University of Southampton

School of Chemistry

Optimization of Protective Coating for Steel-Based Bipolar Plates

by

Jacek Lapinski

Thesis for the degree of the Doctor of Philosophy

November 2010

University of Southampton

Abstract

FACULTY OF ENGINEERING, SCIENCE AND MATHEMATICS

SCHOOL OF CHEMISTRY

Doctor of Philosophy

OPTIMIZATION OF PROTECTIVE COATING FOR STEEL-BASED BIPOLAR PLATES

by

Jacek Lapinski

In this thesis, the possibility to develop a protective coating for carbon steel bipolar plates for H_2/O_2 PEM fuel cells was investigated.

Preliminary studies of the metals (Ni, Cr and Fe) in sulphate medium pH 4 at 333 K (a medium selected to mimic the environment of a bipolar plate in an operating fuel cell) allowed selecting the material suitable for the protection of carbon steel bipolar plate. Ni was chosen for the base coating to prevent the carbon steel from further corrosion degradation. A complete and uniform Ni layer with thickness 3 μm was electroplated from Watts bath at 333 K and this layer significantly decreased the corrosion rate - the corrosion current density was in the range from 0.5 μA cm^{-2} to 1 μA cm^{-2}, whereas for the uncoated carbon steel, the corrosion current density was 30 mA cm^{-2}. An impedance procedure was developed to monitor the quality of the Ni deposits.

In order to increase the electrical contact between bipolar plate and membrane electrode assembly (MEA), a new layer, Ni-graphite composite layer was deposited onto the Ni coated carbon steel. The graphite particles with average diameter 2 μm were added into the Watts bath and a thin layer of Ni-graphite composite was electroplated. The surface of such a layer was intended to be suitable for further modification by PVD; hence minimum surface roughness is required. Furthermore, the corrosion resistance should also be similar to that of the Ni base coating. It was found that the 1 g dm^{-3} graphite particles in the solution were sufficient to deposit Ni-graphite composite with satisfactory surface roughness, i.e., the isolated graphite particles protruding from the Ni layer. The corrosion properties were comparable to the Ni base coating. Such a composite (with 1 g dm^{-3} graphite content in the solution) met the target for the contact resistance (< 25 mΩ cm^2).

However, the corrosion rate of the Ni-graphite layer was still not satisfactory and therefore there was a need for further corrosion protection. Ni-Cr alloys were therefore studied. One approach considered the deposition of a thin Cr layer followed by a heat treatment to diffuse the Cr into the surface of the Ni. A combinatorial approach using physical vapour deposition (PVD) and a 10 x 10 electrode array was used to define the optimum Cr content in the Ni-Cr alloys. It was found that very little improvement in corrosion resistance was observed upon increasing the Cr content

above 20%. Below that value, irreversible changes were observed and those changes had a large negative impact on corrosion properties. Heat treatment performed for the Cr coated bipolar plate lead to coloured surfaces due to oxidation of the Cr. Another approach envisaged the direct electrodeposition of a NiCr alloy. A sulfate bath with additions of thiourea was suitable for the deposition of a thin layer of Ni-20%Cr alloy but the deposit did not thicken because of dominant H_2 evolution reaction. Such a reaction was largely due to the catalytic properties of the Ni-Cr alloy.

Contents

Declaration of Authorship

I, Jacek Lapinski, declare that the thesis entitled: ***Optimization of Protective Coating for Steel-Based Bipolar Plates*****,** and the work presented in this thesis are both my own and have been generated by me as the result of my own original research.

Acknowledgments

After the few years of my study in the University of Southampton, it has been very rewarding and exciting to write this thesis. There were number of people that had a significant influence on my study but the most important person, I would like to express my greatest attitude and respect, was my supervisor, professor Derek Pletcher. His infinite patient, words of critisism and wisdom had a large positive impact on understanding the science and also some aspects of simple everyday life.

I would like to deeply thank my advisors, professor John R. Owen and professor Brian Hayden for support, helpful remarks and scientific comments. To professor Frank C. Walsh for the substantial engineering contribution to the project. Without those stimulating consultations, the thesis would probably have a different scientific content. To my sponsor, CORUS (in Dusseldorf), for providing financial support and surples of materials for experiments.

I also would like to thank the members of staff; in particular to Mr Colin Flowers who largely contributed to the improvement of my language skills.

I would like to express my deepest appreciation to the technical support, to the Alastair Clark for the samples preparation and for any other technical support in the labolatory. To the Mechanical Workshops: in the Chemistry and Engineering Departments. To the Scientific Glassblowing Service for their help and immediate apparatus construction.

I deeply acknowledge a contribution of Jens-Peter Suchland for the detailed instructions of the PVD system, Alexandros Anastasopoulos for his helpful remarks on PVD and the samples preparation for my experiments.

I am also thankful for the marvelous time spent with the Electrochemistry Group from the sixth and the seventh floor and to those I have forgotten to mention…

I. Introduction

I.1. Bipolar plates in the Proton Exchange Membrane Fuel cell

One of the important components of the proton exchange membrane (PEM) fuel cell are the bipolar plates. A single PEM fuel cell comprises of current collectors, gas diffusion layers, catalyst layers and ionic membrane (usually Nafion) that is permeable to hydrogen ions (fig.I.1). A single fuel cell voltage is rather low and therefore they must be connected in series with other cells, to give a higher voltage output. The cells in a stack are separated via current collectors, known as bipolar plates. The bipolar plates also separate the oxygen and hydrogen gases, which are continuously fed to the cell. Metallic plates at the end of the cell stack are used to collect the electricity from all the cells. In fig.I.1, the thickness of the single cell may be approximately 3 – 4 mm. The standard bipolar plates are non-porous, thick graphite. They must be relatively thick because thin graphite bipolar plates are permeable to hydrogen and oxygen gases. Moreover, graphite plates are brittle and difficult to machine. Graphite bipolar plates comprises of 80 % of the total weight in the PEM fuel cell. On the other hand, graphite is the most stable material in a corrosive environment in the PEM fuel cell and also possesses good electrical conductivity. With the graphite bipolar plates, it is rather difficult to fabricate the optimum gas channels due to the brittle structure of the graphite. One of the most promising candidates for bipolar plates is steel and they have a potential to replace the conventional bulky graphite plates. Moreover, the steel bipolar plates are not permeable to the gases, and hence the thickness can be significantly reduced. The steel bipolar plates can be stamped or shaped to give the optimum geometry for gas distribution on both sides of the plate. Detailed solutions of the shape of the metallic bipolar plates can be found in [1] and [2].

One inevitable drawback of the metallic bipolar plates is corrosion in the acidic environment in the PEM fuel cell. On the cathode side of the bipolar plates, where the oxygen is fed, the potential of the plate is estimated between +0.6 V and +0.8 V vs. SHE and this is the potential where the plate must be stable to corrosion.

Moreover, the corrosion may also be enhanced due to decomposition of Nafion at the operating temperature of 333 K - 353 K leading to fluoride ions. Iron ions from the dissolution of the metallic plates may have a contribution to the poisoning of the membrane. Dissolving bipolar plates are also likely to decrease the electrical contact with the MEA because of the dissolution product or corrosion layer deposited on the surface of the steel increasing the contact resistance. Consequently, corrosion of the bipolar plates decreases the efficiency of the fuel cell.

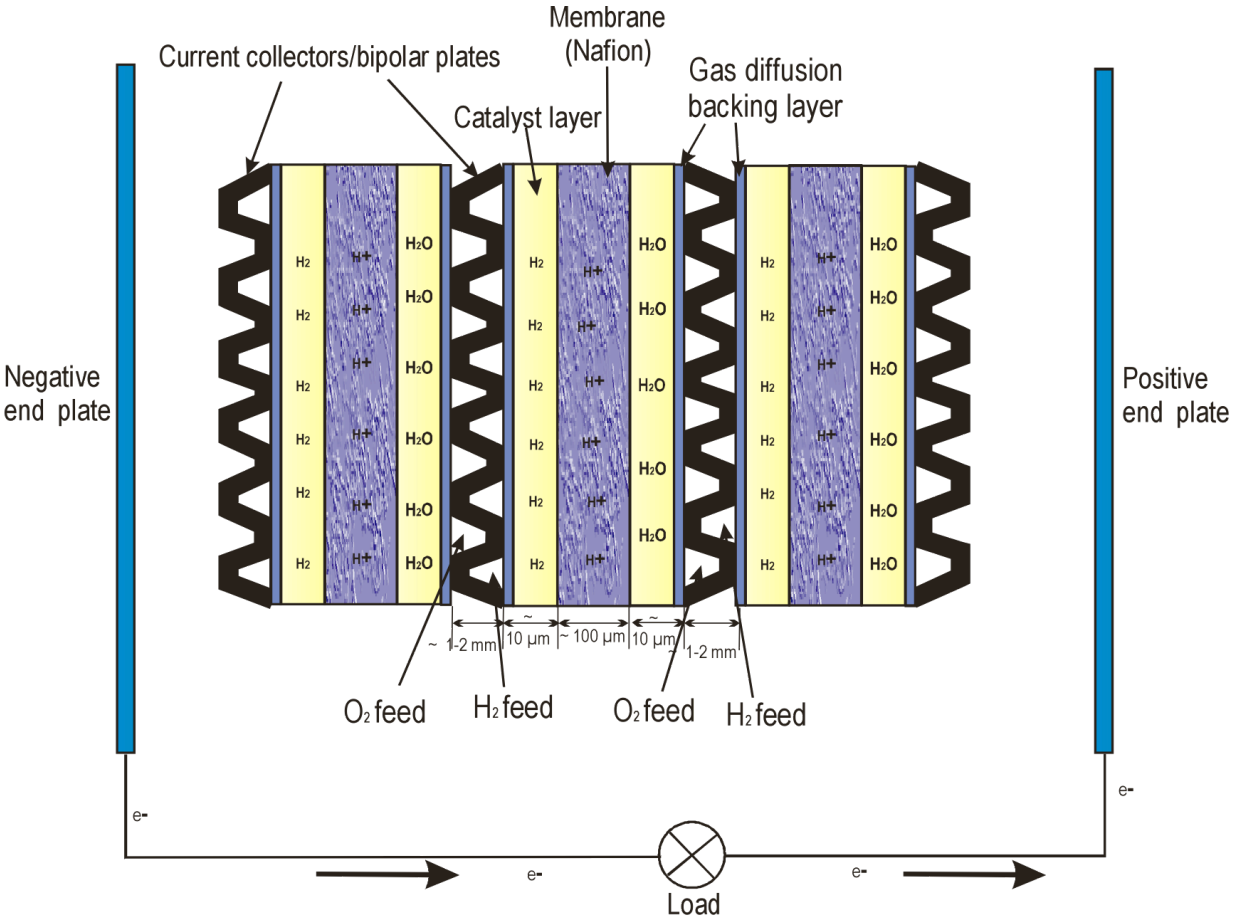

Fig.I.1. A stack of proton exchange membrane fuel cells. The membrane, the catalyst layer and the gas diffusion-backing layer pressed to the catalyst layer in single fuel cell are usually fabricated as one component named the membrane electrode assembly (MEA). The current collectors (preferably carbon steel plates) in the fuel cell stack serve as bipolar plates.

The bipolar plate also serves to remove excess heat resulting from the cell inefficiency (see later discussion). The overall fuel cell reaction can be written as:

$$2\,H_2 + O_2 \rightleftharpoons 2\,H_2O \qquad (1)$$

and the standard cell potential at 298 K and at normal atmospheric pressure is +1.229 V. In practice, due to overpotential and *IR* drop, the cell voltage is approximately +0.7 V and these inefficiencies lead to heat. Although the cell voltage is different to that predicted from thermodynamics, the efficiency of a single fuel cell of approximately 50% - 60 % could be achieved. In order to implement such an attractive source of energy (the only by-product of the chemical reaction is water with no emission of greenhouse gases), a stack comprised of 6 to 500 single fuel cells is used for stationary applications, to power houses, vehicles, trains, plants etc. [3], [4], [5], [6], [7].

I.2. The aim of the project

In this project, the development of a coating for carbon steel bipolar plates to protect it from corrosion on the cathode side of a H_2/O_2 PEM fuel cell is the objective. Even stainless steel is considered too expensive for bipolar plates in a fuel cell and hence the base material should be carbon steel. A schematic illustration of the project pathway is shown in fig.I.2. Carbon steel plates supplied from CORUS in Düsseldorf will be regularly employed. In addition, a 904L stainless steel (SS) also supplied from CORUS, Düsseldorf, will be used and tested for comparison. The protective coating will consist of several layers deposited onto the steel. Ni was chosen as a base material to protect the carbon steel. The electrodeposition of Ni onto carbon steel is the first step to reduce the corrosion rate of the steel. The Ni layer must be relatively thick, complete and uniform. These criteria are vital for the coating to impede the rate of corrosion. However, the Ni layer is not sufficient to maintain the low rate of corrosion and therefore other better corrosion resistant metals or alloys need to be considered. In this project, the metal chosen was chromium. The next layer is intended to increase the electrical contact between the bipolar plates and the MEA. In addition, this layer should have the same low

corrosion rate as the first protective layer. A thin Ni-graphite layer is therefore deposited onto Ni coated carbon steel.

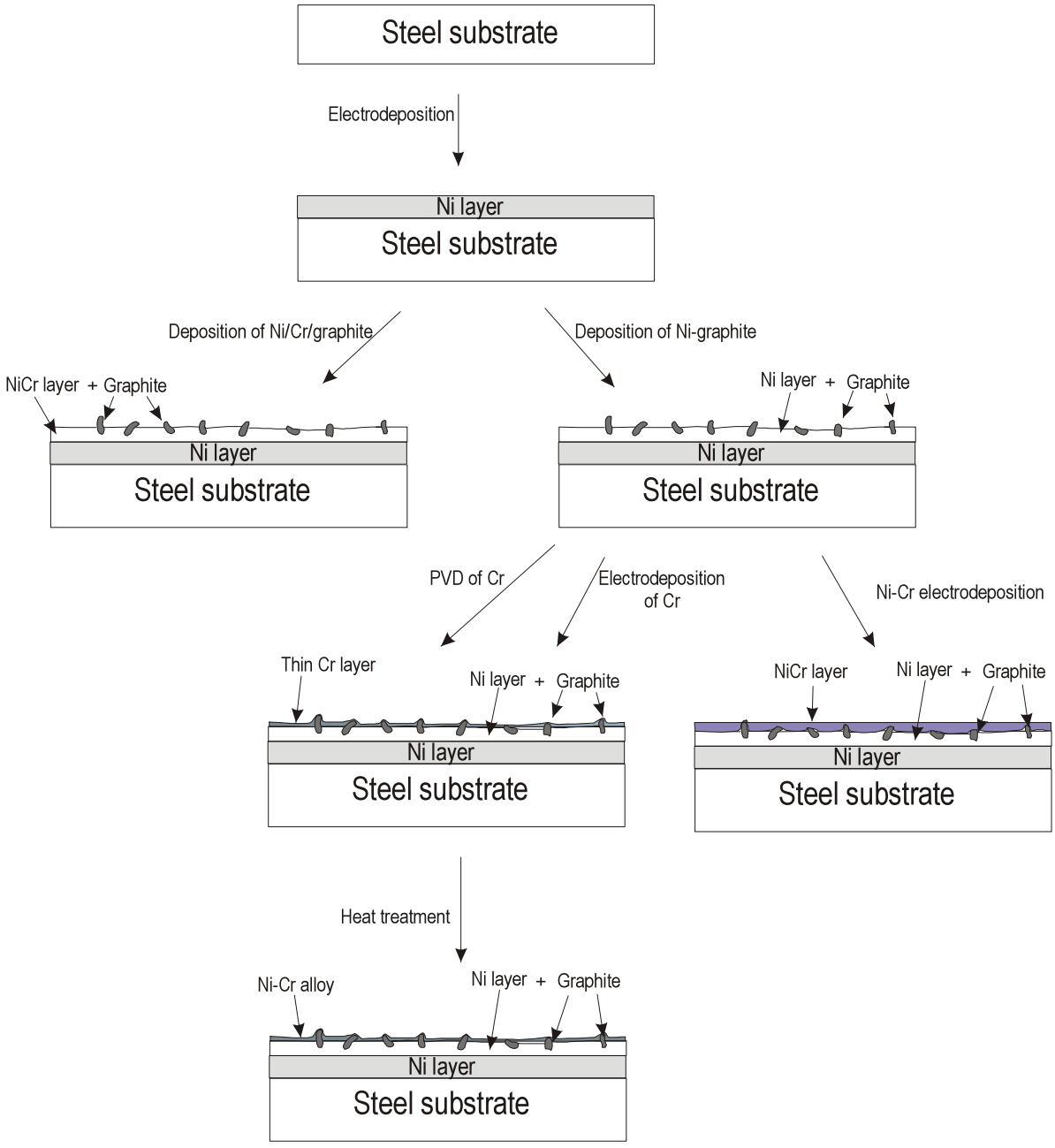

Fig.I.2. Schematic pathway of the possible protective coatings for carbon steel bipolar plates.

Because of the tendency of the metals to form oxides on the surface, the graphite particles were distributed in the Ni to obtain better electrical contact. The influence of different amount of graphite particles in the solution on the corrosion behaviour, contact resistance and surface topology will be a subject of the investigation. After the Ni-graphite layer is successfully deposited onto Ni coated carbon steel, the objective will be to improve the corrosion resistance of the Ni-graphite layer by a further coating with a thin layer of chromium or Ni-Cr alloy. Two possible pathways will be considered:

1. PVD deposition of thin protective film onto Ni-graphite coated carbon steel. A thin layer of chromium with thickness 20 nm or Ni-Cr alloy with Cr ranging from 0% to 100% will be considered and a thickness of the alloy will vary from 20 nm to 100 nm.

2. Electrodeposition of Cr or Ni - Cr alloy. The Ni – Cr alloy will be electrodeposited from a salt solution containing divalent Ni and trivalent Cr sulphate ions. This particular alloy is well known in the literature to be supremely good corrosion resistant material and some applications can be found in our everyday life: electronic devices production [8] or medical applications [9]. An alternative approach would involve the inclusion of graphite particles into an electrodeposited Ni-Cr layer.

A heat treatment will be applied to the coated bipolar plates and the heating temperature as well as dwell time will be investigated. The intention of the heat treatment is to create an alloy from a thin layer of Cr deposited by PVD on the Ni-graphite layer. The structure therefore, will have a form: a thin Cr layer on top of the coating and the mixture of Cr layer and Ni/graphite layer.

It is important to emphasise the significance of the layered structure. Each layer must meet a certain corrosion requirement and therefore after the each stage of fabrication, the surface characterization and one-hour corrosion test will be performed in order to compare the stability of the layered bipolar plates. The solution that mimics the conditions in PEM fuel cell is chosen to be: 0.1 M Na_2SO_4, 2 ppm NaF, pH 4 at 333 K. In addition, the contact resistance measurement for the prepared bipolar plates will be performed and particular interest will be the Ni-graphite layer with different amount of graphite particles, deposited onto Ni coated carbon steel.

The optimum thickness of each layer needs to be determined experimentally.

I.3. Electrode reactions

At the anode side of the fuel cell, when the hydrogen is fed, two hydrogen molecules are oxidized to four protons:

$$2\,H_2 \longrightarrow 4\,H^+ + 4\,e^- \qquad (2)$$

The four protons migrate through the membrane and four electrons move into the external circuit. The potential for this reaction is close to zero volts vs. SHE. On the cathode side, when the oxygen is fed, four electrons and four protons meet an oxygen molecule and combine together producing water:

$$O_2 + 4\,H^+ + 4\,e^- \longrightarrow 2\,H_2O \qquad (3)$$

The electrochemical potential at equilibrium predicted for this reaction for pure oxygen and 1 M proton concentration is +1.229 V vs. SHE. In this way, a closed electrical circuit is obtained and the overall cell reaction is reaction (1). A metallic bipolar plate in contact with O_2/H_2O may corrode and a dissolution product may be metal ions. The metal is corroding and the corrosion will depend on the O_2 concentration, local pH and the nature of the metal (see following discussion on the thermodynamics and kinetics of corrosion).

I.3.1. Thermodynamics of electrode reactions

If the metal is in contact with a solution containing its ions, the potential changes with the concentration (or activity) of the metal ions. The equilibrium reaction for this situation may be written as:

$$M^{n+} + n\,e^- \rightleftharpoons M^0 \qquad (4)$$

and the Nernst equation for the above reaction is:

$$E_e = E_e^0 + \frac{2.3\,RT}{nF} \log \frac{[M^{n+}]}{[M^0]} \qquad (5)$$

where, E_e is the equilibrium potential, R is the gas constant, T is the absolute temperature, n is the number of electrons taking part in the reaction, $[M^{n+}]$ is the activity of metal ion, $[M^0]$ is the activity of metal, E_e^0 is the standard electrode potential for the metal/metal ion couple. The latter quantity can be taken from a table of the standard electrode potentials. Since the reaction is not dependant on the amount of metal, the activity of pure metals (but not alloy) is taken as 1 and the Nernst equation may be written:

$$E_e = E_e^0 + \frac{2.3\,RT}{nF} \log [M^{n+}] \qquad (6)$$

It is impossible to measure the single potential of the metal/solution interface; therefore, a second electrode must be introduced. In order to measure the equilibrium potential, for instance, for Ni, the metal is immersed in solution containing Ni^{2+} ions, and a second electrode (e.g., reference electrode) is immersed at a certain distance apart from the Ni metal. These two electrodes are connected with metal wire and the conductive electrolyte solution is closing the electrical circuit. A potential difference at equilibrium is established. The Gibbs free energy change for the cell reaction is related to the equilibrium cell voltage by:

$$\Delta G_e = - n F \Delta E_e^{cell} \qquad (7)$$

where n is the number of electrons taking part in the reaction, F is the Faraday constant and ΔE_e^{cell} is the equilibrium cell voltage defined as difference in cathode and anode potentials at equilibrium:

$$\Delta E_e^{cell} = E_e^c - E_e^a \qquad (8)$$

I.3.2. Kinetics of electrode reactions

Applying a potential positive or negative to the equilibrium potential, a net anodic or cathodic, current, respectively, starts to flow. The dependence of current density on potential can be described by the Butler-Volmer equation:

$$E_e = E_e^0 + \frac{2.3\,RT}{nF}\log\left[M^{n+}\right] \qquad (9)$$

where j is the net current density measured upon applying an overpotential η. The overpotential is defined as difference between the applied potential and the equilibrium potential: $\eta = E - E_e$. The quantity j_o is known to be the exchange current density and represents the equal rates of cathodic and anodic reactions at the equilibrium. The significance of the j_o can be seen by considering for instance two extreme cases:

1) $j_o \rightarrow \infty$, we have a perfectly reversible electrode, and
2) $j_o \rightarrow 0$, we have an ideally polarisable electrode.

In practical situations, the references electrodes may be treated as reversible electrodes. The values for j_o for real reactions are between ∞ and 0 and two situations can be recognized: when j_o is high, a "fast electrochemical reactions" can be considered. It is more likely that the "fast electrochemical reactions" are limited by mass transport of the species to and from the electrode. When the j_o is low, a "slow electrochemical reactions" can be characterised and here a substantial electrode polarization should be applied for the reaction to occur – the reaction appear to be "sluggish".

It is important to emphasise the significance of the Butler-Volmer equation at different overpotentials applied:

1) When the overpotential is small and in the range of ±10 mV, the arguments in both exponential terms becomes << 1 and therefore the exponent functions may be expanded using power series. This leads to a linear current density-potential relationship:

$$j = j_o \frac{nF}{RT} \eta \qquad (10)$$

2) When the overpotential is large and negative (>> |-10 mV|), the first term in the bracket of the equation (9) becomes negligibly small with respect to the second term and hence it can be omitted in this equation. The reduction reaction is a dominant reaction.

3) Analogously, when the overpotential is large and positive (>> +10 mV), the second term of the equation (9) becomes very small and may be neglected. The oxidation reaction is a dominant reaction. Taking the logarithms for both sides of the oxidation reaction, a linear relationship of current density versus potential can be written:

$$\log |j| = \log |j_o| + \frac{\alpha_a nF}{2.303\, RT} \eta \qquad (11)$$

This equation is known as a Tafel equation for the oxidation reaction. Plotting log | j | versus overpotential, a Tafel plot can be obtained with a slope, (α_anF)/(2.303 RT), that has a units of [V^{-1}] (fig.I.3). A similar equation may be written for the reduction reaction. The extrapolation of the cathodic and anodic branches to η = 0, gives the exchange current density j_0. The transfer coefficient, α, may be obtained from the slope and the sum of the anodic and the cathodic transfer coefficients should give the value 1. For a one-electron transfer reaction at room temperature and for α = 0.5, the Tafel slope should have a value of 1/120 [mV^{-1}] at room temperature. Upon increasing the temperature, the Tafel slope decreases.

The overall rate of anelectrode reaction is limited by the slowest step of a sequence of steps.

1) transport of the reactant from the bulk solution to the electrode. Transport by diffusion, migration or convection may be considered,
2) electron transfer to/from the electrode to the electroactive species. As a consequence, reduction or oxidation of the species is occurring, and
3) removal of the product away from the electrode to the solution bulk

Three modes of mass transport will be briefly discussed for a simple electrode reaction (see reaction (4)):

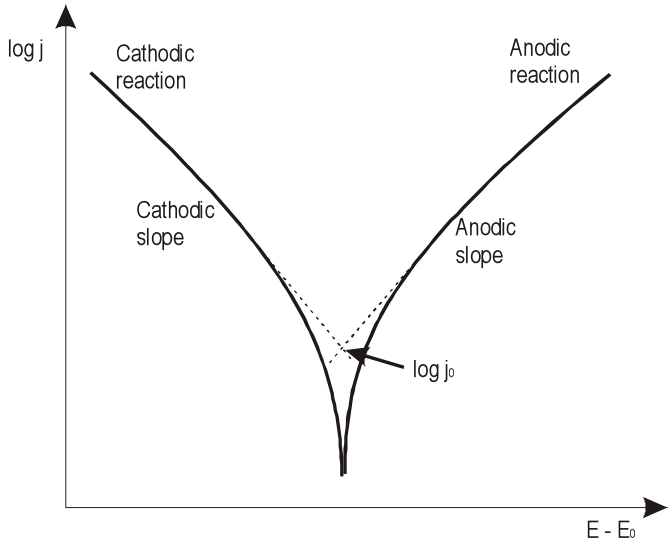

Fig.I.3. Linear relationship of current versus potential presented as a Tafel plot

Diffusion. Diffusion may be regarded as a movement of species in the solution from the higher to the lower concentration until the concentration becomes homogenous everywhere in the solution. Therefore, the driving force for diffusion is the concentration gradient. Adolf Fick gave a mathematical description of the diffusion process in his laws of diffusion. The first law states that the flux of the species is proportional to the concentration gradient and proportionality constant is the diffusion coefficient of the species. The second law relates concentration of the species with distance and time. The equation has the form of a partial differential equation. One initial condition and two boundary conditions appropriate to the experiment are necessary to solve for the concentration profile. A derivation of the second Fick's law can be found in [10] and few solutions of this equation for different electrodes geometry with appropriate boundary conditions can be found in [11]. It is important to emphasise that during the electrochemical reaction in an unstirred solution containing large concentration of electrolyte, diffusion is the only mode of mass transport and transport will be relatively slow process.

Convection. In this mode of mass transport, the solution may be agitated, flowed over the electrode or the electrode may be moving in the stationary solution. It is worthwhile to remember that the natural convection may also occur if there is a slight temperature gradient in the solution. However, natural convection has a rather negligible effect compared to the forced convection.

Moreover, the forced convection allows increasing the mass transport by a large factor compared to when there was no convection present in the solution. The convection used in the laboratory experiments may be well defined in terms of its experimental and theoretical description. As an example, a rotating disc electrode should be quoted here and a vast literature describes influence of electrode rotation on current density [12], [13]. A strong convection can be seen in variety of the flow cell systems. In those systems, the geometry of the cell is usually well defined and the flow of the solution is controlled. The engineering of the system may not necessarily be an easy task but the immediate consequences of the design may have an impact on studying the electrochemical systems that have a practical use in industrial applications [13], [14].

In most industrial applications, a strong convection is desirable. Here, a good example will be an electroplating of nickel in the CORUS strip plating line in Düsseldorf, Germany. Instead of flowing the solution along the cathode, fast moving steel enters a stationary plating bath (see fig.I.4). The strong convection may influence the quality of the deposit together with other electroplating parameters (see later discussion in the chapter on nickel and nickel-base composites). Suffice to say that a beneficial effect of strong convection during the electroplating can be seen in particular, when hydrogen evolution reaction is competing reaction with metal deposition.

Migration. Migration is the movement of the species in the solution due to the electrical gradient. The ions in the solution are charged species and therefore this movement is purely electrostatic in nature. In most laboratory cases, the migration can be neglected in the electrochemical experiments by adding an excess of supporting electrolyte.

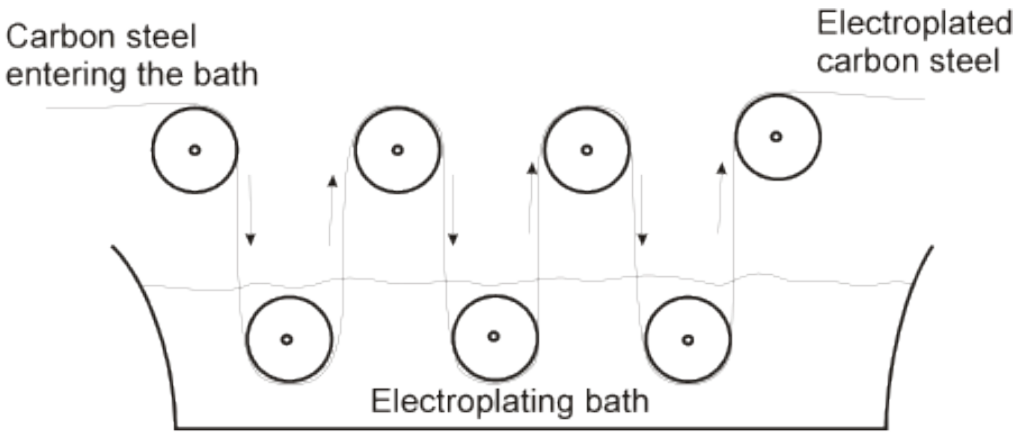

Fig.I.4. Electroplating of Ni in CORUS reel to reel production line in Düsseldorf.

These three modes of mass transport interact with the electron transfer producing some limitations on the rate of electron transfer. As mentioned above, at the equilibrium potential, E_e, the current density $j = 0$ (partial cathodic and partial anodic currents are equal and hence no net current is flowing). Increasing the potential to more positive values, the net anodic current starts to flow and an exponential increase in current density is observed. The Butler-Volmer equation (9) and the Tafel equation (11) will apply while the reaction is electron transfer controlled. Upon increasing the potential further to more positive values, a contribution of mass transport to rate control will be observed. In this region, the rate of electron transfer and mass transport are similar. In practice, the current density is in the range between 0.1 j_{lim} and j_{lim}. Upon increasing the potential even further, the limiting current density for the system is achieved. In this region, the current density is purely dependent on mass transport to the electrode and independent of potential changes.

I.3.3. Corrosion of metals

When a metal is immersed in a solution, it will take up the corrosion potential. This is the potential where no current flows; the current for metal dissolution is balanced by the current for a reduction reaction, usually oxygen reduction or water/proton reduction (see fig.I.5). Assuming that the cathode process is the reduction of the H^+ and that corrosion leads to a metal ion in solution, the corrosion process is:

$$M + nH^+ \rightleftharpoons M^{n+} + \frac{n}{2} H_2 \qquad (12)$$

where n is a stochiometric coefficient of the reaction.

In practice, the dissolution product may be a metal ion, metal oxide or metal hydroxide.

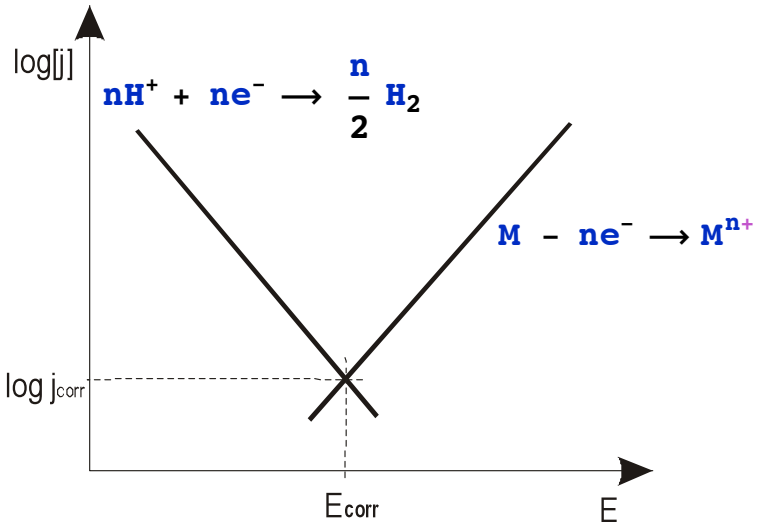

Fig.I.5. A schematic illustration of corrosion at mixed potential.

I.3.3.1. Thermodynamics consideration

If one takes the metal, *M,* in a solution containing metal ions, M^{n+}, the Nernst equation has the form:

$$E_e = E_e^0 + \frac{2.3\,RT}{nF}\log\left[M^{n+}\right] \qquad (13)$$

The equilibrium potential is independent of solution pH. On the other hand, for a chemical reaction such as:

(14)

there is no change in oxidation state but the reaction is dependent on pH.

The corrosion reaction, where the product is an oxygen or hyroxide:

$$M + H_2O \longrightarrow MO + 2H^+ \quad (15)$$

will also depend on pH.

The thermodynamics of corrosion in non-complexing media is often summarised in terms of Pourbaix diagram. Fig.I.6 shows the Pourbaix diagram for Ni – water system at 25°C for a typical activity of Ni^{2+} ions 10^{-6}:

1) The regions of metal immunity, corrosion and passivation can be recognised,

2) Horizontal and vertical lines represent the equilibrium reactions where the electrons and protons are involved. Sloping lines represents equilibrium for the reactions, in which both protons and electrons are taking part.

3) In acid medium, Ni should corrode in association with hydrogen evolution with the formation of Ni^{2+}. In alkaline solution the driving forces for Ni oxidation is much slower and oxides/hydroxides are formed [15].

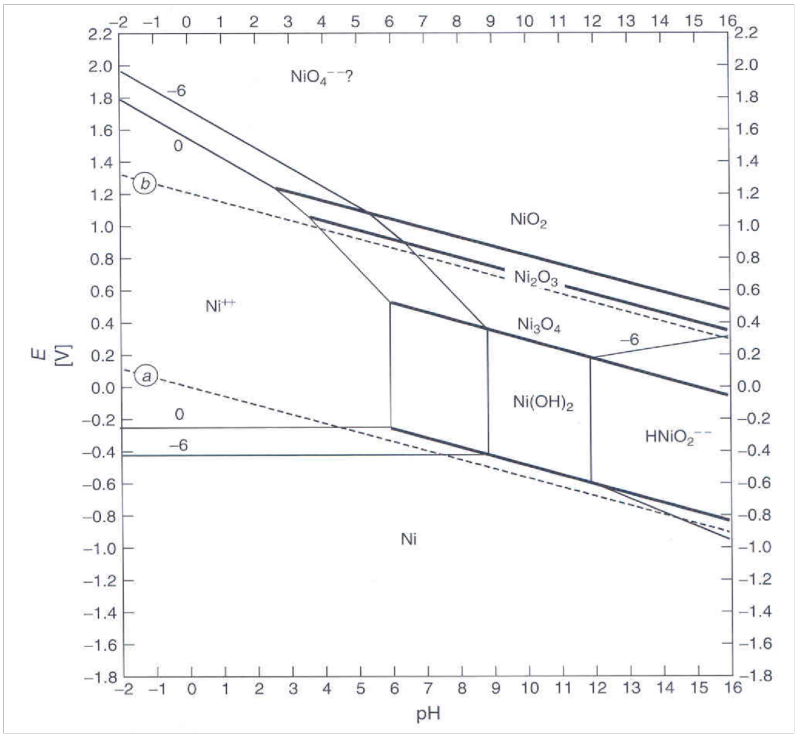

Fig.I.6. Pourbaix diagram for nickel in aqueous medium.

From a thermodynamic viewpoint, Cr should corrode much faster than Ni. In reality, a passive film forms on the Cr surface and strongly inhibits the kinetics of the corrosion reaction. Contact with air is, in fact, usually sufficient to form a passive layer on the surface [15].

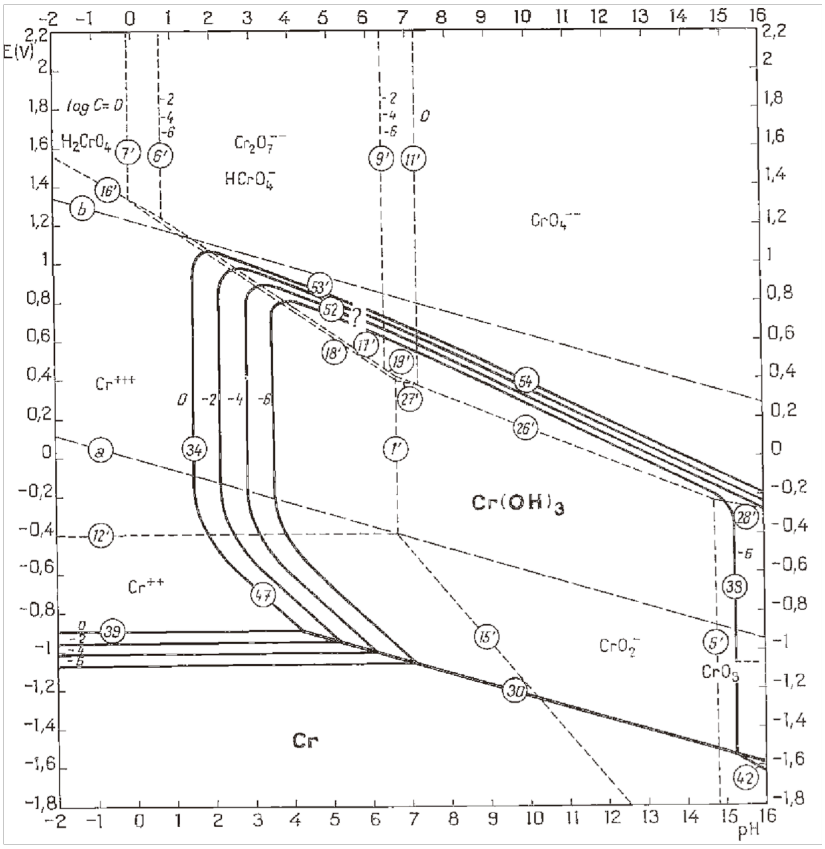

Fig.I.7. Pourbaix diagrams for Cr in aqueous medium.

I.3.3.2. Kinetics of corrosion reaction

Still assuming that the reduction of proton is the only cathode reaction at the open circuit potential, the following reactions are occurring:

(14)

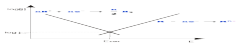

and

$$nH^+ + ne^- \longrightarrow \frac{n}{2} H_2 \qquad (15)$$

The rates of the two reactions are equal, therefore the corrosion reaction occurs at a mixed potential known as the corrosion potential. The kinetics of the corrosion reaction away from the corrosion potential may be described by a current density-potential relationship, similar to the Butler-Volmer equation:

$$E_e = E_e^0 + \frac{2.3\,RT}{nF} \log\left[M^{n+}\right] \qquad (16)$$

where, j is the net current density measured upon departure from a corrosion potential, j_{corr} is current at the corrosion potential, b_a and b_c are anodic and cathodic Tafel slopes. At small polarization, where $E - E_{corr}$ <<10 mV, the current-potential response is linear with the slope $1/R_{corr}$ (see fig.I.8). For known values of the Tafel slopes, the corrosion current density may be calculated from R_{corr} using the Stern-Geary equation [16]:

(21)

$$j_{corr} = \frac{b_a \mid b_c \mid}{2.3\,R_{corr}\,(b_a + \mid b_c \mid)}$$

where R_{corr} is a corrosion resistance, b_a and b_c are the anodic and cathodic Tafel slopes, respectively.

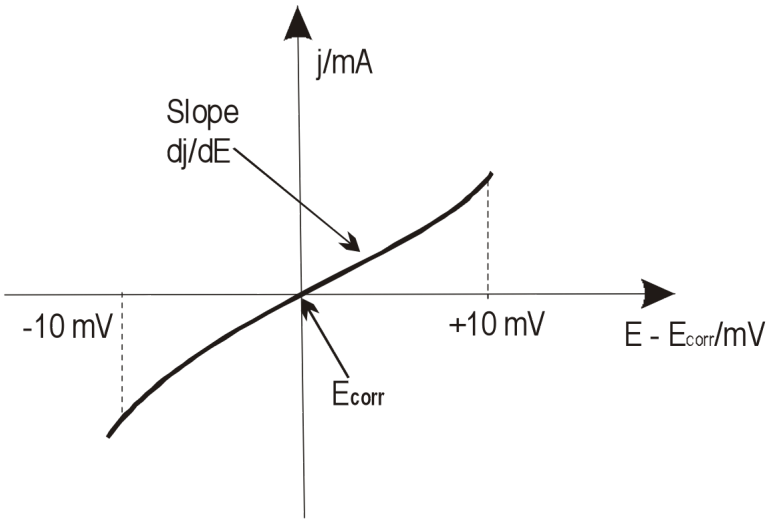

Fig.I.8. Graphical representation of corrosion at low overpotentials.

At larger values of $E - E_{corr}$, either H_2 evolution or metal dissolution will dominate and the j-E data will follow a Tafel equation. On the other hand, the oxygen reduction may be a dominant reaction. Now, the corrosion will largely be dependent on O_2 concentration Fig.I.9 illustrates an influence of the oxygen concentration on changes in the corrosion potential. If the concentration of O_2 is high, the Tafel line for metal dissolution intersects with the oxygen Tafel line and corrosion will occur with association of oxygen reduction. (fig.I.9.a). In general the corrosion potential will be positive to that when the cathode reaction is H^+ reduction and the rate of corrosion will be higher. At lower oxygen concentration, the Tafel line for metal dissolution will intersect the limiting current for oxygen reduction. Convection in solution will increase the mass transport to the electrode and hence the rate of oxygen reduction. Therefore, an increase in the corrosion potential will be observed and corrosion will occur at a higher rate. This situation is illustrated in fig.I.9 b, with the dashed curve.

I.3.4. Passivation of metals

According to the discussion of Pourbaix diagram, chromium should corrode much more easily than nickel in acid solution. This is not the case because of formation of a passive layer. Passive

a)

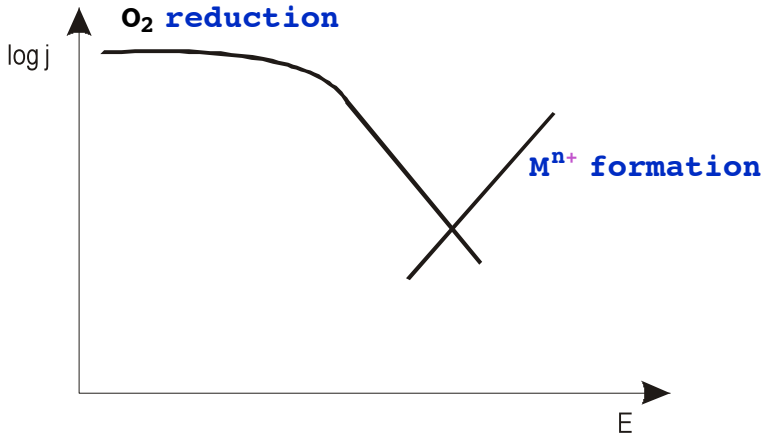

b)

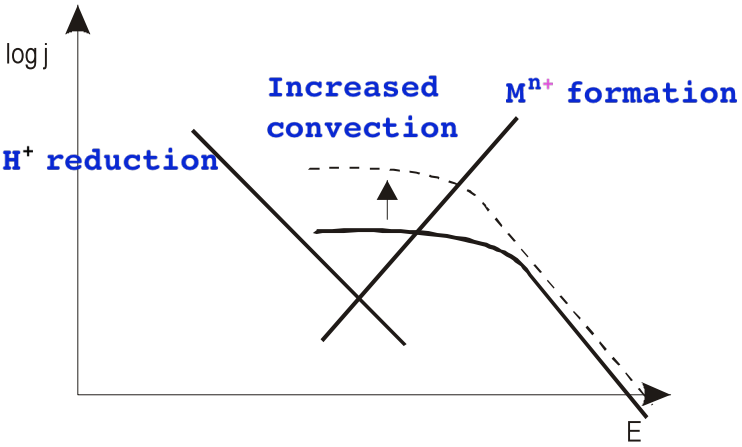

Fig.I.9. The influence of oxygen concentration on corrosion process, a) high O_2 concentration, b) low O_2 concentration.

layers formed on metals act as a barrier from further corrosion degradation and therefore, it can significantly change the kinetics of the corrosion.

Passivation on the surface of the metal will be dependent on potential applied to the metal and properties of the $M(OH)_n$. The thickness of the passive layer usually ranges from 1 nm to 15 nm.

Fig.I.10 presents the change of current density upon scanning the potential to more positive values. The scan starts when the metal is immune to corrosion. If the potential is increased to more positive values, the current density increases rapidly through the active corrosion region. The current density then drops significantly to lower value and upon increasing potential further to more positive, the current density is almost constant and low. A protective oxide barrier is formed on the surface of the metal and this region is called a passive region. At the very positive potentials, in the so-called transpassive region, further formation/conversion of oxides or oxygen evolution may occur.

It is important to recognised that if the corrosion of metal is occurring in the active corrosion region, the rate of metal corrosion will be high. On the other hand, if a passive film was already formed on the surface of the metal, the corrosion rate will be significantly reduced (possibly by orders of magnitude).

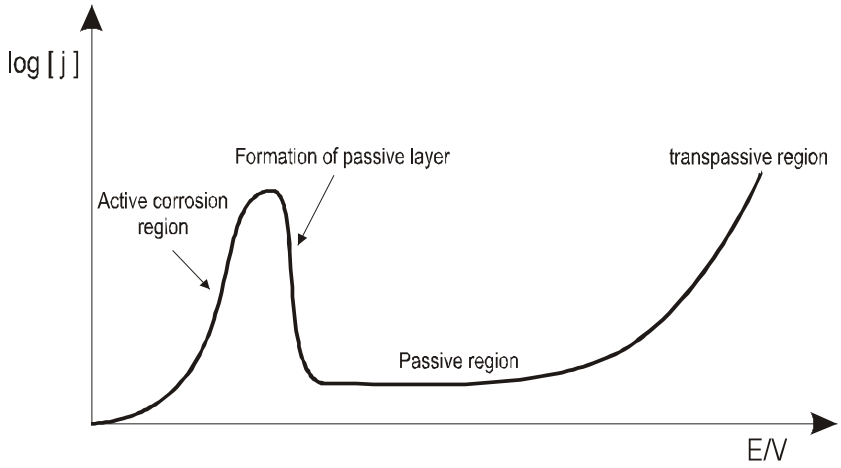

Fig.I.10. Corrosion-potential diagram for a metal upon scanning the surface to more positive potentials.

I.3.5. Corrosion measurements

Several electrochemical methods for corrosion measurement have been reported [11], [17]. Perhaps the most common and widely used methods are linear polarization, Tafel extrapolation and electrochemical impedance spectroscopy. In the linear polarization methods, either the

potential is controlled and the current is measured or the current is controlled and the potential is measured. The controlled parameter is either stepped or scanned.

In order to determine the corrosion current at the corrosion potential, a linear polarization in the potential range of ±10 mV from the open circuit potential can be performed. The potential may by scanned with a slow scan rate and the current is recorded.

In electrochemical impedance spectroscopy, impedance is measured as a function of frequency whilst a small potential perturbation is applied to the system, usually < ±10 mV. In order to analyse the nature of the overall current and potential, an equivalent electrical circuit is developed and the model represents a sum of the impedances in the electrochemical system [18]. For small changes in potential, the measured current is also small and hence the corrosion resistance, R_{corr}, can be estimated. The corrosion current may be calculated from the Stern-Geary equation (21) provided the Tafel slopes are known.

In addition, other electrochemical techniques often used in laboratories are also important. Corrosion rate may be determined by monitoring the current/current density at a particular potential over the period of time (e.g., 5 hours). The transient (current-time) recorded for the system will give an indication of the magnitude of corrosion current/corrosion current density and its variation with time. This technique is rather used when the system is known, for instance, the surface was previously scanned over the certain potential range.

The weight loss is also well known method to determine the rate of corrosion. The steel sample is weighed before and after the immersion in the corrosive medium. The difference in weight of the sample before and after corrosion test is used to estimate the corrosion rate from the Faraday law. The weight loss measurement is often carried out for a long period of time, e.g., 5 days, and the weight measurement is usually conducted with accurate precision.

A salt spray test is commonly employed method in industry to determine the endurance of the material in corrosive environment. The test is carried out in a cabinet and the sample is "immersed" in a salt solution or sprayed with the salt solution, for example, 5 % NaCl with addition of other salts with pH range from 3 to 7. The immersion time may vary from several hours to several days. Some salt solutions may differ as well as the cabinet design and this is dependent on the material tested. Few examples of salt spray tests may be found in the corrosion

standards, internationally accepted and published in, for instance, ASM handbook: Corrosion: fundamentals, testing and protection [19].

I.4. The need for corrosion protection of steel-based bipolar plates

Carbon steel is widely available and has many properties ideal for bipolar plates. However, the rate of corrosion is known to be high compared to stainless steel. Many studies of corrosion of carbon steel in a wide range of media have been reported [20], [21], [22], [23], [24].

In general, carbon steel and low alloy steels do not resist acidic conditions. In 1 N HCl solution, for instance, the corrosion rate is 5 mm $year^{-1}$ in non-stirred conditions at 15°C, and this rate is approximately similar for H_2SO_4 solution with the same concentration. If the concentration of H_2SO_4 is increased to 65 wt. %, the rate of corrosion decreases to 1.27 mm $year^{-1}$ [25]. Similar corrosion properties were observed after the carbon steel was heat-treated [26]. In addition to corrosion, mechanical properties of tempered plain carbon steel described in [27], show low hardness of this steel largely because of absence of other alloying elements. Acidic environments will be the most relevant to the corrosion of metallic bipolar plates.

The main constituents of carbon steel are iron with addition of small amount of carbon; therefore, the corrosion of this steel may be largely attributed to the dissolution of iron. In less aggressive medium, the corrosion of pure iron in 0.1 M Na_2SO_4 at pH 3.3 and 6.4 was investigated by Mayouf in [28]. It was found that the corrosion current density recorded in this medium at pH 3.3 was 12.6 mA cm^{-2} (equivalent to a corrosion rate of 143 mm y^{-1}) whereas at pH 6.4, the corrosion current density decreased to 5.6 mA cm^{-2}.

The corrosion rate of carbon steel containing 0.31% carbon in different acids was compared. The rate of corrosion measured by weight loss in 5% HCl and 5% H_2SO_4 acids was: 2.1 mg cm^{-2} h^{-1} and 2.7 mg cm^{-2} h^{-1}, respectively [29]. Reihim at al. [30] studied corrosion of low carbon steel in 4 M H_2SO_4 solution. The weight loss measurement showed that the longer the immersion time the larger the rate of corrosion. The weight loss after 6 h was 100 mg cm^{-2} h^{-1} and after 10 h, an increase to 150 mg cm^{-2} h^{-1} was observed. A polarization curve in narrow potential range with scan rate 0.1 mV s^{-1} was recorded. The corrosion current density at corrosion potential was

determined from the Tafel plot. It was found that the corrosion current density was 3.85 mA cm^{-2}. Khaled [31] studied corrosion of mild steel with 0.15% carbon in 0.5 M HCl by electrochemical impedance spectroscopy measurement.

The corrosion current density for this steel was 1.9 mA cm^{-2}. The carbon steel is indeed prone to corrosion and therefore, an effective protective coating must be applied. The coating must be relatively thick, uniform and complete in order to successfully impede the rate of corrosion. Noble metals are among those that can be successfully employed to protect the steel. In practice, however, the costs of manufacturing of the protective coatings with noble metals may lead to difficulties on the industrial scale. The final coated product should have a relatively low rate of corrosion and exhibit properties internationally established in, for instance, the Annual Book of ASTM Standards [32]. In addition, by alloying metals or incorporating particles and fibers within the metal matrix, the protection may be more effective, enhancing mechanical, corrosion or electrical properties of the coating. Different techniques for protective coatings are employed. In most cases, those techniques are rather developed and practically used for industrial applications, for instance, to galvanize the steel [33] or to sputter the metal for electronic devices [34]. On the other hand, the significance of investigations carried out in the university laboratories may be considered as a vital bridge between transferring the product into the industrial line.

I.5. Electrodeposition

The first commercial electroplating began about 170 years ago and manufacturing considered the minimum requirements needed, i.e.: electroplating tank, plating solution, cleaning and a power source. Throughout the history of the electroplating, safety issues, costs of the production and environmental concerns gradually began to develop. Modern electroplating nowadays satisfies a series of regulations that help to protect the environment, in particular, water and air pollution [35]. The electroplating is widely applied to protect carbon steel and particular interest of this technology was found in the automobile industry and the electronic industry.

I.5.1. Kinetics and mechanism of metal deposition

The electrodeposition of metals occurs by the reaction:

$$M^{n+} + n\,e^- \rightleftharpoons M^0 \qquad (22)$$

in which metal ions from the solution are reduced to metal. Electroplating baths are essentially one of two types, acid or complexing. Acidic baths may be free from complexing agents and may contain some additives in order to catalyse the electrodeposition process (in the case of Cr deposition, see later chapter).

Early stages of metal deposition involve nucleation of the new metal phase and initial growth. A detailed description of phase formation can be found in [7] and [35]. The surface structure of the substrate may have a beneficial effect on nucleation and growth. The importance of substrate pre-treatment is crucial before metal deposition is commenced. In practice, usually before the metal is electroplated, the surface of the substrate is pre-treated by: mechanical treatment – cleaning the surface by sandblasting, abrasion or chemical treatment – degreasing or electrodegreasing the surface. All those preparations are intended to decrease (or "minimise") the passivation layer on the steel and enhance uniformity and adhesion. As it is relatively easy to pretreat the carbon steel, the stainless steel on the other hand, requires more effort in order to decrease the level of oxide on the surface (see experimental chapter *II.1.2.2 Stainless steel 904L*).

Parallel with metal formation, very often hydrogen evolution reaction is a competing reaction. This reaction is clearly, an unwanted reaction and should be minimised during a deposition process. It is important to stress that upon increasing the rate of deposition, the rate of hydrogen evolution may also increase.

I.5.2. Nickel and Ni-based composites

One of the plating solutions for Ni is a Watts bath. This bath has been significantly improved over the years and many applications of Ni electrodeposited from the Watts bath can be seen nowadays [36]. Another plating bath is the sulphamate bath. Both plating solutions, see table I.1, are used for functional deposition.

Watts bath	***Sulphamate bath***
• 225 – 400 g dm^{-3} $NiSO_4.6H_2O$ • 30 – 60 g dm^{-3} $NiCl_2.6H_2O$ • 30 – 45 g dm^{-3} H_3BO_3	• 500 g dm^{-3} $Ni(SO_3NH_2)_2$ • 0 – 30 g dm^{-3} $NiCl_2.6H_2O$ • 30 – 45 g dm^{-3} H_3BO_3

Table.I.1. Composition of Watts bath and sulphamate bath for Ni electrodeposition.

Typically, an acid electroplating bath will contain:

1) a high concentration of the metal ion
2) electrolyte or acid to enhance solution conductivity
3) acid/buffer to prevent hydrolysis of the metal ion
4) additives to modify the structure/properties of the deposit
5) additives to catalyse the reduction of M^{n+}

Since the sponsor already used the Watts bath, this was employed throughout the project.

Electroplated Ni from the Watts bath without additives in the plating solution has a dull appearance, but the appearance as well as mechanical and corrosion properties may by enhanced upon addition of additives and levelling agents. The most common are: saccharin,

pyridinium propyl sulfonate, or other aromatic compounds containing sulphur, for example, 1,3,6-naphthalene sulfonic acid (sodium salt). In the sulphamate bath, the concentration of Ni metal ions is slightly higher than in the Watts bath. Sulphamate ions decrease the stress of the deposit and therefore almost stress free Ni layer can be electroplated. This plating bath is preferred in some engineering applications [37], [38], [39].

Apart from the solution composition, the electroplating conditions like current density (charge density), plating temperature, solution pH and hydrodynamics determine the properties of the deposit [40], [41], [42].

Current density. The current density is well known to be a driving force for the deposition process. It determines the size of the grains and the thickness of the deposited layer can be controlled. It also determines the rate of the competing reaction, i.e., H_2 evolution. Rashidi at al. [43] investigated the effect of current density on grain size of the electrodeposited Ni. The Ni was electroplated from Watts bath with addition of 5 g dm^{-3} of saccharin. They found that at the current density ranged from -10 mA cm^{-2} to -75 mA cm^{-2}, the grain size decreased from 182 nm to 24 nm. Further increase in current density, i.e., from -75 mA cm^{-2} to -300 mA cm^{-2} had no significant effect on the grain size. Wu at al. [44] investigated the effect of current density on the quality of the Ni surface. At a relatively low current density, -142 mA cm^{-2}, small nodules of Ni were observed on the surface and the size of the nodules was 10 μm on a 20 μm scale. The size of the nodules increased significantly to approximately 40 - 50 μm at the current density of -314 mA cm^{-2}. In addition to the current density, the metal deposition can be influenced by the current distribution [45] and the electrical conductivity of the solution [46]. The influence of current density distribution can be investigated using a Hull cell. In this cell, the anode is tilted with respect to the cathode and therefore non-uniform current density distribution is achieved on the cathode panel. A primarily, secondary or tertiary current density distribution may be studied during the deposition in the Hull cell [47], [48], [49],

The throwing power can be improved by increasing the conductivity of the plating bath, increasing solution temperature and also decreasing the current density. On the other hand, electroplating of Ni with higher current density and with strong convection very often improves the quality of the deposit [50]. [51].

As mentioned in the previous chapter, the operating current is the sum of the current for Ni deposition and the hydrogen evolution. It is important to recognise that the hydrogen gas may be trapped inside the metal during the electroplating, causing reduction in ductility (hydrogen embrittlement), may escape from the metal surface leaving pores or voids in the coating or adsorbed on the metal surface.

Surfactants and Additives. The effect of additives or surfactants may enhance the mechanical properties of the Ni deposition, in particular intrinsic stress or strain of the deposit. The adhesion of the deposited metal to the substrate is improved by reducing the surface tension in the plating bath. The surface of the deposited metal may seem to be smoother upon addition of levelling agents. The appearance of the deposit may be bright, semi bright, or dull. It is well known that a small amount of saccharin added to the Ni plating bath improves brightness of the Ni deposit. The detailed role of surfactants and additives on electroplating of Ni may be found in [52], [53].

Impurities. Different types of impurities may influence the electroplating of Ni and usually the impurities have a negative impact on mechanical and corrosion properties. Those impurities may arise from the purity of chemicals, purity of added particles, corrosion of the substrate or plating bath and decomposition of additives. Solid particles and metallic impurities in the Ni plating bath (zinc, copper, lead, chromium, calcium and iron) are constantly filtered out and removed from the plating solution [38].

Ni composites. Metallic or non-metallic particles and fibers are added to the Watts bath in order to improve mechanical and corrosion properties of the coating. The size of the particles may vary from nanometers to micrometers. It is worthwhile to mention that some elements like phosphorus or boron present in the electrolyte of the plating bath to enhance the Ni properties. Spyrellis at al. [54] investigated Ni deposit electroplated from Watts bath with addition of 0.1 mol dm^{-3} NaH_2PO_2 in the solution. The amorphous structure of this alloy was obtained and after the heat treatment, the coating crystallised to Ni_3P and Ni_2P. In addition, nickel-phosphorous was intensely examined because of good wear and corrosion resistance. The effect of current density, solution pH, and the amount of phosphorus added to the Watts bath was studied in order to optimise the corrosion properties [55].

Ferkel at al. [56] investigated Ni-alumina composites with nanosized alumina particles (average alumina particles' size was 14 nm in diameter) and with different concentrations of particles in the

plating bath. They found that the nanoparticles largely suppress grain growth during the heat treatment at 850°C in argon atmosphere for 20 h. The hardness of the composite was significantly affected by the amount of particles added and the highest hardness, 118 ± 6 HV, was observed for 1.7 g dm^{-3} alumina powder in solution. The beneficial effect of particles in the coating may be seen in the work of Zhao at al. [57]. The Ni-graphite composites with different graphite content (diameter of the particles were < 4 μm) were prepared by electrodeposition. Friction and wear resistance were investigated. They found that upon increasing the graphite content from 0 to 26 % graphite in the Ni-graphite composite, the coefficient of friction decreased from 0.41 to 0.11 and wear loss, measured in mg cm^{-2} h^{-1}, also decreased from 9.64 x 10^{-3} to 1.47 x 10^{-3}, respectively. Wu at al. [58] performed similar study for the Ni-graphite composite with the size of graphite particles < 10 μm. In this investigation, the Ni-graphite composite comprised of 15 vol. % of graphite in the Ni-graphite composite revealed the best wear resistance properties. Moreover, the morphology of the Ni-graphite composites was studied and it was shown that at higher graphite concentration in the solution, the graphite agglomerations on the surface were observed although the distribution of particles was uniform (see fig.I.11).

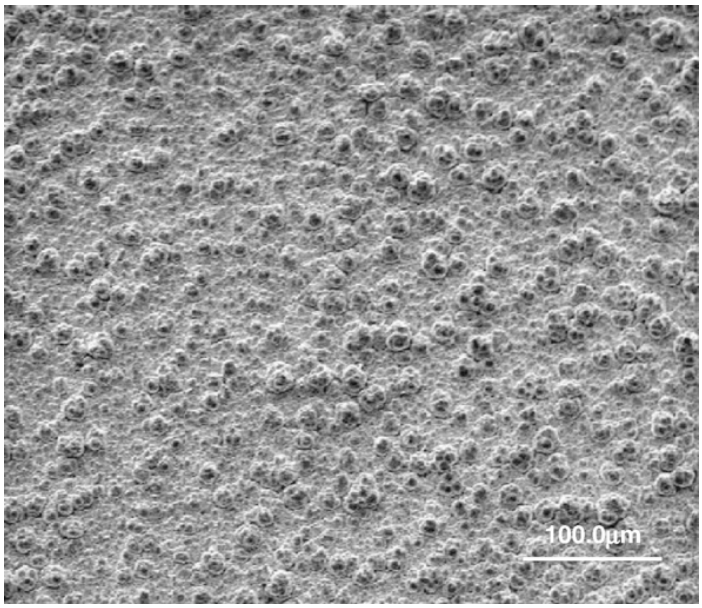

Fig.I.11. SEM picture of Ni-graphite composite with 10 g dm^{-3} graphite in solution (reference [58]).

The hardness of the coating may be significantly increased by embedding diamond particles into the Ni layer. Ogihara at al. [59] investigated a synthesis of super hard Ni-B/diamond alloy coating by eletrophoretic and electroless deposition. The hardness of the coatings was controlled by the content of incorporated particles. They found that the hardness for the Ni-B alloy was 558 HV whereas for the Ni-B/diamond, the hardness reached value of 1940 HV. This clearly indicated the significance of the diamond particles in the coating. The hardness of the coating was compared with the hardness of TiN coating deposited by dry sputtering or supersonic plasma spraying. The results were similar. Bean at al. [60] studied the influence of Ni-SiC composite coating. The SiC nanoparticles with average diameter 20 nm, were dispersed in the Watts bath. The electrochemical impedance spectroscopy was employed to investigate corrosion behaviour of the pure Ni coating and Ni-SiC composite coating. It was found that the charge transfer resistance was lower for Ni-SiC composite than for pure Ni coating, hence the composite coating had higher corrosion rate. The surface topology for the Ni-SiC composite was different than for pure Ni coating; smaller grain size was observed for Ni-SiC composites (see fig.I.12).

Vaezi at al. [61] performed similar study for Ni and Ni-SiC composite coatings, however, the size of the SiC particles was 50 nm. Both samples, Ni coating and Ni-SiC composite, had an active and passive region but the current density in the active region for Ni-SiC composite was lower than that for Ni. Moreover, Ni-SiC composite showed wider passive region and smaller passive current. This could be attributed to the fact that the SiC particles acted as an inert physical barrier against corrosion.

Aal at al. [62] investigated Ni-RuAl composite coating. The RuAl particles, with average particles' size 10 μm, were added to the Watts bath. A morphology of the Ni-RuAl composite showed protruding particles from the Ni coating (thickness of the Ni coating was 10 μm). The corrosion test measured by AC impedance in 3.5% NaCl solution at room temperature, revealed the smallest charge transfer resistance for pure Ni coating, 17 kΩ and the charge transfer resistance increased with amount of RuAl particles in the composite. This suggested that Ni-RuAl composites were better corrosion resistant materials than pure Ni coating. Ciubotariu at al. [63] investigated Ni-nano Al_2O_3 composites with alumina particles' size 13 nm. The corrosion of the composite was studied in two different solutions: 0.5 M sodium chloride and 0.5 M potassium sulphate.

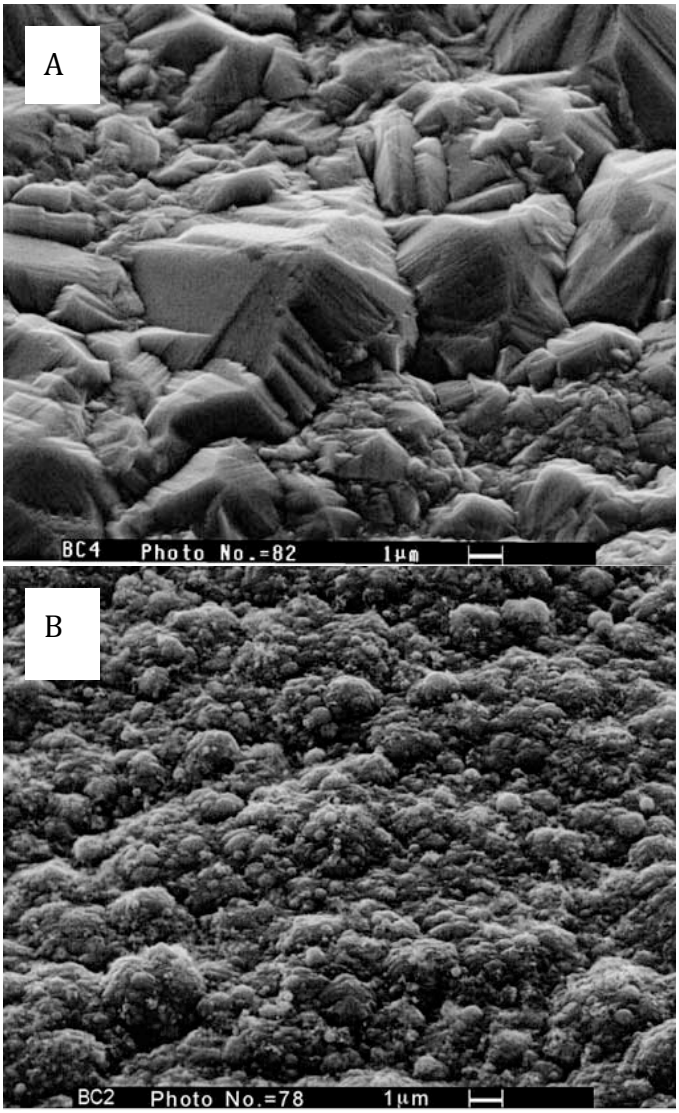

Fig.I.12. SEM pictures for A) Ni coating and B) Ni-SiC composite taken from reference [59]. The electroplating current density was -40 mA cm^{-2}.

The electrochemical impedance spectroscopy showed that polarization resistance were similar after the samples were immersed for 0.5 h in both solutions. After 30 h immersion, polarisation resistance was two times larger for the sample immersed in 0.5 M potassium sulphate solution than in 0.5 M sodium chloride solution. The corrosion current density for Ni coating in 0.5 M potassium sulphate decreased to 360 nA cm^{-2} and for Ni-alumina composite, the corrosion current was three times lower. The study of carbon nanotubes-Ni composite coatings conducted by Chen at al. [64] revealed significant improvement in corrosion resistance. A carbon steel, Ni

coated carbon steel and Ni-carbon nanotubes composite deposited onto carbon steel were immersed in 3.5 wt. % NaCl solution for 240 h. The Ni-carbon nanotubes composite coating gave three times better corrosion protection than Ni coated carbon steel. The open circuit potential measurement for the samples in the same solution gave the most positive corrosion potential for the Ni-carbon nanotubes composite coating.

Incorporation of particles into the Watts bath may also result in structure modification. Spanou at al. [65] studied the effect of TiO_2 nanoparticles with diameter 21 nm on structure of Ni-TiO_2 composite. Pure Ni coating was electrodeposited for comparison. In addition to preferred orientation for pure Ni coating, (211) and (110), a new plane (100) was observed for Ni-TiO_2 composite.

I.5.3. Chromium deposition

The first successful electrodeposition of chromium may be attributed to Geuther [66]. A detailed description of chromium electroplating was published in Gottingen in 1856.

The most common chromium bath was based on hexavalent chromium ions in solution with sulphate and organic acids as catalysts. A thick chromium layer (in the range of 10 – 20 μm) can be deposited from hexavalent chromium plating bath and practical problems and solutions of the electroplating may be found in [67], [68], [69], [70]. The current efficiency during the electroplating is very low and ranged from 10 % to 25 % and almost constant temperature must be maintained during the plating process. This current efficiency is much lower than the efficiency for Ni plating and hence deposition of Cr is mainly carried out at very high current densities, -100 mA cm^{-2} to -400 mA cm^{-2}. Therefore, “burning” of the deposit at these current densities may be possible and poor throwing power make the electroplating rather difficult to control. Moreover, chromic acid is highly toxic as well as a strong oxidizing agent and therefore a potential fire hazard.

Trivalent chromium electroplating bath have started to replace traditional hexavalent chromium bath and this was largely due to the health and safety regulations [38]. A novel Cr electroplating can be seen in the work of Smart at al. [71]. The chromium bath was prepared from a mixture of chromium(III) sulphate and sodium sulphate (named “Chrometan”, where the concentration of

chromium(III) was 5 - 6 g dm^{-3}), organic additives - thiourea, saccharin or sodium 2-ethyl hexylsulphate, potassium sulphate, and boric acid.

The thiourea is a vital component in the plating bath. This organic additive makes the Cr deposition possible. The thiourea can be compared to complexing agents that promote reduction of the chromium(III) ions during the deposition [72], [73]. The chemistry of the chromium(III) complex can be found in [74], [75], [76]. Some other sulphur based organic compounds have been reported to improve the quality of the Cr(III) deposit [77], [78]. The electroplating of Cr(III) from salt solutions can be found in [79], [80].

Potassium sulphate or other alkaline metal salts are added to the Cr plating bath to increase the conductivity of the bath. Weak buffer, boric acid maintains the pH at the constant level 3.5. The electrodeposition of chromium from Cr(III) was studied with the Hull cell and the experiment revealed the range of possible current densities [81]. The optimum current densities were in the range of -40 mA cm^{-2} to -110 mA cm^{-2}. In addition, the deposition rate at -70 mA cm^{-2} was estimated to be 0.1 μm min^{-1}. As a consequence of a relatively low current density, there was no "burning" of the deposit and the properties of the electroplated Cr were comparable to that obtained from the hexavalent chromium solution. It was also emphasised that no greater health and safety procedures must be applied than those for the nickel electroplating. This was clearly a large achievement in the chromium electroplating.

Like electroplating of other metals, a decorative and functional classification can be distinguished. The thickness of a decorative deposit is usually less than 0.80 μm and that is sufficient to offer reflective appearance and also corrosion resistant layer. Exceeding this thickness, hard chromium is deposited largely for industrial applications, where the coating properties might be: resistance to heat, wear and corrosion or low coefficient of friction.

I.5.4. Alloy deposition

As mentioned in chapter 1.5.2, a deposition of Ni with particles added to the plating bath, indeed, may have a positive impact on mechanical or corrosion properties. On the other hand, alloying

metals may offer a new structure that may give benefits in mechanical or corrosion properties to a larger extent [82], [83].

Eletrodeposition of alloys are governed by the same electrochemical principles as the single metal deposition. However, difficulties in the alloy plating may arise due to a difference in equilibrium potential for the metal/metal ion couple in the solution. If, for instance, Cu-Zn alloy is electroplated, the rate of Cu deposition will be clearly higher that the rate of Zn deposition. The standard equilibrium potential measured for those metal/metal ions couples are different: for Cu^{2+}/Cu, E_e^0 = +0.34 V vs. SHE and for Zn, E_e^0 = -0.76 V vs. SHE. Hence, at any applied potential, the overpotential for Cu deposition will always be much higher than for Zn deposition. It should therefore be difficult to plate the alloy containing Zn. In practice, however, this is not always the case and other electroplating parameters must be considered: solution complexing agents, pH, solution temperature and composition, surfactants and additives [84], [85], [86].

Particular examples of alloy deposition are Ni-Fe alloy [87] and Ni-Zn alloy [88], [89]. Deposition of those alloys is considered to be an anomalous deposition. This may be attributed to: a) a difference in the equilibrium potential for metal/metal ion couples in the solution and the kinetics of the metal ion complexes, b) a reduction of thermodynamically less noble metal ions. In addition, the influence of one metal ions present in the solution may suppress or enhance deposition of the other metal ions. As a consequence of that, different content of metals in the alloy may be deposited comparing to the ratio of metal ions added to the solution. Further explanation of this mechanism can be found in [90], [91].

Alloying nickel with other elements, for instance iron or cobalt, a high performance of soft and hard magnetic materials can be achieved. In the work of Myung at al. [92], Ni-Co, Ni-Fe and Ni-Co-Fe alloys were studied. All alloys showed magnetic saturation but upon addition of Fe up to 50% to Co-Ni thin film, the magnetic saturation increased. The corrosion resistance was dependent on film composition, crystal structure, grain size and impurity content. All those properties can be controlled by current density, solution pH, and solution temperature. In addition, the corrosion rate decreased substantially with Ni content up to a critical value of 34%. Exceeding this value, the corrosion rate for alloy was approximately similar to pure Ni. Electrical resistivity of the Ni-Fe alloy decreased with increasing Ni content from 40% to 100 %.

The number of electrodeposited Ni alloys is growing and interesting properties of those alloys are still not fully difined. Suffice to say that in the *Journal of Electrochemical Society*, about 200 publications were recorded between 2001 and 2006 for alloy depositions [38].

One particular metal alloyed with Ni, gives remarkable corrosion properties. Bojinov at al. [93] reports the study of high purity Ni-Cr alloys. Three alloys were investigated: 10% Cr, 15% Cr and 20 % Cr in Ni-Cr alloy. Cyclic voltammetry and AC impedance measurement were conducted in 0.1 M sodium borate solution at pH 9.3. The behaviour of pure Ni and pure Cr was compared with the alloys. They found a wide potential region corresponding to passive region for all the Ni-Cr alloys upon scanning the surface. The maximum resistance for different Ni-Cr alloys was higher with higher Cr content. It was also found that the Ni - 20% Cr alloy behaved almost like pure Cr. Similarly, the study of transpassive behaviour of commercial Ni - 10% Cr and Ni – 20% Cr can be seen in the work of Bojinov and Saario at al. [94]. Sodium sulphate solution with pH 0 – 5 was used to study a transpassive region of Ni-Cr alloys. The behaviour of all Ni-Cr alloys was similar to pure Cr metal.

In addition to the mechanical and corrosion properties, the electrical contact resistance for alloys was studied. Aql [95] investigated the electrical resistivity for Ni-Cr alloy upon heating in different temperatures. At 663 K, a rapid increase in electrical resistivity was observed and this was explained due to changes in phases in the alloy. Kotobnko at al. [96] measured the electrical resistance for industrial Ni and Cu-based alloys. The resistivity of the conventional Ni-Cr alloy with 20% Cr was compared. It was found that resistivity for Ni-based alloys were different in liquid state, near the melting point than in the solid state. For Ni - 20% Cr alloy, the resistivity was 110.8 μΩ cm, whereas for pure Ni, the resistivity was 59 μΩ cm. Togasaki at al. [97] studiedcontact resistance for electroplated Ni-Au alloy. The data were compared to hard Co-Au alloy. The contact resistance was measured for the alloys with thickness 0.2 μm. It was found that contact resistance for Ni-Au alloy was 2.21 mΩ and for hard Co-Au alloy, 2.16 mΩ.

Although the commercial Ni-Cr alloy was thoroughly characterised and corrosion study revealed the optimum composition at 20 % Cr in the Ni-Cr alloy, very little work has been performed on electroplating of Ni – 20% Cr alloy. One of the method of the Ni - 20% Cr alloy preparation is to electroplate 16 μm Ni layer followed by 9 μm Cr layer on top and then applying heat treatment at 1273 K for 4 to 5 h [39]. This procedure, however is lengthy and certainly, costly. An attempt to

electroplate the Ni-Cr alloy from solution containing Cr and Ni ions was performed with little success. Huang at al. [98] studied Cr rich - Ni alloy deposition from $CrCl_3$ and $NiCl_2$ solution using SEM and EDX analysis (including cross section area). The electroplating of the alloy was carried out applying pulse current for 1 minute and each current density pulse varied from -100 mA cm^{-2} to -300 mA cm^{-2} for 2 – 6 s. In the work of Lin at al. [99] a Cr-Ni electroplated alloy from trivalent chromium chloride and divalent nickel chloride solution was presented. The current density was in the range of -100 mA cm^{-2} to -400 mA cm^{-2}. The surface of the deposited alloy was polarized in a narrow potential range with scan rate 5 mV s^{-1} in 0.5 M sulphuric acid. The surface topology was investigated with SEM and EDX analysis and X-ray diffraction analysis was performed for 2θ angle between 20^o and 80^o. In all cases, [98] and [99], the deposits were highly cracked and the cracks were leading to the substrate. The corrosion test conducted in the latter reference, gave poor results. Moreover, the emphasis was rather put on Cr rich - Ni alloy than on Ni - 20% Cr.

Further work is needed to investigate electrodeposition of Ni – 20% Cr alloy. This will clearly reduce the costs of the alloy. Moreover, the electrodeposition of Ni-Cr alloy from trivalent chromium and divalent nickel bath seems to satisfy health and safety regulations.

I.6. Combinatorial method - Physical vapour deposition

Physical vapour deposition (PVD) is frequently employed techniques for the deposition of metals and alloys. Vacuum technology can allow deposition of several multilayers of single metals or alloys, uniformly and with high reproducibility and also high purity of the deposited metals. Moreover, the deposition process can be controlled by adjusting the temperature of the metal, residual gas pressure in the chamber and in the case of alloys, its composition. The principles of the PVD can be found in [100].

A combinatorial approach to the deposition of several metals will be briefly discussed. As a substrate for alloy deposition, a silicon or silicon nitride wafer cut into squares with 3.1 cm x 3.1 cm was used. On top of the silicon substrate, a 10 x 10 gold array was deposited and individual electrical contact was provided to each gold electrode. This arrangement allowed simultaneous investigation of 100 deposits and therefore this method became very convenient approach to

study a broad range of composition. The application of this method can be seen in the work of Guerin at al. [101]. The effect of particles' size on supported electrocatalysts was investigated. A uniform titanium oxide layer was first deposited onto 10 x 10 array and then gold with a fixed "wedge' shutter was deposited on top. As a result, variation of Au across 100 electrodes was obtained and catalytic activity of the oxygen reduction was studied.

Guerin and Hayden at [102] studied wide range of composition in ternary alloys. The following elements were used: Pd, Pt, Ru, Au, Sb, Ge and Te. Again, the same substrate, 10 x 10 gold array, was employed to investigate electrochemical properties of the alloys across the 100 electrodes.

Some applications of combinatorial approach for investigation of electrochemical properties can also be found in [103] or [104].

Indeed, this could be a powerful and very convenient method to investigate the alloy properties. The combinatorial method of metal deposition will be employed in this thesis to study the composition and electrochemical properties for Ni-Cr alloy with Cr range from 0% to 100%.

II. Experimental

II.1. Chemicals and solutions

CHEMICAL NAME	CHEMICAL FORMULA	SUPPLIER/GRADE
Acetone	CH_3COCH_3	Charles Tennant Distribution/n'Grade
Boric acid	H_3BO_3	Alfa Aesar/purity 98%
Deionised water	H_2O	WhatMan International Ltd, UK, Analyst 25/ 1MΩ cm
Hexadecyltrimethyl-ammonium hydroxide	$CH_3(CH_2)_{15}N(OH)(CH_3)_3$	Sigma Aldrich/purity 99%
Hydorchloric acid	HCl	Fisher Scientific/analytical grade
Nickel(II) chloride hexahydrate	$NiCl_2.6H_2O$	Alfa Aesar/purity 98%
Nickel(II) sulphate heptahydrate	$NiSO_4.7H_2O$	Acros Organic/purity 98%, for electrodeposition
Nickel(II) sulphate hexahydrate	$NiSO_4.6H_2O$	Alfa Aesar/purity 98%
Potassum chloride	KCl	Fisher Scientific/ analytical reagent grade
Sodium sulphate anhydrous	Na_2SO_4	Fisher Scientific/analytical grade
Sulphuric acid	H_2SO_4	Fisher Scientific/analytical grade

CHEMICAL NAME	*CHEMICAL FORMULA*	*SUPPLIER/GRADE*
Alkaline cleaner for industrial applications: P3Percy 702	-	Henkel, Germany
Alkaline soap	-	Multipurpose detergent – Teepol
Aluminum oxide	Al_2O_3, grade 0.05 μm	Buhler/powder 99%
Chromium (III) sulphate	$Cr_2(SO_4)_3.15H_2O$	BDH
DispersionMittel 01926	-	Dr Hesse, Germany
Dodecylsulphate sodium salt	$CH_3(CH_2)_{11}OSO_3Na$	Fisher Scientific/ electrophoresis grade 98%
Mercury	Hg	Aldrich/99.99%
Mercury sulphate	$HgSO_4$	Aldrich/99%
Mercury(I) chloride	Hg_2Cl_2	Aldrich/99.5+%
Paraffin liquid	-	Fisher Scientific
Potassium sulphate	K_2SO_4	Timstar Laboratory Supplier LTD
Saccharin	$C_7H_5NO_2S$	Aldrich
Sodium fluoride	NaF	AnalaR/analytical grade
Sodium hydroxide, pellets	NaOH	Fisher Scientific/analytical grade
Thiourea	CH_4N_2S	Timstar Laboratory Supplier LTD

CHEMICAL NAME	CHEMICAL FORMULA	SUPPLIER/GRADE
Argon gas	Ar_2	BOC Gases/99%
Argon/5% Hydrogen mixture	$Ar/5\%H_2$	BOC Gases/99.99%
Nitrogen gas	N_2	BOC Gases/99%
Oxygen gas	O_2	BOS Gases/99%

Table II.1. Lists of chemicals and gases

SOLUTION	COMPOSITION
1. Watts bath	• 267 g dm^{-3} $Ni_2SO_4.6H_2O$ • 50 g dm^{-3} $NiCl_2.6H_2O$ • 35 g dm^{-3} H_3BO_3 • pH 3-3.5
2. Ni-graphite solution	• Watts bath, pH 3 – 3.5 • 1 – 10 g dm^{-3} of graphite particles • 10 mg DispersionMittel 01926 per gram particles, or • 1 mg DispersionMittel 01926 per gram particles
3. Woods strike	• 100 ml dm^{-3} HCl (concentrated) • 240 g dm^{-3} $NiCl_2.6H_2O$
4.Electrodegreasing solution	• 30 ml dm^{-3} P3 Percy 702 • 60 ml dm^{-3} 45% NaOH
5. Cleaning solution	• 25 g dm^{-3} alkaline soap (Teepol) • 40 g dm^{-3} NaOH
6. Sodium hydroxide solution	• 1 M NaOH,
7. Solution for corrosion test	• 1 M Na_2SO_4 • 2 ppm NaF • pH 4, adjusted by adding few drops of 50:50 H_2SO_4:H_2O

Table II.2. Solutions that have been used during the course of the project

II.2. Materials

2.1. Pure metals - Iron, chromium and nickel

Three metals, Fe foil with thickness 0.5 mm, Cr foil with thickness 0.5 mm and Ni foil with thickness 0.125 mm, were supplied from GoodFellow Metals (purity 99%). The Fe foil was thoroughly washed with acetone, then rinsed with deionised water and dried with warm air.

Cr foil was wet polished with silicon carbide paper in grade 600, followed by 1200 and then wet polished with alumina powder in grade 0.05 μm (Buhler) using a polishing cloth (Buhler) for 5 minutes. Finally, the sample was rinsed with plenty of deionised water and dried with warm air.

Ni foil was thoroughly washed with acetone, rinsed with deionised water, and dried with warm air.

Cleaned and prepared samples were stored in a dessicator to avoid moisture from the air.

2.2. Cold rolled carbon steel

Cold rolled carbon steel with grade DC04 LC supplied from Hille & Muller GmbH & Co, Special Corus Strip, Dusseldorf, Germany arrived in the form of A4 sheets with thickness 0.4 mm. The surface of the carbon steel was already polished to a mirror finish and according to the data sheet from CORUS, the surface roughness was 0.5 μm.

The composition of the carbon steel in a weight percentage is shown in table II.3. The steel contains C and Mn, with some P and S.

Grade	C wt%	Mn wt%	P wt %	S wt%
DC04 LC	0.08	0.4	0.03	0.03

Table.II.3. Chemical composition of DC04 LC carbon steel supplied from CORUS [105].

Each sheet of the carbon steel was individually wrapped and the surface of the steel was covered with protective lubricant that preserved the steel from corrosion. This required special pre-treatment to remove the grease or fingerprints etc, before the sample was tested. The sample was cut into small pieces; usually 2 cm x 5 cm and working area was depended upon the cell used (see chapter II.3 *Electrochemical cells*). Different methods of cleaning the substrate are listed in table II.4.

It follows from the table that *pre-treatment A* was the simplest one in terms of preparation time. Applying this pre-treatment, it is unlikely to damage the surface either mechanically or chemically. *Pre-treatment B* consists of five steps and required much more time for degreasing the sample than *pre-treatment A*. The last pre-treatment, *pre-treatment C*, was suggested by CORUS, Dusseldorf, Germany and one of the ingredients for electrodegreasing solution – P3Percy 702 - was supplied from this company (for detailed composition see section II.1 Chemicals and solutions).

The electrodegreasing cell, consisting of two Ni coated carbon steel anodes immersed in the solution, situated parallel to each other and the steel cathode was placed between the anodes.

	DC04 LC
Pre-treatment A	1) Rinsing with deionised water, 2) Thorough rinsing with acetone, 3) Rinsing with deionised water again and 4) Dried with warm air
Pre-treatment B	1) Immersing the steel for 2 – 5 h in an aqueous solution consisting of an alkaline soap (multi-purpose detergent from Teepol), 2) Rinsing with deionised water, 3) 5 – 10 minutes dipping in two concentrations of HCl (1:5, $HCl:H_2O$ and 2:5 $HCl:H_2O$), 4) Rinsing in deionised water and 5) Dried with warm air
Pre-treatment C	1) Electrodegreasing in alkaline solution pH 11 by applying a cathodic current density -5 to -80 mA cm^{-2} for t = 15 – 60 s, 2) Rinsing with deionised water and 3) Dried with warm air

Table.II.4. Pre-treatments applied for DC04 LC.

Cathodic current density in the range of -5 to -80 mA cm^{-2} was used for a short period of time 15 – 60 seconds depending upon the degree of greasiness. After the electrodegreasing, the sample was thoroughly rinsed with deionised water to remove the residue of the solution and dried with warm air. If, however, after the drying of the sample, some water marks on the surface were observed, the two last steps of the pre-treatment from the table II.4 were repeated.

2.2. Stainless steel 904L

Austenitic stainless steel (SS) with grade 904L was also supplied by Hille & Muller GmbH & Co, Special Corus Strip, Dusseldorf, Germany in form of the sheets with dimensions 30 mm x 1000 mm and with thickness 0.10 mm. The composition of the steel is presented in table II.5. Significant amounts of Cr and Ni are added to the steel. During the manufacturing of stainless steel, it is important to have a right ratio of C to Cr. C to Cr ratio is needed to retain austenite phase. The addition of Ni stabilises this phase.

Grade	***C wt%***	***Mn wt%***	***Si wt%***	***P wt%***	***S wt%***	***Cr wt%***	***Mo wt%***	***Ni wt%***	***Cu wt%***
904L SS	0.02	2	1	0.045	0.035	19-23	5	23-28	2

Table.II.5. Chemical composition of 904L SS – source: Atlas Steel Australia.

Cr to a large extent and to a less extent Ni, contribute to the corrosion resistance of the alloys in a wide range of environments, in particular, acidic and chloride environments.

Analogous to carbon steel, 904L SS was cut onto small pieces with similar dimensions as the carbon steel and was exposed to several pre-treatments. All the pre-treatments used for 904L SS are listed in table II.6.

Pre-treatments 1 and *3* for 904L SS were exactly the same as for the carbon steel. The intention of those pre-treatments was to compare behaviours of the samples in the same acidic environment that mimics the conditions in proton exchange membrane fuel cell.

Pre-treatment 4 was suggested by CORUS in order to successfully electroplate Ni onto 904L SS.

Woods strike, mentioned in the table, was defined in chapter II.1 and plays a key role before electrodeposition of thick layers of Ni onto stainless steel.

	904L SS
Pre-treatment 1	1) Rinsing with deionised water, 2) Thorough rinsing with acetone, 3) Rinsing with deionised water again
Pre-treatment 2	1) Rinsing with deionised water, 2) Dipping in 10 % HCl solution, for 4 minutes 3) Rinsing with deionised water and
Pre-treatment 3	1) Electrodegreasing in alkaline solution pH 11 by applying a cathodic current density -5 - -80 mA cm^{-2} for t = 15 – 60 s, 2) Rinsing with deionised water and
Pre-treatment 4	1) Dipping in 50:50 H_2SO_4 acid solution for 10 seconds, 2) Rinsing with deionised water, 3) Electrodegreasing in alkaline solution pH 11 by applying an anodic current density +15 mA cm^{-2} for t = 60 s, 4) Rinsing with deionised water and, 5) *Woods strike: current density -100 mA cm^{-2} for 30 seconds

* Woods strike was used only before electroplating of Ni

Table.II.6. Pre-treatments applied for 904L SS. After each step of pre-treating, the sample was rinsed with deionised water.

2.3. Ni coated carbon steel supplied from CORUS

Ni coated carbon steel substrate, produced on the commercial, continuous plating line, arrived in the form of A4 sheets. The thickness of the coating was estimated to be 3 μm and Ni was electroplated on both sides of the carbon steel. The surface finish was bright Ni with surface roughness 0.5 μm. The sample was cut into pieces with area 10 – 60 cm^2, and the surface of the sample was cleaned using two following pre-treatments:

1. Thorough wash with acetone, then rinse with deionised water and dry with warm air,
2. Electrodegreasing in electrodegreasing solution (please refer to the section II.1. Chemicals and Solutions), applying cathodic current density in the range of -5 to -30 mA cm^{-2} for 5 - 10 seconds, depending upon the amount of grease on the surface then rinsing with deionised water and drying with warm air.

2.4. Ni coated steels prepared in Southampton laboratory

Ni was electrodeposited onto carbon steel with grade DC04 LC and the stainless steel 904L SS from Watts bath, pH 3 – 3.5. The solution temperature was in the range of 323 – 333 K. The pre-treatments used for carbon steel and 904L SS before electrodeposition were described in table II.4 and II.6.

Two electroplating cells, a parallel plate beaker cell and a rectangular flow cell, described in the following sections, were employed for Ni deposition. Ni anode plate and carbon steel or 904L SS cathodes were used for deposition of nickel. Cathodic current density in the range of -10 to -200 mA cm^{-2} was applied from regulated power supplies described in section *II.3.Equipment*.

All the power supplies were used interchangeably depending upon the current density and working area used for electroplating. Once the Ni was electrodeposited, the sample was wet polished to a mirror finish using polishing cloth (Buhler) with alumina powder (Buhler) in grade 0.05 μm for 2 - 3 minutes, then rinsed with deionised water and dried with warm air. Prepared samples were stored in a desiccator in order to avoid moisture from the air.

2.5. Ni-graphite composites

Two types of graphite particles from NGC Naturgraphit GmbH, Germany were employed for Ni-graphite deposition. SEM pictures for flake graphite with grade MF2/99.5-99.9 in 2 μm in diameter and flake graphite in grade MF5/99.5-99 in 5 μm in diameter are shown in fig.II.1.

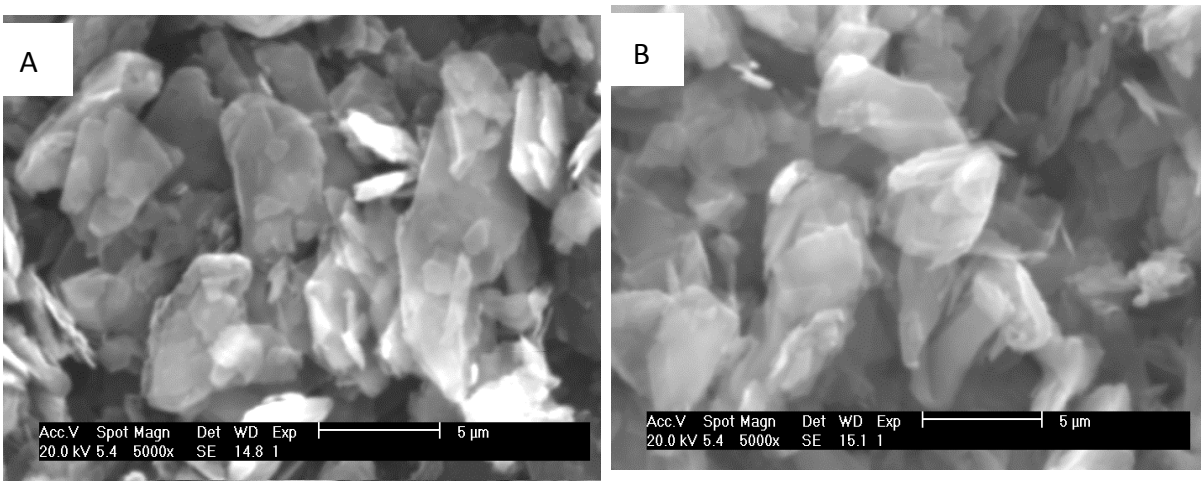

Fig.II.1. SEM pictures of two types of graphite used for Ni-graphite composites a) MF5/99.5-99, 5 μm in diameter and b) MF2/99.5-99, 2 μm in diameter

It can be seen that the graphite flakes with 2 μm in diameter (fig.II.1b) were slightly smaller than the graphite flakes with 5 μm in diameter (fig.II.1a), although the difference is smaller than expected.

Anionic surfactant, DispersionMittel 01926 supplied from Dr. Hesse, Germany was used for electrodeposition of Ni-graphite composites from Ni-graphite solution (see section II.1 Chemicals and solutions). In addition to that, the influences of other surfactants like cationic surfactant hexadecyltrimethyl-ammomium hydroxide (Sigma Aldrich) and dodecylsulphate sodium salt (Fisher Scientific) on Ni-graphite composites were investigated.

Watts bath, pH 3 – 3.5 was heated to 333 K and the appropriate ratio of graphite particles with surfactant was added to the bath: 1 mg DispersionMittel 01926 per 1 g particles or 10 mg DispersionMittel 01926 per 1 gram particles. The solution was stirred using magnetic bar stirrer for about 1 h until a uniform distribution of graphite was achieved.

Once the solution was prepared, two electroplating cells described in section II.4.5 and II.4.6 were used for Ni-graphite composites preparation. The Ni coated carbon steel and Ni coated 904L SS were employed as cathodes. Cathodic current density in the range of -10 to -100 mA cm^{-2} was applied from a regulated power supplies (see section II.3.*Equipment*). Prepared Ni-graphite composites were dried with warm air and stored in a desiccator, in order to avoid moisture from the air.

2.6. Cr onto Ni coated carbon steel

Chromium with thickness 20 nm (Agar Scientific, high purity chromium) was evaporated onto Ni coated carbon steel using Edwards Surface Coating E306A. The chamber was vacuum pumped and the deposition was carried out under the maximum pressure of 10 mBars. The substrate preparation for Cr deposition is described in section II.2.4. Prepared samples were stored in a desiccator to avoid moisture from the air.

II.3. Equipment

3.1. Measurement of pH

The pH for all solutions was measured using microprocessor pH meter 210 from Hanna Instruments. The pH meter was calibrated with acidic buffer with pH 3.5.

3.2. Electrochemical instrumentation

PAR Potentiostat/Galvanostat PG&G model 263A and Electrochemical Power Suit software was used to record voltammetry and monitor current and/or potential with respect to time.

PCI-DAS6402/16 data acquisition card (Talisman Electronic) and Pentium 4 (2.2 GHz) desktop computer operating under Windows XP operating system was used to acquire and control electrochemistry on the arrays. Data was analysed and presented using software specifically designed for the laboratory purposes to control and monitor electrochemical responses. More detailed description of the software can be found in [106].

Regulated power supplies: Farnell AP 60 - 150 with maximum current 60 A and voltage 150 V, PLPowerLine LAB 505 with maximum current 5 A and voltage 30 V and ISO-Tech IPS 2303D with maximum current range 3 A were employed interchangeably to apply constant current to the electroplating cells.

3.3. SEM and EDX

Two scanning electron microscopes were used to characterize the surface of the samples: Phillips SEM model XL-30 ESEM coupled with EDX Digital Control SW, model XL from EDAX, UK and JSM-5910, JEOL coupled with EDX analysis from Oxford, Inca 300. The latter was used to run the macro for 100 electrodes in electrochemical arrays.

3.3. X-Ray diffraction equipment

X-Ray powder diffractometer Bruker C2 with Cu Kα radiation with a wavelength 1.5405 Å was used to characterise the structure of metals.

3.4. Atomic force microscopy (AFM)

A ThermoMicroscope Autoprobe M5 from Veeco in tapping mode with a silicon cantilever with a resonance frequency ~365 kHz, and spring constant of 20 - 80 N m^{-1} was employed for thickness measurement of deposits on electrochemical arrays.

3.5. Contact resistance measurement

Two different methods were used for contact resistance measurement:

1. One set-up is shown in fig.II.2. The sample with area 25 cm^2 was inserted between two thick copper plates with Au contact plates and the force measured in Newton's was applied to the one of the copper plates, to compress the sample. A constant current of 1 A was applied from power supply ISO-Tech IPS 2303D and the voltage across the sample was measured with digital voltmeter. The resistance was measured as a function of compressive force.

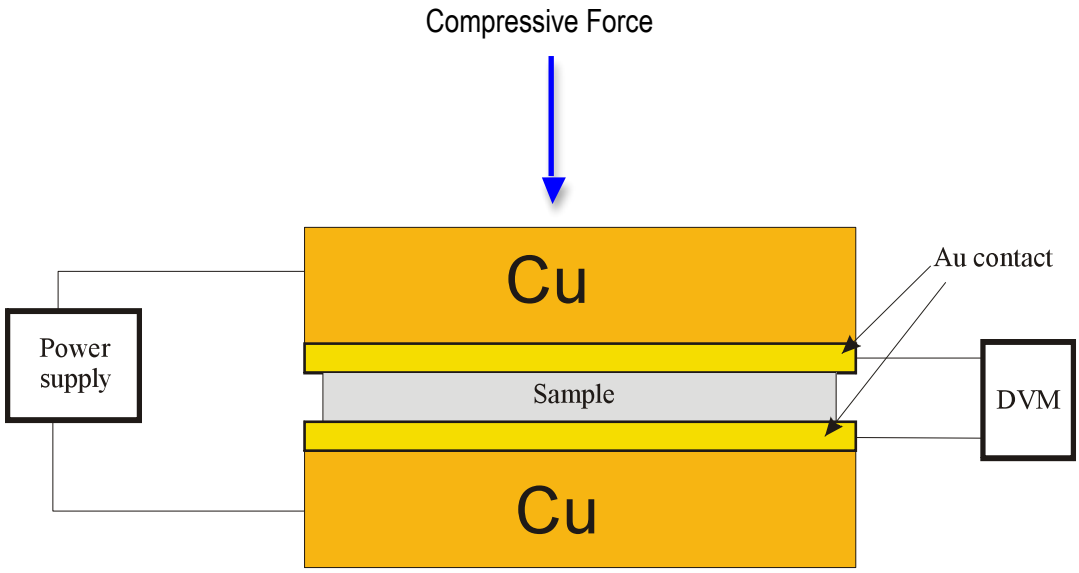

Fig.II.2. Equipment for contact resistance measurement – sample area was 25 cm^2.

2. The other equipment for contact resistance measurement was used in Amsterdam Research and Development Laboratory in CORUS, Netherlands (fig.II.3). The method of the measurement was similar as previously described but the force applied to the sample was better controlled and varied with a wide range of pressure (from 2 to 40 bars) resembling that used in proton exchange membrane fuel cells.

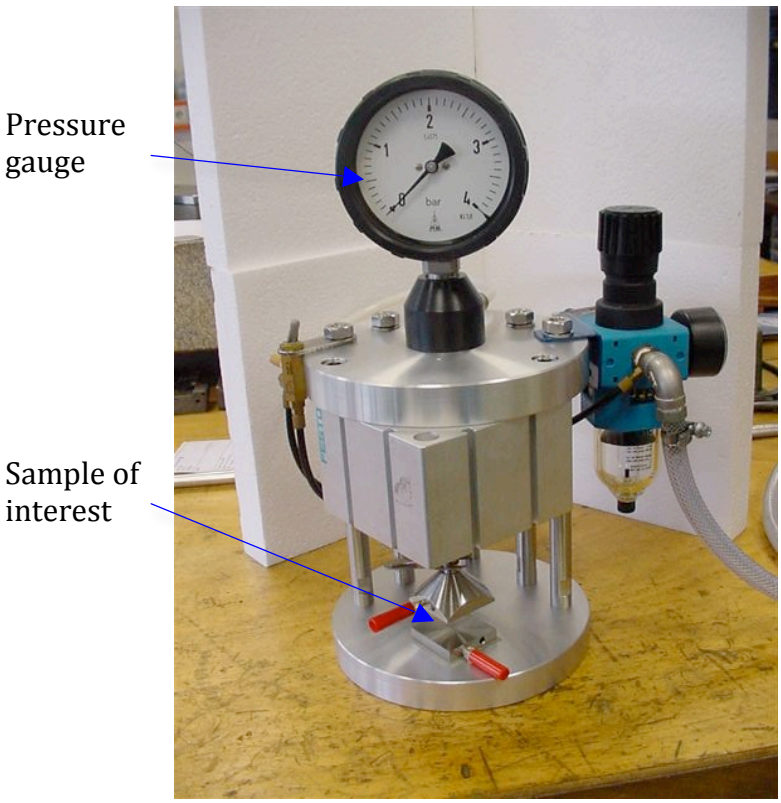

Fig.II.3. Equipment for contact resistance measurement – sample area was 16 cm².

3.6. Equipment for heat treatment

Heat treatment of all samples was performed in a tube furnace supplied by Lenton, UK with a Eurotherm temperature controller. Before the heat treatment, the sample was cleaned with deionised water and dried, then placed in a glass tube with internal diameter 2 cm (fig.II.4). The sample was inserted into the glass tube and the glass tube was pushed into the glass head. A paraffin liquid (Fisher Scientific) was used as a lubricant to decrease the friction between the glass tube and the head. N_2 and Ar/5%H_2 (BOC, purity 99.99%) were employed in order to perfome heat treatment in reducing atmosphere. One of thoses gases was connected to the one end of the glass head and the other end was left opened. This opened end gives a possibility to replace the air with inert gas. The procedures of the sample heating are described in section II.6.

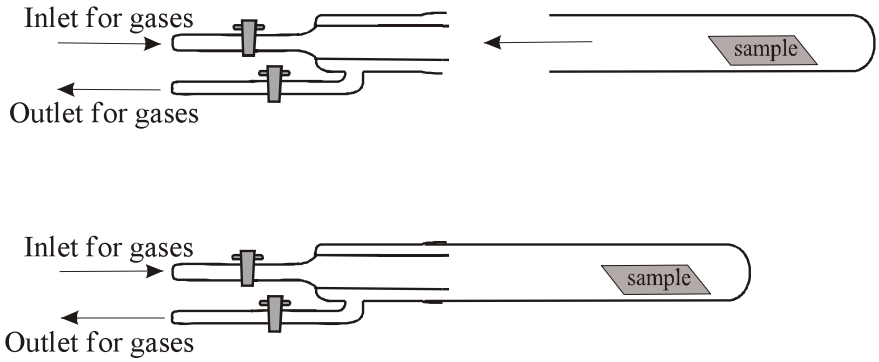

Fig.II.4. Glass tube for heating the samples.

II.4. Electrochemical Cells

For voltammetry and constant potential experiments, small, three-electrode cells were used.

4.1. Reference and counter electrodes

A Pt mesh with area 1 cm^2 was used as a counter electrode. Two references electrodes: saturated calomel electrode (SCE) and Hg/Hg_2SO_4 electrode were assembled and used. The electrodes were prepared in the following way. A SCE is used for the description.

- A paste consisting of 3 g of Hg_2Cl_2 + 4 drops of Hg was mixed together for 30 - 60 minutes,
- A saturated KCl solution was prepared
- One drop of Hg + paste + glass wool soaked in KCl (saturated) was layered together in a first compartment of the electrode as shown in fig.II.5. Each layer was evenly distributed

in the glass tube and the next layer was slightly “thicker” than the previous one. The whole structure was gently pressed using a wooden stick and the remainder of the glass was filled with KCl solution. Second compartment of the electrode was completely filled with KCl in such a way that the solution formed a convex surface. This procedure prevents formation of air bubble in the glass electrode whilst combining those two compartments together. The next step was to merge both glass compartments and screw them together. If the air bubble was noticed whilst the electrode was assembled, the procedure of refilling with electrolyte and combining the two glass compartments was repeated.

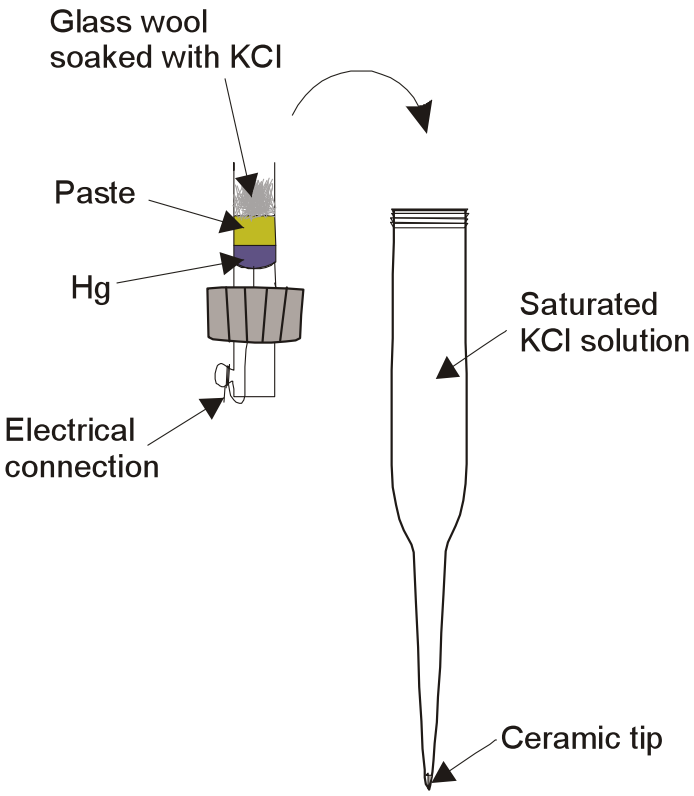

Fig.II.5. Reference electrode assembly

A number of corrosion tests were performed in different cells that are presented below:

4.2. Cells with working area above 1 cm^{-2}

The cell made of Perspex, with working area 7 cm^2 is shown in fig.II.6. The cell consists of cylindrical tube with a flange at the end. The steel sample was placed between the flange and the base of the cell and tightened up with four screws at the corners. In order to prevent solution leakage, Viton™ rubber gasket from Altec Products Limited, UK, with thickness 1.6 mm was cut out according to the diameter of the working area and placed between the working electrode and the flange. The saturated calomel electrode (SCE) as a reference electrode and Pt mesh counter electrode were inserted from the top of the cell.

The N_2 and O_2 gases (BOC Gasses) were used to saturate the solution before experiment was started. The experiment was performed at room temperature.

.

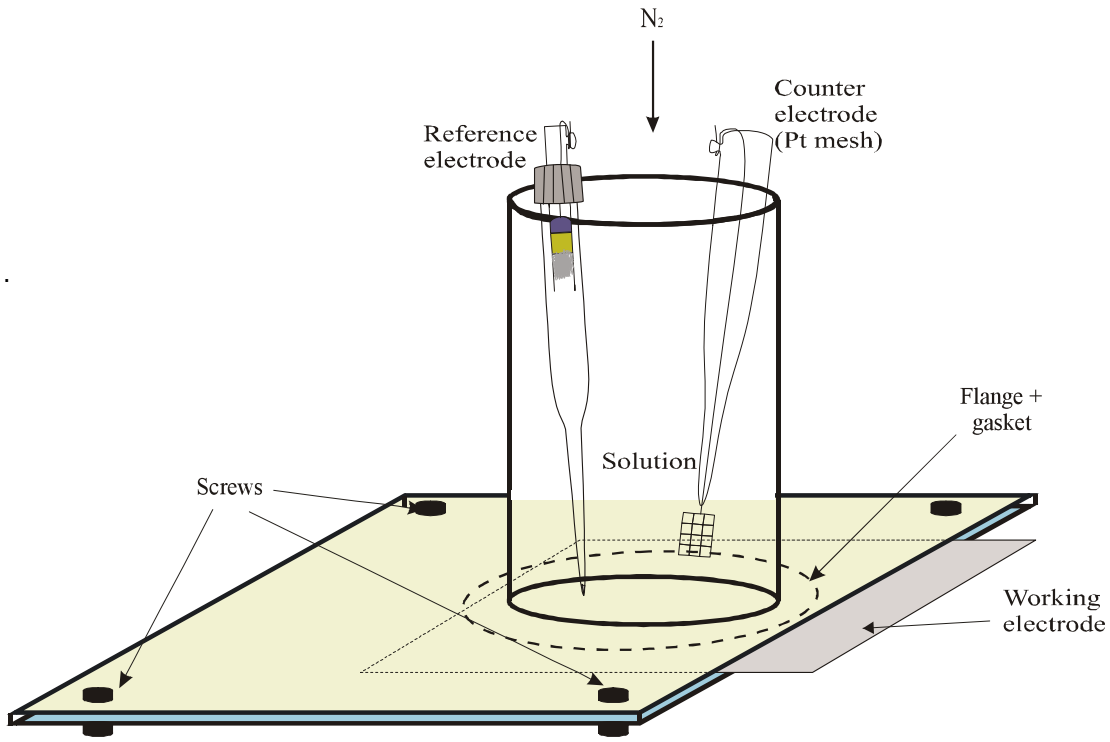

Fig.II.6. The cell with working area 7 cm^2 used for corrosion tests.

4.3. Cells with working area below 1 cm^{-2}

Cell 1. A three-electrode cell with working area 0.17 cm^2, Pt mesh electrode with area 1 cm^2 (counter electrode) and Hg/Hg_2SO_4 as a reference electrode is shown in fig.II.7. The cell design was similar to the cell from fig.II.6 except that the body of cell was made of glass. In addition, the cell was glass jacketed allowing the solution temperature to be controlled and maintained using water from a thermostatic bath, Julabo F20.

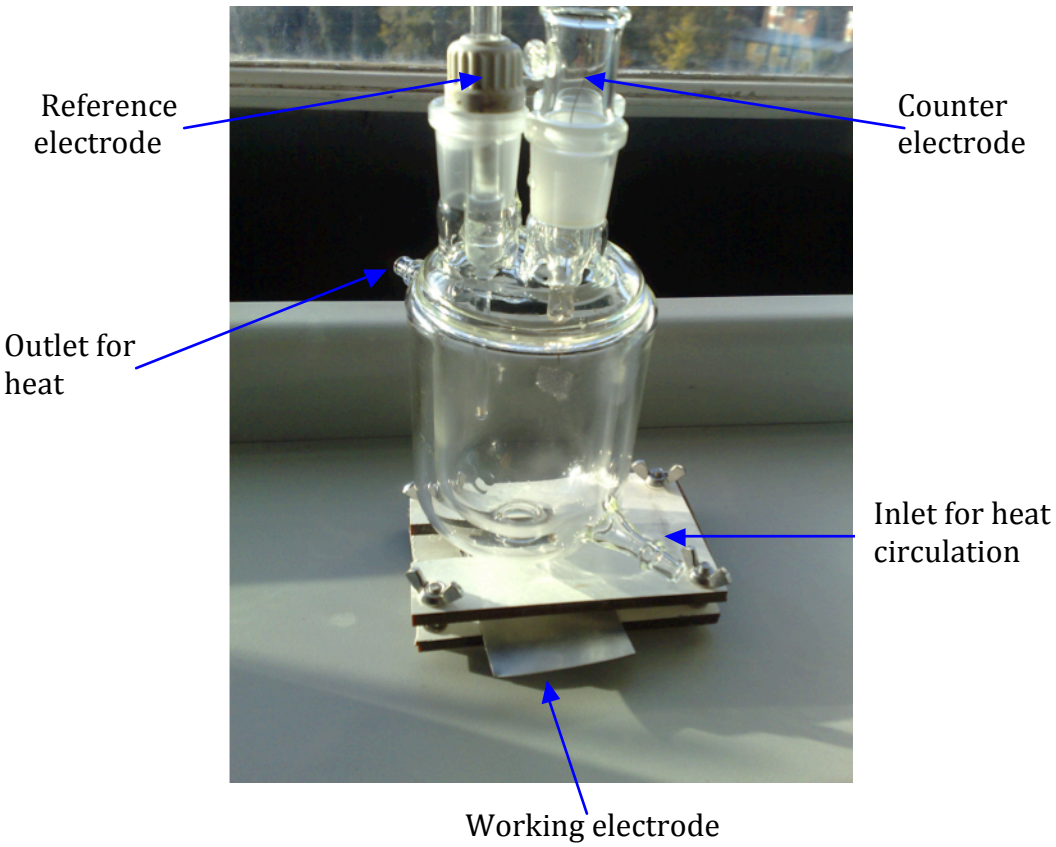

Fig.II.7. The cell with working area 0.17 cm^2.

Cell 2. A three-electrode cell with an electrochemical array as a working electrode, Pt mesh counter electrode and Hg/Hg_2SO_4 reference electrode was employed for some experiments. Fig.II.8a presents schematically the electrochemical cell. The cell was glass jacketed, enabling the control of the solution temperature during the test. Fig.II.8b shows sample holder with the electrochemical array - each gold electrodes in the array had an area 0.016 cm^2 and had an individual electrical contact; te array is described further in section II.5.2.

The electrochemical array can be positioned very precisely between printed circuit board (PCB) and PTFE block (PTFE block is shown in fig.II.8a). The gasket was incorporated into PCB in order to seal the array and prevent the solution leaking. The PTFE cell body was clamped from the top of the array with Viton gasket seal. Four long screws at the corners of the PCB were used to mount the sample holder to the cell.

a)

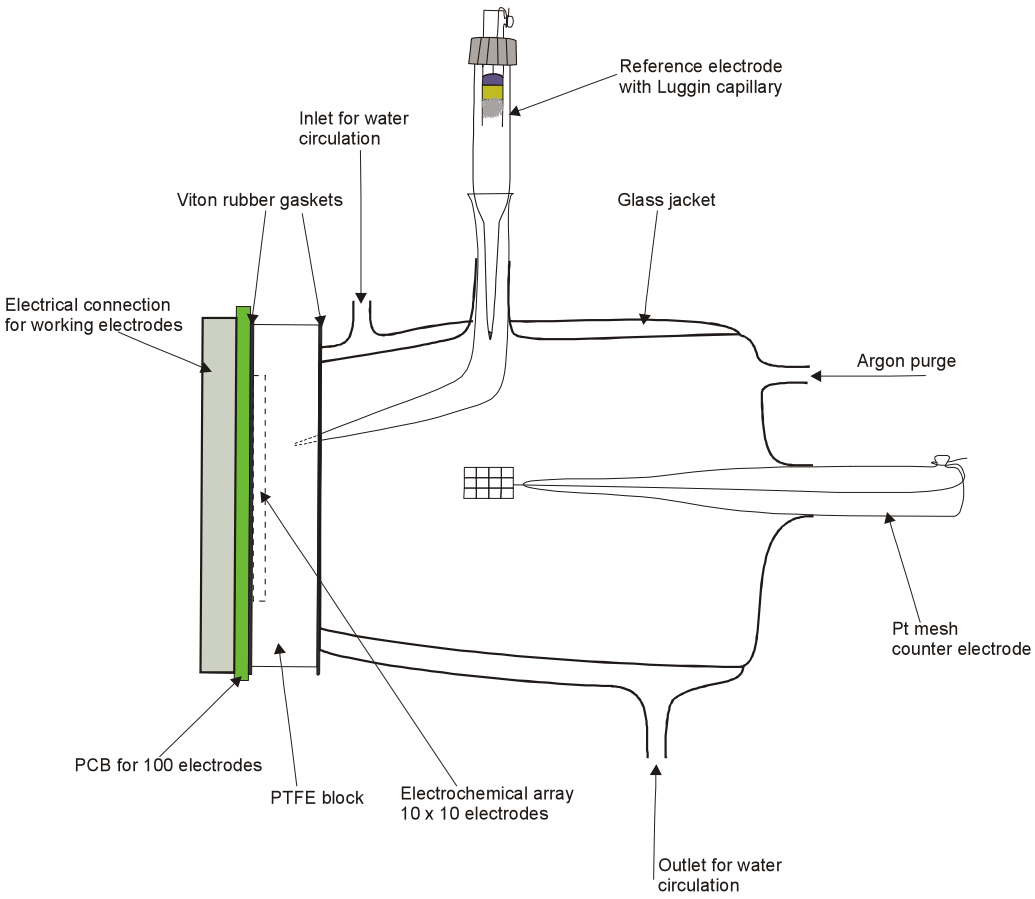

b)

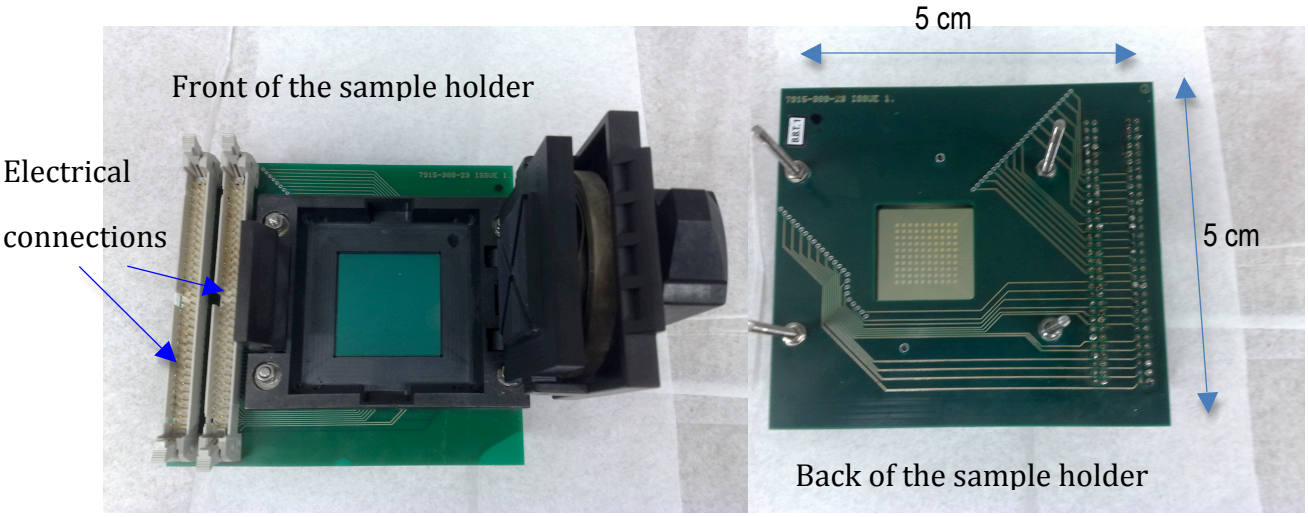

Fig.II.8. The three-electrode cell (a) and a sample holder (b) used for experiments.

Before the experiment was started, the solution was saturated with Argon (BOC Gases, 99.9%) and Argon was passed over the solution surface whilst experiment was running.

4.4. Hull cell

Fig.II.9 shows schematically a Hull cell with its dimensions. Its trapezoidal geometry was design in a particular way, to give a known current density distribution across the cathode. The body of the cell was made from Perspex with the height of 7 cm and overall capacity 267 ml. The cathode was tilted with respect to the anode. The Ni anode plate with dimensions 6 cm x 6 cm and thickness 1.24 mm and the steel cathode dimensions 11 cm x 7 cm were used for electroplating. A constant current 1 A was supplied from a power supply ISO-Tech IPS 2303D for 10 minutes. This current gives a current density ranging from 2 mA cm^{-2} to 60 mA cm^{-2} across the cathode.

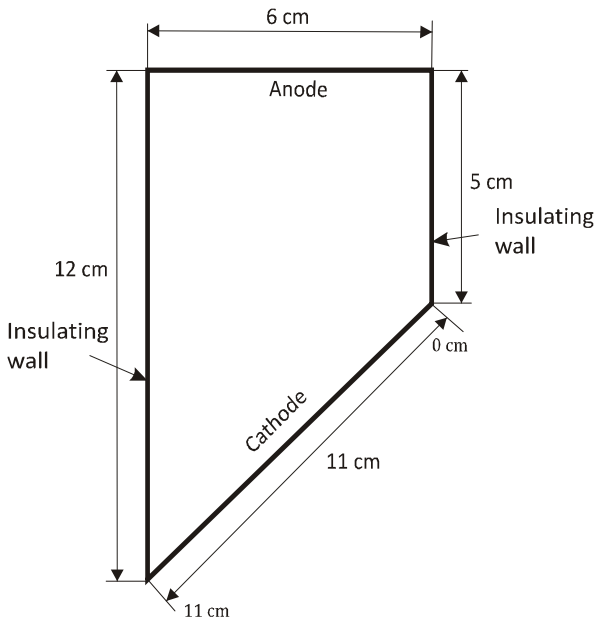

Fig.II.9. Hull cell and its dimensions – cell capacity 267 ml.

4.5. Parallel plate beaker cell

Beakers, with capacity ranging from 200 ml to 1000 ml were used as a cell for metal deposition (fig.II.10). Two Ni anode plates with maximum dimensions 6.5 cm x 10 cm with thickness 1 – 1.24 mm situated opposite to each other were employed. Carbon steel, stainless steel or Ni coated carbon steel with maximum dimensions 5 cm x 6 cm was placed parallel between the two anodes, served as a cathode. A magnetic bar stirrer was employed especially for Ni/graphite deposition where the graphite particles have to be constantly suspended in the solution. Constant current density was applied from the power supply ISO-Tech IPS 2303D. A magnetic hot plate supplied from Fisher Scientific and thermometer was employed to maintain a constant temperature for electrodeposition.

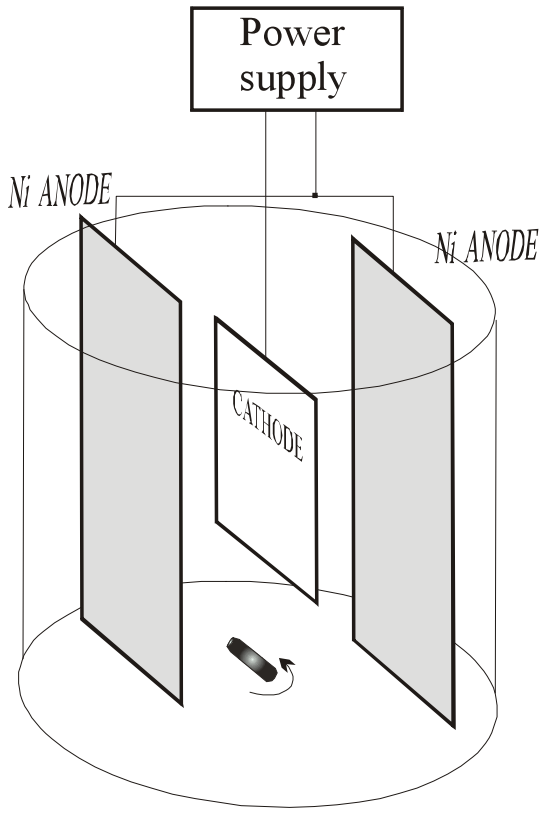

Fig.II.10. Parallel plate beaker cell used for deposition of Ni and Ni-graphite composites.

4.6. Rectangular laminar flow cell

Ni and Ni-graphite were electrodeposited in a parallel plate flow cell. The flow system and rectangular cell are shown in fig.II.11a and fig.II.11b, respectively. The flow system was designed to have two circuits: a main circuit and a second smaller circuit called the bypass (fig.II.11a) [107],[108]. In both circuits, PVC valves with internal diameter 1 cm were incorporated into the reinforced PVC heat resistant tubes with internal diameter 1 cm using jubilee clumps.

a)

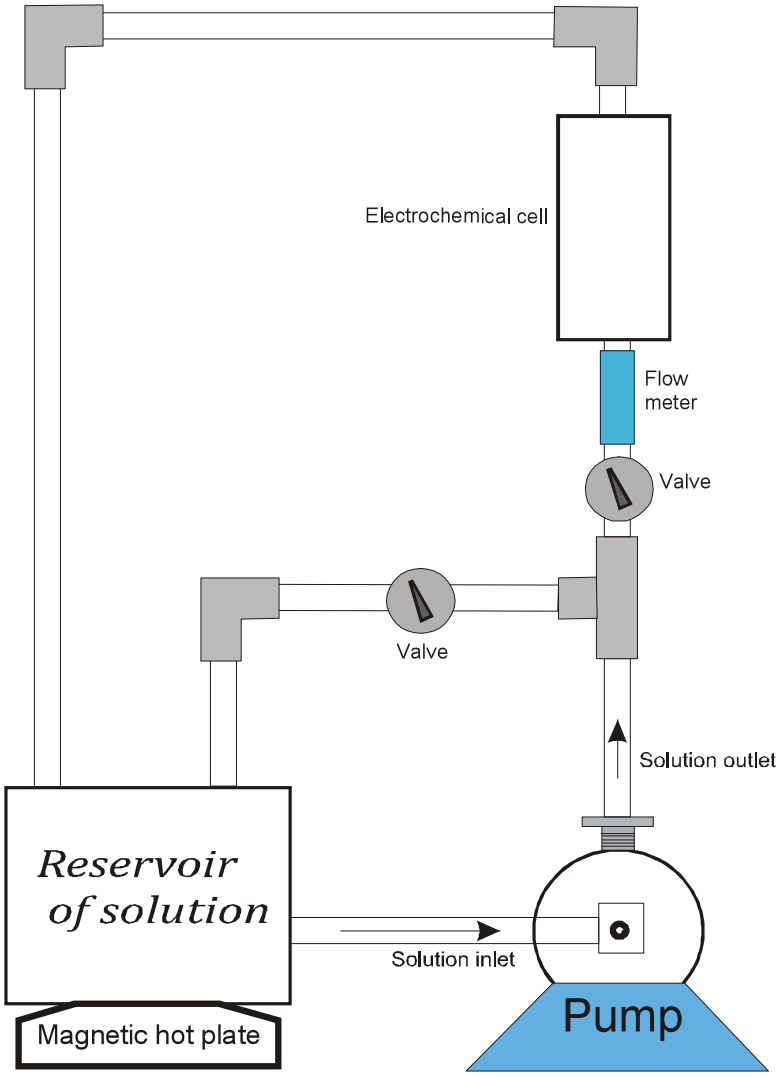
Electrochemical cell
Flow meter
Valve
Valve
Solution outlet
Reservoir of solution
Solution inlet
Pump
Magnetic hot plate

b)

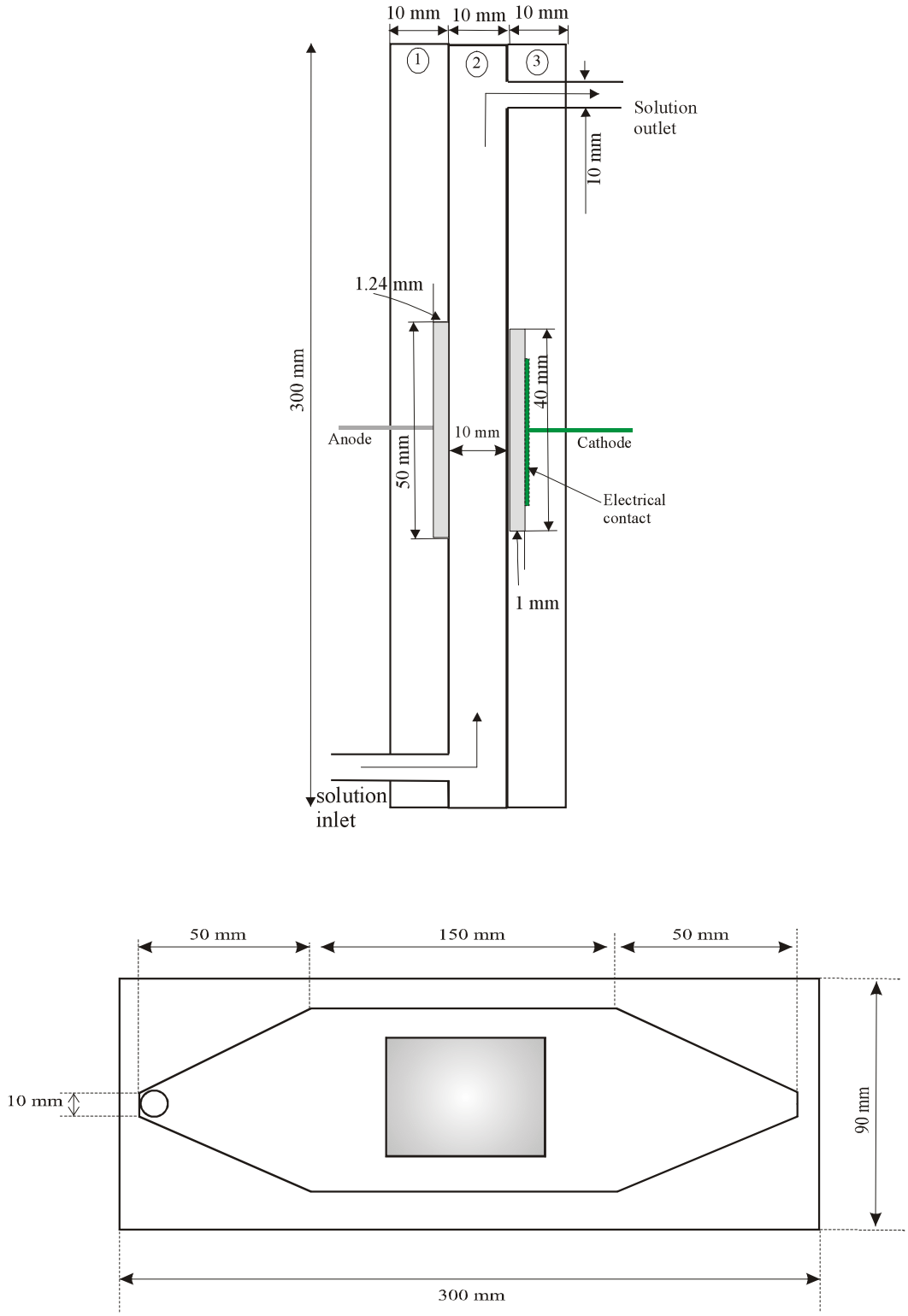

Fig.II.11. Flow cell design for deposition of Ni and Ni/graphite deposition.

These valves enabled the control of the solution flow rate in the system, measured with a flow meter type SK52 and SK62 (George Fisher +GF+) ranged from 10 l/h to 100 l/h and 10 l/h to 200 l/h, respectively. The tubes were connected to the electrochemical cell and to the pump with jubilee clamps.

The 5-litre reservoir with the solution was placed on the magnetic hot plate (Fisher Scientific) to maintain the solution temperature at 333 K. The linear velocity of the solution studied was in the range of 7 cm s^{-1} to 46.6 cm s^{-1}. Two pumps with 0.25 kW type TE BK MD and 0.37 kW type TE GK MD from March May, UK were employed interchangeably to circulate the electrolyte through the system.

The body of the flow cell was made of polypropylene blocks and consisted of three compartments (fig.II.11b). Each compartment was 1 cm thick, 9 cm wide and 30 cm long. The middle compartment served as a separation between the steel cathode and the Ni anode plate. Thin trenches with dimensions 5 cm x 5 cm for the Ni anode and 4 cm x 4 cm for the cathode was cut out in the compartment 1 and 3, respectively. The depths of the channels were 1.24 mm for the NI anode plate and 1 mm for the cathode. In order to prevent solution leakage through the compartments, a Viton™ rubber sheets from Altec Products Limited, UK, with thickness 1.6 mm were cut out and put between compartments 1 and 2 and between compartments 2 and 3. Compression of the three polymer blocks held the electrodes in place and the cell was designed to have a flat electrode/polymer interface so that linear flow was not disturbed. 1 mm holes in the middle of the trenches in the compartment 1 and 3 were drilled for electrical connection of the anode and the cathode with the power supply. On the cathode side, a copper plate was inserted to improve electrical contact. Steel rod with 1 mm in diameter and 3 cm long was welded to the Ni anode plate and cables, which can withstand the current load up to 10 A, were used to connect the electrodes with the power supply. To prevent the solution leaking, all purpose interior and exterior sealant, UniBond, Henkel was used to seal the electrical connections on the anode and the cathode to the polypropylene blocks. The diameter for the solution inlet in the compartment 1 and the solution outlet in the compartment 3 was 1 cm. The assembled cell was clumped using G-clamps.

4.7. Physical vapour deposition

This system was designed to enable the growth of layers with a compositional gradient across the area of the substrate by simultaneous deposition of component elements. The system was designed to work under ultrahigh vacuum with base pressure 1 x 10^{-10} mBar, with two cryopumped physical vapour deposition (PVD) chambers, ion-pumped surface analysis and reaction chamber, and turbomolecularly pumped LPCVD (Low Pressure Chemical Vapour deposition) chamber specifically designed to carry out high-throughput synthesis of thin film materials. In this work, only one modified PVD chamber, shown in fig.II.12, was used for single metals and alloy deposition. The PVD chamber consists of six off-axis sources, three e-beam and three Knudsen cells, cryopanels and shields, a manipulator with heating range 300K – 900K, quartz crystal microbalance which monitor metal deposition rate and a number of shutters for the control of material deposition. Shutter and source temperatures are computer controlled to allow automated deposition of predetermined thicknesses and composition gradients of the thin films. It is important to emphasise the role of shutters during the deposition. Depending upon the shutter's position within the molecular beam, the gradient can be controlled from the natural profile of the source to a fully controlled gradient. Each source profile is controlled independently using its own shutter so that each material can be evaporated with its own gradient. Such a deposition is referred as a "wedge" growth and these fixed shutters as "wedge" shutters because of deposition profile they achieve. Using the wedge growth method on several sources simultaneously and controlling the intrinsic source fluxes, it is possible to vary the composition as a function of position across the sample [109].

Fig.II.13a presents the position of the sources: K-Cells and e-beams with respect to the sample. Two e-beam sources: Ni and Cr were used for deposition of Ni-Cr alloy and Ni layer and the growth of the metals are presented in fig.13b.

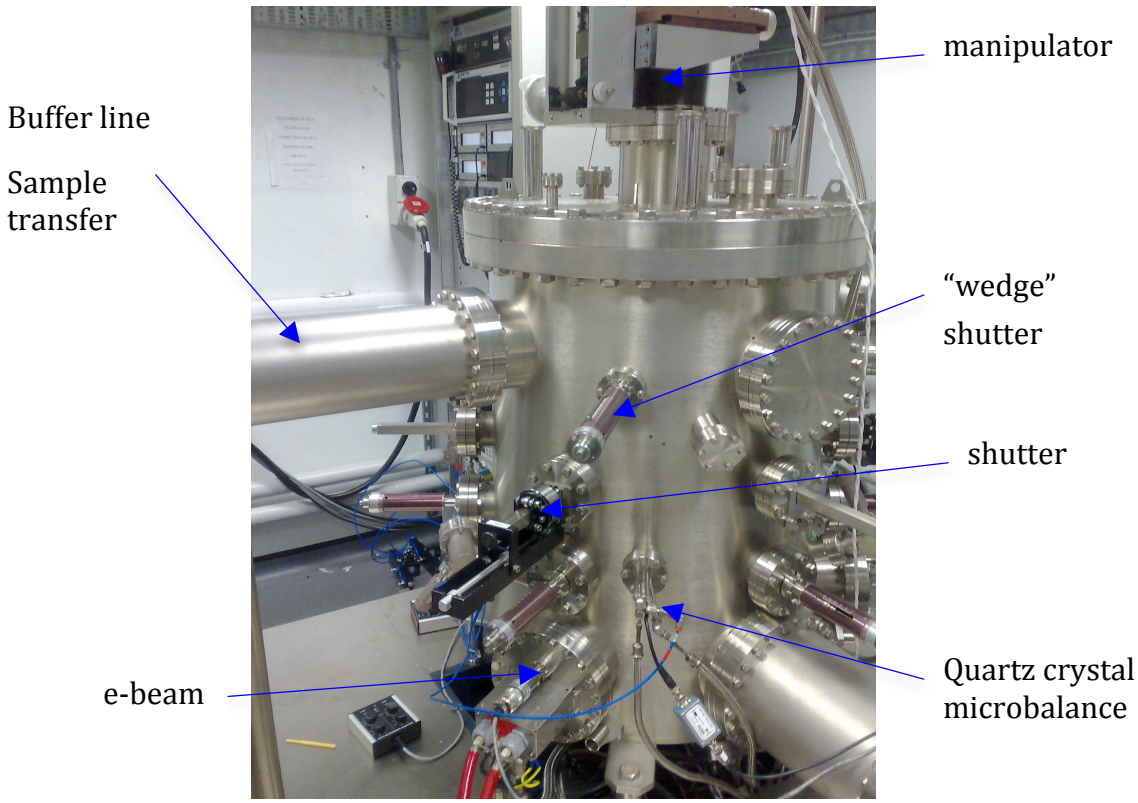

Fig.II.12. Vacuum chamber for metal deposition.

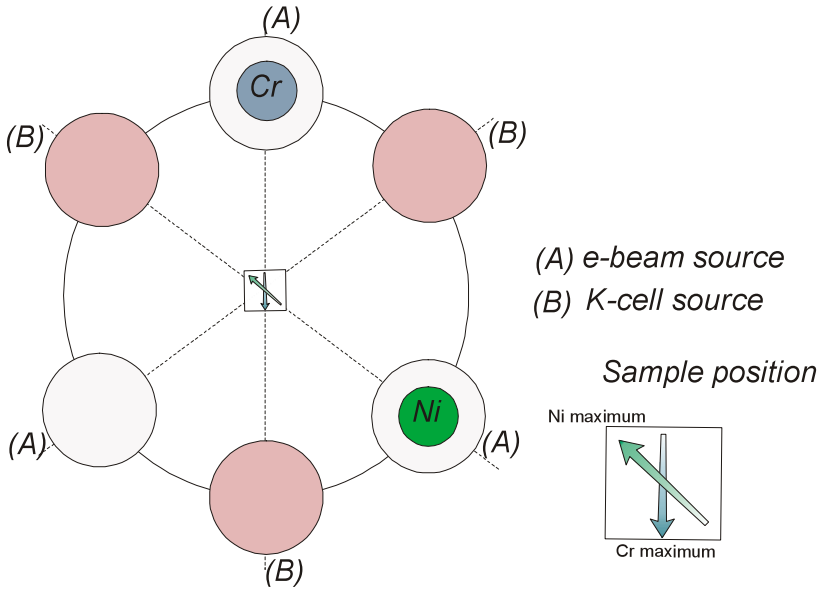

Fig.II.13. Representation of K-Cells and e-beams sources in the PVD chamber with respect to the sample's position

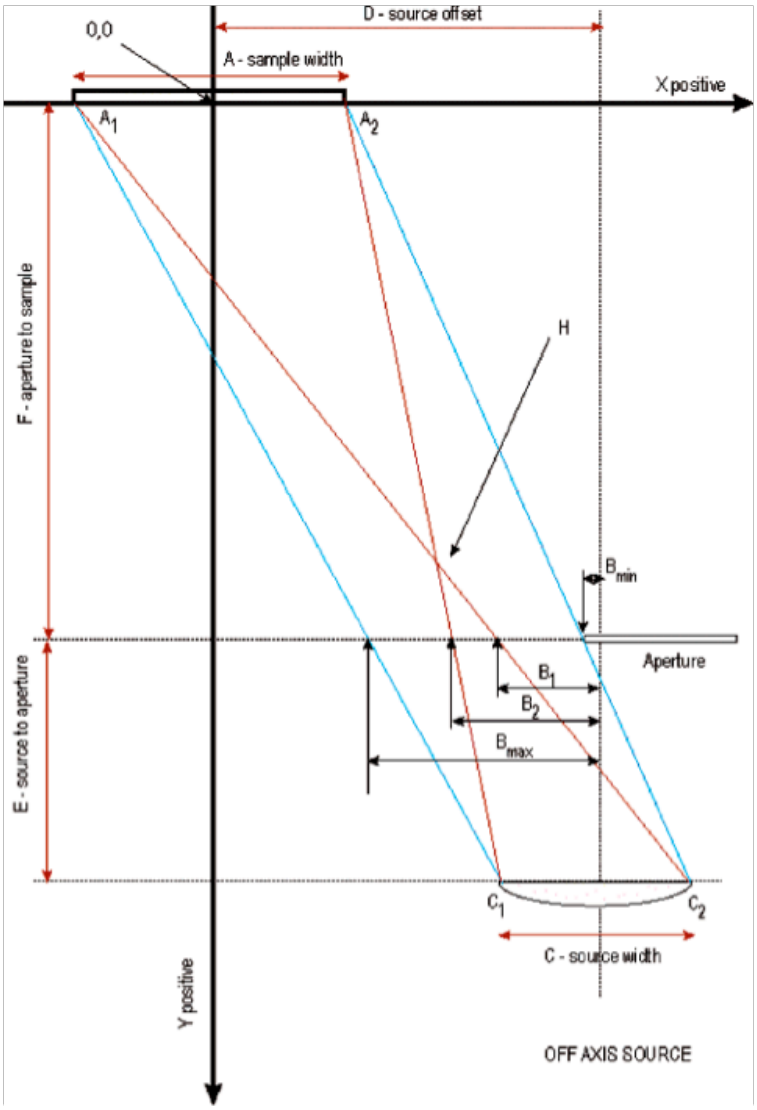

Fig.II.14. A geometrical representation of deposition chamber in PVD.

A geometrical representation of the PVD chamber is shown in fig.II.14. According to the model presented in the figure below, few important features can be distinguished. The source *C* is offset at a distance *D* with respect to the sample *A* situated well above the source. The aperture $B_{min.}$ refers to the minimum wedge position, where the source "sees" whole sample, *E* is the distance between the source and wedge shutter and *F* is a distance between wedge shutter and sample. The lines A_1C_2 and A_2C_1, which are geometrical representation of source flux, intersect at point *H*.

The triangle defined by H, C_1 and C_2 gives the region in which the wedge shutter cutting the source flux will give rise to a linear gradient across the entire sample. By changing the position of wedge shutter to B_1, B_2 or B_{max}, it is possible to control the gradient across the sample [2]. An example of the two alloying metals can be schematically seen in fig.II.15.

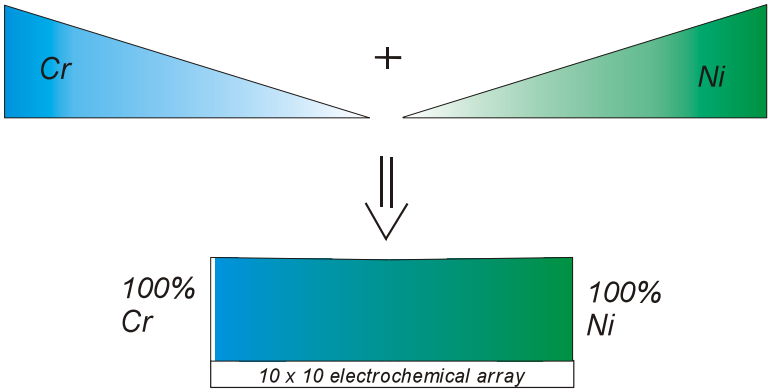

Fig.II.15. When the two metals are deposited using wedge shutters, they combine together to give the alloy with composition variation across the array.

II.5. Metal deposition

II.5.1. Electrodeposition procedures

For the electrodeposition of metals, whether it was carried out in the parallel plate beaker cell or in the rectangular flow cell, the electronic set up is shown in fig.II.16. Regulated power supplies, described in section II.3.2 were used interchangeably to apply constant current to the cell. When parallel plate beaker cell was used, two Ni anode plates were employed and the steel cathode was inserted centrally between the anodes, whereas in the case of the rectangular flow cell, only one Ni anode plate opposite to the cathode steel was employed as it was shown in fig.II.11b. The magnetic hot plate from Fisher Scientific was used to keep the constant temperature of the

electrolyte. The electrodeposition time varied with thickness and thickness of the deposited film was estimated using Faraday's law transformed to the equation (1) below [110]:

$$\mathbf{thickness} = \frac{\mathbf{j\,M\,t}}{\mathbf{n\,F}\,\rho} \qquad (1)$$

where j is applied current density, M – atomic weight of the metal, t – deposition time, n – number of electrons involved in reaction, F – Faraday constant and ρ - is the density of the metal. The thickness calculated assumes 100 % current efficiency for the metal deposition.

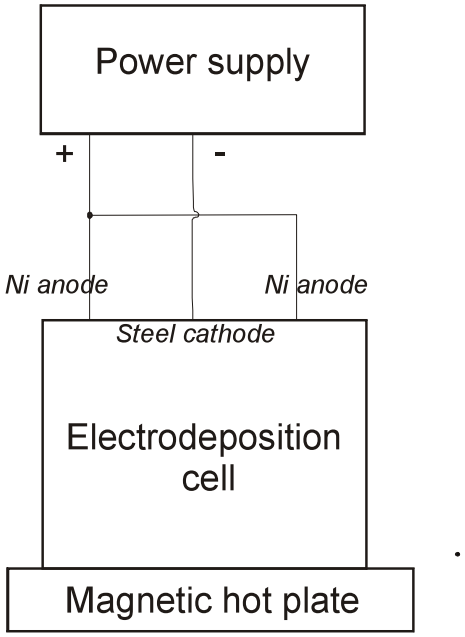

Fig.II.16.Electronic set up for electrodeposition of metal.

II.5.2. Physical vapour deposition (PVD) procedures

PVD deposition was carried out on a specifically designed 10 x 10 array shown in fig.17. The following procedure was used to design the array:

- Squares with dimensions: 35 mm x 35 mm and with thickness 1 mm were cut from silicon chip,
- The squares were covered with 20 nm TiW layer and on top of the layer, 100 gold electrodes 1.4 mm x 1.4 mm with gold tracks and contact pads at the edge of the square were deposited.
- The array was covered with passive layer, silicon nitride with thickness 320 nm, except the square gold electrodes and gold contacts [111].

A stainless steel mask, designed in such a way that enabled the deposition only onto the gold squares, together with sample holder and array is shown in fig.18. The array with the mask was secured at the corners with four pieces of metal mounted in the back of the sample holder, that can be tightened up with a screw.

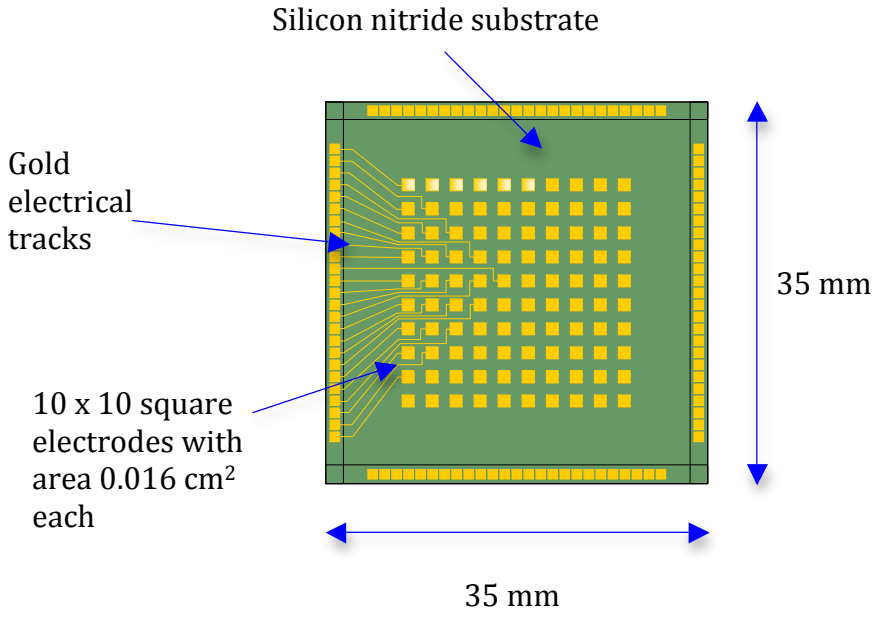

Fig.II.17. Electrochemical array with its dimensions.

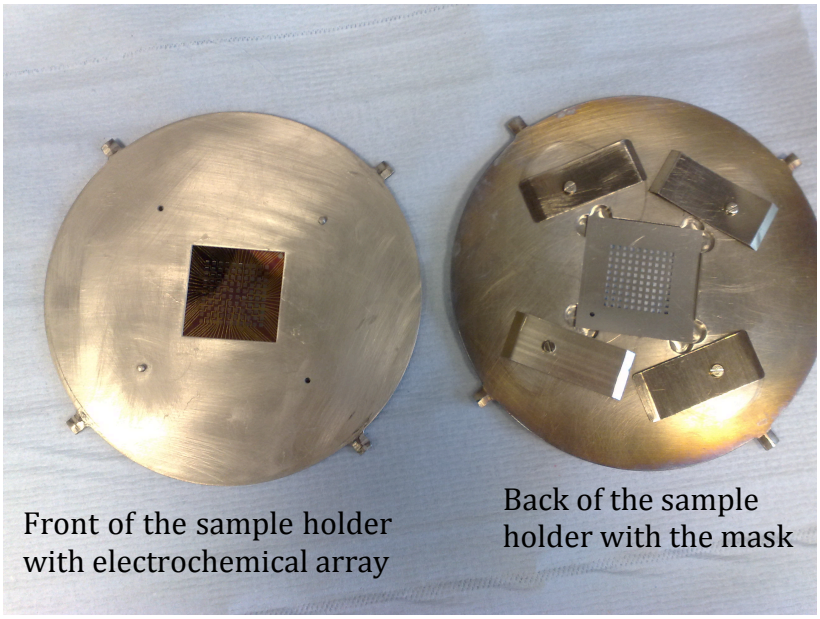

Fig.II.18.Sample holder with mask used for electrochemical array.

Before the deposition of metal was carried out, the sources were calibrated in the following way:

1) *Ni calibration:*

Three depositions were performed with different deposition times: 10 minutes, 20 minutes and 30 minutes. The thicknesses of the as deposited samples were measured using AFM. Having the thickness and the deposition times, the least square method was used to fit the data points and to find the best linear approximation. The slope gave the value for the rate of the deposition. The rate of deposition for Ni was estimated to be 0.6 nm per minute.

2) *Ni and Cr wedge calibration*

Two sources: Ni and Cr crucibles (Testbourne Ltd) were calibrated to give Ni-Cr alloys with maximum composition range of 0 % – 100% Ni, 0 % – 100% Cr.

Three depositions (for each metal) were performed with different times (30 minutes, 45 minutes and 60 minutes) for three wedge shutter positions. Deposited samples were analysed by SEM JSM-5910, JEOL coupled with EDX Inca 300 and the composition for 100 electrodes (in weight percent) was estimated. An example of Cr content in the Ni-Cr alloy across 100 electrodes is shown in fig.II.19.

At % of Cr in NiCr alloy

0.2	1	1	1	1	1	2	3	3	4
4	4	4	5	5	5	5	6	6	8
8	8	10	10	10	11	12	12	12	14
17	18	19	20	21	21	24	25	27	28
29	31	32	35	35	36	37	41	41	43
45	45	45	48	50	51	53	54	54	58
59	61	63	64	65	66	66	67	68	68
70	71	72	72	76	79	80	84	84	84
85	86	88	88	88	89	90	90	90	92
92	94	95	96	97	99	100	100	100	100

Fig.II.19. The composition of Cr in Ni-Cr alloy deposited onto 10 x 10 electrochemical array.

Once the sources were calibrated, two plain Ni films with thickness 100 nm, two Ni-Cr alloys with maximum composition range 0% to 100% of Ni and 0% to 100% of Cr were deposited onto electrochemical array. The deposition time was kept constant at 45 minutes. The estimated thickness was approximately 20 nm.

II.6. Heat treatment procedures

Ni coated carbon steel prepared in Southampton and Cr onto Ni coated carbon steel were heat treated in a tube furnace described in section *II.3.6 Equipment for heat treatment*. Before the heat treatment, the samples were rinsed with deionised water and dried and the heat treatment was perfomed in the following way:

A mixture of Ar/5%H_2 or N_2 gas (BOC) was purged to the glas tube for 40 minutes allowing the air to escape through the exit "bubbler", connected to the other end of the glass tube. The "bubbler" had a shape of a small glass tube with a spherically expanded bottom and partially filled with a paraffin oil. The paraffin oil allowed the gas to be detectable whilst purging. Two different procedures for heating the samples can be distinguished:

1) After 40 minutes, the samples were inserted into hot furnace and subjected to the heat treatment. After the heat treatment, the samples were cooled down to the room temperature (approximately 300 K) in Ar/5%H_2 or N_2 in the following way: the glass tube was pulled away from the hot zone of the furnace toward the entrance of the furnace – less hot zone and kept there for 10 minutes. After that time the sample was completely removed from the furnace and cooled down to the room temperature for 30 minutes.

2) After 40 minutes, the samples were inserted into the cool furnace (room temperature) and subjected to the heat treatment. After the heat treatment, the samples still remained in the furnace and were cooled down to the room temperatare in the inert gas atmosphere.

The heating temperature as well as heating time was varied from 573 K to 1273 K. After the cooling to the room temperature, the glass tube was opened and the sample was transferred to and kept in dessicator in order to avoid moist air.

II.7. Corrosion tests

For corrosion tests, the electronic set up is shown in fig.II.20. In all electrochemical characterisation, the three-electrode cell, described above, was employed and placed in a grounded Faraday cage to minimise noise. The solution temperature was controlled with water from a thermostatic bath Julabo F20. The working electrode, counter electrode and reference electrode were connected to the potentiostat PG&G model 263A from Princeton Applied Research, USA. Potentiostat was connected via USB port to the computer with operating system Windows XP and Electrochemical Power Suit software was used to record current and/or potential with respect to time.

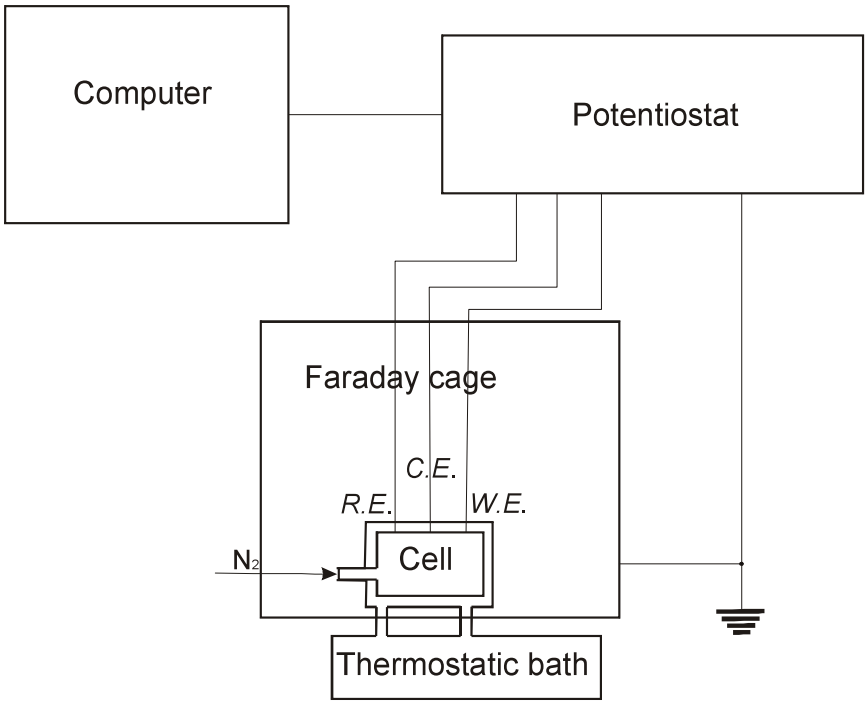

Fig.II.20.Electronic set up for corrosion tests.

7.1.Cyclic voltammetry

The surface of the samples was characterised by linear cyclic voltammetry (CV). The potential was scanned with scan rate 20 mV s^{-1} and current versus potential was recorded. The usual potential limits were from -1.2 V vs. Hg/Hg_2SO_4 to +0.2 V vs. Hg/Hg_2SO_4. The solution used for all electrochemical experiments mimicked the conditions in the cathode side in the PEM fuel cell, i.e., sulphate medium with 2 ppm NaF, pH 4 at T = 333 K. The solution was saturated with N_2 for 5 minutes before experiment, and N_2 was passed over the surface whilst experiment was running. All potentials in this thesis were quoted versus Hg/Hg_2SO_4 electrode and the correction factor from SCE was 0.4 V vs. SHE.

7.2.Corrosion potential measurement

The open circuit potential versus Hg/Hg_2SO_4 was measured for the samples as received. The experimental time ranged between 1000 s and 3600 s. The solution temperature was 333 K. The solution was saturated with N_2 before experiment and N_2 was passed over the solution whilst corrosion potential was recorded.

7.3.Potential step experiments

In this experiments, the potential was held at 0.0 V vs. Hg/Hg_2SO_4 (oxygen potential at the cathode in the PEM fuel cell) and current versus time was recorded for 1 h. The solution temperature was 333 K. The solution was saturated with N_2 before experiment started and N_2 was passed over the solution surface whilst the test was running.

III. Results and Discussion

In this chapter, a number of materials and coatings have been fabricated and there was a requirement for standard corrosion tests to compare their performance. The conditions selected to mimic the environment of a bipolar plate in contact with an oxygen cathode in a PEM fuel cell with a Nafion electrolyte were:

- An electrolyte consisting of 0.1 M Na_2SO_4 + 2 ppm NaF at pH 4. It was considered that the protonic polymer electrolyte would lead to a slightly acidic environment and that some F^- might result from decomposition of the Nafion,
- A temperature of 333 K,
- A potential of 0 V vs. Hg/Hg_2SO_4 electrode (+0.65 V vs. SHE). This is an estimate of the potential seen by the bipolar plate in electrical contact with an oxygen cathode. Such a potential drop is largely due to the kinetics of the reaction on the catalyst layers.

III.1. Metallic substrate for bipolar plates

1.1. Iron, nickel and chromium

In the initial experiments Fe, Ni and Cr were examined; these are the three metals central to the materials studied. SEM images of the metals as received are shown in fig.III.1. On each of the metals, there is no evidence for surface structure on a µm scale. Some white patches were seen and these probably result from non-conductive material such as thin layer of oxide from reaction of the surface with oxygen from the atmosphere.

Each of the metals were characterised by scanning the potential from a negative limit of -1.2 V vs. Hg/Hg_2SO_4 to a positive limit of +0.2 V vs. Hg/Hg_2SO_4 in the standard electrolyte of 0.1 M Na_2SO_4 + 2 ppm NaF, pH 4 at 333 K. Complete first cycles are shown in fig.III.2.The voltammogram for Fe shows only an increasing current density as the potential was made more positive. Indeed, the current density reached a very high value of 30 mA cm^{-2} towards the positive

potential limit. Clearly the iron is corroding at a very high rate; a current density of a 30 mA cm^{-2} is equivalent to a uniform corrosion rate of 330 mm $year^{-1}$. There was also little hysteresis when the direction of the scan was reversed. No passivation was observed.

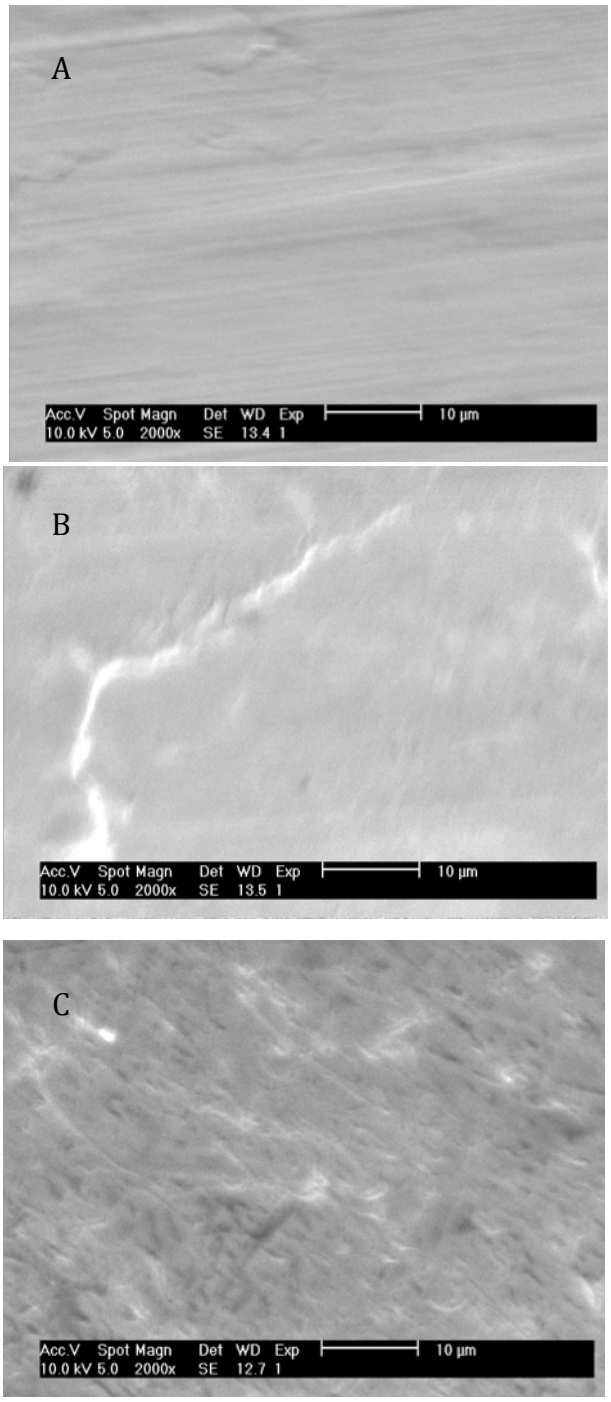

Fig.III.1. SEM pictures of a) Fe, b) Ni and c) Cr as received.

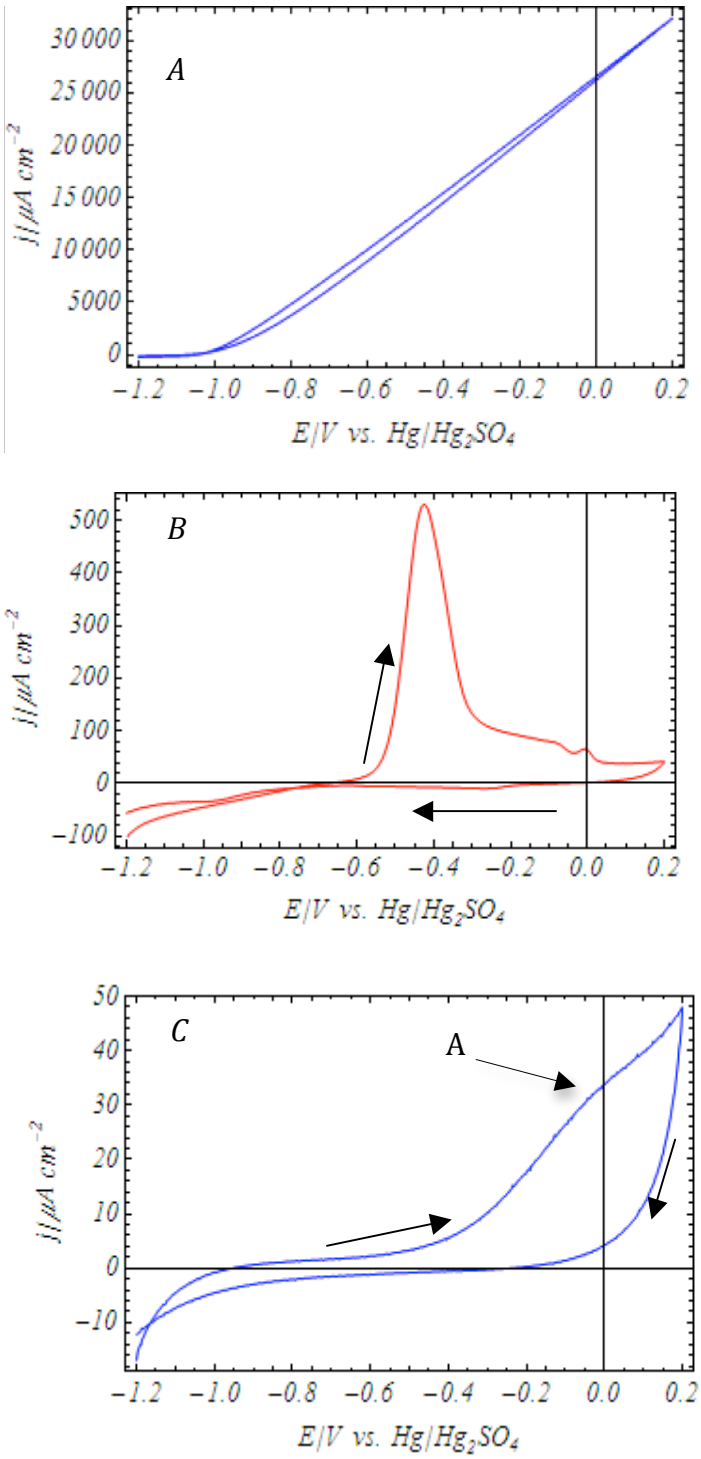

Fig.III.2. Cyclic voltammograms, first cycle for a) Fe, b) Ni and c) Cr. CV, scan rate 20 mV/s. Sulphate medium, pH 4 at T = 333 K was used. The solution was saturated with N_2 and N_2 was passed over the solution surface whilst experiment was running.

In fact, the voltammogram was rather drawn out along the potential axis and there may be some *IR* drop at these high currents but the response was very reproducible.

A completely different response for Ni can be seen in fig.III.2b. The same potential limits were used and during the potential scan toward more positive, Ni started to dissolve at approximately -0.6 V Hg/Hg_2SO_4. Active dissolution was observed over the potential range -0.6 V vs. Hg/Hg_2SO_4 < *E* < -0.4 V vs. Hg/Hg_2SO_4. The current density at the peak was 520 μA cm^{-2}. At potential -0.4 V vs. Hg/Hg_2SO_4, the passivation occurred due to formation of an insoluble corrosion film - current density decreased rapidly to the values of 100 μA cm^{-2} and was still decreasing until the potential was reversed. The Ni surface was passivating. On reversing the potential scan, the current density dropped to a few μA cm^{-2} at 0.0 V vs. Hg/Hg_2SO_4 and when passing -0.1 V vs. Hg/Hg_2SO_4, changed to a negative value until the potential scan was stopped. The chemistry involved in the small cathodic wave at -0.22 V vs. Hg/Hg_2SO_4 is unknown. Hydrogen evolution is not possible and the solution is deoxygenated. A slow reduction of a passivation layer is the most likely reaction. If the scan is repeated without repolishing the surface, the anodic peak is much reduced, typically 100 – 300 μA cm^{-2} and with continued cycling it drops to the very low value of 10 - 30 μA cm^{-2}. The passivation was not reversible.

Chromium was investigated in a similar manner as Fe and Ni and the first scan is shown in fig.III.2c. The current density was in the range of a few μA cm^{-2}. However, the current density started to increase at potential -0.4 V vs. Hg/Hg_2SO_4 and continued to increase until potential was reversed. A point of inflection *A* was noticed at *E* = -0.05 V vs. Hg/Hg_2SO_4. As the potential was reversed, a very rapid decrease in current density was observed and at 0 V vs. Hg/Hg_2SO_4, current density was approximately 2 μA cm^{-2}. At about -0.2 V vs. Hg/Hg_2SO_4, the current density changed its direction to negative in a similar manner as for Ni, but no clear wave was seen and the current density for Cr was about 10 times lower than for Ni. The first scan gave already low value of current density only in the range of 40 – 50 μA cm^{-2} but on continuous cycling the current density decreased to approximately 10 μA cm^{-2} and the inflection point *A* disappeared; the current showed only a slow increase with potential.

The corrosion potentials for Fe, Cr and Ni are more clearly seen from the Tafel plots (fig.III.3). A shift in potential for zero current, between forward and reverse scan was observed for all metals.

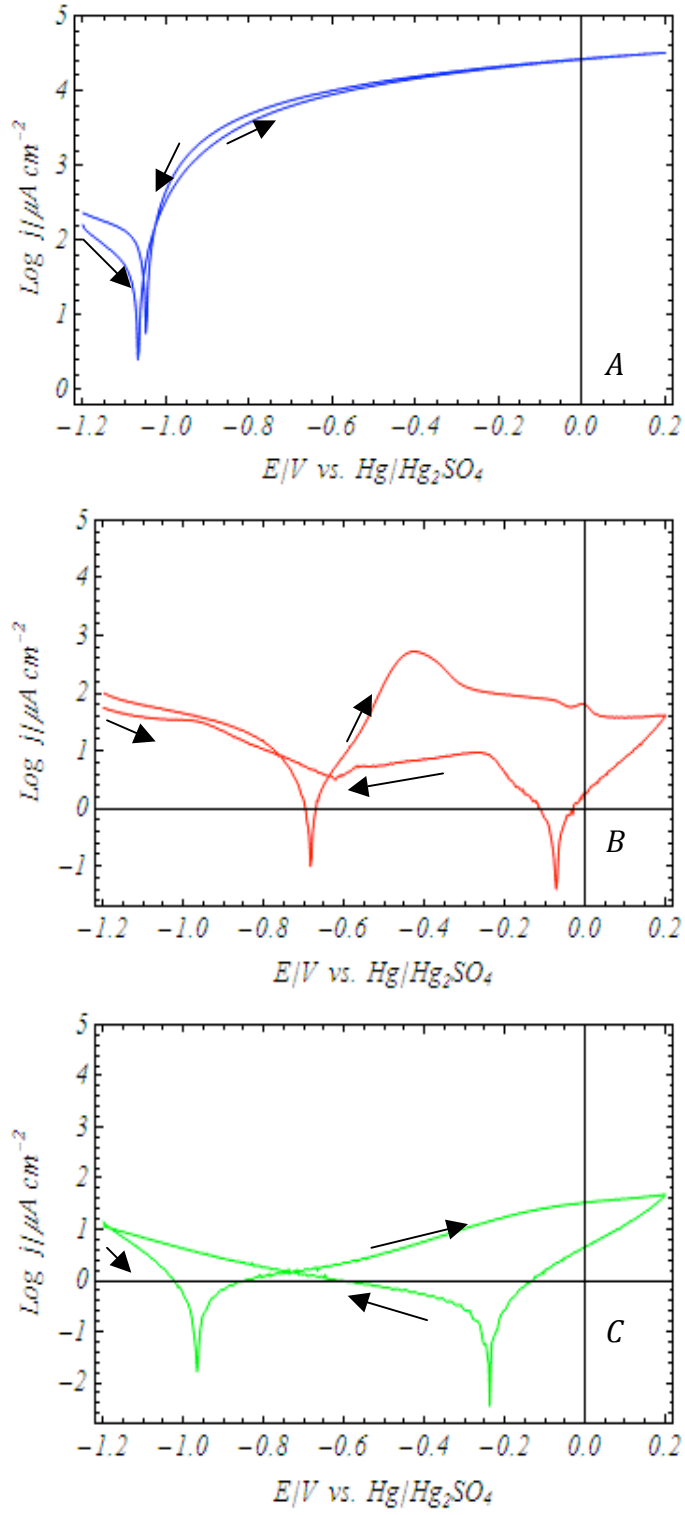

Fig.III.3.Tafel plots for a) Fe, b) Ni and c) Cr as received.

This shift was small for Fe. Any passivation is ineffective. Approximately -0.6 V and -0.7 V difference between forward and reverse scans was observed for Ni and Cr, respectively. This shift in xero current potential results from the low rate cathodic process already seen of the voltammograms and it is unfortunate that the nature of this process is not defined. Even so it is clear that that upon scanning the potential more positive values, a passive layer was formed causing the potential of zero current to shift to more positive. It is believed that Cr passivates in atmosphere before the experiment. Therefore, the shift in the potential of zero current can be interpreted as a "pseudo" shift in corrosion potential of zero current. In the case of Ni, however, an active corrosion region, discussed earlier (see fig.III.2b), can be seen as an increase in the current density at -0.6 V vs. Hg/Hg_2SO_4 and then decrease to the value of approximately 100 μA cm^{-2}. Hence, it can be concluded:

1. Fe dissolved rapidly in sulphate medium, pH 4 at almost all potential scanned positive to -1.0 V vs. Hg/Hg_2SO_4, and there was no passivation,

2. Ni dissolved rapidly only in a certain potential range: -0.6 V vs. Hg/Hg_2SO_4 < *E* < -0.4 V vs. Hg/Hg_2SO_4. More positive to that potential, passivation of Ni occurred. During the reverse scan, reasonable stability to corrosion was observed.

3. Even greater stability to corrosion was found for Cr. The current density was very low in both directions of the potential scan.

Corrosion rates in the conditions of a bipolar plate in contact with an O_2 in a PEM fuel cell was monitoring for one hour after applying a potential of 0.0 V vs. Hg/Hg_2SO_4. A very large current density was observed for Fe. The current density was noted to be 30 mA cm^{-2} and remained almost constant whilst the experiment was running. Again with Cr, the current density was constant but significantly lower with respect to Fe and the value was 2 μA cm^{-2}. This current for Cr may be attributed to the fact that the current density in the forward direction shown in fig.III.2.C, started to increase at potential -0.4 V vs. Hg/Hg_2SO_4. At 0.0 V vs. Hg/Hg_2SO_4 the current was still increasing.

The response observed for Ni was different as the current decreased with time. After 500 seconds, the current density decreased to the value lower than 1 μA cm^{-2} and continued to decrease whilst the experiment was running. Fig.III.3 shows three *i-t* responses for Ni, recorded

for three different samples. After the initial time, each of the responses behaved similar – a tendency of the current density to decrease with time as the experiment was running. At the end of the experiment, the current density was noted to be 0.8 μA cm^{-2} < *j* < 0.5 μA cm^{-2}. Passivation of Ni prevailed over dissolution.

The open circuit corrosion potentials were measured before and after the metal was held at a potential of 0.0 vs. Hg/Hg_2SO_4 for one hour. The corrosion potential for Fe was -1 V vs. Hg/Hg_2SO_4 and after one hour corrosion test, it was -1.1 V vs. Hg/Hg_2SO_4, which implied that surface area of Fe had increased by forming pits in the surface.

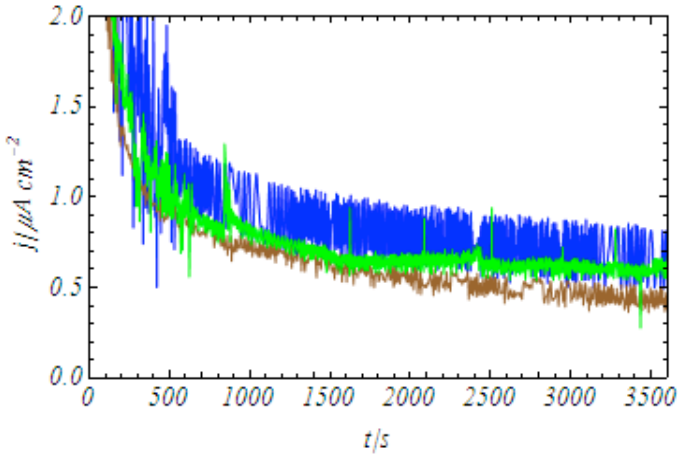

Fig.III.3 i-t response for Ni foil at E = 0.0 V vs. Hg/Hg_2SO_4 for t = 1 h repeated three times for fresh sample. Sulphate medium, pH 4 at T = 333 K was saturated with N_2 and N_2 was passed over the solution surface whilst experiment was running.

For Ni, there was a shift in the corrosion potential of zero current from -0.6 V vs. Hg/Hg_2SO_4 to -0.2 V vs. Hg/Hg_2SO_4 resulting from passivation. Clearly, this behaviour can be seen while scanning the potential to more positive direction (fig.III.2b). Some passive layer probably already existed on the surface before the experiment, therefore it is believed that during the potential hold at 0.0 V vs. Hg/Hg_2SO_4, ”more” oxide layer was formed on the surface, which contributed to the overall decrease of the dissolution rate of Ni.

The results discussed above are summarized in table III.1. The corrosion current, j_{3600}, at the end of the one-hour experiment and estimation of the equivalent uniform corrosion rate measured in mm/year was included for the metals. The examination of Fe, Cr and Ni in sulphate medium,

pH 4 gave clear evidence that the Fe possesses a much higher corrosion rate compared to Cr and Ni. Iron based materials are unlikely to be suitable for the fabrication of bipolar plates but Ni and Cr containing alloys or surface coatings may offer the possibility of more stable components.

	Fe	Ni	Cr
E_{corr} as received/ *V vs. Hg/Hg$_2$SO$_4$*	-1.00	-0.60	-0.60
E_{corr} after/ *V vs. Hg/Hg$_2$SO$_4$*	-1.10	-0.20	-0.60
j_{3600s}/μA cm^{-2}	30 000	0.60	2.00
Equivalent uniform corrosion rate in mm year^{-1}	330	0.006	0.02

Table.III.1. Open circuit potential values before and after one-hour potential hold at 0.0 V vs. Hg/Hg$_2$SO$_4$ in sulphate medium pH 4 at T = 333 K, corrosion current after one-hour potential hold and equivalent corrosion rate for Fe, Cr and Ni. The solution was saturated with N_2 and N_2 was passed over the solution surface whilst experiment was running.

1.2. Carbon steel DC04 LC and 904L SS - stability in corrosive environment

SEM pictures for DC04 LC carbon steel and 904L austenitic stainless steel are shown fig.III.4. Grooves along the surface were due to the rolling of both steel substrates. On a micrometer scale, the surface was relatively smooth for both substrates.

The cyclic voltammogram with the scan rate 20 mV s^{-1} was recorded for the steel substrates in a similar manner as for Ni, Cr and Fe. For carbon steel sample the potential was scanned from negative -1.2 V vs. Hg/Hg$_2$SO$_4$ to positive +0.2 V vs. Hg/Hg$_2$SO$_4$ then reversed to the initial potential -1.2 V vs. Hg/Hg$_2$SO$_4$. Very little hysteresis was observed and the voltammogram resembled that for pure Fe (fig.III.2a). With the carbon steel, the current density was, however, lower. For example at 0.0 V vs. Hg/Hg$_2$SO$_4$ the value was 26 mA cm^{-2} for Fe and only 8 mA cm^{-2} for the carbon steel.

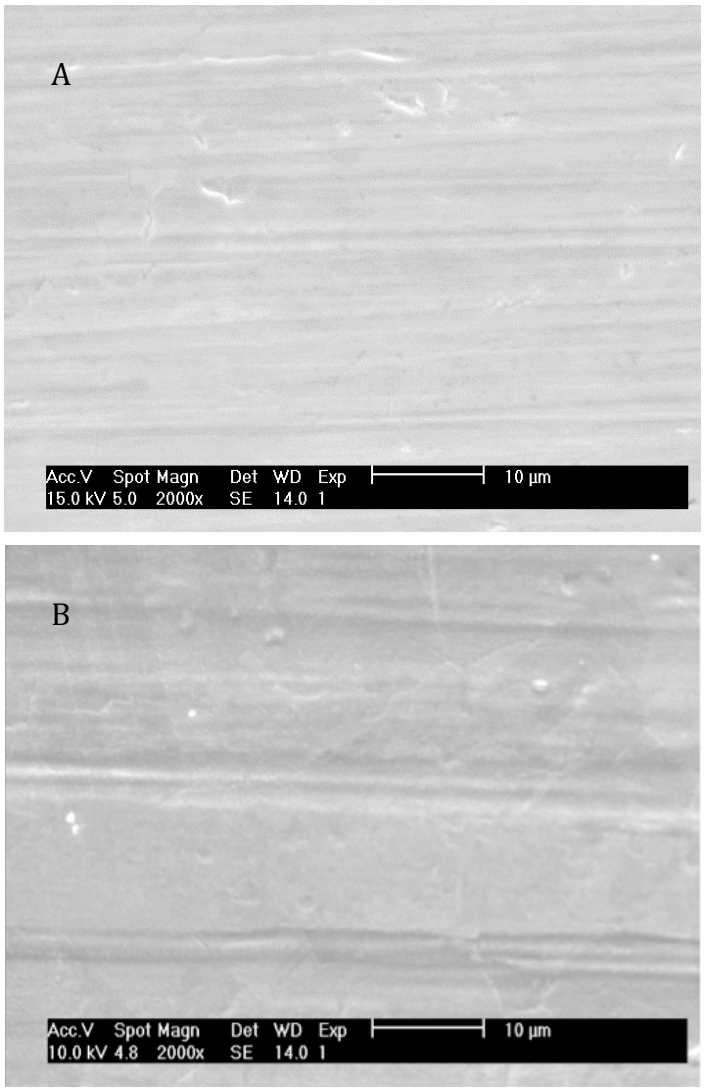

Fig.III.4. SEM for a) carbon steel DC04 LC and b) austenitic stainless steel 904L supplied from CORUS.

Voltammogram recorded for 904L SS with the same scan rate as for the carbon steel is shown in fig.III.5a. The scan started from negative potential -1.2 V vs. Hg/Hg_2SO_4. The voltammogram is essentially featureless. As the potential was scanned to positive direction, the current density became more positive but low in the range of few µA cm^{-2}. Upon the reversing the potential at +0.2 V vs. Hg/Hg_2SO_4, the current density immediately dropped and as it passed through 0.0 V vs. Hg/Hg_2SO_4, the current density slowly became more negative until the potential was stopped at -1.2 V vs. Hg/Hg_2SO_4.

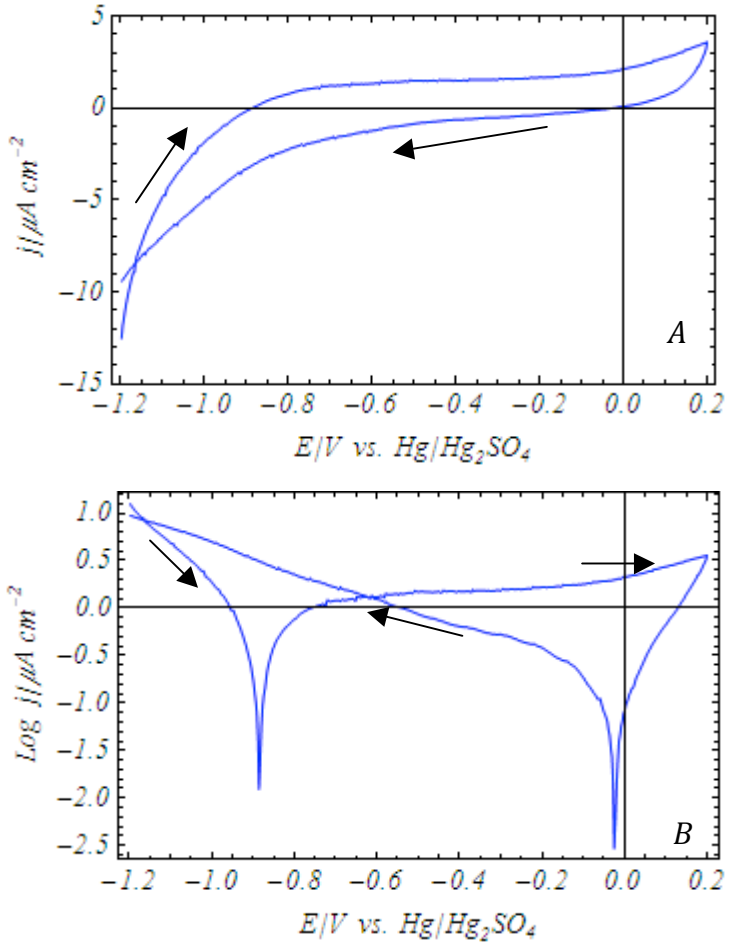

Fig.III.5. Surface characterisation for 904L SS supplied from CORUS. a) cyclic voltammogram, first scan with scan rate 20 mV s^{-1}, b) Tafel plot in sulphate medium, pH 4 at T = 333 K. The solution was saturated with N_2 and N_2 was passed over the solution surface whilst experiment was running.

Clearly, the voltammogram resembled that for pure Cr after few cycles with low (in the range of μA cm^{-2}) current density, which again is an indication of a surface, passivated in air before commenced of electrochemistry.

Fig.III.5b presents Tafel plot for 904L SS. The shift in the potential for zero current from -0.9 V vs. Hg/Hg_2SO_4 to -0.05 V vs. Hg/Hg_2SO_4 was observed. Indeed, this difference was larger than observed with the Cr and Ni (see fig.III.3b and c. Despite the low current density, the surface undergoes a large change as a result of the scan to positive potentials.

One-hour corrosion test was performed for carbon steel and 904L SS at potential 0.0 V vs. Hg/Hg_2SO_4. The results repeated three times for each sample are shown in fig.III.7a and b for carbon steel and 904L SS, respectively.

Very high and almost constant current – time responses were recorded for carbon steel. With 904L SS (fig.III.7b), after the initial time, the current density decreased slowly to 0.8 – 0.4 μA cm^{-2} after 500 seconds and at the end of the experiment, it was recorded to be 0.1 – 0.4 μA cm^{-2}. Fig.III.7b in fact shows three experiments. Some oscillations of the current were always seen and the transients were not identical but in all experiments, the current density was low.

a)

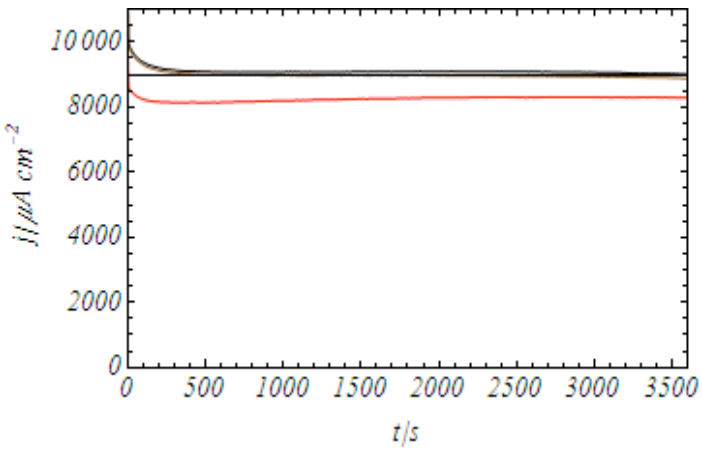

b)

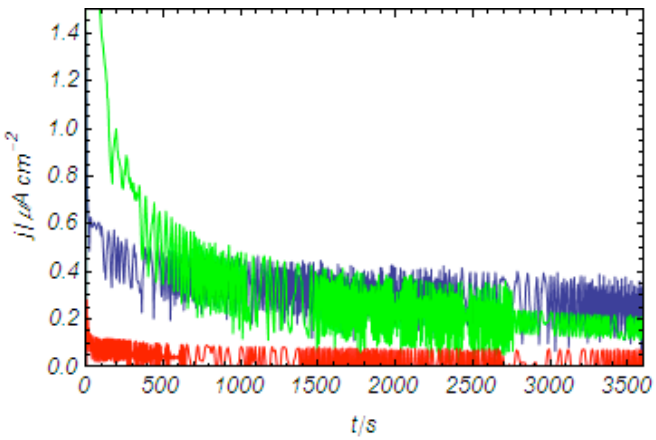

Fig.III.7. Steel samples supplied from CORUS: i-t responses repeated three times at E = 0.0 V vs. Hg/Hg_2SO_4 in sulphate medium, pH 4 at T = 333 K for a) carbon steel, b) 904L SS. The solution was saturated with N_2 and N_2 was passed over the solution surface whilst experiment was running.

The carbon steel substrate dissolved with a high rate at 0.0 V vs. Hg/Hg_2SO_4, but very slow corrosion was observed for 904L SS. The addition of Cr and Ni to the steel decreases the corrosion rate significantly. This is of course consistent with the literature [1]. Carbon steel suffers large degradation in corrosive environment but 904L SS could be a sufficient material for bipolar plates on its own. There is however, an important issue regarding the costs of the fuel cell and its components.

In order to market a fuel cell at an acceptable price, the costs of the production must be reduced to a minimum. Even if 904L SS meets requirements for steel-based bipolar plates, it is still expensive for automotive application. Therefore, the carbon steel, which is alternative replacement for steel-based bipolar plates, needs to be protected in order to bring the rate of corrosion down to the values similar to 904L SS. One of the forms of the steel protection is electrodeposition of more noble metals.

In order to successfully deposit any metal onto metallic substrates, a special pre-treatment of the substrate must be applied. Two methods of pre-treating the steel were considered:

1. Exposing the sample to acidic solution (solution pH ~2),
2. Electrodegreasing the surface using cathodic current (solution pH ~11).

The behaviour of the corrosion current tested at 0.0 V vs. Hg/Hg_2SO_4 for 1 h for 904L SS after 10% HCl acid dip for 4 minutes and after electrodegreasing in P3Percy702 solution (applying cathodic current density -80 mA cm^{-2} for 60 s) were similar for both pre-treatment used. Three samples of the stainless steel were tested and in each case the current density was very low and in the range of 0.2 – 1.5 μA cm^{-2} at the end of the test. Regardless the pre-treatment applied to the steel, there was almost no differences after the corrosion test.

The same pre-treatments with the same conditions as for 904L SS were applied to the carbon steel. The results gave very large current density in the range of mA cm^{-2} and there was no difference whether the steel was dipped in acid or electrodegreased. The corrosion current was always high. As it was true for 904L SS, this substrate gave reproducible data regardless the pre-treatment applied.

III.2. Protective coatings for steel-based bipolar plates

It was shown in the previous section that the carbon steel bipolar plates corrode rapidly in a harsh enviroment in the PEM fuel cell. On the other hand and for the reason of cost, carbon steel is preferred to stainless steel and this places much greater stress on the coating to prevent corrosion.

Nickel corrodes only in certain potentials and this was observed in the voltammogram shown in the fig.III.2b. In the simulated potential in the PEM fule cell, a passivation of Ni was observed.

As mentioned in the Introduction of this thesis, the protective coating consists of layered structure and the first layer to protect the carbon steel from further degradation is Ni layer.

2.1. Electrodeposition of Ni

The Ni was deposited onto carbon steel from a Watts bath, pH 3 – 3.5 at T = 333 K. The composition of the Watts bath was: 267 g dm^{-3} $Ni_2SO_4.6H_2O$, 50 g dm^{-3} $NiCl_2.6H_2O$ and 35 g dm^{-3} H_3BO_3. A typical voltammogram for Ni^{2+} reduction at a stationary carbon steel disc is shown in fig.III.8. It can be seen that the current is low when the potential was positive to -1.10 V vs. Hg/Hg_2SO_4. The nucleation and growth of the Ni started at about -1.17 V vs. Hg/Hg_2SO_4 and the metal continued to grow and thicken until the potential was reversed. Interestingly, at the current density of about -40 mA cm^{-2}, noise was observed during the deposition and the curve was not as smooth as for the lower values of the current density. This noise was correlated to a hydrogen evolution that occurred on the cathode in parallel with Ni deposition. Clearly, it should be emphasized that the efficiency of the electroplating from Watts bath can be 95 – 98% and the other charge leads to hydrogen evolution. The ratio of the currents for Ni deposition and hydrogen evolution depends strongly on electrolyte composition and potential. On the reverse scan, the hydrogen evolution may still have a contribution to the current but, as the potential was made positive, the curve started to become smooth again. Also a 'nucleation loop' is evident. This means that at low potential there was very little hydrogen contribution to the current density and

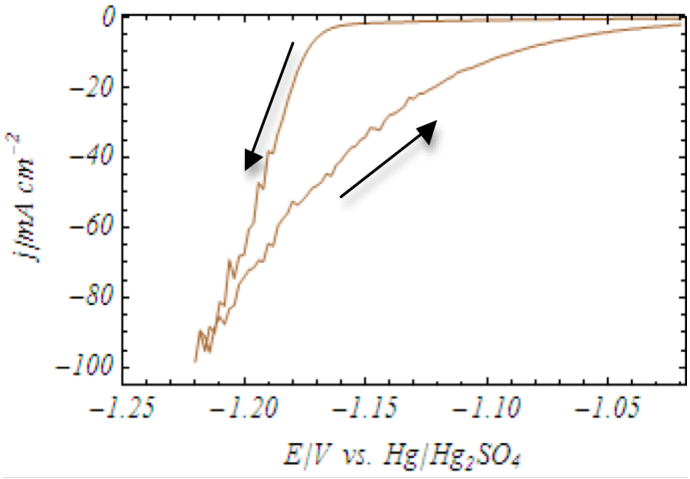

Fig.III.8. A reduction curve recorded in a stationary carbon steel disc from Watts bath, pH 3–3.5 at T = 333 K. Scan rate 20 mV s^{-1}.

Ni deposition was a dominant reaction. In addition, there was no change in shape of the voltammogram when stirring or agitating the electrolyte; the deposition is under electron transfer control.

It can be therefore concluded that at low overpotentials (or current density) it is relatively safe to deposit Ni with little concern about significant contribution from hydrogen evolution. Provided that the current density is low, Faraday's law can be used to estimate the thickness from the charge passed. Even at current densities of 10 – 100 mA cm^{-2}, Ni deposition appears to be a major reaction, although the contribution from hydrogen evolution increases with current density. This conclusion is consistent with the literature [2], [4].

The protective layer must be thick enough to ensure complete coverage of the steel and corrosion current density of the coated surface should certainly be lower than 1 μA cm^{-2}. From the cyclic voltammogram (fig.III.8), we know that the current density applied during the deposition in a stationary solution should be low in order to minimize hydrogen evolution and favour Ni deposition. A Hull cell was used to investigate how the current density influences the roughness of the deposit.

2.1.1. Hull cell electroplating

The Hull cell shown in fig.III.9 (see experimental section, chapter *II.4.4.Electrochemical cells* for more details) was used for the deposition of Ni, in order to define the influence of current density distribution along the cathode was studied. The electroplating conditions were as follows:

- Watts bath (267 g dm^{-3} $Ni_2SO_4.6H_2O$, 50 g dm^{-3} $NiCl_2.6H_2O$ and 35 g dm^{-3} H_3BO_3), pH 3 – 3.5 at T = 333 K,
- Applied constant current i = 1 A for t = 10 minutes,
- Unstirred solution.

The current density along the cathode surface was calculated using an equation of the form [112]:

$$j = j_{average}\ (3.26 - 3.04\ ln[x]) \qquad (1)$$

where $j_{average}$ - average current density applied, x - cathode length in cm from the shortest distance to the anode.

Table.III.2 shows changes in the current density along the cathode. It can be recognised from the table that the current density decreased as the gap between anode and cathode increased. This reflects increasing voltage drop through the electrolyte and corresponding decrease in the local overpotential for Ni deposition. The thickness of the Ni deposit increased with the current density and assuming 100% current efficiency for Ni depostion, the thickness ranged from 0.4 μm at the lowest current density to 13 μm at the highest current density.

x/cm	0.5	1.5	2.5	3.5	4.5	5.5	6.5	7.5	8.5	9.5	10.5
j/mAcm^{-2}	58	37	29	22	18	14	11	8	6	4	2

Table.III.2. Calculated current density vs. distance on the cathode according to the equation (1)

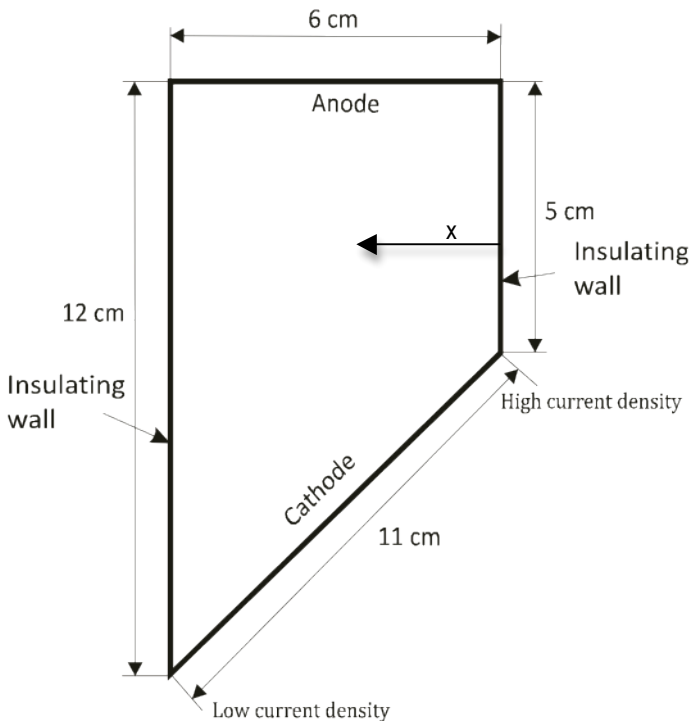

Fig.III.9. Hull cell (view from above) with its dimensions – cell capacity 267 ml.

Fig.III.10 presents SEM pictures of Ni deposition as a function of the current density *j*, deposit thickness and the cathode length *x*. The plot was split into six regions, where six SEM pictures revealed changes in the deposition quality with current density variation. Rough Ni deposit was formed on the cathode at the higher current densities - SEM pictures 5 and 6. The thickness at this current density (-40 mA cm^{-2} to -60 mA cm^{-2}) was in the range of 8 μm to 13 μm. As the distance between cathode and anode increased, the current density dropped to the value of -20 mA cm^{-2}. This current density drop also affected the appearance of the deposit (SEM picture 4). Apart from some rough areas, some smooth patches were observed. The thickness decreased from 8 μm to 4 μm as the current density decreased from -40 mA cm^{-2} down to -20 mA cm^{-2}. At the largest gap between the anode and the cathode, the current density was very small and ranged from -2 mA cm^{-2} to -20 mA cm^{-2}. SEM pictures 1, 2 and 3, show the surface of the deposited Ni under this current densities. A smooth deposit can be observed on a 1 μm scale. In this range of current density, the thickness decreased further from 4 μm to 0.4 μm. Considering the surface roughness of the deposited Ni, the SEM pictures 1, 2 and 3 were acceptable.

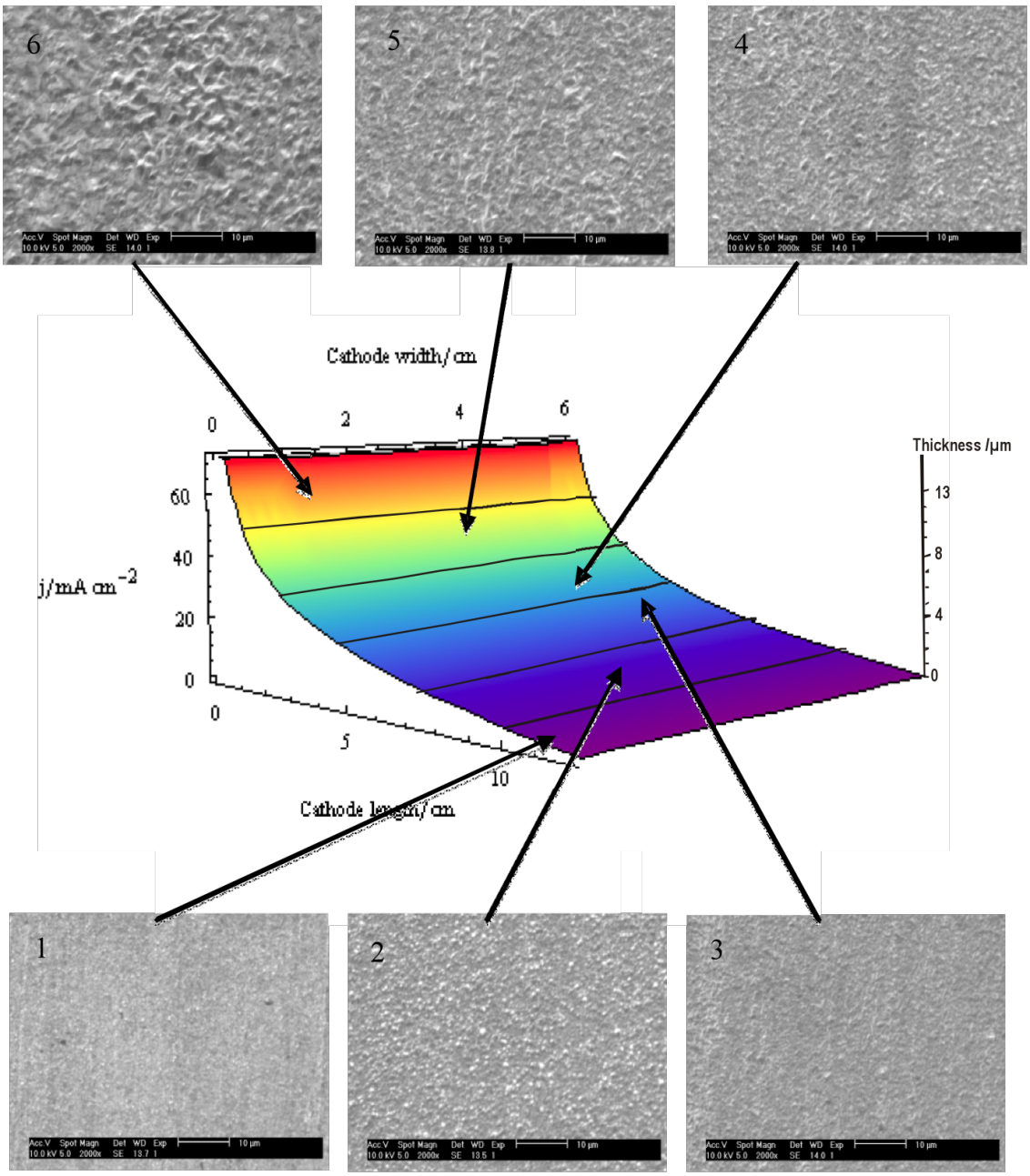

Fig.III.10. A three-dimensional representation of current density distribution in the Hull cell along the area on the cathode and SEM analysis. The SEM pictures show changes on the Ni surface upon varying the current density along the cathode panel. The thickness corresponding to the particular current density was estimated from the Faraday's law (assuming 100% current efficiency)

The current density was indeed low, ranging from -2 mA cm^{-2} to -20 mA cm^{-2}. This range of the current density will generally be used while employing the parallel plate beaker cell. It should be again stressed that in flowing the solution or stirring the solution, the deposit quality may improve at the higher current densities, for example, because of the removal of H_2 bubbles from the surface.

Considering the cyclic voltammogram for Ni in Watts bath from fig.III.8, it can be seen that the optimum current density applied for the deposition should be in the rage of -5 mA cm^{-2} to -20 mA cm^{-2}. If a larger in magnitude current density is used for the deposition, for instance –50 mA cm^{-2}, the curve from fig.III.8 becomes distorted due to the possible hydrogen contribution to the deposition. According to the experiment conducted in the Hull cell, we can further see that at the particular current density, for instance –50 mA cm^{-2}, in addition to the hydrogen evolution, the surface of the deposited Ni became rough. If the current density was decreased to -5 mA cm^{-2} or to -10 mA cm^{-2}, the surface was relatively smooth (fig.III.10 SEM picture 2 and 3). Interestingly, even if the current density was low, the structure of Ni appeared to be grainy. This is a typical structure for Ni. The grains seem to have 0.5 or 1 μm diameter.

2.1.2. Parallel plate beaker cell

In the Hull cell, Ni was deposited from a pure Watts bath containing 267 g dm^{-3} $Ni_2SO_4.6H_2O$, 50 g dm^{-3} $NiCl_2.6H_2O$ and 35 g dm^{-3} H_3BO_3, pH 3 – 3.5 with no surfactant or additives. The Hull cell experiment provided compelling evidence that the appearance of the deposit depends on the current density along the cathode. At higher current densities, the deposited material was thicker and rougher in structure. In this chapter, a preliminary study of Ni deposition in the parallel plate beaker cell was conducted to further understand the effect of current density on Ni coated carbon steel. The thickness of the Ni layer was estimated based on Faraday's law and assuming 100% efficiency for Ni deposition.

Prior to Ni deposition, the substrate was pre-treated by applying electrodegreasing with a cathodic current density in the range of -15 mA cm^{-2} to -30 mA cm^{-2} for 30 s, then rinsed with deionised water and dried. The electrodegreasing solution consisted of 30 ml dm^{-3} P3Percy702

(Henkel), 60 ml dm^{-3} 45% NaOH. A small beaker with two Ni anodes situated parallel to each other and the steel cathode placed between and in the middle of the anodes was set up to pre-treat the steel substrate.

A parallel plate beaker cell was used as a first electroplating cell to study the changes in Ni deposit whilst varying the current density (for the detailed description of the cell see the experimental chapter *II.4.5. Parallel plate beaker cell*). Based on the Hull cell experiment in the stationary electrolyte, the following electroplating conditions were selected: the solution temperature 333 K, deposition charge 6 C cm^{-2} and the current density -10 mA cm^{-2}. Three samples were fabricated: Ni coated carbon steel without surfactant and with addition of 200 mg dm^{-3} and 400 mg dm^{-3} sodium dodecyl sulphate (SDS) salt (fig.III.11). Significant changes on the surface of Ni layer can be observed. The Ni coated carbon steel with no surfactant (fig.III.11a) had rather coarse and grainy structure. Upon addition of surfactant, the surface appeared to be less grainy and smoother. As the amount of surfactant increased from 200 mg dm^{-3} to 400 mg dm^{-3}, the smooth regions prevailed over the grainy structure. The coating seemed to be complete. Certainly, the presence of the surfactant has decreased the surface roughness largely because of addition of sulphur containing surfacant to the Watts bath.

Ni was chosen to protect the carbon steel from corrosion, because of its good corrosion properties. With or without addition of surfactant, the Ni layer must be complete. With electroplated films, there is always certain amount of porosity present but the pores should not lead directly to the substrate. Pores leading to the carbon steel substrate are likely to result in very rapid local corrosion, i.e. crevice corrosion.

In order to further investigate the “completeness” of the coating, three samples of the Ni coated carbon steel with coating thicknesses: 1 μm, 5 μm and 10 μm were prepared and the thicknesses were estimated using the Faraday’s law and assuming 100% current efficiency. No surfactant was added to the electroplating bath. AC impedance at the open circuit potential was conducted in 1 M H_2SO_4 solution at room temperature. A three-electrode cell with working eletrode area 5 cm^2, Pt mesh electrode (1 cm^2) and Hg/Hg_2SO_4 reference electrode was employed for measurement. Small amplitude was applied to the cell, +5 mV and frequency ranges from 10 mHz to 10 kHz. The AC impedance data, recorded in Autolab, from the three electroplated samples and two standards (carbon steel and Ni) are reported in fig.III.13 and fig.III.14 as Nyquist plots. In addition to that, Ni coated carbon steel supplied from CORUS plating

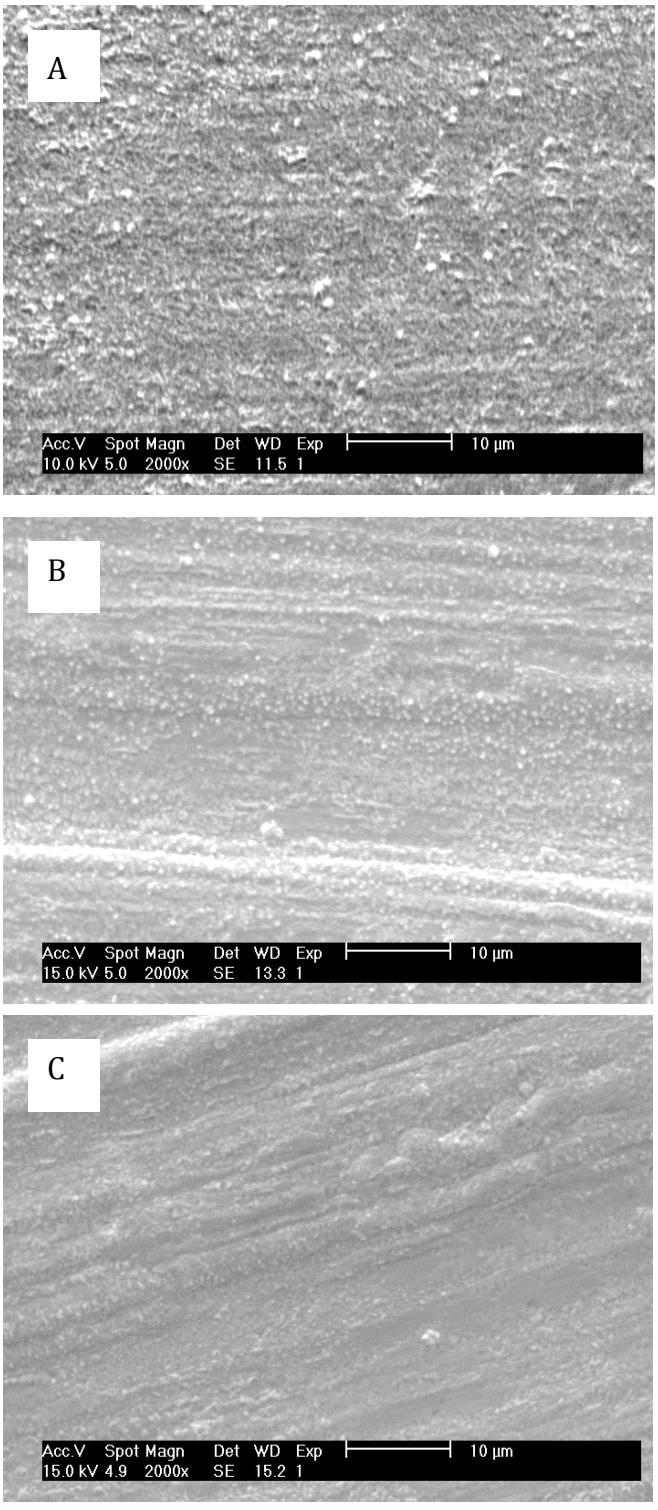

Fig.III.11. SEM pictures of Ni coated carbon steel with coating thickness 2 μm. The electroplating conditions were: Watts bath pH 3 – 3.5 at T = 333 K, j = -10 mA cm^{-2}, A) no surfactant, B) with 200 mg dm^{-3} SDS and C) with 400 mg dm^{-3} SDS. No stirring were applied.

line was examined. Well-formed semicircles were obtained for each sample and hence the data can be interpreted in terms of a very simple circuit (see fig.III.12). The corrosion resistances calculated from the diameters of the semicircles are summarized in table III.3 and double layer capacitances were also estimated from the frequencies at the top of the semicircle. The double layer capacitance was used to compare surface roughnesses. Fig.III.13 presents two standard samples: pure Ni and carbon steel supplied from CORUS after wet polishing with alumina powder. From the semicircles shown in fig.III.14, the corrosion resistance, R_{ct}, for pure Ni was larger than for polished carbon steel, suggesting much lower corrosion rate.

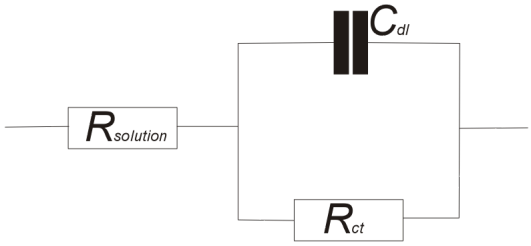

Fig.III.12. An equivalent electrical circuit for AC impedance experiment.

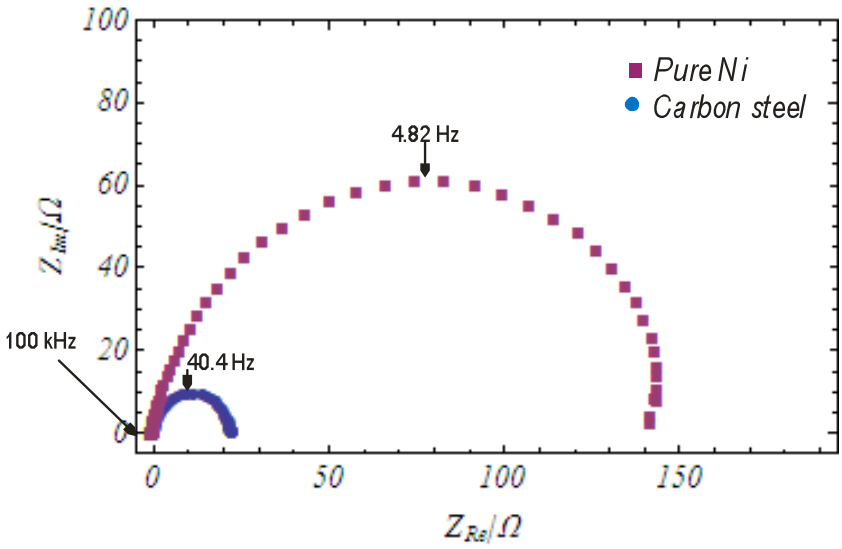

Fig.III.13. AC Impedance analysis for pure Ni and uncoated carbon steel at their corrosion potentials. The experiment was performed in 1 M H_2SO_4 at room temperature and at open circuit potential; frequency ranged from 10 mHz to 10 kHz and small amplitude +5 mV was applied. Working electrode area was 5 cm^2.

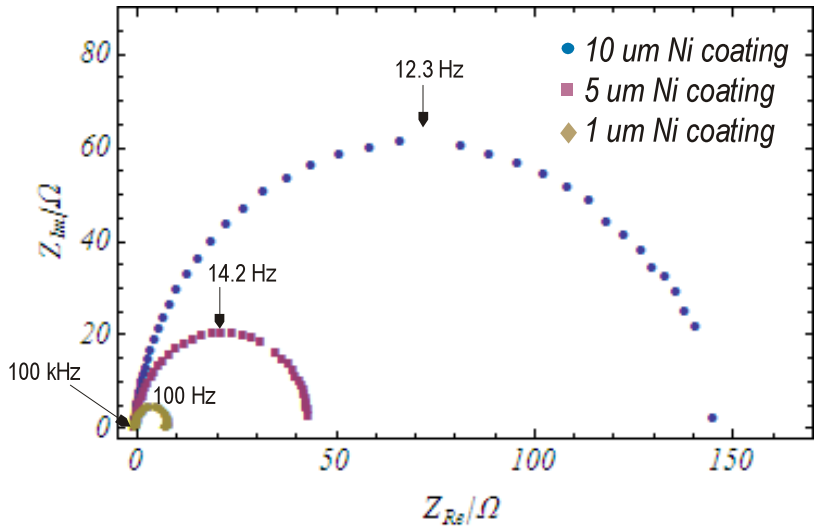

Fig.III.14. AC Impedance analysis for Ni coated carbon steel with different coating thicknesses. The experiment was performed at the open circuit potential in 1 M H_2SO_4 at room temperature; frequency ranged from 10 mHz to 10 kHz and small amplitude 5 mV was applied. Working electrode area was 5 cm^2.

Perhaps the Fe surface increased to a larger extent than Ni due to pitting. The lower value for capacitance for polished carbon steel, C_{dl}, however, may indicate a smoother surface. The samples prepared in Southampton laboratory, gave a clear trend for the diameter of the semicircles as the coating thickness increased – an increase in R_{ct}, with increasing coating thickness. As a consequence of that, the corrosion rate of the coated carbon steel decreases as the coating becomes thicker. A decreasing trend in C_{dl} as the coating thickness increases can be seen in table III.3. This may suggest changes in surface area of the plated metal as well as different thicknesses of the oxide formation. For 10 μm Ni coated carbon steel, the R_{ct} was similar to pure Ni; therefore, the corrosion properties of the coating will also be similar. Moreover, the Ni coated carbon steel supplied from CORUS (produced in the reel-to-reel plating line) was examined and the results for R_{ct} and C_{dl} are shown in table III.3. The corrosion resistance was larger than for pure Ni, but the capacitance indicates a low surface area presumably an indication of additives in the plating bath and also pressing the sample whilst electroplating (see chapter *I.Introduction* for more details). The AC impedance experiment showed that the coating thickness with a similar corrosion property to pure Ni should be 10 μm. This is a very thick deposit and for an industrial application, it can be a time-consuming and expensive deposition process.

Sample	***Deposition time/s***	***Thickness/μm***	***R_{ct}/Ω***	***C_{dj} /μF cm^{-2}***
Carbon steel (polished)	-	-	22	180
Ni coated carbon steels prepared in Southampton	300	1	5	318
	1500	5	42	266
	3000	10	145	89
Ni foil	-	-	143	227
Ni coated CORUS sample	-	3	275	31

Table.III.3. The experimental data obtained from the impedance measurement conducted at open ciruit potential in 1 M H_2SO_4. Deposition was carried out at j = -10 mA cm^{-2} from a stationary Watts bath pH 3 – 3.5.

The deposits in the parallel plate beaker cell were not entirely satisfactory:

1. It did not give good enough protection for carbon steel when electroplating thin layers, in the order of 1 μm or 2 μm.
2. The beaker cell does not mimic the reel-to reel plating line used commercially.

2.1.3. Rectangular flow cell

The electroplating conditions for Ni were modified in such a way that the electrolyte was flowing along the cathode. This modification was made to allow deposition of Ni at higher rates and to achieve a strong convection during the electroplating in a similar manner as it was performed in CORUS electroplating line. A rectangular flow cell was designed to have the electrodes facing towards each other with separation 1 cm and with the electrolyte chamber entry length 7.5 cm.

The volumetric flow ranged from 24 ml s^{-1} to 240 ml s^{-1} and the linear flow rate 6 cm s^{-1} to 50 cm s^{-1}. The Reynolds number was estimated to be in the range of 2 – 16. Those low values for the Reynolds numbers gave a laminar flow of the solution. Such a well-defined geometry and uniform solution flow will become of great importance, particularly when graphite particle composites are deposited. Two modes of mass transport are considered for a flow cell: convection – as a dominant mode of mass transport and diffusion, which always occurs close to the surface. The solution was flowing through the channel, in which the cathode and the anode were embedded into the polypropylene block to give a smooth solution flow. Upon electrodeposition, the current density and deposition charge were kept constant at -100 mA cm^{-2} and 9 C cm^{-2}, respectively. The linear solution velocity was varied from 6 cm s^{-1} to 50 cm s^{-1}. The Ni coated carbon steel electroplated with three different solution velocities is shown in fig.III.15. With the solution velocity equal to 6 cm s^{-1}, the deposit had a significant number of "black spots". Those black spots could possibly arise from hydrogen evolution occurring alongside Ni deposition as the potential is driven to more negative direction. Increasing the solution velocity from 6 cm s^{-1} to 23 cm s^{-1} and 46 cm s^{-1} (fig.III.15b and fig.III.15c), the improvement of the Ni coated carbon steel could be observed - no visible black spots and the Ni layer seemed to be complete. The electroplated Ni in the flow cell significantly affected the appearance of the coating. The Ni layer was more compact and less rough than the Ni coated carbon steel electroplated in the parallel plate beaker cell. Moreover, the quality of the deposit improved as the solution flow was equal to and larger than 23 cm s^{-1}.

Keeping the solution flow relatively high and constant, the effect of the current density was investigated. The deposition charge was also maintained constant at 9 C cm^{-2}. The appearance of the deposit under the different current densities can be seen in the fig.III.16. The electrodeposition was carried out at: -50 mA cm^{-2}, -100 mA cm^{-2} and -200 mA cm^{-2}. In all cases, the carbon steel substrate was completely covered with Ni. The deposit was free from visible pinholes or voids. The surface of the electrodeposited Ni was usually semi bright. An interesting result was observed for the Ni plated carbon steel where the current density was equal to -50 mA cm^{-2} (fig.III.16a). At this current density, the surface of the plated Ni appeared to be slightly dull than the surface of the samples electroplated with higher current densities i.e., -100 mA cm^{-2} or -200 mA cm^{-2} (fig.III.16b and fig.III.16c). The difference in brightness was subtle but distinguishable by eye on close inspection.

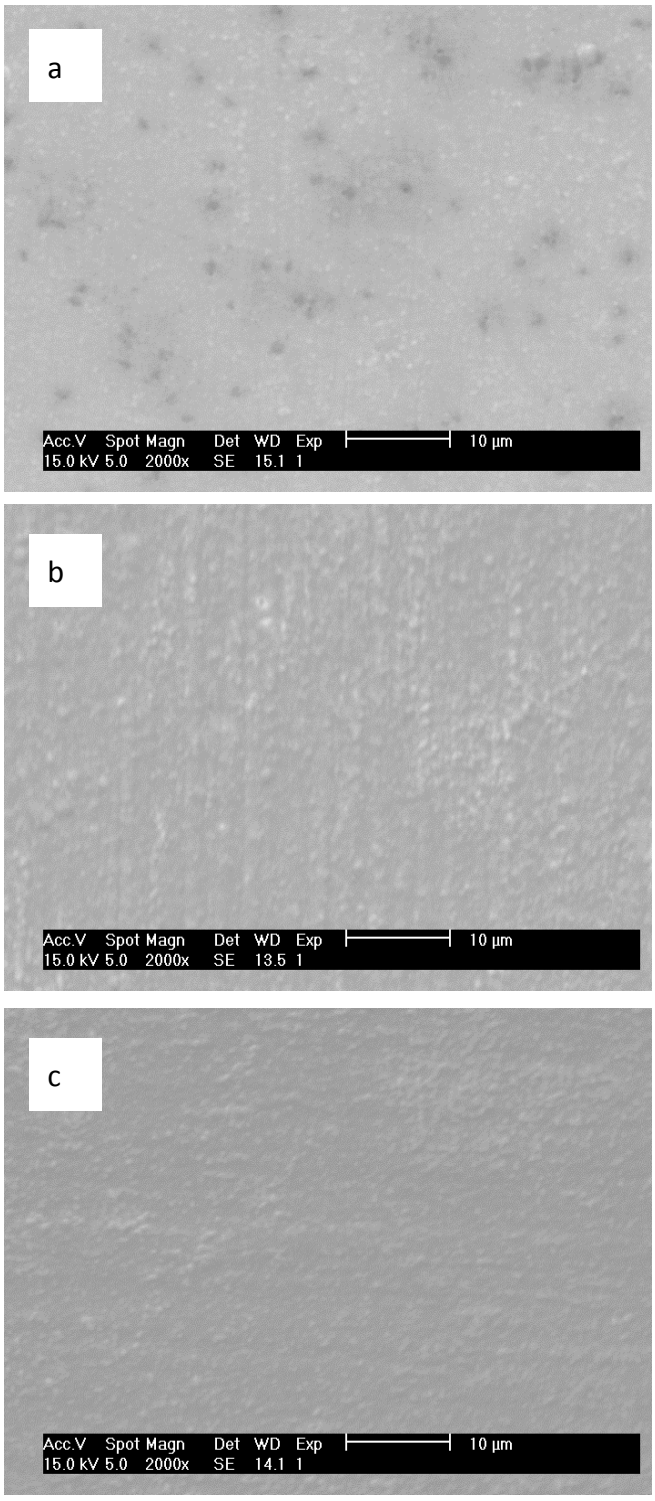

Fig.III.15. SEM picture for Ni coated carbon steel electroplated in flow cell from Watts bath, pH 3-3.5, with constant current density -100 mA cm^{-2}, deposition charge 9 C cm^{-2} and linear velocity of the solution a) 6 cm s^{-1}, b) 23 cm s^{-1} and c) 46 cm s^{-1}.

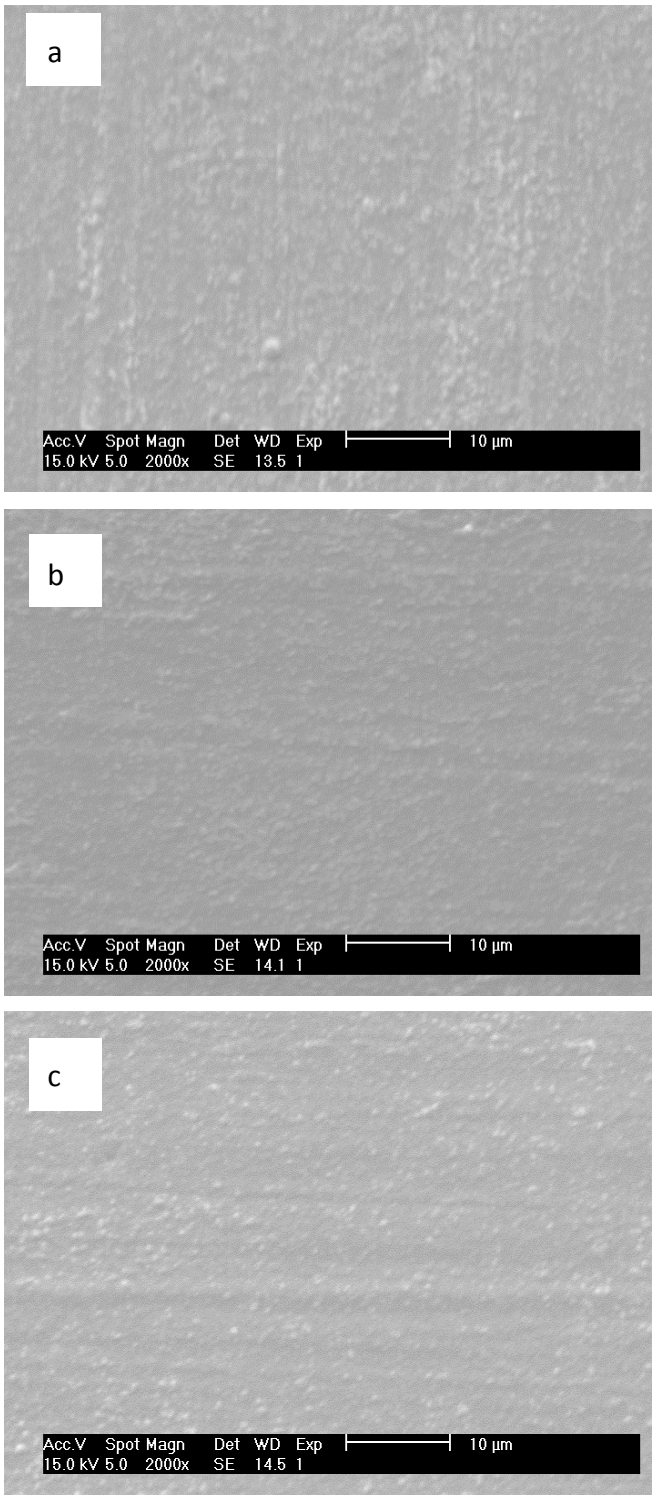

Fig.III.16. SEM picture for Ni coated carbon steel electroplated in flow cell from Watts bath, pH 3-3.5, with constant linear velocity of the solution 46.6 cm s^{-1}. Deposition charge applied was 9 C cm^{-2}, current density was a) -50 mA cm^{-2}, b) -100 mA cm^{-2} and c) -200 mA cm^{-2}.

It should also be noted that the smooth deposits were obtained in the flow cell without surfactant in the plating bath. It was found that upon addition of sodium dodecyl sulphate salt to the plating bath, foam was generated whilst flowing the solution. The foam generation in the flow system was so large that the electroplating process had to be halted. Therefore, no surfactant was used during the electroplating of Ni.

Flowing the solution along the cathode may be comparable with the commercial reel-to-reel plating line used in CORUS, Dusseldorf. The Ni coated carbon steel from CORUS was supplied directly from the production line and the sample was examined in Southampton. The electroplating conditions used in CORUS were: the minimum steel strip speed was 10 cm s^{-1}, the current density was -100 mA cm^{-2} and the solution temperature was 333 K. SEM picture of the Ni plated steel is shown in fig.III.17. This electroplated Ni coated carbon steel was somehow different to those prepared in Southampton laboratory. Smooth, white non-conductive patches of Ni and Ni grains were observed. The smooth patches may be attributed to the rolling the sample during the electroplating process. The coating also seems to be complete and compact, free from pinholes or voids.

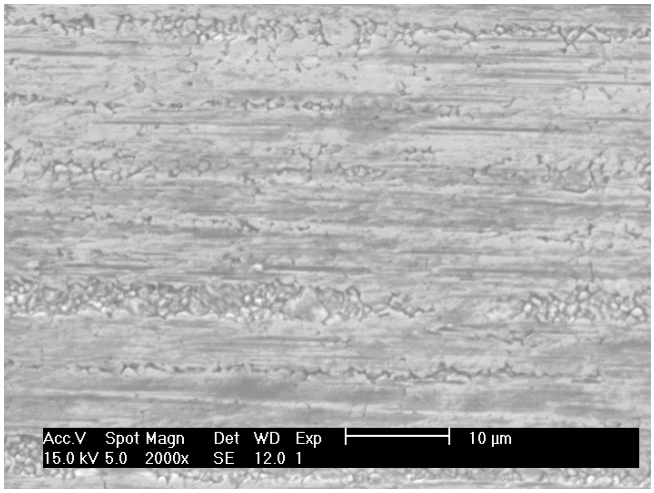

Fig.III.17. SEM pictures of Ni coated carbon steel supplied from CORUS.

Interestingly, no white patches were observed upon electroplating in Southampton laboratory and AC impedance experiment showed smoother surface. This may suggest the surface of the Ni coated carbon steel supplied from CORUS had oxidized after leaving the plating line.

2.1.4. Crystallographic structure of the deposited Ni layer

XRD analysis was performed on the Ni coated carbon steel electroplated in the flow cell with current density -200 mA cm^{-2}, deposition time 45 s and linear solution velocity 46.6 cm s^{-1}. The XRD data is shown in fig.III.18. Two very well defined peaks were seen: one peak characterises the plane (111) at two theta equal to 44 and the second peak characterizes the plane (200) at two theta equal to 53. Those peaks are those expected for the bulk structure of the deposited Ni [113]. According to the selection rules for reflection in cubic crystals, the peaks correspond to the face centred cubic (fcc) crystal structure with a centro-symmetric space group m3m [114].

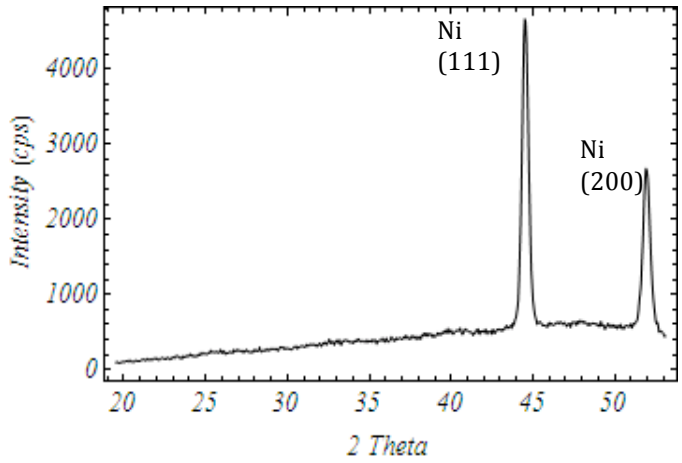

Fig.III.18. XRD analysis for Ni coated carbon steel deposited in the flow cell with the solution T = 333 K, current density j = -200 mA cm^{-2}, deposition time t = 45 s and linear solution velocity v = 46.6 cm s^{-1}.

2.1.5. Significance of the electroplating methods

Two methods of electrodeposition of Ni were presented in section 2.1.2 and 2.1.3 with different mode of mass transport to the electrode. It was found that the electrodeposition in the stationary solution (parallel plate beaker cell), could limit the full potential of the electroplating. The deposit electroplated with higher current density was rough and had a significant amount of pinholes or

pores that may lead to the substrate. The substrate therefore could be exposed to the harsh environment, which triggers very good conditions for an accelerating corrosion process. The porosity of the coating depends also on the thickness of the deposited metal, as it was clearly indicated in the AC impedance experiment. In order to have a good corrosion resistant layer, a very thick coating, of the order of 10 μm, should be deposited.

Electrodeposition of Ni performed in the flow cell, on the other hand, mimicked the reel-to-reel electroplating line and therefore it was possible to apply higher current densities. Moreover, the solution flow was a crucial factor during the electroplating. The example of the effect of solution flow during the electroplating was shown in fig.III.16a. Black spots were observed while the linear velocity of the solution was 6 cm s^{-1}, and constant current density -100 mA cm^{-2}. The surface of the coating became free from faults, when the solution velocity was increased above 20 cm s^{-1} and only smooth and continuous layer of Ni was seen. The quality of the deposit was strongly depended on the current density and to a certain extends, on the solution flow. Moreover, unlike in the parallel plate beaker cell, the quality of the deposited Ni in the flow cell was comparable to the Ni electroplated in the CORUS plating line.

2.2. Corrosion of the Ni coated carbon steel under fuel cell conditions

At the cathode side of the bipolar plates, where the oxygen is fed and the potential is more positive, the corrosion of this component is most likely to occur. Moreover, there is also a possibility of the membrane decomposition, introducing another uncertainty factor to the corrosion of bipolar plates.

Since carbon steel corrodes much more rapidly than Ni (see section *III.1. Metallic substrates for bipolar plates*) in the simulated positive electrode environment, the Ni deposit should be continuous and pit free in order to impede the corrosion rate. It is worthwhile to emphasize that the protective coating for bipolar plates will consist of several layers superimposed on each other. Here the attention will be drawn to the first protective layer, which is the Ni electroplated onto carbon steel. The final coated bipolar plate must have a corrosion current density < 0.01 μA cm^{-2}

in the cell operating conditions; the Ni coated carbon steel is unlikely to meet this requirements but the corrosion current should be as low as possible.

In order to test the quality of deposits, a one-hour corrosion test was performed for the Ni coated carbon steels. The electrolyte mimicked the conditions at the cathode side in the fuel cell, i.e., sulphate medium with 2 ppm NaF, pH 4 at T = 333 K and the samples were tested in the three-electrode cell (see experimental chapter *II.4. Electrochemical cells*), where the working electrode was the Ni coated carbon steel, the secondary electrode was Pt mesh with mesh area 1 cm^2 and potential was measured versus Hg/Hg_2SO_4 reference electrode. The potential applied to the cell was similar to the potential at the cathode side in the fuel cell i.e., 0.0 V vs. Hg/Hg_2SO_4 (+0.65 V vs. SHE). The current response was monitored with respect to time. The corrosion test for the Ni coated carbon steel electroplated in the parallel plate beaker cell without and with surfactant is shown in fig.III.19a and fig.III.19b. The corrosion test for the Ni coated carbon steel fabricated in the flow cell is shown in fig.III.19c. In addition, the CORUS Ni coated carbon steel electroplated in the reel-to-reel plating line was tested and the results are compared in the fig.III.19c. The Ni coated carbon steel from fig.III.19a was deposited from pure Watts' bath with no surfactant addition. The coating thickness was estimated to be 2 μm (see sample from fig.III.11a). At the beginning of the test, the corrosion current density was low and in the range of few μA cm^{-2}. After about 90 s, the current density increased rapidly to the value of several mA cm^{-2} and after 250 s, the current density continued to increase with a slower rate than at the first 90 seconds. The electrolyte was creeping through the pores in the coated steel into the substrate, giving rise to a rapid increase in corrosion current density. At the current density of approximately 30 mA cm^{-2}, a plateau was achieved. Such a high current density corresponds to the dissolution of the carbon steel (see chapter *III.1.Metallic substrate*). This current density is equivalent to a uniform corrosion rate of 30 mm $year^{-1}$. The experiment shows a large porosity in the Ni coated carbon steel. Indeed, the AC impedance experiment confirmed those results and clearly, the coated steel with 2 μm Ni layer was not ideal protection for the carbon steel substrate. A different response can be observed when small amount of sodium dodecyl sulphate salt (SDS) was added to the electroplating medium. Fig.III.19b reports the current-time response for the Ni coated carbon steel with addition of 400 mg dm^{-3} surfactant. The corrosion current was very low and in the range of tens of μA cm^{-2}. After an initial period, the current density decreased to the value of 20 μA cm^{-2}

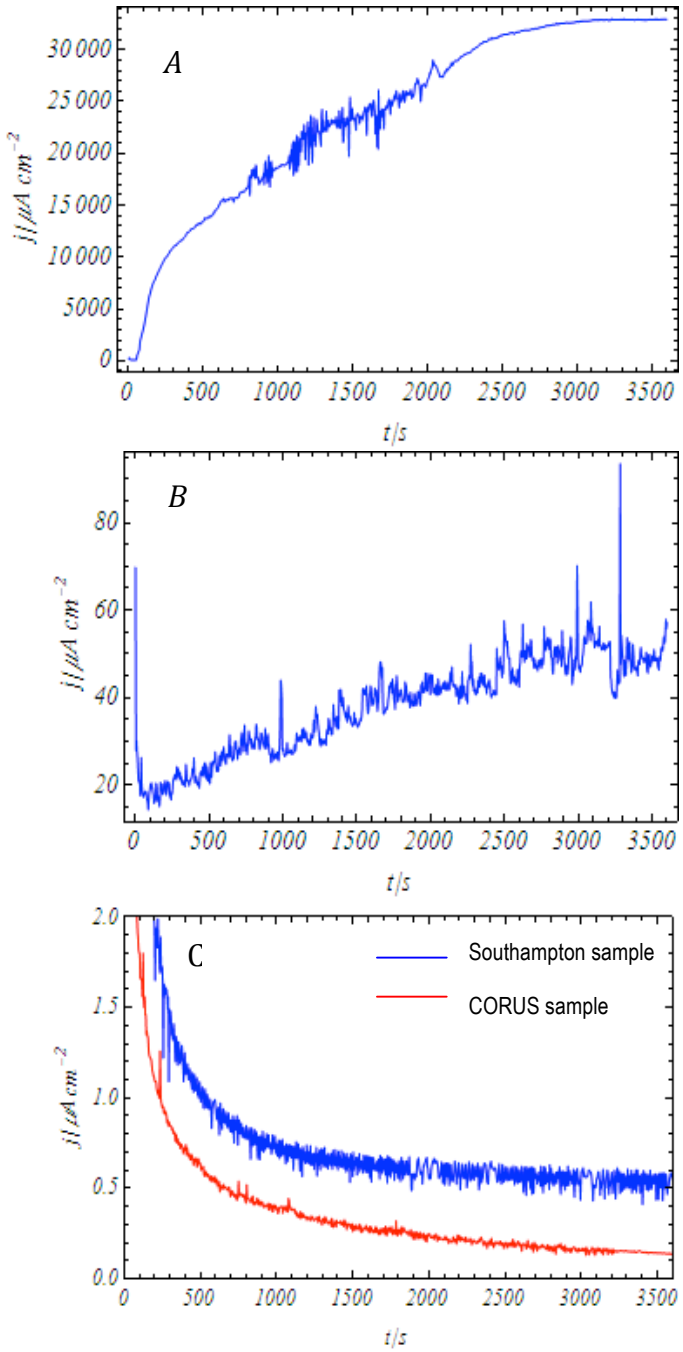

Fig.III.19. One-hour corrosion test at 0.0 V vs. Hg/Hg_2SO_4 in sulphate medium, pH 4 at T = 333 K for Ni coated carbon steel with coating thickness 2 μm, electroplated with j = -10 mA cm^{-2}, charge density 6 C cm^{-2}, A) without surfactant, B) with addition of 400 mg dm^{-3} of SDS, and C) Ni coated carbon steel electroplated in the flow cell, coating thickness 3 μm with j = -100 mA cm^{-2}, charge density 9 C cm^{-2}. Corrosion test for the CORUS sample was also shown in the plot C) - sample from fig.III.17. The solution was saturated with N_2 and N_2 was passed over the solution surface whilst experiment was running.

and then slowly started to increase to 45 μA cm^{-2}. After 3000 s, a plateau at about 45 μA cm^{-2} was observed. The addition of surfactant strongly influenced the quality of the deposited layer. Indeed, large improvement in corrosion current was observed, however the magnitude of the corrosion current was still not satisfactory. Fig.III.19c shows the corrosion test for the Ni coated carbon steel prepared in the rectangular flow cell and for the CORUS sample from the fig.III.17. It can be seen that the corrosion current in all cases was below 1 μA cm^{-2}. The samples prepared in the flow cell had a much better coverage by Ni of the steel. It is worthwhile to stress again that the corrosion current recorded for the Ni foil (see fig.III.3) was in the range of 0.5 μA cm^{-2} to 0.9 μA cm^{-2}. The corrosion current for the Ni coated carbon steel prepared in the flow cell (blue curve, fig.III.19c) was slightly larger than for the CORUS Ni coated steel (red curve, fig.III.19c). One of the possible explanations for this was a difference in surface roughness for each sample, which was attributed to a different method of the samples fabrication. The CORUS sample was rolled and pressed during the electroplating. This led to a smoother surface; hence, the corrosion current was lower. At this stage of fabrication of the bipolar plates, it is very important that the coated surface must be smooth with minimum roughness possible. Moreover, the oxide film formation on the Ni coated carbon steel is unwanted product that may decrease the electrical contact between bipolar plates and the MEA. Therefore, the condition that satisfies the first protective layer should be: the coating with minimum possible thickness, which is complete and relatively smooth.

According to the corrosion tests presented above, it can be concluded that 1) the choice of electroplating conditions for the deposition of Ni is vital, 2) the minimum coating thickness that prevents steel substrate from further degradation should be 3 μm. The rectangular flow cell seems to be promising electroplating cell for the Ni deposition. It was also found that the electroplating conditions should be: solution temperature 333 K, current density in the range of -100 mA cm^{-2} to -200 mA cm^{-2}, the linear solution velocity equal to or more that 20 cm s^{-1}. Those conditions were clearly close to the industrial electroplating and could satisfactory be introduced for the deposition of Ni. Therefore this sample will be further used as a substrate for the Ni-graphite layer and the flow cell with this electroplating conditions will be used to fabricate series of Ni coated carbon steel substrates.

2.3. Electrodeposition of Ni-graphite composites

A Ni-graphite composite was the next layer for the proposed steel-based bipolar plates intended to minimize contact resistance between the bipolar plate and the catalyst layer of the MEA. CORUS routinely produce Ni-graphite coated steel for a different application. The graphite content in the solution for the production of the Ni-graphite composites was 40 g dm^{-3}. The solution was stirred with large magnetic bar stirrer in order to keep the graphite particles suspended during the electroplating. A large electroplating tank was used with two Ni anodes and the carbon steel cathode (A4 in size) to produce the Ni-graphite layer. The electroplated samples prepared in CORUS laboratory were examined in Southampton and a SEM picture for the Ni-graphite composites is shown in fig.III.20. The graphite content in the Ni-graphite composite was very high and therefore a thick multilayer with highly porous structure was observed. This structure was certainly not suitable for further modification of the Ni-graphite surface by PVD or similar technology. The "throwing power" of PVD would be insufficient to coat the metal within below the porous structure. A few important modifications were introduced to the electroplating of Ni-graphite composites. A "small" system mimicking that for reel to reel plating of pure Ni was set up during a visit by me to the CORUS laboratory and the solution was flowing between the two Ni anodes nd the carbon steel cathode with solution velocity 6 m min^{-1}. The amount of graphite in plating bath was 30 g dm^{-3} and the electroplating conditions were: current density -100 mA cm^{-2}, charge passed 3 C cm^{-2}. The Ni-graphite composite fabricated with such conditions is shown in fig.III.21. A very different surface was produced with much less graphite particles. The particle aggregation was significantly reduced and mainly isolated graphite particles in the Ni were observed. However, some aggregations were also seen and the "mountainous" structure of the surface would lead to areas unmodified by PVD in the shadow of the peaks. The amount of graphite in the plating bath was still large. The aggregations markedly influenced the surface of the Ni-graphite composite and this classified the surface to be very rough. It is believed that if the amount of graphite is decreased from 30 g dm^{-3} to 10 g dm^{-3} and the electroplating speed is maintained at the same rate, the Ni-graphite composite might have a more suitable surface for further modification. Clearly, the graphite "concentration" and hydrodynamics of the electrolyte have a strong influence. In parallel with CORUS electroplating, the Ni-graphite composites were deposited in the Southampton laboratory.

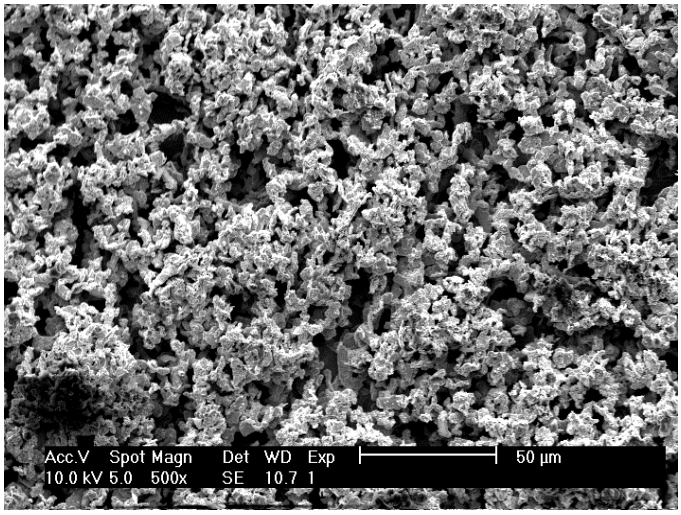

Fig.III.20. SEM picture for Ni-graphite composite prepared from the Watts bath containing 40 g dm^{-3} graphite in the solution. The composite was prepared in a beaker cell in the CORUS laboratory.

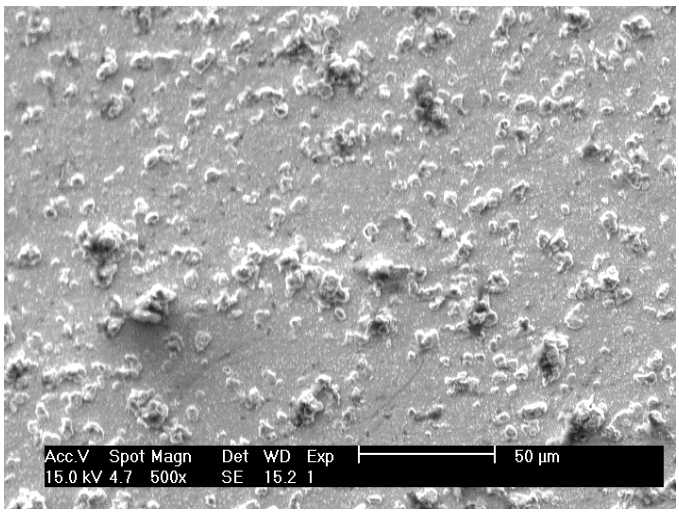

Fig.III.21. SEM picture for Ni-graphite composite prepared from the solution containing 30 g dm^{-3} graphite in the solution and electroplated onto Ni coated carbon steel in CORUS laboratory. The electroplating was carried out in a small plating line with solution flow 6 m min^{-1}.

Parameters such as the amount of graphite particles in the plating bath, current density, deposition charge, different surfactants and different methods of the solution preparation were examined. Two electroplating cells were used: the parallel plate beaker cell and the rectangular flow cell.

2.3.1. Results obtained in the parallel plate beaker cell

1. The influence of graphite size on Ni-graphite composites. The Watts bath, pH 3 – 3.5 with two types of graphite particles, MF2/99.5-99.9, 2 μm in diameter and flake graphite MF5/99.5-99, 5 μm in diameter (a detailed description of the graphite particles can be found in the experimental chapter *II.2.5. Ni-graphite composites*), were employed for electrodeposition of Ni-graphite composites. The graphite particles were thoroughly soaked in the solution and electrodeposited onto the Ni coated carbon steel. A magnetic bar stirrer was used to keep the particles suspended whilst electroplating. The graphite content used to fabricate the Ni-graphite composites was much lower than the graphite content used in CORUS experiments. The amount of graphite particles in the plating bath commenced at 10 g dm^{-3}. All the electroplated Ni-graphite composites were deposited onto Ni coated carbon steel. Preliminary experiments were conducted to deposit Ni-graphite composites in order to investigate whether the 2 μm or 5 μm in diameter graphite particles were more suitable for the application. It is worthwhile to emphasize that the aim of the Ni-graphite deposition was to electroplate a Ni-graphite layer with protruding, single graphite particles that are uniformly distributed along the surface, hence to achieve a contact resistance below 25 mΩ cm^2 upon applying pressure of 12 bars in a simulated environment in PEM fuel cell (see experimental chapter *II.3.5.Contact resistance measurement*).

Fig.III.22 presents the Ni-graphite composite electroplated with two types of graphite particles. The electroplating conditions were: solution temperature 333 K, current density -40 mA cm^{-2}, deposition charge 3 C cm^{-2}. It can be clearly seen that in both cases, single particles and aggregates were deposited on the surface but very little differences were observed upon electroplating of Ni-graphite composite with different size of graphite particles. Both materials contain a range of particle sizes and it is not clear that "2 μm particles" are smaller than the "5 μm particles". This is not surprising because upon inspection of pure graphite using the SEM (see experimental chapter *II.2.5 Ni-graphite composites*), it could immediately be seen that there was little differences in the particles' size. However, if the particles aggregations are considered, it may be convincing to use graphite particles with 2 μm diameter rather than graphite particles with 5 μm diameter, since the former tend to give smaller aggregates. Therefore, the graphite particles with 2 μm in diameter will be further used for electroplating of Ni-graphite composites.

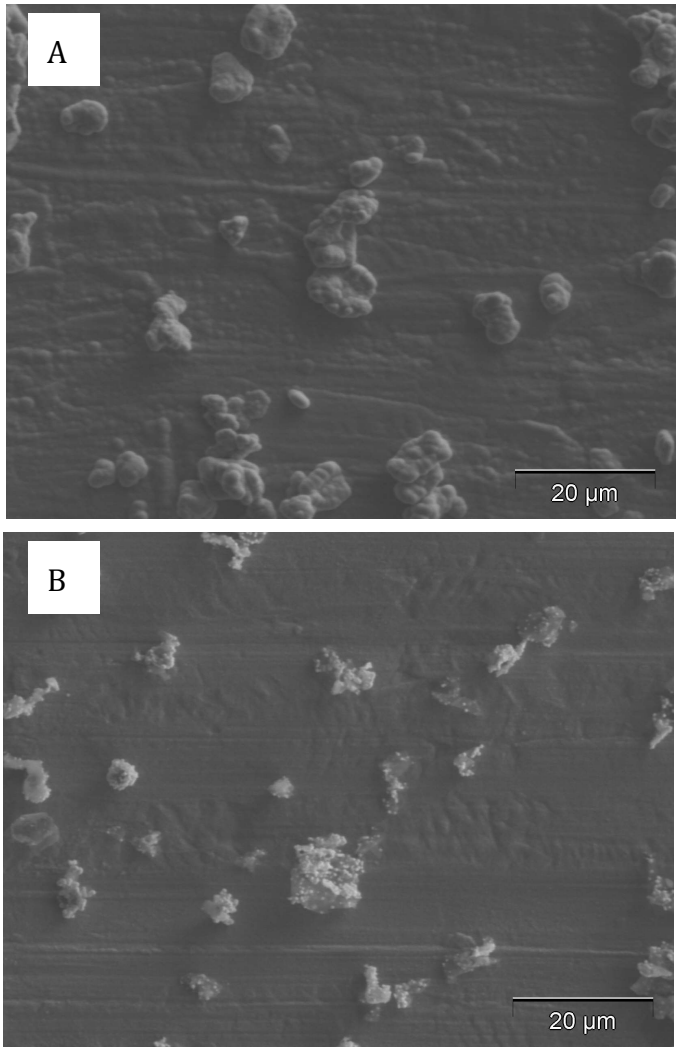

Fig.III.22. SEM pictures for Ni-graphite composites with 10 g dm^{-3} graphite in the solution, electroplated in the parallel plate beaker cell with the following conditions: solution T = 333 K, 1% DispersionMittel per gram particles, j = -40 mA cm^{-2}, deposition charge 3 C cm^{-2}, strong convection was applied using a large magnetic bar stirrer. The size of graphite particles was: A) 5 µm B) 2 µm.

In the Ni-graphite composites, it is always interesting to know to what extend the graphite particles are covered by Ni. The Ni-graphite composite was prepared onto the 904L SS substrate and this required special pre-treatment for the steel (see experimental chapter *II.2.2 Stainless steel 904L SS*). Again, 10 g dm^{-3} graphite particles in the solution were added to electroplate Ni-graphite composite. The following electroplating conditions were used: solution temperature

333 K, the solution was stirred with magnetic bar stirrer to keep the particles suspended, current density -25 mA cm^{-2}, deposition charge 3 C cm^{-2}.

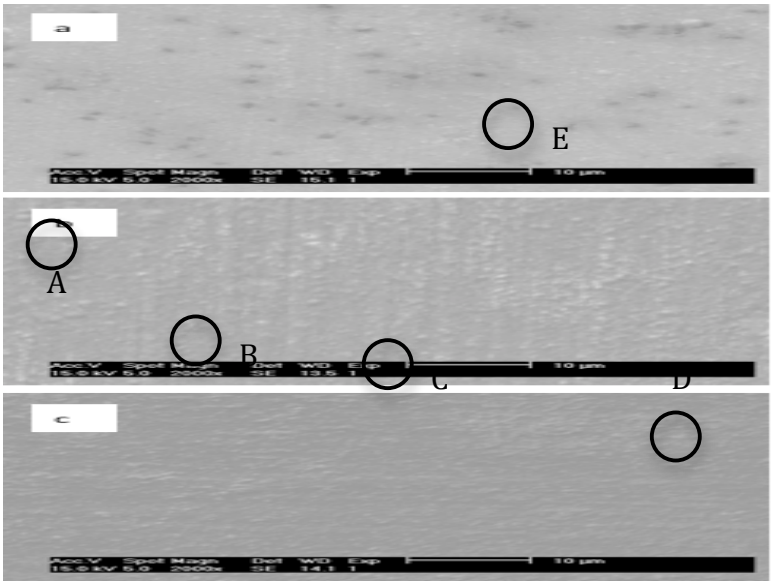

Elements	At %				
	A	B	C	D	E
C	82	-	90	49	71
Cr	0.2	5.3	0.3	3	1
Ni	17	85	9	43	26
Fe	0.8	9.7	0.7	-	2

Fig.III.23. SEM and EDX analysis for Ni-graphite composite from 10 g dm^{-3} graphite in the solution, electroplated onto 904L SS.

The table above the SEM picture shown in fig.III.23 presents EDX analysis for five points on the Ni-graphite composite electroplated onto Ni coated 904L SS. The EDX analysis allows confirmation of the inclusion of the graphite particles in the Ni layer and also the presence of the

surface where there is no graphite. The graphite particles can also be seen to have some coverage by Ni although a quantitative interpretation of the percentage of Ni must be avoided because of the uncertainty about the precise area of the surface examined by the e-beam. The observation of the some Fe and Cr results from the e-beam going through the coating.

2.The influence of current density. In a similar manner as for Ni deposition (see chapter *III.2.2.1.1. Hull cell electroplating*), the Hull cell was employed to determine a distribution of the particles in the Ni-graphite composites as a function of current density. A detailed description of the electroplating cell can be found in experimental chapter *II.4.4.Hull cell*. It should be again stressed here that the Hull cell was specifically designed, to give a broad range of current densities distribution, by tilting the cathode with respect to the anode and hence only the primary current density distribution was considered during the calculation o the current distribution. The Watts bath with 10 g dm^{-3} graphite in the solution and cationic surfactant Cetyltrimethylammonium chloride (CTAC) with concentration of 0.4 g dm^{-3} was used to electroplate the Ni-graphite composite. The electroplating conditions were: applied current was 1 A for 30 minutes, the solution temperature 333 K, the solution was stirred with magnetic bar stirrer whilst electroplating. These conditions led to rather thick deposit and, of course, the structure of the deposit (and charge density) varies with the current density across the cathode plate. The SEM analysis was conducted for different regions on the cathode as the current changes. Fig.III.24 reports four SEM pictures for the Ni-graphite composite prepared in the Hull cell. Clearly, the loading with graphite particles is always high but also increases with the current density (or charge density). At the lowest current density, i.e., -5 mA cm^{-2}, within the deposition time 30 minutes, the deposit thickness is 3 μm and the graphite particles appear as "isolated aggregates". By -50 mA cm^{-2}, the whole surface was covered by a porous graphite structure.

3. The influence of solution preparation. The Ni-graphite surface of fig.III.23 shows some aggregates and this surface topology seems likely to lead to "shadowing" in a PVD deposition and hence ineffectual protection of Ni. There is however, other important aspect that needs to be addressed here: whether it is 10 g dm^{-3} graphite or 1 g dm^{-3} graphite, an appropriate procedure for mixing particles in the solution should be applied.

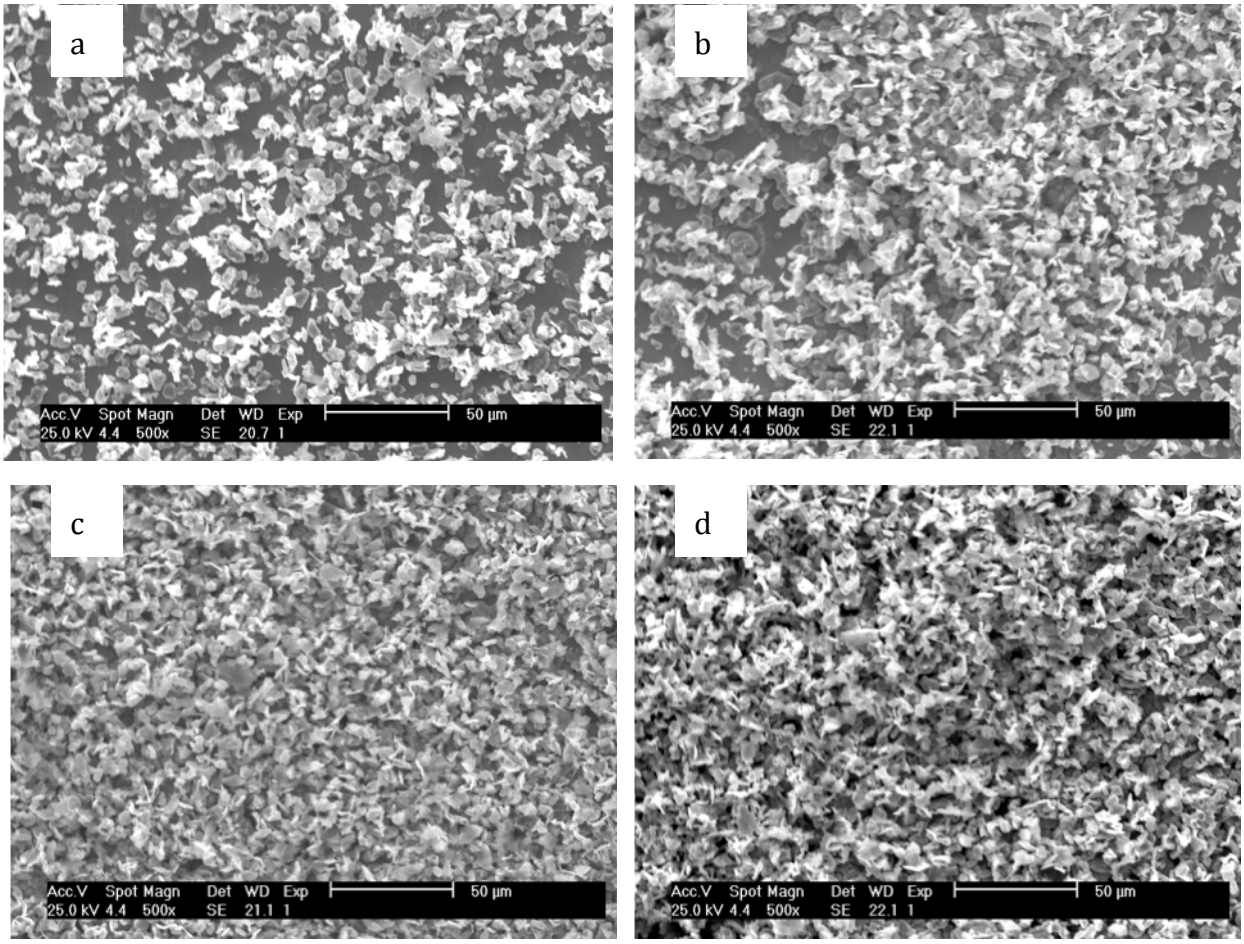

Fig.III.24. The SEM pictures for the Ni-graphite composite with 10 g dm^{-3} graphite in the solution electroplated in the Hull cell with the current density a) - 5 mA cm^{-2}, b) - 10 mA cm^{-2}, c) - 40 mA cm^{-2} and d) - 60 mA cm^{-2}.

This allows maintaining the original structure and properties of the particles. Another aspect is the influence of different surfactants in the plating bath (discussed later in this chapter). Considering the Ni-graphite solution preparation, two methods were applied:

- The graphite particles were mixed in the solution using magnetic bar stirrer. The particles dispersion took approximately 60 to 90 minutes (depending upon the amount of graphite particles) in order to completely soak with electrolyte and obtain a uniform suspension.
- The graphite particles were mixed using a fast shear blade-mixing machine – SILVERSON L4RT. The maximum rotation of the head of the machine used was 3000

rpm. The particles suspended in the Watts bath were sucked from the bottom into the fast rotating head and passed to the shear blades. When the particles passed the blades, they were dispersed in all directions into the solution. The following preparation was used employing the SILVERSON L4RT (for 1 g dm^{-3} graphite particles): a concentrated slurry consisting of 150 ml Watts bath, 1 g/l graphite particles and 0.6 % anionic surfactant DispersionMittel 01926 per gram particles was well mixed using SILVERSON L4RT machine for 20 min. The slurry then was added to the remaining 750 ml of the Watts bath and mixed for further 20 min.

Once the solutions were prepared, the electroplating was carried out under the following conditions*: j* = -10 mA cm^{-2}, deposition charge 3 C cm^{-2}, the solution temperature was 333 K and the solution was stirred with magnetic bar stirrer (with rotation 350 rpm) in order to keep the particles suspended whilst electroplating. The SEM pictures of prepared Ni-graphite composite with 1 g dm^{-3} graphite particles and with different methods of mixing graphite particles are compared in fig.III.25. The electroplated Ni-graphite composite from fig.III.25a shows a mixture of single particles and agglomerates on the surface. The aggregates were small because the amount of graphite particles in the solution was 1 g dm^{-3}. If, however, the amount of graphite was increased to 10 g dm^{-3} larger aggregates with porous structure were deposited. Considering the deposit from fig.III.25b, where the graphite particles were mixed with magnetic bar stirrer, practically, there appeared to be more single particles and less aggregation. The graphite particles mixed with magnetic bar stirrer maintained the original dimensions and its structure, i.e., it was not possible to damage the structure of the particles because the rotation of the magnetic bar stirrer was too low. Upon mixing the graphite particles with the SILVERSON L4RT machine, it is believed that the particles were milled into smaller in size whilst passing through the fast shear blades. As a result of that, more particles were suspended in the solution and deposited onto the steel cathode forming small aggregation. The deposition of Ni-graphite composites with larger amount of graphite particles (5 g dm^{-3} and 10 g dm^{-3}) was also performed with two different mixing methods and it was found that the larger amount of particles with some aggregations were formed upon mixing the graphite particles using SILVERSON L4RT machine rather than the magnetic bar stirrer. Therefore, the SILVERSON L4RT mixing machine was no longer used for the Ni-graphite solution preparation and magnetic bar stirrer was employed instead.

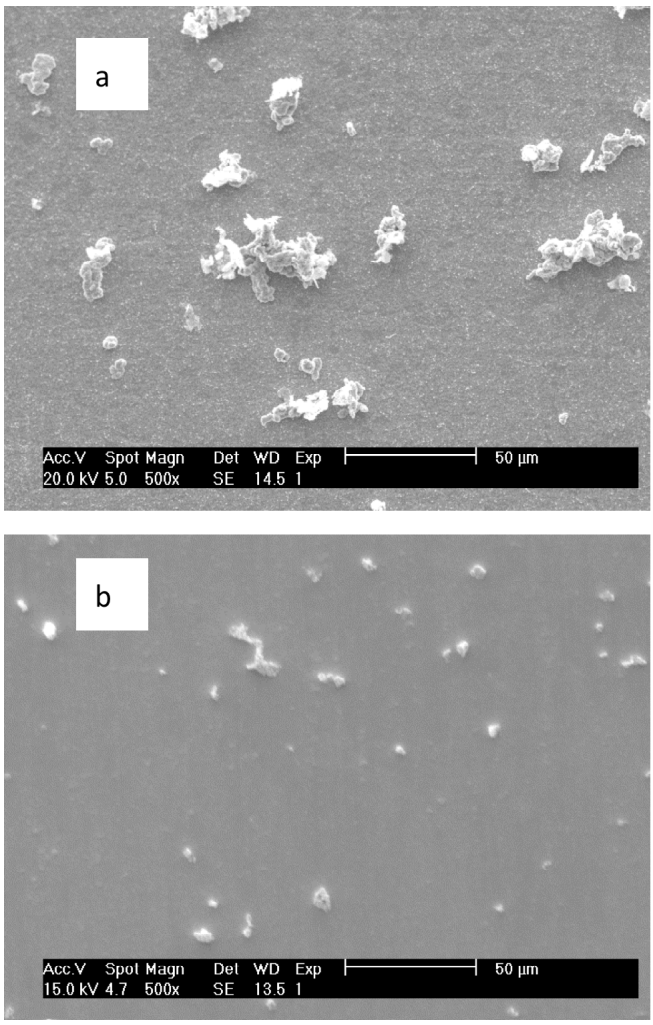

Fig.III.25. SEM pictures for Ni-graphite composites with 1 g dm^{-3} graphite in the solution, electroplated onto Ni coated carbon steel from CORUS. The suspension was prepared with two different mixing methods a) using SILVERSON L4RT, b) using magnetic bar stirrer.

4.The influence of surfactant. Another aspect, as important as the solution preparation, was the influence of different surfactants on Ni-graphite electroplating. The deposition of particles requires an addition of appropriate surfactant in the solution in order to prevent their agglomeration. Anionic DispersionMittel 01926 supplied from Dr Hesse, Germany and one of the common cationic surfactants, Cetyltrimethylammonium Chloride (CTAC) were used to study the influence of those surfactants on graphite particles in the Ni-graphite composite. The anionic DispersionMittel 01926 was developed in German laboratory, Dr Hesse, especially for the deposition of graphite particles. The Ni-graphite composites with different surfactants are shown

in fig.III.26. A 10 g dm^{-3} graphite was suspended in the Watts bath. The following electroplating conditions were used: current density -20 mA cm^{-2}, solution temperature 333 K, deposition charge 6 C cm^{-2}, the solution was stirred with magnetic bar stirrer in order to keep the graphite particles suspended in the bath. The Ni-graphite composites deposited with cationic surfactant gave large aggregates with pseudo three-dimensional growth (fig.III.26a). The particles were deposited onto each other to form complex structure. There were some regions on the cathode where no particles were deposited and bare Ni coated carbon steel was exposed.

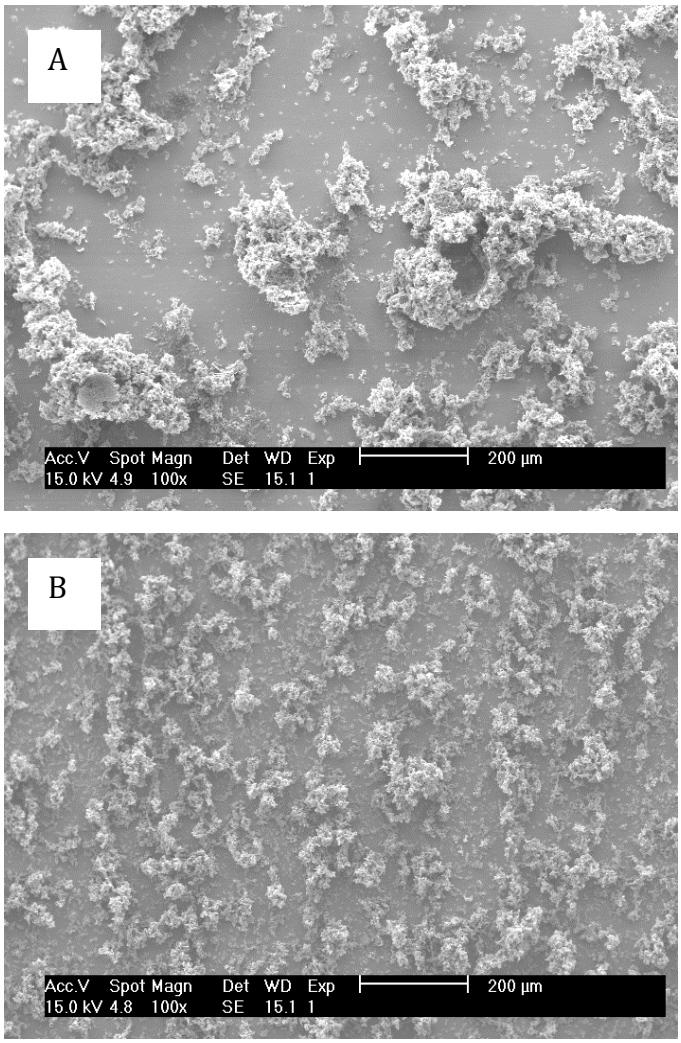

Fig.III.26. Ni-graphite composites (10 g dm^{-3} graphite in the solution) electroplated onto Ni coated carbon steel with addition of a) cationic surfactant Cetyl Trimethylammonium Chloride, b) anionic surfactant DispersionMittel 01926.The electroplating conditions were: j = -20 mA cm^{-2}, t = 300 s, the solution T = 333 K, the solution was stirred with magnetic bar stirrer, 1 mg per 1 gram particles of both surfactants was used.

In the case of Ni-graphite composites deposited with anionic DispersionMittel 01926 (fig.III.26b), less clumping was seen and the graphite particles were growing approximately uniformly over the cathode. In addition, less "free space" on the cathode among the graphite aggregates was observed. The aggregations were smaller than those, if the cationic surfactant was used. In all cases, however, the aggregates were always formed. Those results led to the use of the anionic DispersionMittel 01926 instead of cationic surfactant for further investigations of the Ni-graphite composites in order to find the optimum surfactant concentration and hence minimize the aggregations on the surface. A significant advantage of using this surfactant was that no foam was generated during the electroplating. Foam was always present when the cationic surfactant was used.

5.The influence of deposition charge. In general, the charge density for the Ni-graphite composites was kept constant in order to obtain 1 μm coating thickness onto Ni coated carbon steel with coating thickness 3 μm; however, the effect of a deposition charge can be crucial. The experiment performed in the Hull cell (see fig.III.24) showed that the effect of the current (or charge) density was a critical factor determining the appearance of the Ni-graphite deposit, therefore the current density was kept relatively low and constant. The experiment was performed on 904L SS substrate and therefore a special surface preparation was applied before the Ni-graphite deposition (see Experimental chapter *II.2.2. Stainless steel 904L*). Fig.III.27 shows the effect of charge density applied for deposition of the Ni graphite composites. It is clear that the larger the charge passed, the more deposited material was observed on the cathode. Applying 3 C cm^{-2} (fig.III.27a), a mixture of aggregated and single graphite particles was deposited on the surface. Upon applying 12 C cm^{-2} (fig.III.27b), the graphite particles formed large aggregates with pseudo three-dimensional growth. The particles growth was a dominant process and the substrate was almost completely covered with Ni-graphite aggregates. There were no single particles deposited on the cathode. The study of different parameters, which significantly influenced the quality of the Ni-graphite composites prepared in the parallel plate beaker cell, allowed the fabrication of thin layer of the Ni-graphite composites with the following conditions: different amount of graphite in the solution with fixed amount of surfactant (1 % surfactant per gram particles) in the plating bath, the graphite particles were mixed with the Watts bath using magnetic bar stirrer, current density -10 mA cm^{-3}, deposition charge 3 C cm^{-2}, the solution temperature was 333 K.

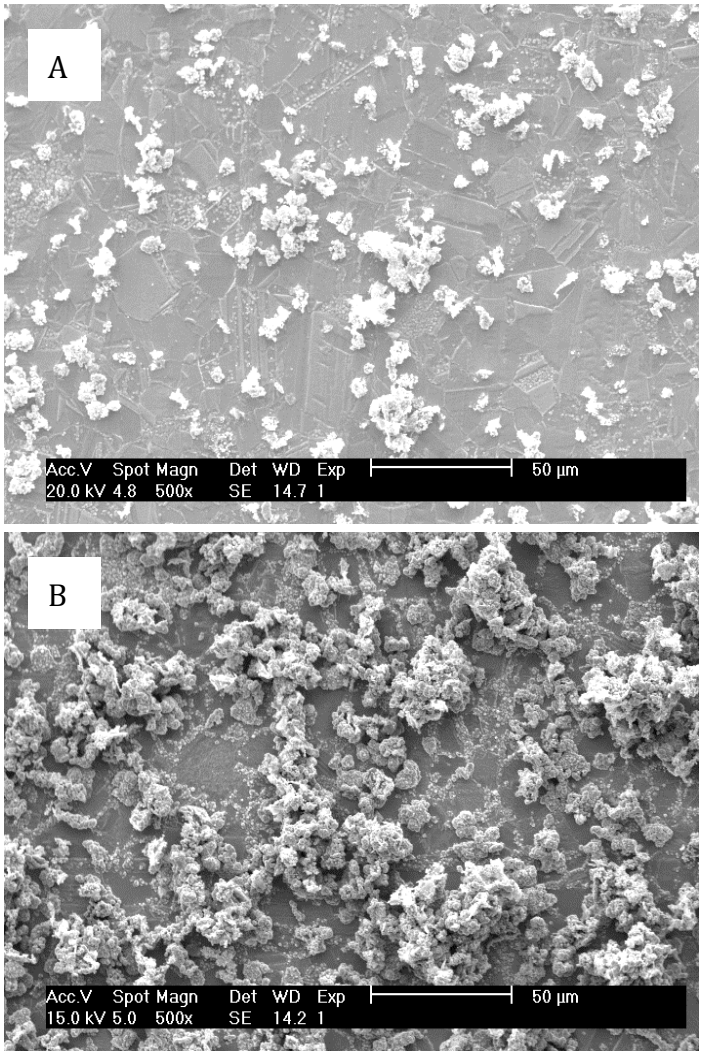

Fig.III.27. Ni-graphite composite deposited onto 904L SS with 10 g dm^{-3} graphite in the solution. The electroplating conditions were: j = -10 mA cm^{-2}, solution T = 333 K, the solution was stirred with magnetic bar stirrer, deposition charge density was A) 3 C cm^{-2}, B) 12 C cm^{-2}.

SEM pictures of the Ni-graphite composites with 1 g dm^{-3}, 3 g dm^{-3} and 10 g dm^{-3} graphite are shown in fig.III.28. It can be immediately seen that the graphite particles deposited on the cathode surface varied with the amount of graphite in the suspension whilst applying the same deposition charge. Almost no agglomeration and predominantly single particles were observed upon electrodeposition of the Ni-graphite composites with 1 g dm^{-3} (fig.III.28a). As the graphite content increased from 1 g dm^{-3} to 3 g dm^{-3} (fig.III.28b), the particles started to form aggregates and were deposited onto each other.

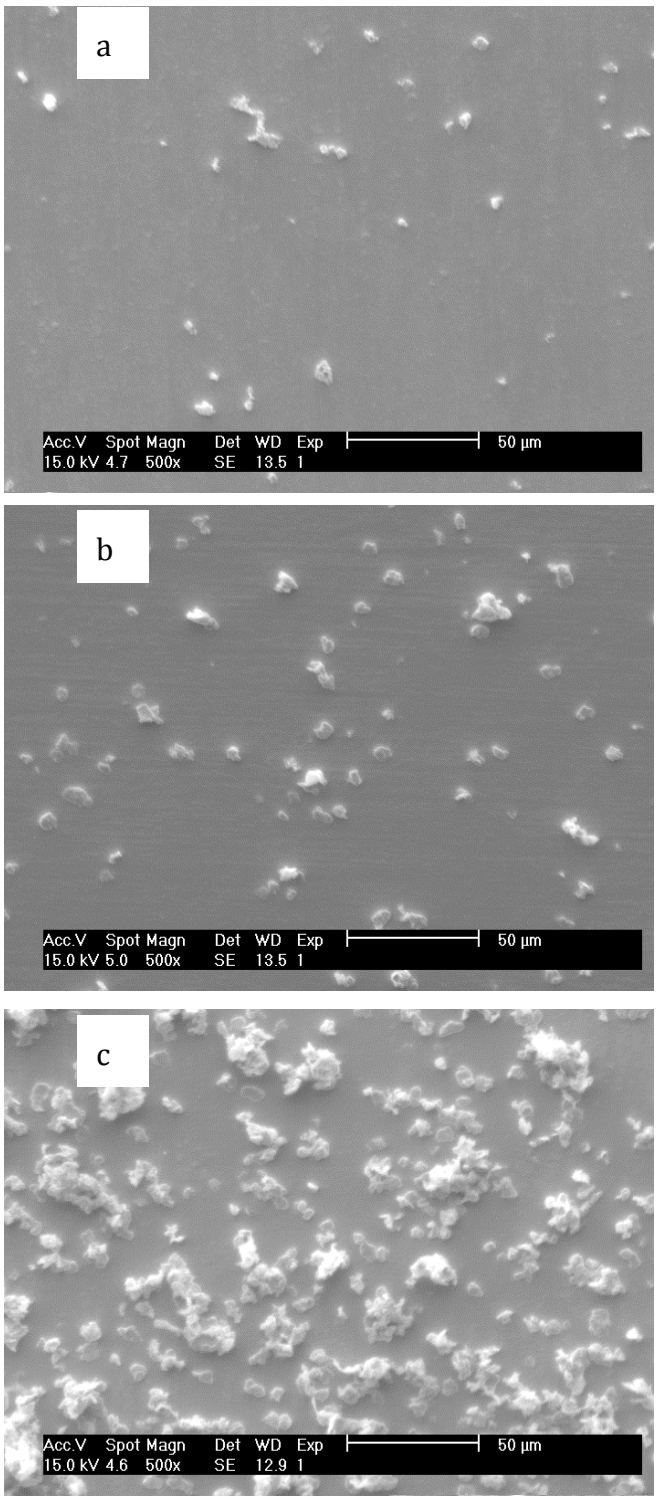

Fig.III.28. SEM pictures of Ni-graphite composites onto Ni coated carbon steel prepared in the parallel plate beaker cell. Electroplating conditions were: 1% DispersionMittel 01926 per gram particles was added, solution T = 333 K, j = -10 mA cm^{-2}, deposition charge 3 C cm^{-2}, with a) 1 g dm^{-3}, b) 3 g dm^{-3} and c) 10 g dm^{-3} graphite particles suspended in the solution.

The vast majority of the graphite particles shown in fig.III.28b were still single particles. The immediate effect of particles agglomeration can be seen in fig.III.28c. The particles started to grow onto each other forming large aggregates. 10 g dm^{-3} graphite particles seem to have a significant effect on the aggregates formation. Indeed, more particles' aggregates were observed in the Ni-graphite composite with 10 g dm^{-3} graphite than in the Ni-graphite composite with 3 g dm^{-3} graphite, even if the amount of surfactant seemed to be appropriate. Electrodposition of Ni-graphite composite with 1 g dm^{-3} graphite prepared in the parallel plate beaker cell may be considered as a successful coating in terms of single particles deposition but the distribution of particles in Ni-graphite composites needs to be examined further.

2.3.2. Results obtained in the rectangular laminar flow cell

In the flow cell, the hydrodynamics are closer to those in the reel-to-reel plating line in Dusseldorf allowing the use of higher current densities.

The 2 μm in diameter graphite particles were dispersed in the Watts bath, pH 3.5 and mixed with magnetic bar stirrer until a uniform distribution was achieved. The solution temperature was kept constant at 333 K whilst mixing the graphite particles. A 1 % by weight of surfactant per gram particles was added to the bath. The electroplating conditions were as follows: current density -100 mA cm^{-2}, charge density 3 C cm^{-2}, linear solution velocity was set constant at the value of 23.5 cm s^{-1}. Two substrates were used for the electroplating: 904L SS and Ni coated carbon steel. Fig.III.29 shows SEM pictures for the Ni-graphite composites electroplated with 1 g dm^{-3}, 5 g dm^{-3} and 10 g dm^{-3} graphite onto 904L SS and Ni coated carbon steel. The electrodeposit shows six SEM pictures: three for the Ni-graphite composites with 1 g dm^{-3}, 5 g dm^{-3} and 10 g dm^{-3} graphite particles electroplated onto 904L SS and another three SEM pictures, for the Ni-graphite composites with the same amount of graphite but electroplated onto Ni coated carbon steel. The deposits on the two substrates were very similar and clearly, the amount of graphite in the deposit increases with the graphite content in the electrolyte. Also the tendency to form aggregates decreases with low graphite content in the solution and the surface from 1 g dm^{-3} graphite in solution had the better topology for further modification by PVD. The uniformity of the deposition over the cathode plate is also important.

904L SS substrate

Ni coated carbon steel substrate

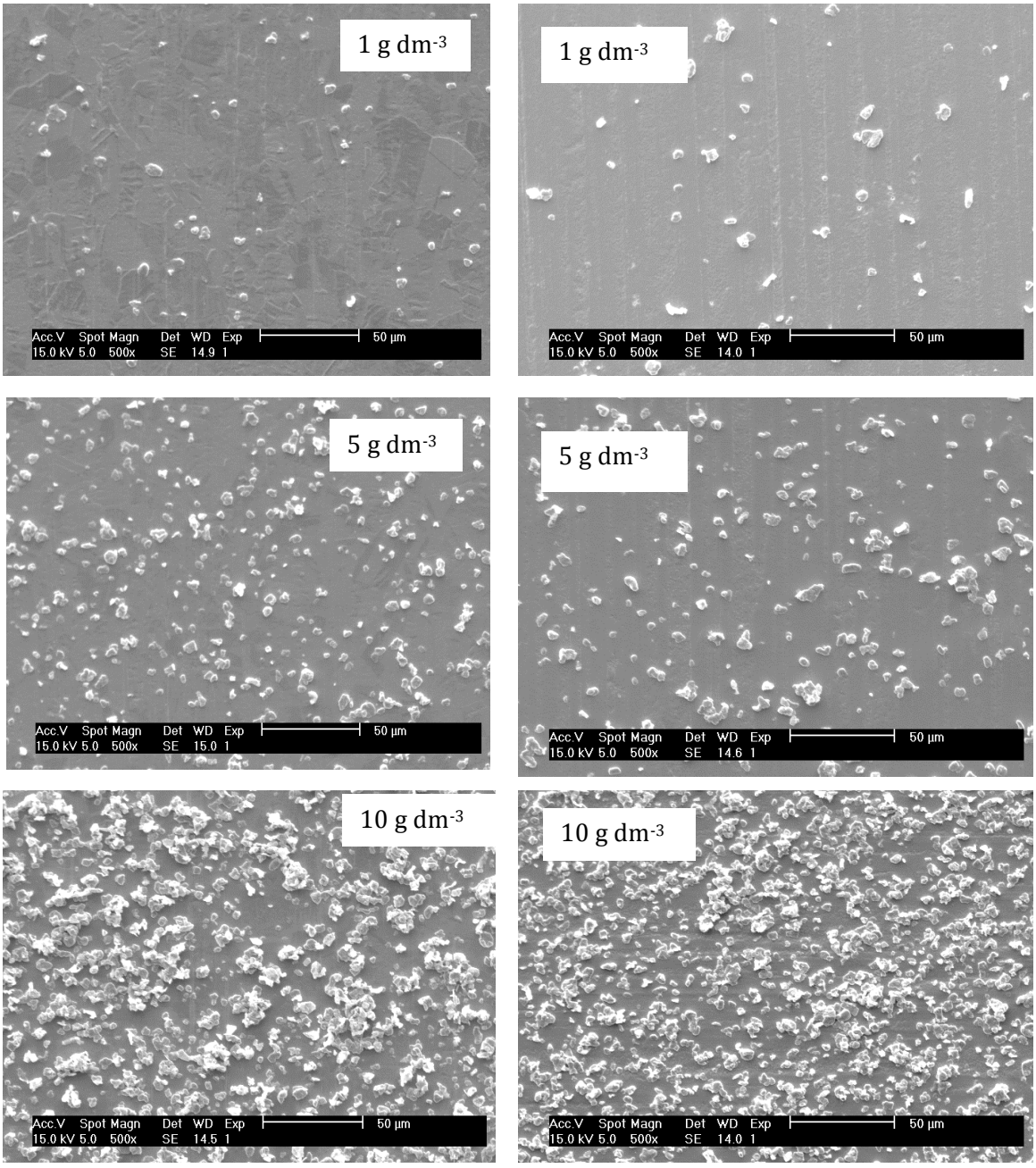

Fig.III.29. SEM pictures for Ni-graphite composites electroplated onto 904L SS and Ni coated carbon steel (prepared in the flow cell) with different amount of graphite particles in the solution. The electroplating conditions were: j = -100 mA cm^{-2}, t = 30 s, solution T = 333 K and linear solution velocity v = 23.5 cm s^{-1}.

Fig.III.30 shows schematically the regions of investigation performed on the Ni-graphite composites. The SEM pictures for those five regions are shown in fig.III.31. Every time the electroplating was preformed, the distribution of graphite particles on the cathode was reproducible. The particles distribution was relatively uniform in all five regions investigated. This was not observed upon electroplating in the parallel plate beaker cell, however for 1 g dm^{-3} graphite in the Ni-graphite composite very little and almost no aggregation was observed in both electroplating cells. The electroplated Ni-graphite composites with 5 g dm^{-3} and 10 g dm^{-3} graphite in the solution also gave uniform particles distribution but the particles started to form aggregates as the graphite was increased in the plating bath. Fig.III.32 presents SEM pictures for the Ni-graphite composites electroplated onto Ni coated carbon steel with different graphite content in the solution at two different flow rates. The pictures were taken from the middle of the cathode although there were no differences, which region was considered. The Ni-graphite composites were electroplated with two linear solution velocities: 12 cm s^{-1} and 23.5 cm s^{-1}. Indeed, the amount of graphite particles, where the solution was flowing with 12 cm s^{-1} seems to be larger than the amount of graphite where the solution velocity was 23.5 cm s^{-1}. For example, in the Ni-graphite composite with 1 g dm^{-3} graphite electroplated with the solution velocity 12 cm s^{-1}, 12 particles were seen, whereas for the same deposition but with the linear solution velocity 23.5 cm s^{-1}, 9 particles were detected. However, for the 10 g dm^{-3} graphite particles in the electrolyte some particles agglomerations were seen upon flowing the solution with both velocities but there was more aggregation with slow flow rate.

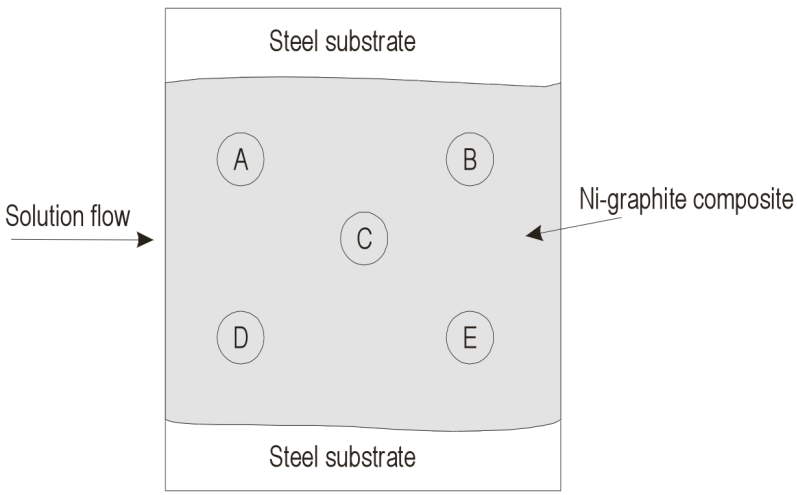

Fig.III.30. A diagram of the sample electroplated in the flow cell. Five regions on the Ni-graphite coated sample were investigated. A detailed SEM analysis for each region is shown in fig.III.30.

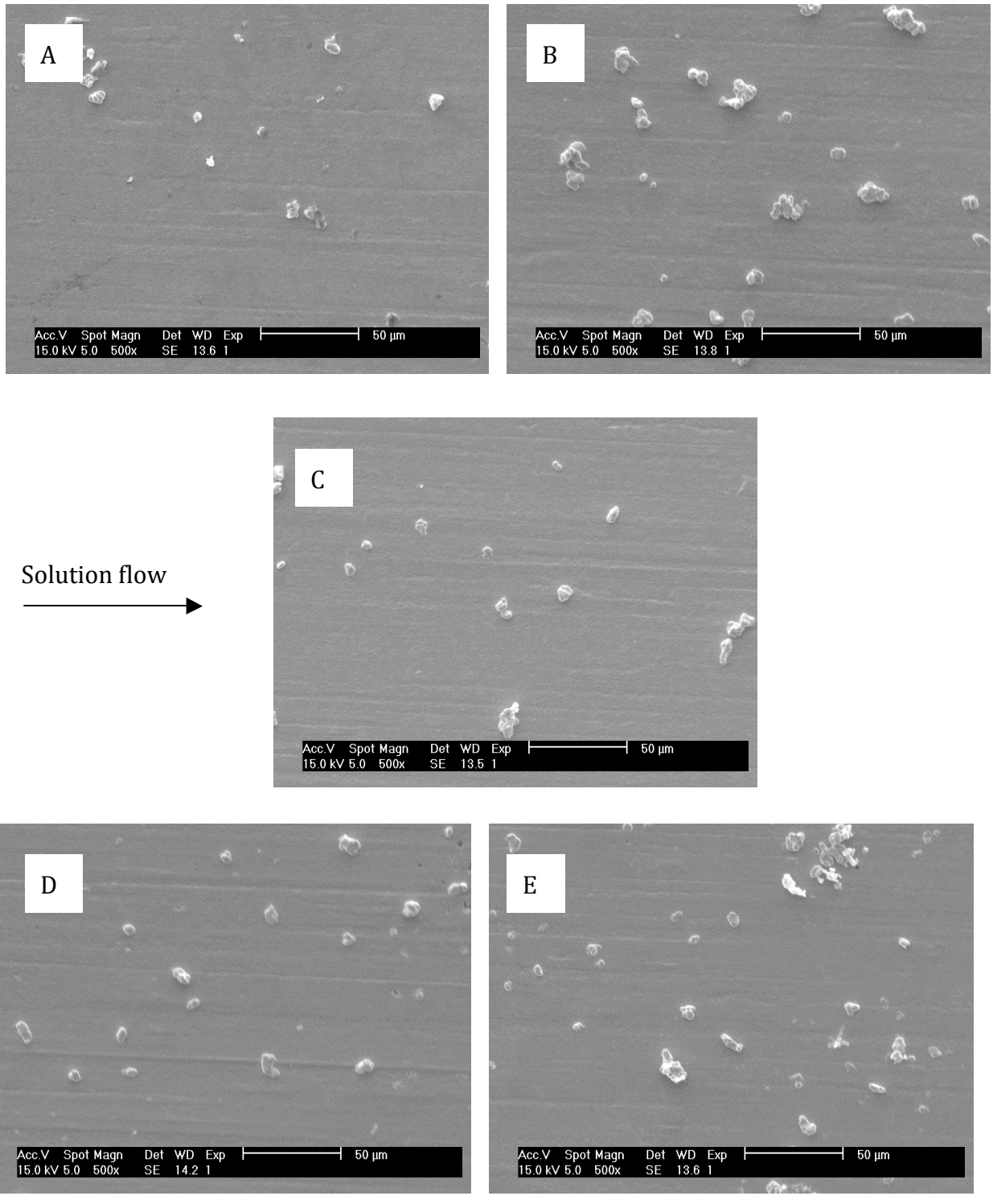

Fig.III.31. SEM pictures for Ni-graphite composite with 1 g dm^{-3} graphite electroplated onto Ni coated carbon steel (linear solution velocity was 23.5 cm s^{-1}). The pictures were taken from five regions on the cathode presented schematically in fig.III.40.

v_1 = 12 cm/s

v_2 = 23.5 cm/s

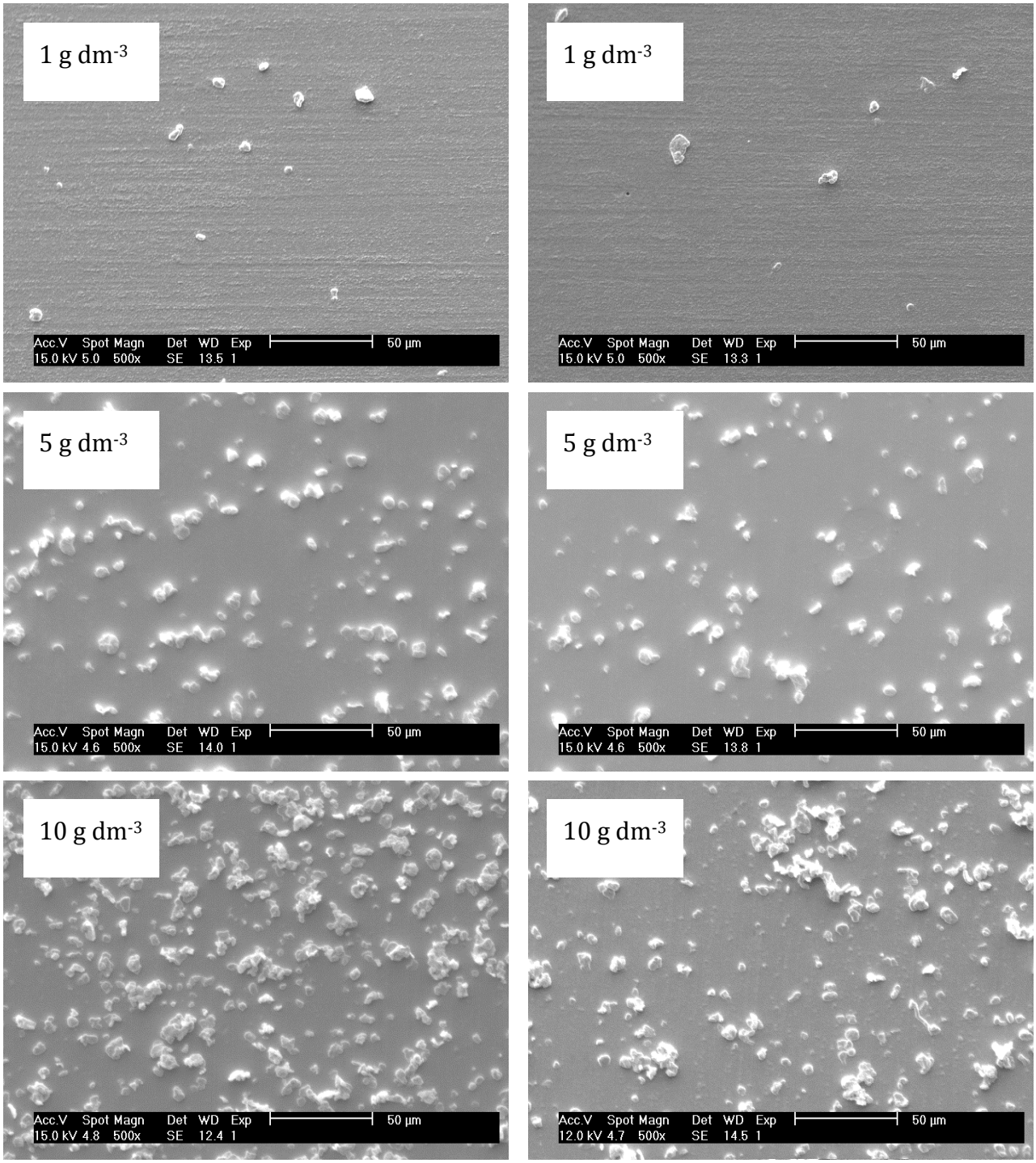

Fig.III.32. SEM pictures for Ni-graphite composites onto Ni coated carbon steel with different graphite content electroplated with different linear solution velocity.

2.3.4. Contact resistance measurement for bipolar plates

The electrical contact between the bipolar plates and catalyst layer of the MEA is critical in determining the output voltage of the fuel cell. Bipolar plates conduct electrons and feed the current to the external circuit. Therefore, the conductivity must be very high. The aim of the project was to fabricate the bipolar plates with acceptable low contact resistance below 25 mΩ cm^2 under the simulated gas pressure of 12 bars in the fuel cell stack.

Three Ni-graphite composites were chosen to measure the contact resistance: the Ni-graphite composites with 0.5 g dm^{-3} graphite, 5 g dm^{-3} graphite and 10 g dm^{-3} graphite - both sides of the samples were coated with the Ni-graphite layer (see table.III.5) in order to give good contact on both sides of the bipolar plate. In fact, the Ni-graphite composites were prepared in the early stage of the Ni-graphite fabrication and the deposits would resemble that for instance, shown in fig.III.25a. As a result, the deposits contained more graphite than those shown in fig.III.31 and there were more aggregations but the trend was similar. The test for the contact resistance was performed in the CORUS laboratory, Ijmuiden, Holland with different pressure applied to the samples. The equipment for contact resistance was described in experimental chapter *II.3.5. Contact resistance measurement*.

The carbon paper, used to mimic the gas diffusion layer in the fuel cell, was placed on both sides of the sample and sandwiched between the sample and the press. The measured samples area was 16 cm^2. The pressure commenced at 2 bars and increased to 40 bars. Upon increasing the pressure, the reading was performed each time. The values for contact resistance, measured in mΩ cm^2, are shown in table.III.6. As the pressure increases, the contact resistance for all the samples decreases. At the low pressure, i.e. 2 bars, the contact resistance measurement for the Ni-graphite composite with 0.5 g dm^{-3} graphite was two times higher than for the Ni-graphite composite with 10 g dm^{-3} graphite. This was not surprising because there were more “contact points” in the Ni-graphite composites with 10 g dm^{-3} graphite than in the Ni-graphite composite with 0.5 g dm^{-3} graphite. Increasing the pressure further to 40 bars, there were almost no differences for all the Ni-graphite samples and the contact resistance measurement gave very low values in the range of 3 – 5 mΩ cm^2. In the simulated PEM fuel cells, the pressure of gasses is about 12 bars. By comparing the pressure applied to the samples with the contact resistance measurement, it can be seen that all our samples meet the target resistance.

Sample number	Sample	Details
1	1 μm layer Ni-graphite with 0.5 g dm^{-3} graphite	Both sides coated with Ni-graphite composite
2	1 μm layer Ni-graphite with 5 g dm^{-3} graphite	Both sides coated with Ni-graphite composite
3	1 μm layer Ni-graphite with 10 g dm^{-3} graphite	Both sides coated with Ni-graphite composite

Table.III.5. Ni-graphite coated 904L SS samples used for the contact resistance measurement.

Pressure /bars	Sample number		
	1	2	3
2	30	26	15
6	7	14	8
12	4	9	4
17	5	8	2
20	4	8	3
26	4	9	4
32	5	4	5
28	4	6	4
40	3	5	3

Table.III.6. Contact resistance measurement (in $m\Omega$ cm^2) for three samples presented in table.III.5.

In addition to that, the Ni-graphite composites with graphite content ranged from 0.5 g dm^{-3} to 10 g dm^{-3} under the simulated pressure in the fuel cell may be satisfactory fabricated as a layer to increase the conductivity. It was shown in the previous section that the surface of the Ni-graphite composites with graphite content higher than 1 g dm^{-3} was rough and certainly not suitable for further modification by PVD. The only 1 g dm^{-3} graphite content was found to be acceptable in the Ni-graphite composite for further surface modification. Based on the results shown in the table III.6, and considering the range of graphite in the Ni-graphite composites measured for the contact resistance, the Ni-graphite composite with 1 g dm^{-3} graphite is included in the range of graphite investigated and hence, it may also be classified for the contact resistance measurement as a successful deposit.

2.3.5. Corrosion of Ni-graphite composites

Although the Ni-graphite layer was intended to improve contact resistance measurement to be graphite layered gas diffusion layer, it must also be stable to corrosion. The bipolar plates coated with two layers: Ni coated 904L SS steel with coating thickness 3 μm and the Ni-graphite composite with coating thickness 1 μm, electroplated on top of the Ni base, were examined in sulphate medium with 2 ppm NaF, pH 4 at 333 K. The solution was saturated with N_2 prior to experiment and N_2 was passed over the solution surface whilst experiment was running. The Ni-graphite composites were prepared in the flow cell with the current density -100 mA cm^{-2}, deposition charge 3 C cm^{-2} and with the linear solution velocity 23.5 cm s^{-1}. The only samples examined were prepared in the flow cell because the distribution of graphite particles in the Ni-graphite composites was uniform and the electroplated layers were found to be more compact. Three-electrode cell was employed with the Ni-graphite coated bipolar plate as a working electrode; Pt mesh electrode with mesh area 1 cm^2 as a secondary electrode and the potential was measured versus Hg/Hg_2SO_4 reference electrode. Fig.III.33 reports three voltammograms recorded for the Ni-graphite composites with 1 g dm^{-3}, 5 g dm^{-3} and 10 g dm^{-3} graphite in sulphate medium, pH 4 at 333 K. In addition, a voltammogram for the Ni coated carbon steel is also compared in the same figure. Large anodic peaks positive to -0.5 V vs. Hg/Hg_2SO_4 were observed for all Ni-graphite composites and the current increased with graphite particles.

No corresponding cathodic peak in the reverse scan was seen although the hydrogen evolution current towards the negative limits increased with graphite particles. The charges under the peak for the Ni-graphite composites with 1 g dm^{-3} and 5 g dm^{-3} graphite may be compared with deposition charge of approximately 44 mC cm^{-2} and 162 mC cm^{-2}, respectively. Those charges correspond to the dissolution/deposition of 16 nm and 60 nm of Ni layers, respectively. Clearly, either the graphite is corroding or much of the Ni has dissolved.

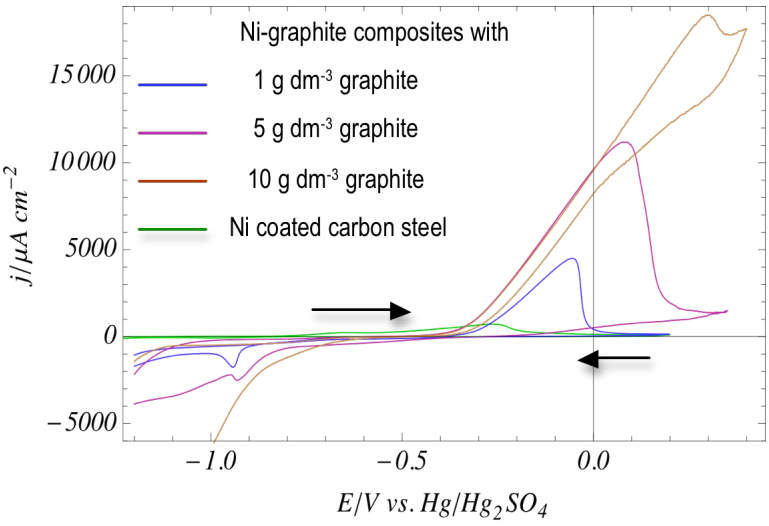

Fig.III.33. Cyclic voltammograms recorded for the Ni-graphite composites with different graphite content in the solution. The surface was scanned with 20 mV s^{-1}. The sulphate medium, pH 4 at T = 333 K was saturated with N_2 and N_2 was passed over the solution surface whilst experiment was running.

Various papers consider the corrosion mechanism for graphite in different media [115], [116] and [117]. In order to understand further the corrosion of graphite, 2 μm graphite particles were sprinkled onto a Pt surface and the potential was scanned from negative -1.2 V vs. Hg/Hg_2SO_4 to positive +0.2 V vs. Hg/Hg_2SO_4. The voltammogram is shown in fig.III.34. No anodic and cathodic peaks were observed upon scanning the potential from positive to negative values. The substantial anodic current may be attributed to the charging current for the high area graphite electrode.

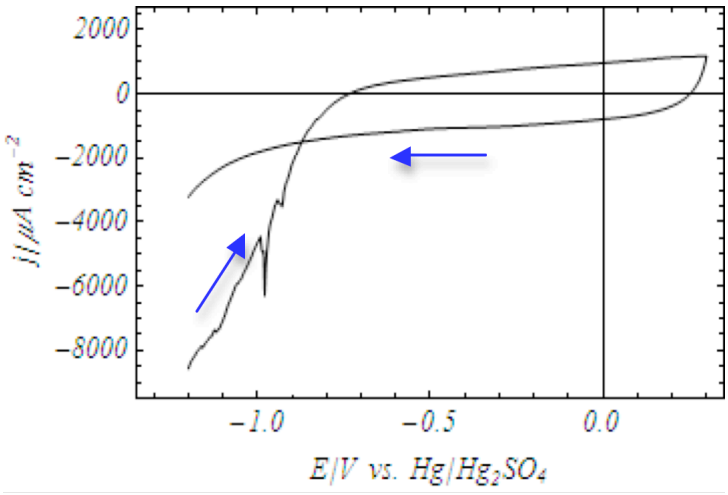

Fig.III.34. Voltammogram for graphite particles sprinkled onto Pt surface.Scan rate 20 mV s^{-1}. Sulphate medium, pH 4 at 333 K was saturated with N_2 and N_2 was passed over the solution surface whilst experiment was running.

Therefore, the surface area of the Ni-graphite composite was much increased with respect to the Ni layer.

In order to further investigate the corrosion of the Ni-graphite layer, one-hour test was performed in a similar manner as for the Ni coated carbon steel (see chapter *III.2.2 Corrosion of Ni coated carbon steel with and without heat treatment*) at the potential similar to cathode potential in the fuel cell. Again, a three-electrode cell described earlier was employed for the corrosion tests with the same solution. The corrosion current responses at the end of one-hour test, j_{3600}, for the Ni-graphite composites prepared with different amount of graphite in the solution are listed in table.III.7. In addition, the dependence of the corrosion current for the Ni-graphite composites on the solution flow is also included.

The magnitude of the corrosion current for the Ni-graphite composites electroplated with solution velocity 12 cm s^{-1} was larger than for the Ni-graphite composites electroplated with solution velocity 23.5 cm s^{-1}. Those results were not surprised because the amount of graphite particles deposited on the surface with the solution velocity 12 cm s^{-1} was larger than the amount of particles deposited with 23.5 cm s^{-1} (see fig.III.32). Clearly, the Ni-graphite composites with larger than 1 g dm^{-3} graphite content, gave relatively high value for the corrosion current and therefore

Ni-graphite composites	Linear solution velocity 12 cm s^{-1}	Linear solution velocity 23.5 cm s^{-1}
	$j_{3600}/\mu A\ cm^{-2}$	$j_{3600}/\mu A\ cm^{-2}$
1 g dm^{-3} graphite	2	0.4
5 g dm^{-3} graphite	2	4.5
10 g dm^{-3} graphite	21	5.5

Table.III.7. The current-time responses for the Ni-graphite composite with different graphite content in the solution prepared in the flow cell with two different linear solution velocities.

those sample are likely to corrode faster on the cathode side of the bipolar plate in the PEM fuel cell. The lowest corrosion current was noted for the Ni-graphite composite with 1 g dm^{-3} graphite in the solution electroplated with solution velocity 23.5 cm s^{-1}. Interestingly, the voltammograms shown in the fig.III.33 gave a large current density at the simulated potential in the PEM fuel cell, whereas a low current density was recorded within the one-hour corrosion shown in the table.III.7.

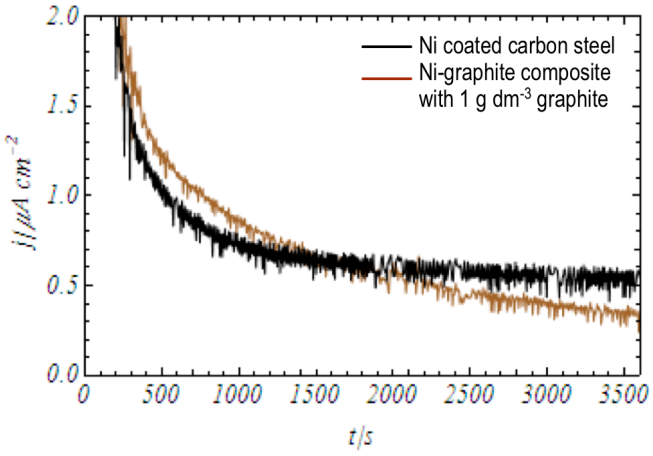

Fig.III.35. Current-time responses or the Ni coated carbon steel and Ni-graphite composite with 1 g dm^{-3} graphite in the solution. Both layers were electroplated in the flow cell with linear solution velocity 23.5 cm s^{-1}.

This sample, parallel with the Ni coated carbon steel is compared in the fig.III.35. The result clearly illustrate similar transients for both samples - very low current density in the range of 0.4 to 0.6 μA cm^{-2}. The Ni-graphite composite with 1 g dm^{-3} graphite in the solution, not only had an acceptable surface for further modification (see SEM picture in fig.III.35), but may also be successfully deposited with little concern about the corrosion susceptibility. Therefore the following structure can be proposed for the metallic bipolar plates: a protective Ni base with coating thickness 3 μm and a 1 μm layer of the Ni-graphite composite with 1 g dm^{-3} graphite in the solution to increase the conductivity between the bipolar plate and the MEA. Although the corrosion current was similar to the corrosion of Ni coated carbon steel, the magnitude of the corrosion current was still high. It is important to emphasize that the aim of the final coated bipolar plate is to decrease the corrosion current density down to 0.01 μA cm^{-2}. There is a need, therefore to deposit another protective layer on top of the Ni-graphite composite in order to further impede/decrease corrosion current and enhance the life of the bipolar plate.

2.4. Ni-Cr alloy

The Ni-Cr alloys, in particular Ni alloyed with approximately 20% Cr have received considerable attention because of their excellent corrosion resistance in many environments [118], [119], [120]. Here, the attention will be drawn to a preparation of the Ni – Cr alloy as a thin protective layer intended to be deposited onto the Ni-graphite layer. Two methods for the Ni-Cr alloy deposition were investigated: physical vapour deposition (PVD) and electrodeposition from a sulphate bath.

2.4.1. Ni-Cr alloy prepared by physical vapour deposition (PVD)

The deposition chamber and the procedures for PVD were described in The Experimental chapter *II.4.7 Physcial Vapour Deposition* and *II.5.2 Physical Vapour Deposition Procedures*. It is worthwhile to emphasize that the alloy was deposited from two independent sources: Ni and Cr sources at an angle of 120° with respect to each other and the metals were combined in the form

of two wedges over the 10 x 10 array to give an alloy composition on each electrode that needs to be determined by EDAX. The emphasis was put on the composition of the alloy rather than the thickness, however the estimated thickness was approximately 20 nm. Several Ni-Cr arrays with the maximum Cr range from 0 to 100 at. % Cr were deposited onto a 10 x 10 electrochemical array. In addition, pure Ni was uniformly deposited onto a 10 x 10 array with thickness of approximately 100 nm. Preliminary experiments in 1 M NaOH solution at room temperature were conducted before sulphate solution with 2 ppm NaF, pH 4 at 333 K, was used. From the experiment point of view, the tests performed in 1 M NaOH at room temperature were an interesting "bridge" before the experiments were conducted in more aggressive and less understood medium.

In all experiments, a specially designed three electrode cell with the working electrode a 10 x 10 array, the Pt mesh counter electrode and the Hg/Hg_2SO_4 reference electrode was employed (for more detailed description of the cell, see The Experimental chapter *II.4.3. Cells with working area below 1 cm^2*).

Nickel array. The first set of experiments was performed on the 10 x 10 array with only Ni deposited uniformly over the array with thickness of approximately 100 nm. In this experiment, reproducibility for each electrode and the possibility to deposit a smooth (on an atomic scale) Ni layer was investigated.

Voltammograms with scan rates of 20 mV s^{-1} and 100 mV s^{-1} were recorded for the Ni array in 1 M NaOH solution at room temperature. The voltammograms for 100 electrodes are shown in fig.III.36a and an example of one voltammogram is presented in fig.III.36b. The charge ratio of the cathodic to anodic peaks for the 100 electrodes is shown in fig.III.37 and further data are reported in table III.8. The blank responses in the fig.III.36 indicate no electrical contact with those electrodes due to mechanical damage to the contact network.

The presentation of the 100 voltammograms from fig.III.36a allows the conclusion that all the active "Ni electrodes" in the array behaved essentially in the same way: the voltammograms featured the symmetrical anodic peak in the forward scan and symmetrical cathodic peak on the reverse scan. Such reproducibility is crucial to the combinatorial approach to the study of corrosion.

a)

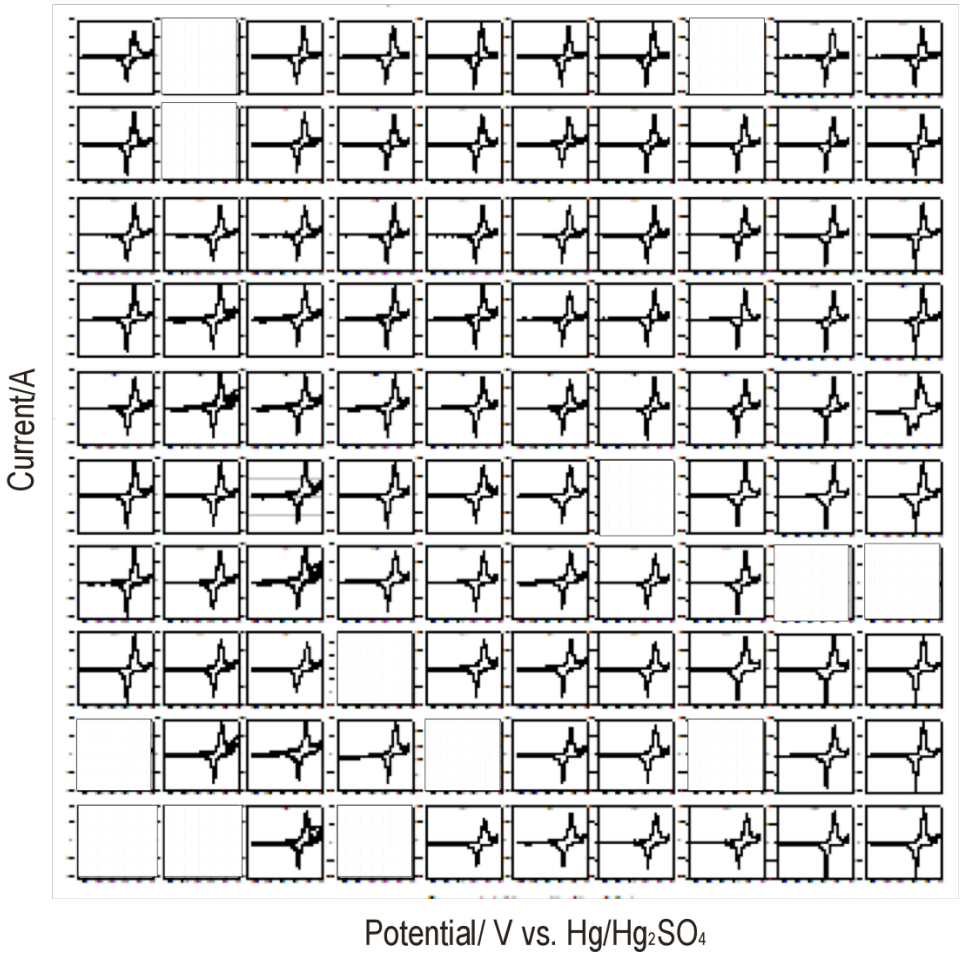

b)

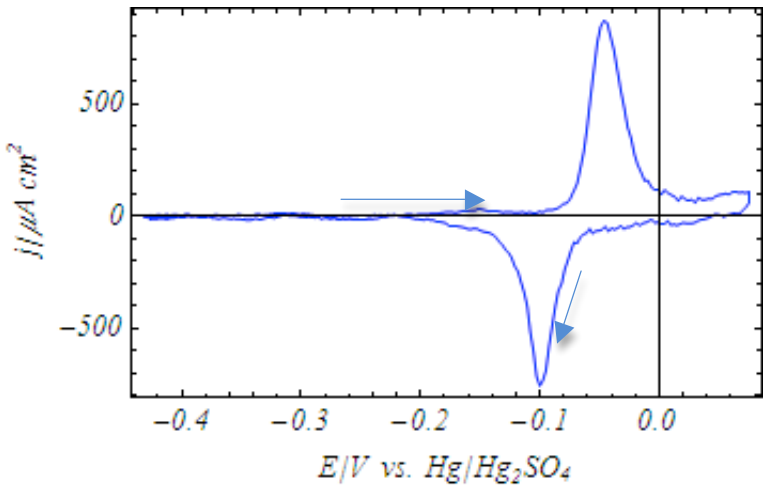

Fig.III.36. Cyclic voltammograms recorded for the Ni deposited onto a 10 x 10 Au array: a) representation of 100 voltammograms, b) one chosen voltammogram. The surface was scanned from -1.2 V vs. Hg/Hg_2SO_4 at 20 mV s^{-1} in 1 M NaOH at room temperature.

Expanding individual responses allows more detailed analysis of the curves and comparison of each voltammogram, hence analyzing one of the voltammograms from the fig.III.36a, the anodic peak commencing at potential -0.09 V vs. Hg/Hg_2SO_4 is symmetrical implying the conversion of surface layer. The current density reached maximum, 900 $\mu A\ cm^{-2}$ at a peak potential of -0.05 V vs. Hg/Hg_2SO_4 and then decreased to a very low value (see fig.III.36b). On the reverse scan, a symmetrical cathodic peak was again recorded. It is known from the literature [121], [122], [123], [124], [125], that when Ni is contacted by a hydroxide solution it covers spontaneously with a thin layer of $Ni(OH)_2$. The anodic peak corresponds to the oxidation of the $Ni(OH)_2$ layer to a higher oxidation state oxide, generally written:

$$Ni(OH)_2 + OH^- - e^- \rightleftharpoons NiO(OH) + H_2O \qquad (1)$$

and the cathodic peak corresponds to the reverse reduction process.

Further analysis of the voltammogram shows that:

1) The anodic peak current density was proportional to the scan rate: for the scan rate 20 $mV\ s^{-1}$, the peak current density was 900 $\mu A\ cm^{-2}$ and for the scan rate 100 $mV\ s^{-1}$, the peak current density increased five times (see table.III.8).

2) The charges under the anodic and the cathodic peaks were similar and about 1.8 $mC\ cm^{-2}$ and independent of scan rate. This value implied conversion of a few monolayers of oxide on an atomically smooth surface or a single monolayer on slightly rough surface (one monolayer of an atomically smooth surface corresponds to the charge of about 0.1 – 0.2 $mC\ cm^{-2}$). In addition, the cathodic to anodic charge ratio was estimated for the all electrodes and the results are reported in the fig.III.37. Little variation was seen.

3) Second cycle was identical to the first scan one confirming that the oxidation of the metal hydroxide is chemically reversible.

4) The anodic and cathodic peak potentials (peak separation) suggested that the electrochemical reaction was irreversible. If the anodic peak was a mirror image of the cathodic peak, i.e., the potential peak separation was zero, then the reaction would be reversible. However this was not the case and the anodic and cathodic peak were separated from each other. The potential separation between the peaks was 50mV for

the scan rate 20 mV s^{-1} and approximately 80 mV for the scan rate 100 mV s^{-1}. Therefore, the peak potential is a function of scan rate.

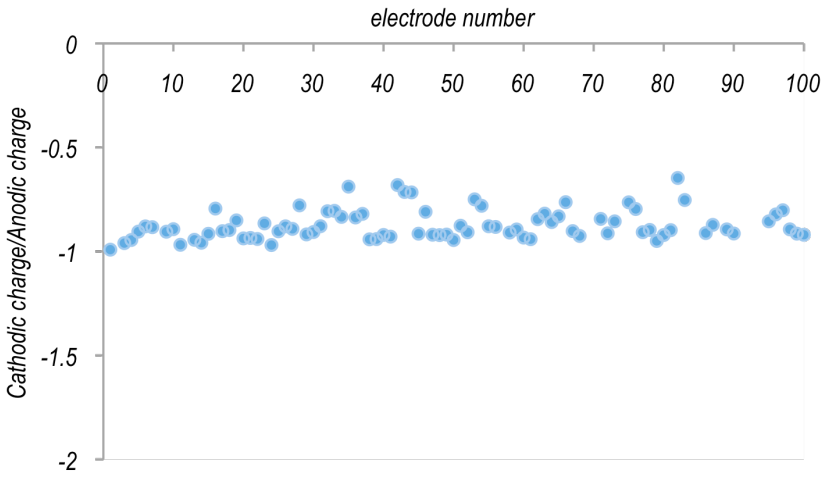

Fig.III.37. Ratio of the anodic to the cathodic charge density for 100 electrodes (except the blank electrodes – see fig.III.40).

Scan rate / mV s^{-1}	***j_{anodic}/μA cm^{-2}***	***E_{anodic}/V vs. Hg/Hg_2SO_4***	***$j_{cathodic}$/μA cm^{-2}***	***$E_{cathodic}$/ V vs. Hg/Hg_2SO_4***
20	+900 ± 51	-0.040 ± 0.009	-815 ± 60	-0.092 ± 0.006
100	+4519 ± 215	-0.018 ± 0.007	-4064 ± 289	-0.101 ± 0.008

Table.III.8. Anodic and cathodic current and potential peak characterization for two different scan rates. The values with its errors were averaged from 100 electrodes except for those, in which the electrical contact was uncertain (see fig.III.36 blank electrodes).

The experiments for Ni confirm the reproducibility of the responses across the array. Not surprisingly the responses were similar to those obtained for bulk Ni in1 M NaOH with scan rate 20 mV s^{-1}. The charge under the anodic peak for bulk Ni was larger, approximately 2.5 mC cm^{-2}.

This happened because the surface of bulk Ni was slightly rougher than the surface of the Ni deposited by the PVD.

Ni-Cr array. The Ni-Cr alloy deposited onto 10 x 10 array was next studied and the Ni-Cr alloy with the Cr content across the 100 electrodes detected by EDAX is shown in fig.III.42. The amount of Cr varied from 21 to 69 at. %. The stability of the Ni-Cr alloy was investigated initially in 1 M NaOH solution. It is important to emphasize that the Ni-Cr array was studied in the as deposited state without heat treatment. Hence, the structure was either in an amorphous or metastable phase, i.e., the alloy was not crystallized, as the commercial Ni-Cr alloys.

The 100 voltammograms recorded for the Ni-Cr alloys with scan rate 20 mV s^{-1} are shown in fig.III.38 together with atomic percent of Cr corresponding to each alloy. Clearly, some trend can be observed in the first scan. With low Cr content, between 20 at. % and 40 at. %, well-defined anodic peaks occur in the forward scan and a small cathodic peak on the reverse scan was seen. The charge balance for the anodic and cathodic reaction was not equal. More charge passed in the anodic process than in the cathodic suggesting the surface reaction was at least partially irreversible. As the Cr content increased from 40 at. % to 69 at. %, a “triangular-like” shape of the voltammgrams was observed. The anodic current density was increasing as the potential was scanned more positive and no peaks were observed. The cathodic peak on the reverse scan became smaller with increasing Cr content and eventually was negligible with the highest Cr content.

Three voltammograms from the fig.III.38 were chosen for expansion in order to analyze in more detail the surface reactions of the Ni-Cr alloy with different Cr content. The first and the second scan for the Ni – 22% Cr, Ni – 54% Cr and Ni – 69% Cr are shown in fig.49A, B and C, respectively. With 22 at. % Cr in the Ni-Cr alloy (fig.III.49A) the first scan gave two anodic peaks and one cathodic peak. The surface scan started from -0.4 V vs. Hg/Hg_2SO_4. The current density was rather high at the beginning of the scan, approximately 90 $\mu A\ cm^{-2}$ and increased even higher to 500 $\mu A\ cm^{-2}$ upon increasing the potential to -0.1 V vs. Hg/Hg_2SO_4. A large charge in this potential region, 3.7 mC cm^{-2} was observed. The first anodic peak was recorded at the potential of -0.04 V vs. Hg/Hg_2SO_4 suggesting oxidation of nickel hydroxide.

At % of Cr in the Ni-Cr alloy

37	34	33	34	30	30	26	31	22	23
40	43	36	33	35	33	30	26	28	30
47	36	37	40	36	37	34	29	32	29
49	45	41	40	38	36	37	37	34	31
44	49	43	43	40	41	35	38	35	34
48	47	56	41	39	41	39	40	37	36
54	54	49	44	46	39	41	39	39	37
59	53	51	44	46	52	44	40	42	37
69	57	63	56	50	51	45	43	43	41
63	63	57	54	54	55	49	44	44	45

Fig.III.38. Cyclic voltammograms with scan rate 20 mV s^{-1}, recorded for the Ni-Cr alloy onto 10 x 10 array in 1 M NaOH and percentage of the Cr in the Ni-Cr alloy corresponding to each electrode, detected by EDAX. The initial potential was -1.2 V vs. Hg/Hg_2SO_4.

A)

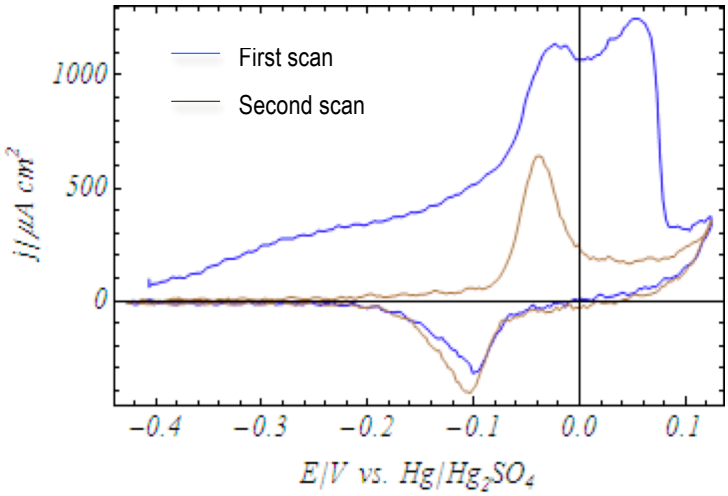

B)

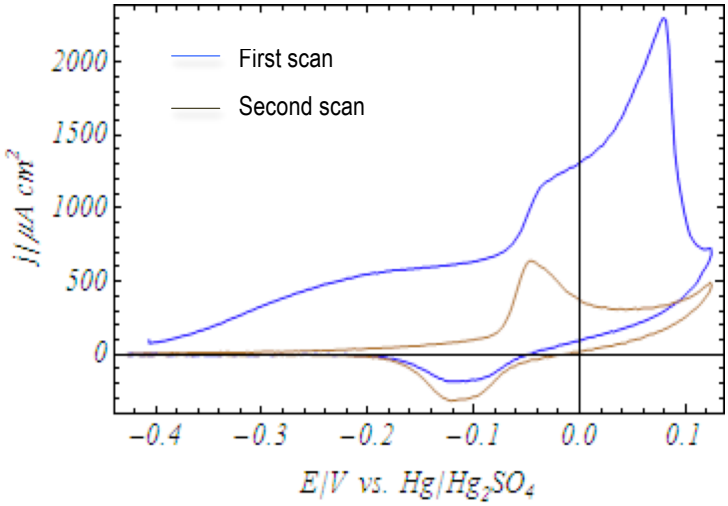

C)

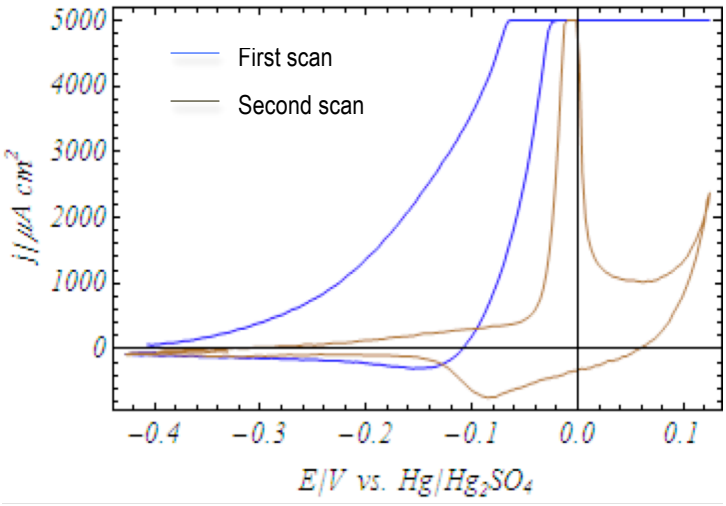

Fig.III.39. First and second scan for the Ni-Cr alloy with A) 22 at. % Cr, B) 54 at. % C and C) 69 at. % Cr in 1 M NaOH solution. Scan rate 20 mV s^{-1}.

The second anodic peak at more positive potential, +0.06 V vs. Hg/Hg_2SO_4 may suggest oxidation of chromium hydroxide. On the reverse scan, a cathodic peak was recorded, similar to the peak for the pure Ni. The second scan shows voltammogram, which resembled pure Ni in 1 M NaOH solution, although both peaks seemed to be slightly broader.

The oxidation of the Ni-Cr surface in the first cycle was clearly irreversible process, however in the second cycle the reaction on the surface seemed to proceed as it would be for the bulk Ni. Comparison with Ni suggests:

1) the surface before commencement of the first scan was not fully passivated,

2) On the first scan the most likely reactions are: a) nickel oxidizes to give nickel(II) hydroxide and b) chromium oxidizes to give chromium(III) hydroxide, in the potential range from -0.4 to -0.1 V vs. Hg/Hg_2SO_4, with b) the more probable.

3) In the potential range from -0.1 V vs. Hg/Hg_2SO_4 to +0.1 V vs. Hg/Hg_2SO_4 further oxidation of the oxide/hydroxide occurred but oxidation of the chromium component was irreversible.

4) On second scan, only features for nickel(II) hydroxide leading to nickel oxyhydroxide were observed with similar charge (about 1.7 - 1.8 mC cm^{-2}) as it would be for the uniform Ni deposited by PVD onto 10 x 10 array. However, oxide formation of the mixed oxide/hydroxide retards the kinetics making the peaks broader and the reaction, proceeding from nickel(II) hydroxide to nickel(II) oxyhydroxide, more irreversible.

If the Cr content in the Ni-Cr alloy was increased to 54 at %, the voltammogram shown in fig.III.39B was similar to that from the fig.III.39A. However, the first peak in the fig.III.39B, corresponding to the oxidation of nickel(II) hydroxide was smaller with respect to the first peak shown in fig.III.39A. Moreover, on the second cycle, the $Ni(OH)_2$/NiOOH peaks are similar. These differences may be attributed to the increasing Cr content in the alloy.

Upon further increasing the Cr content to 69 at. % of Cr in the Ni-Cr alloy, the voltammogram shown in the fig.III.39C had a different characteristics. In the first scan, the anodic current density increased as the potential was increased. However, due to the limitation in the experimental equipment, the current density was saturated at the value of 5000 $\mu A\ cm^{-2}$ and no further

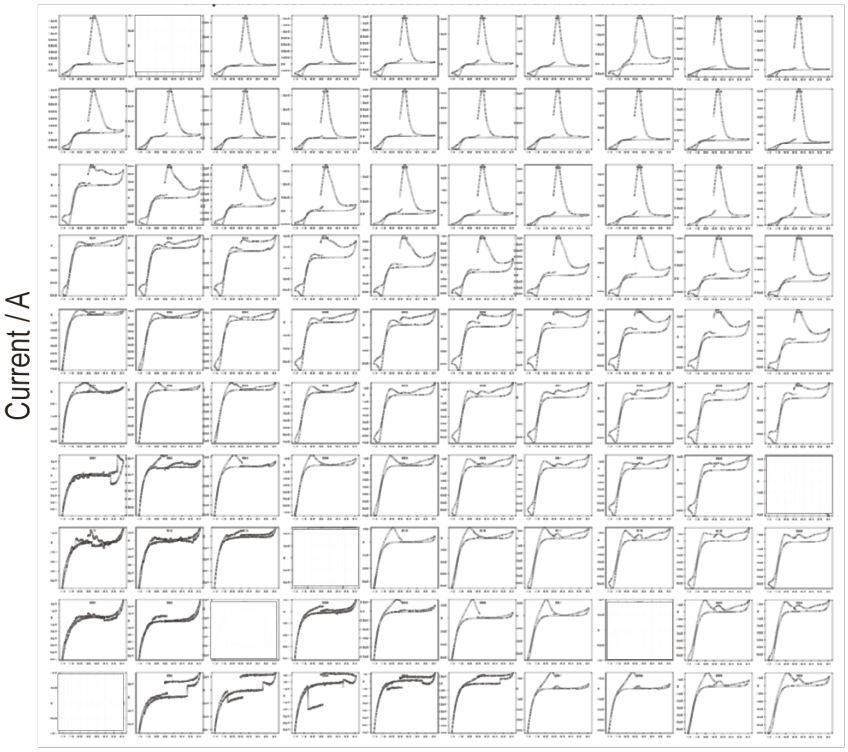

At % of Cr in the Ni-Cr alloy

1	2	2	3	3	4	4	5	5	5
5	5	5	6	6	6	6	6	6	7
7	7	8	9	9	9	10	10	11	11
11	11	12	12	12	12	13	13	13	13
14	14	15	15	16	16	16	16	17	18
19	20	21	21	21	22	22	22	22	23
23	23	23	27	28	29	30	30	31	31
32	32	34	36	37	38	40	40	40	44
48	51	52	53	54	55	55	57	60	60
61	67	68	69	69	71	75	77	81	86

Fig.III.40. CV with scan rate 20 mV s^{-1} recorded for 100 electrodes and corresponding Cr content for 10 x 10 Au pads. The potential scan was recorded in sulphate medium, pH 4 at T = 333 K. The solution was saturated with N_2 and N_2 was passed over the solution surface whilst experiment was running. The initial potential was -1.2 V vs. Hg/Hg_2SO_4.

changes in the current density were recorded upon increasing the potential to more positive values. The charge under the potential from -0.4 V vs. Hg/Hg_2SO_4 to -0.1 V vs. Hg/Hg_2SO_4 was 37 mC cm^{-2} – 10 times larger than the charge for the same potential region in the voltammograms shown in the fig.III.39A and B. In the reverse scan, no corresponding cathodic peak was recorded, suggesting much thicker corrosion layer and clearly irreversible reaction. In the second scan, a large anodic peak was recorded with the charge density of 10 mC cm^{-2} still probably resulting from $Ni(OH)_2$ oxidation but in a thicker surface layer. In the reverse scan, a broad cathodic peak with much smaller charge density, 2.6 mC cm^{-2} was observed. The anodic charge was about 4 times larger than the cathodic charge; therefore the addition of this amount of Cr leads to even larger irreversibility. It was observed that the charge on the surface of the Ni – 69% Cr alloy was "building up". In fact, the charge was "building up" with increasing Cr content in the Ni-Cr alloy. The most reproducible surface was observed for the Ni – 22%Cr alloy, after the first cycle. The results imply changes in the hydroxide layer properties with composition. Also the PVD materials are less readily passivated than bulk materials.

However, the solution that mimics the conditions on the cathode side in the PEM fuel cell for studying the stability of the alloy is the acid sulphate solution. A new array of the Ni-Cr alloy was deposited with the Cr content ranged from 0 to 100 at. % Cr and the test was performed in 0.1 M Na_2SO_4 with 2 ppm NaF, pH 4 at 333 K. The solution was saturated with N_2 and N_2 was passed over the solution surface whilst experiment was running.

Voltammograms for 100 electrodes and a table of the Cr content corresponding to each Ni-Cr alloy are shown in fig.III.40. The scan rate was 20 mV s^{-1} and the potential scan started from a potential close to the open circuit potential for Ni – 50% Cr alloy. The open circuit potential will, however vary with composition and a single starting potential had to be selected. A very clear trend can be seen from the 10 x 10 array presentation. The top three rows of the 10 x 10 array, where the Cr content was low with maximum 11 %, gave voltammograms with distinct anodic peaks in the forward scan with peak potential at approximately -0.45 V vs. Hg/Hg_2SO_4 and no corresponding catholic peak on the reverse scan. This voltammetry was similar to that for Ni (see section *III.1.1. Iron, nickel and chromium*); the peak arose from an active corrosion region just positive to the corrosion potential and passivation at more positive potentials. At the end of the reverse scan at the potential of approximately -1.0 V vs. Hg/Hg_2SO_4, a small cathodic peak was recorded. With increasing Cr content, above 13 %, the anodic peak at potential -0.45 V

vs. Hg/Hg_2SO_4 in the forward scan is much diminished and eventually, no anodic peak at this potential in the voltammograms with Cr content exceeding 20% was observed. However, in the forward scan and at the potential of approximately -0.7 V vs. Hg/Hg_2SO_4, a small peak was recorded. Also the cathodic current negative to -1.0 V vs. Hg/Hg_2SO_4 is much increased and this result from water reduction to H_2. The small anodic peak at -0.7 V vs. Hg/Hg_2SO_4 may result from H_2 oxidation. More detailed analysis for some selected Ni-Cr alloys is shown in fig.III.41. In this figure, four Ni-Cr alloys are compared. Fig.III.41A presents Ni – 5%Cr alloy, fig.III.41B compares the Ni – 20% Cr alloy, fig.III.41C shows Ni – 55% Cr alloy and fig.III.41D presents the Ni – 86% Cr alloy.

In the Ni – 5%Cr, a large anodic peak in the forward potential at -0.45 V vs. Hg/Hg_2SO_4 was recorded with the charge density of 31 mC cm^{-2}. Such a large charge corresponds to the oxidation of approximately 11 nm of metal layer. On the other hand, an active corrosion region and passive region for the Ni in the sulphate medium, pH 4 was observed. Therefore, this amount of charge may equally contribute to the dissolution of the layer as well as formation of corrosion product, known as a passive film. However, the thickness of the film was approximately 20 nm and the charge under the anodic peak suggested clearly that almost all of the Ni film dissolved. It is important to note that for the complete dissolution of 20 nm layer, the charge of approximately 58 mC cm^{-2} is needed. A passivation of the Ni was also observed in positive potentials to -0.2 V vs. Hg/Hg_2SO_4. The current density decreased to 400 μA cm^{-2} and remained constant until the potential was reversed. On the reverse scan, no corresponding cathodic peak was recorded but a small cathodic peak at potential of -1.0 V vs. Hg/Hg_2SO_4 was observed. It is interesting to note that after the first scan, the gold electrode pads were visible by eye in these three rows, confirming the rapid dissolution of the alloys with very low Cr contents.

For the Ni – 20% Cr alloy (fig.III.41B), the oxidation peak almost completely disappeared and the voltammogram resembled rather that for pure Cr (see fig.III.2c). The anodic current density in the forward scan was low and in the range of 25 to 50 μA cm^{-2} until the potential was reversed. The surface of the alloy was passivated. It is believed that the passive film was formed on the alloy on the open circuit potential while the Ni-Cr alloy was in contact with the solution, before the experiment started. On the reverse scan, the current density was also low and the peak observed at -1.0 V vs. Hg/Hg_2SO_4, disappeared – the current was shifted to more negative direction.

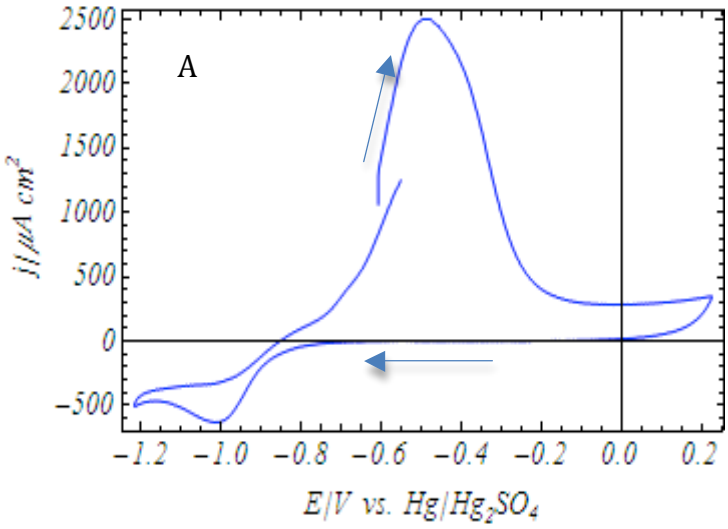
A
2500
2000
1500
1000
500
0
−500
−1.2 −1.0 −0.8 −0.6 −0.4 −0.2 0.0 0.2
j/μA cm²
E/V vs. Hg/Hg₂SO₄

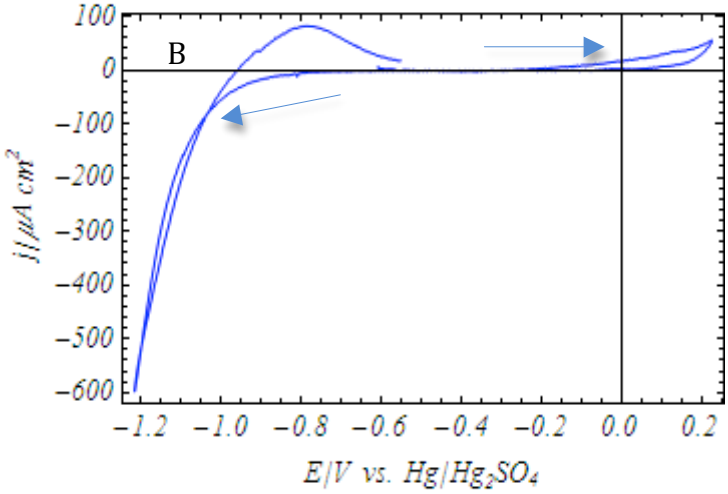
B
100
0
−100
−200
−300
−400
−500
−600
−1.2 −1.0 −0.8 −0.6 −0.4 −0.2 0.0 0.2
j/μA cm²
E/V vs. Hg/Hg₂SO₄

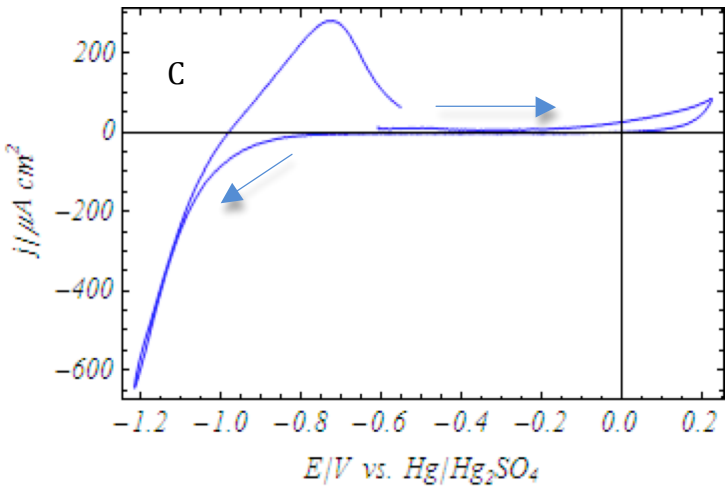
C
200
0
−200
−400
−600
−1.2 −1.0 −0.8 −0.6 −0.4 −0.2 0.0 0.2
j/μA cm²
E/V vs. Hg/Hg₂SO₄

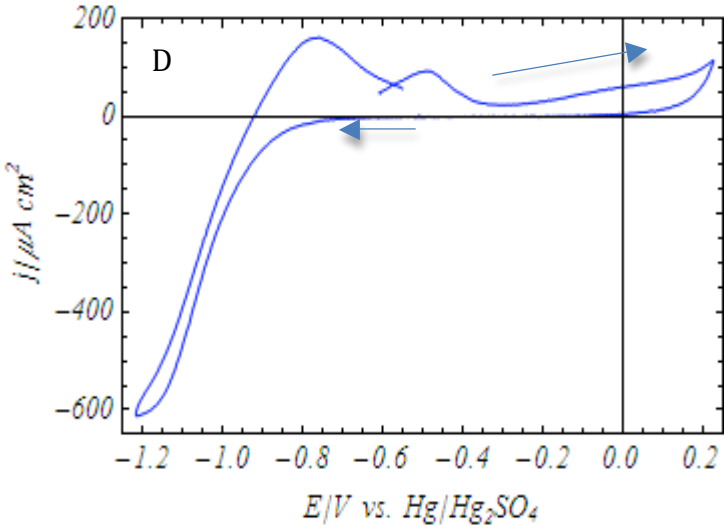

Fig.III.41. A comparison of voltammograms for A) Ni – 5% Cr, B) Ni - 20% Cr, C) Ni – 55% Cr alloy and D) Ni -86% Cr. Scan rate 20 mV s^{-1} in sulphate medium, pH 4 at T = 333 K.

The voltammograms for the alloys with 55% Cr and 86% Cr in the Ni-Cr alloy shown in fig.III.41C and D, respectively, were similar to the voltamogram for the Ni – 20% Cr alloy. The anodic current density was low at all potentials during the scan to more positive potentials – the surface was passivated. However, if the charge under the anodic scan in the potential range from -0.6 V vs. Hg/Hg_2SO_4 to +0.2 V vs. Hg/Hg_2SO_4 is compared in those voltmmograms, it can be noticed that the largest charge was estimated for the Ni – 86% Cr alloy and the lowest, for the Ni – 20 % Cr alloy. All the voltammograms featured large cathodic current density at the negative end of the reverse scan, which may be attributed to the reduction of water.

In the Ni-Cr alloys containing 20% Cr, 55%Cr and 86% Cr, the gold pads were never observed; the electrodes remained shiny and metallic gray. This was attributed to the formation of passive film on the surface of the alloys upon contacting with the solution. As a result of that the anodic current density shown in the voltammograms (fig.III.41B, C and D) was very low. Therefore, upon increasing the Cr content in the Ni – Cr alloy to 20 %, and above, much greater stability in the acidic medium can be achieved.

This corrosion behaviour of the Ni-Cr alloys was shown to be dependent on Cr content in the Ni-Cr alloy. Therefore, the application of PVD deposition allows the selection of a particular Ni-Cr alloy that gives acceptable corrosion behaviour in the potential similar to that in the simulated

environment on the cathode side in the PEM fuel cell. This behaviour can be clearly observed, if the current density on the reverse scan at 0.0 V vs. Hg/Hg_2SO_4 (the simulated potential on the cathode side of the PEM fuel cell) versus the Cr content of the 100 electrodes in the array (see fig.III.42).

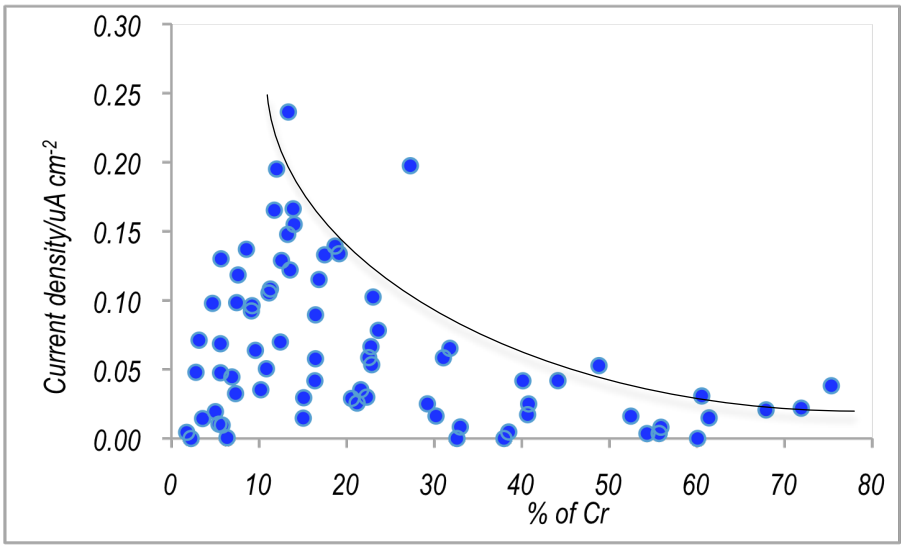

Fig.III.42. A plot of the current density (in the reverse scan) versus Cr content in the Ni-Cr alloy for 100 electrodes. The current density was chosen at the potential of 0.0 V vs. Hg/Hg_2SO_4.

The trend is clear. The surface passivates more strongly as the Cr content increases. Below 20% Cr, the data is rather scattered although the current density at 0.0 V vs. Hg/Hg_2SO_4 is always low. It is clear whether with very low Cr content (<10%) the data may represent largely a gold surface. As noted above, it could be seen by eye that dissolution occurred. There appears little advantage in adding more than 20% Cr.

From the experiments conducted on the 10 x 10 array, the following conclusions might be drawn:

1) A thin Ni layer (100 nm) was deposited onto 10 x 10 electrochemical array by PVD and the reproducibility was examined in 1 M NaOH solution at room temperature. Voltammograms were recorded for 100 electrodes and it was shown that indeed, good reproducibility was achieved when employing the PVD system. This experiment was crucial in order to consider the next step – deposition of the Ni-Cr alloy with different Cr content.

2) The Ni-Cr alloy with different Cr content prepared onto 10 x 10 array was tested in 1 M NaOH solution at room temperature and in 0.1 M Na_2SO_4 with 2 ppm NaF, pH 4 at 333 K. In 1 M NaOH solution the surface of the alloy was passivated and the reaction $Ni(OH)_2$/NiOOH became more irreversible with increasing Cr content in the Ni-Cr alloy.

   In the sodium sulphate solution pH 4, dissolution was observed for the Ni – 5% Cr alloy after the first cycle and the charge under the anodic peak clearly suggested dissolution of almost all Ni layer – gold pads were visible after the experiment. A relatively good stability was observed with increasing Cr content in the Ni-Cr alloy. In fact, the alloys containing 20% Cr (fig.III.45B), 55% Cr (fig.III.45C) and 86% Cr (fig.III.45D) in the Ni – Cr alloy indicated similarities during the anodic scan – low anodic current density as a result of formation of passive layer formed upon contacting the alloys with solution.

3) As a result of formation of the passive layer and upon scanning the potential to the more positive, a low anodic current density was recorded in the forward and in the reverse scan for the alloys with Cr content equal to and greater than 20%. At the potential of 0.0 V vs. Hg/$Hg/_2SO_4$, the current density was low for all alloys with Cr content greater than 20%.

4) A thicker Ni-Cr film would be advantageous for the corrosion studies; the thicker film would allow performing a larger series of investigations, for instance, surface scan before and after the one-hour corrosion test. Moreover, as mentioned above, the deposited Ni-Cr alloy was either in amorphous or metastable phase; therefore heating the alloy and examine stability in sulphate medium, pH 4, could be valuable in order to investigate the changes in corrosion after the crystallization. Those materials could also be compared with the commercial Ni-Cr alloys.

2.4.2. Ni-Cr alloy prepared by electrodeposition

The literature and experience showed that deposition of Ni is facile process but Cr only deposits from Cr(III) bath in restricted conditions. The experiments have intended to define conditions where 80% Ni – 20% Cr alloy could be deposited. This required inhibiting Ni deposition whilst catalysing Cr deposition.

Cr electroplating. Cr was first electrodeposited onto a carbon steel cathode and the conditions were based on work described in [126]. The electroplating bath consisted of chromium(III) sulphate (10 g dm^{-3}), thiourea (0.1 g dm^{-3}), boric acid (60 g dm^{-3}) saccharin (0.4 g dm^{-3}) and potassium sulphate (100 g dm^{-3}). The parallel plate beaker cell with two lead anodes and the carbon steel cathode was employed for the Cr electroplating and the electroplating conditions were: solution temperature 318 K, current density -70 mA cm^{-2}, deposition charge 2.1 C cm^{-2}. This current density was suggested in [17]. The authors estimated the rate of deposition for this current density to be 0.1μm min^{-1}. During the deposition at such current density, a large amount of hydrogen on the cathode was evolved. Considering those data and comparing to the calculated thickness from the Faraday's law, the current efficiency for the Cr electroplating was rather low about 10 – 15 %. However, with those electroplating conditions, a Cr layer was deposited onto the carbon steel substrate. After the electroplating, the metallic deposit with bluish appearance was observed.

Ni electroplating. The Ni was electroplated onto carbon steel disc from four times diluted Watts bath, pH 3.5 consisting of 65 g dm^{-3} nickel(II) sulphate, 12.5 g dm^{-3} nickel(II) chloride and 35 g dm^{-3} boric acid. The electroplating was performed in a three-electrode glass cell with carbon steel disc working electrode with area 0.2 cm^2, Pt mesh counter electrode, with mesh area 1 cm^2 and a reference saturate calomel electrode at room temperature. A continuous layer of Ni with dull appearance was observed using a current density of -12 mA cm^{-2} for 1 minute. When saccharin was added to the Watts bath with the same amount as it was used in the Cr plating bath, a bright metallic deposit was obtained.

Ni – 20% Cr plating. The first attempts to electroplate Ni – 20%Cr alloy was to add various amounts of chromium(III) sulphate or chromium(III) chloride to the concentrated and diluted Watts bath and also nickel(II) sulphate to the Cr plating bath. The parallel plate beaker cell with two Ni anodes and the carbon steel cathode was employed for electrodeposition of the alloy. The very first plating bath contained a mixture of 50 g dm^{-3} nickel(II) chloride, 250 g dm^{-3} chromium(III) chloride, 35 g dm^{-3} boric acid, 30 g dm^{-3} thiourea. The bath temperature was 318 – 328 K. The electroplating current density was -100 mA cm^{-2} and deposition charge 6 C cm^{-2}. Uneven Cr and Ni distribution was obtained in the middle and on the edge of the cathode. The sample had a brownish colour in the middle and metallic on the edges. This brownish deposit may be attributed to the chromium hydroxide.

In another plating bath, nickel(II) and chromium(III) chlorides were replaced by nickel(II) and chromium(III) sulphates. The new plating bath contained of 10 g dm^{-3} Cr(III) sulphate, 1 g dm^{-3} Ni(II) sulphate, 0.6 g dm^{-3} of thiourea, 0.4 g dm^{-3} saccharin, 100 g dm^{-3} potassium sulphate and 60 g dm^{-3} boric acid. The solution pH was 4. The current density was -65 mA cm^{-2} and the deposition charge was 2.2 C cm^{-2}. The plating bath temperature was in the range of 318 – 328 K. Precipitation of green nickel hydroxide was observed in the middle of the deposit and metallic colour was seen on the edges after the deposition on the carbon steel cathode. Those attempts to electroplate the Ni-20%Cr alloy, indeed gave clear evidence of the complex nature of the Ni-Cr deposition. However, based on those observations, it was decided to test a bath consisting of different amount of nickel(II) sulphate and chromium(III) sulphate, fixed amount of potassium sulphate, 100 g dm^{-3}, saccharin, 0.4 g dm^{-3} and various amounts of boric acid and thiourea. Therefore the following parameters were investigated in order to obtain an appropriate composition (20%Cr in the Ni-Cr alloy), uniform coverage and metallic appearance:

1) the ratio of Ni(II) sulphate to Cr(III) sulphate in the plating bath,
2) the effect of thiourea on the deposition of Ni-Cr alloy,
3) the effect of boric acid,
4) the effect of current density.

The surface topology and the elemental analysis for the electroplated Ni-Cr alloy were conducted each time a deposition was carried out in the parallel plate beaker cell. Fig.III.43 explains the procedure used for the SEM and EDX analysis for the Ni-Cr alloy. Three regions were investigated, indicated as 1, 2 and 3. Each of those regions contained four-point measurement analysis and therefore the overall 12 points were analyzed and average percentage of the composition for the Ni-Cr alloy was determined.

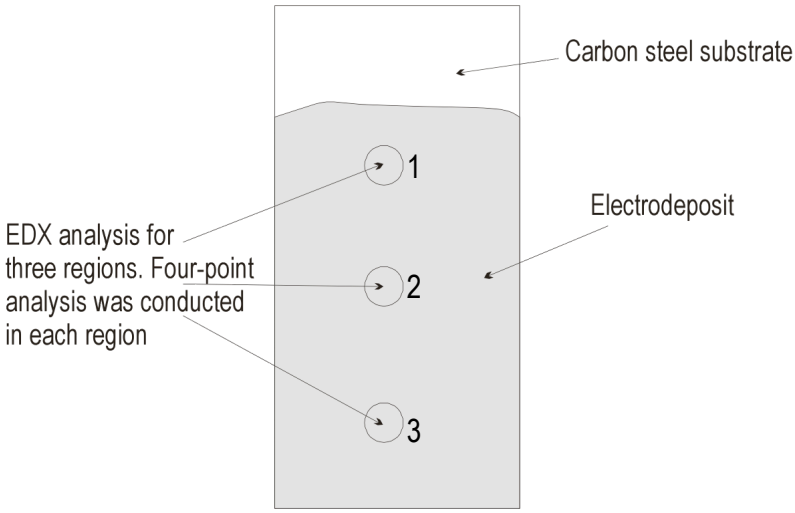

Fig.III.43. EDX analysis for the Ni-Cr alloy electroplated in the parallel plate beaker cell from the Ni(II) and Cr(III) salt solution. Each region, marked as 1, 2 and 3, contains four-point measurement, so the overall 12 points were analyzed on the Ni-Cr alloy.

The effect of thiourea was separately investigated for the Cr and Ni plating baths. The starting amount of thiourea was 0.1 g dm^{-3}. In the Cr plating bath the thiourea had a great impact on electroplating. Patchy deposit and almost no Cr were detected with thiourea free Cr plating bath (see table.III.9). Upon addition of 0.05 g dm^{-3} thiourea, the appearance of the Cr deposit was improved. A good appearance was obtained with 0.1 g dm^{-3}. Similar experiments were conducted in the Watts bath, pH 3.5 with addition of 0.1 g dm^{-3} thiourea (see table.III.10). The electroplating of Ni was performed with typical conditions, as it would be for depositing 2 μm of Ni layer: solution temperature 318 K, current density -10 mA cm^{-2} and deposition charge 6 C cm^{-2}. Patches of Ni with exposed bare carbon steel substrate were observed after the electroplating. The amount of thiourea, therefore was decreased by a factor of two and the electroplating was

performed again with the same experimental conditions. The steel substrate was completely covered with Ni. Clearly, the thiourea promotes Cr deposition in the Cr plating bath but inhibits the Ni deposition in the Watts bath.

Amount of thiourea in Cr plating bath / g dm^{-3}	***Appearance of the deposit***
0	No deposit
0.05	Patches of the metallic deposit, the carbon steel substrate was exposed
0.1	Metallic bluish appearance

Table.III.9. The effect of thiourea on the deposition of Cr from Ni-Cr plating bath consisting of 10 g dm^{-3} $Cr_2(SO_4)_3.15H_2O$, 0.4 g dm^{-3} saccharin, 60 g dm^{-3} boric acid and 100 g dm^{-3} K_2SO_4. Bath temperature was 318 - 328 K. The electroplating conditions were: j = -70 mA cm^{-2}, deposition charge 2.1 C cm^{-2}.

Amount of thiourea in Watts bath/ g dm^{-3}	***Appearance of the deposit***
0	Semi bright deposit
0.05	Semi bright Ni complete layer, no carbon steel was exposed through the Ni coating
0.1	Semi bright deposit, the Ni layer was not complete, patches of Ni and exposed carbon steel substrate

Table.III.10. The effect of thiourea on electrodeposition of Ni comes from Watts bath, pH 3.5 at T = 318 – 328 K. The electroplating conditions were: j = -10 mA cm^{-2}, charge density 6 C cm^{-2}.

On the other hand, the individual consideration of this additive in the Ni and Cr plating baths may also give misleading information for Ni-Cr deposition.

Increasing the thiourea concentration further and electrodepositing the alloy, it was found that in order to deposit Cr and Ni alloy on the carbon steel substrate, the amount of thiourea should be 0.66 g dm^{-3}. With this amount of thiourea, the Ni-Cr alloy was successfully deposited but precipitation of nickel hydroxide was observed on the cathode. Therefore, the ratio of Ni(II) sulphate to Cr(III) sulphate was next investigated keeping the amount of thiourea constant. For instance, in the Ni-Cr plating bath consisting of 10 g dm^{-3} chromium(III) sulphate, 2 g dm^{-3} nickel(II) sulphate and 0.66 g dm^{-3} thiourea, a metallic deposit was obtained with an average (average value estimated from 12 points detected by EDX, shown schematically in fig.III.43) composition of 53% Ni and 47% Cr, whereas for 4.26 g dm^{-3} of chromium(III) sulphate and 3.06 g dm^{-3} nickel(II) sulphate in the plating bath, the average composition was 75% Ni and 25% Cr, which was very close to the desired Ni – 20% Cr alloy. Green nickel hydroxide precipitation was no longer observed after the electrodeposition. The above results implied that the ratio of Ni(II) sulphate to Cr(III) sulphate, the amount of thiourea and boric acid in the solution was important in order to obtain metallic deposit and therefore the emphasis was next put on the finding the exact ratio of Ni(II) sulphate to Cr(III) sulphate to obtain the appropriate alloy composition.

The influence of current density on the Ni-Cr deposition was carried out in the parallel plate beaker cell and the range of current densities started from -40 mA cm^{-2} to -100 mA cm^{-2} while the deposition charge was kept constant at 2.2 C cm^{-2}. With lower current densities, very little Cr was detected in the Ni-Cr alloy; on the other hand, with high current densities a precipitation of Ni hydroxide was observed. It was found that the optimum current density should be -65 mA cm^{-2}. At this current density metallic deposit was observed after the electroplating. On the other hand, at such high current density, a large amount of hydrogen gas was always generated during the deposition process.

Fig.III.44 shows SEM and EDX analysis for the Ni-Cr alloy prepared in the parallel plate beaker cell from the solution contained 5.73 g dm^{-3} Cr(III) sulphate, 4 g dm^{-3} Ni(II) sulphate, 0.66 g dm^{-3} of thiourea, 0.4 g dm^{-3} saccharin, 100 g dm^{-3} potassium sulphate and 6 g dm^{-3} boric acid. The electroplating conditions were: solution temperature 318 K – 328 K, current density was -65 mA cm^{-2} and deposition charge 2.2 C cm^{-2}. After the electroplating, a metallic deposit was observed

on the surface of the carbon steel substrate. The SEM analysis showed a smooth surface with some white patches. The EDX analysis (shown in the same figure) revealed the composition of the alloy, and the percentage of the Ni and Cr was resonalbe uniform. Interestingly, no oxygen was detected on the surface of the alloy and hence no bulk metal hydroxide is being formed. The deposits were also clearly thinner than predicted by the Farday's law as iron from the substrate is major element detected.

1)

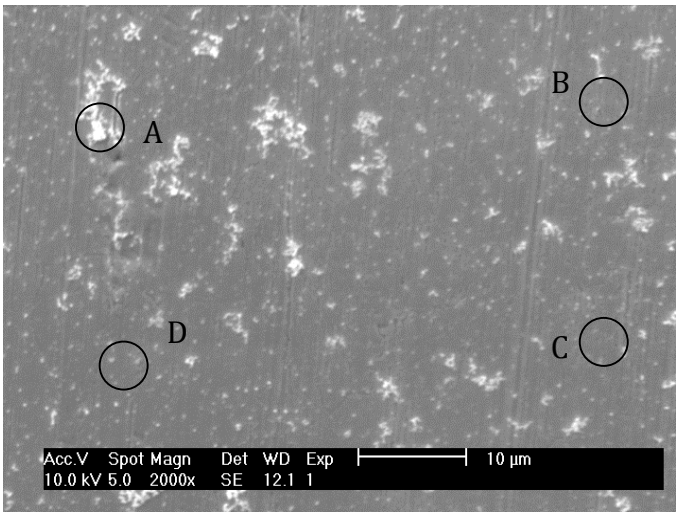

Element	At %			
	A	B	C	D
O	-	-	-	-
Cr	2	2	2	2
Fe	88	92	93	91
Ni	9	6	5	6
%Ni / %Cr	81/19	80/20	76/24	75/25

2)

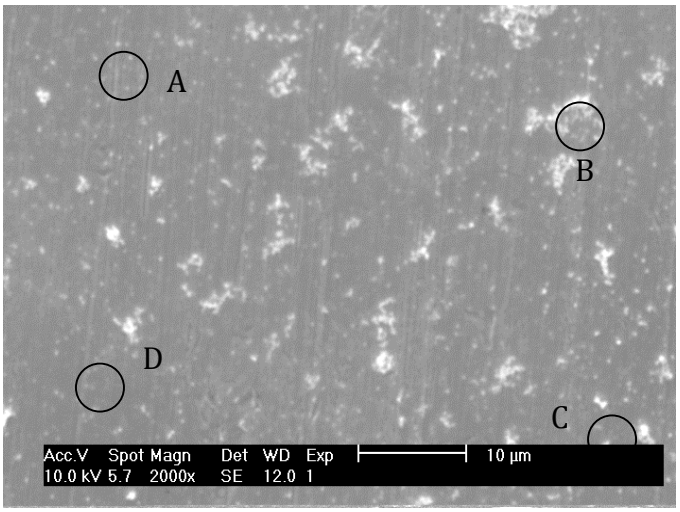

Element	At %			
	A	B	C	D
O	-	-	-	-
Cr	2	2	2	2
Fe	91	96	89	92
Ni	7	2	8	6
%Ni / %Cr	77/23	50/50	78/22	76/24

3)

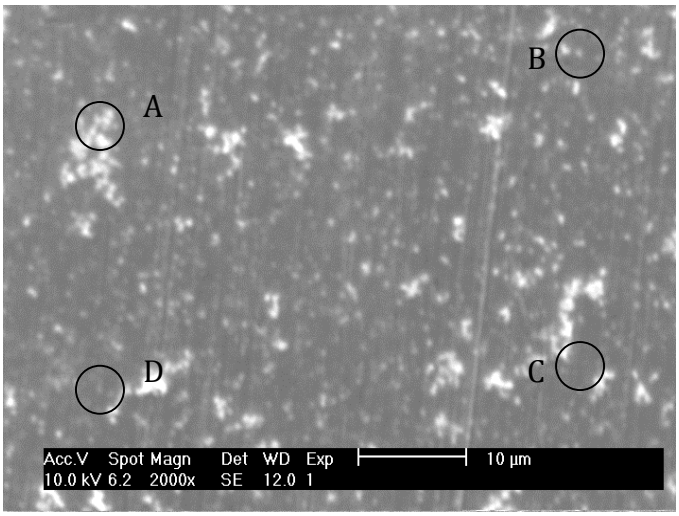

Element	At %			
	A	B	C	D
O	25	-	-	-
Cr	4	2	2	2
Fe	69	91	92	90
Ni	2	7	6	8
%Ni / %Cr	29/71	75/25	73/27	80/20

Fig.III.44. SEM and EDX analysis for the Ni-Cr alloy electroplated in the parallel plate beaker cell from the bath consisting of 5.73 g dm^{-3} Cr(III) sulphate, 4 g dm^{-3} Ni(II) sulphate, 0.66 g dm^{-3} of thiourea, 0.4 g dm^{-3} saccharin, 100 g dm^{-3} potassium sulphate and 6 g dm^{-3} boric acid. The electroplating conditions were: plating bath temperature 318 K – 328 K, j = -65 mA cm^{-2}, deposition charge 2.3 C cm^{-2}. The images were taken at the positions indicated in the fig.III.43.

A few examples of latest Ni-Cr plating baths with different amount of nickel(II) sulphate and chromium(III) sulphate, fixed amount of thiourea and boric acid can be seen in table.III.11. In addition, the appearance of the deposit was included. The selected Ni-Cr plating bath is shown in table.III.12.

Fig.III.45 shows SEM pictures for the electroplated Ni–20%Cr alloy in the parallel plate beaker cell and the composition of the alloy estimated by EDX. The plating bath is listed in table.III.12. The SEM image of the alloy was similar to that in the fig.III.44 – white patches on the surface of the alloy but the alloy had a metallic colour. The EDX analysis showed relatively uniform Cr distribution in the Ni-Cr alloy. The measurement was performed for 12 points according to the fig.III.43 and all of those gave relatively uniform Cr distribution around 20% Cr. Again, there was no oxygen present on the surface of the alloy.

	The amount of Ni(II) sulphate and Cr(III) sulphate in the plating bath/g dm^{-3}	***Appearance***
1	10 g dm^{-3} $Cr_2(SO_4)_3.15H_2O$ 3.33 g dm^{-3} $NiSO_4.7H_2O$	Metallic; Cr present at the edges and in the middle of the sample approximately: 50% Ni – 50% Cr
2	10 g dm^{-3} $Cr_2(SO_4)_3.15H_2O$ 3.06 g dm^{-3} $NiSO_4.7H_2O$	Metallic at the edges with uneven ratio of Ni to Cr and approximately 53% Ni – 47% Cr in the middle
3	4.4 g dm^{-3} $Cr_2(SO_4)_3.15H_2O$ 2 g dm^{-3} $NiSO_4.7H_2O$	Metallic; an average value calculated from three regions shown in fig.III.46: 65% Ni – 35% Cr
4	5.86 g dm^{-3} $Cr_2(SO_4)_3.15H_2O$ 4 g dm^{-3} $NiSO_4.7H_2O$	Metallic; an average value calculated from three regions shown in fig.III.46: 77% Ni – 23% Cr

Table.III.11. The effect of different amount of Ni(II) sulphate and Cr(III) sulphate on deposition of the Ni-Cr alloy. The other constituents of the bath were: 0.66 g dm^{-3} thiourea, 0.4 g dm^{-3} saccharin, 6 g dm^{-3} boric acid and 100 g dm^{-3} potassium sulphate. Electroplating conditions were: solution temperature 318 – 328 K, j = -65 mA cm^{-2}, deposition charge 2.3 C cm^{-2}.

	Composition of the bath	Appearance
Ni-Cr bath used in the parallel plate beaker cell	4.26 g dm^{-3} $Cr_2(SO_4)_3.15H_2O$ 3.06 g dm^{-3} $NiSO_4.7H_2O$ 0.66 g dm^{-3} thiourea 0.4 g dm^{-3} saccharin 6 g dm^{-3} H_3BO_3 100 g dm^{-3} K_2SO_4	Metallic

Table III.12. The selected Ni-Cr plating bath used in the parallel plate beaker cell. The electroplating conditions were: solution temperature 318 – 328 K, j =-65 mA cm^{-2}, deposition charge 2.2 C cm^{-2}

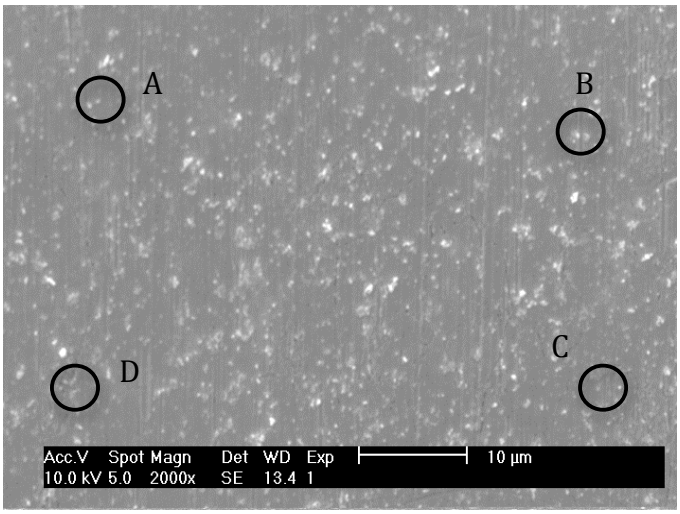

Element	At %			
	A	B	C	D
Cr	2.5	2.6	2.9	2.5
Fe	87.5	88.2	87.6	87.6
Ni	10.1	9.2	9.5	9.9
%Cr/%Ni	20/80	22/78	23/77	20/80

Fig.III.45. SEM and EDX point analysis for the Ni-Cr alloy prepared in the parallel plate beaker cell from the plating bath containing 4.26 g dm^{-3} Cr(III) sulphate, 3.06 g dm^{-3} Ni(II) sulphate, 0.66 g dm^{-3} thiourea, 0.4 g dm^{-3} saccharin, 6 g dm^{-3} boric acid and 100 g dm^{-3} potassium sulphate. The solution temperature was 318 – 328 K. The alloy was electrodeposited with current density -65 mA cm^{-2} and charge density was 2.3 C cm^{-2}. The EDX analysis for the alloy was conducted according to the fig.III.43.

While the deposit was far from perfect in the parallel plate beaker cell, this composition seemed a reasonable basis for further studies in the rectangular flow cell. The starting plating bath consisted of 4.26 g $Cr_2(SO_4)_3.6H_2O$, 5.37 g $NiSO_2.6H_2O$, 6 g H_3BO_3, 0.66 g NH_4Cl, 0.4 g saccharin and 100 g K_2SO_4. The solution temperature was 318 K – 328 K, the electroplating current density was -60 mA cm^{-2} and deposition charge was 15 C cm^{-2}. The solution was flowing between the carbon steel cathode and the Ni anode with the linear solution velocity 25.5 cm s^{-1}. This linear solution velocity was the same as was used for electrodeposition of Ni. It was found that during the deposition of Ni, the hydrogen gas was successfully removed and the deposited layer was complete. After the electroplating of Ni-Cr alloy, SEM pictures showed similar appearance as for the alloy prepared in the parallel plate beaker cell. The EDX analysis was performed for the alloy for five regions and each region contained four-point measurement analysis (see fig.III.46). It was found that the percentage of Cr in the Ni-Cr alloy, averaged from those five regions, was approximately 18%. There was no bulk oxide or hydroxide detected after the electroplating and the sample had a metallic colour.

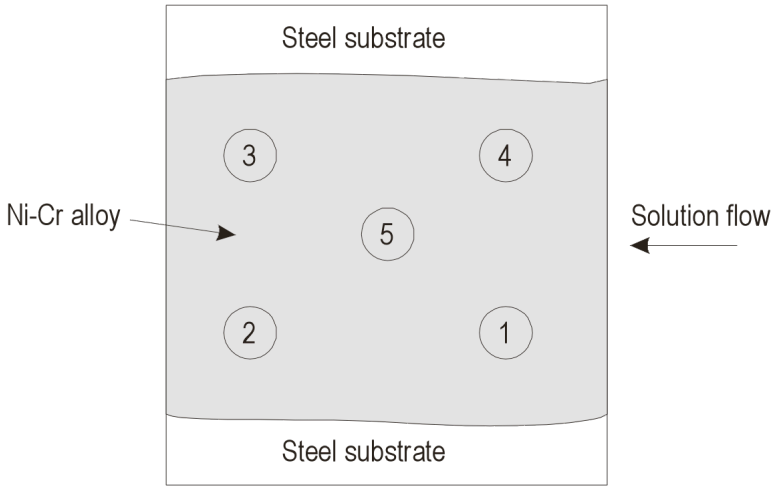

Fig.III.46. The procedure for the elemental analysis of the Ni-20%Cr alloy electroplated in the flow cell from the solution containing 4.26 g dm^{-3} Cr(III) sulphate, 5.37 g dm^{-3} Ni(II) sulphate, 0.66 g dm^{-3} thiourea, 0.4 g dm^{-3} saccharin, 6 g dm^{-3} boric acid and 100 g dm^{-3} potassium sulphate. The electroplating conditions were: solution temperature 318 – 328 K, current density -60 mA cm^{-2}, deposition charge 15 C cm^{-2}. Five regions on the alloy were examined and percentage of Cr and Ni in the Ni-20%Cr alloy was estimated.

1)

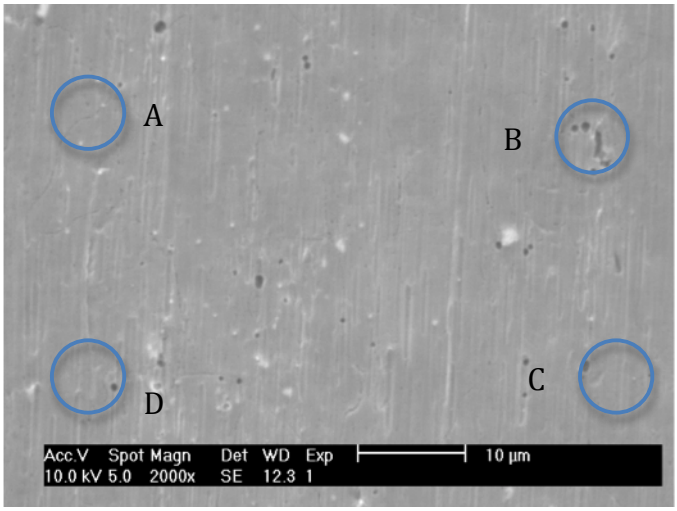

Element	At %			
	A	B	C	D
Cr	2	2	2	2
Fe	94	88	89	91
Ni	4	9	9	6
%Cr/%Ni	29/71	17/83	14/86	23/77

2)

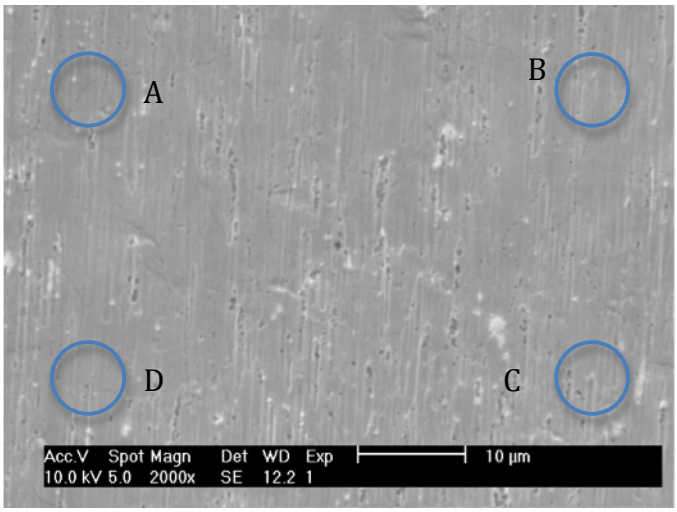

Element	At %			
	A	B	C	D
Cr	1	1	1	1
Fe	93	95	93	93
Ni	6	3	5	6
%Cr/%Ni	20/80	30/70	21/79	12/88

3)

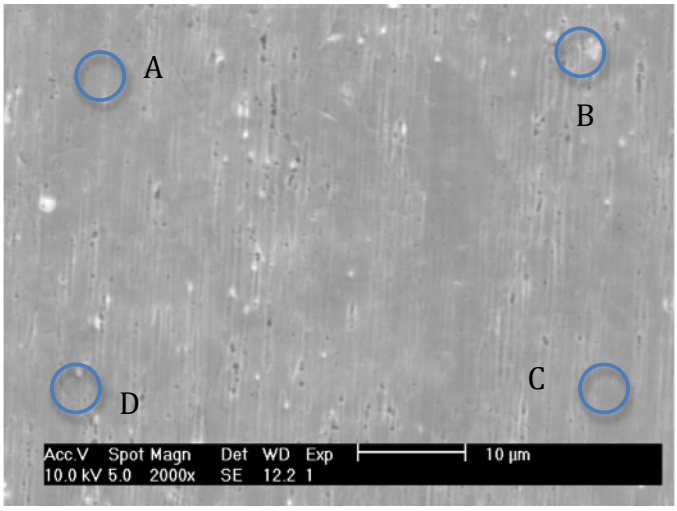

Element	At %			
	A	B	C	D
Cr	1	2	1	3
Fe	90	92	93	90
Ni	8	5	5	6
%Cr/%Ni	15/85	26/74	23/77	30/70

4)

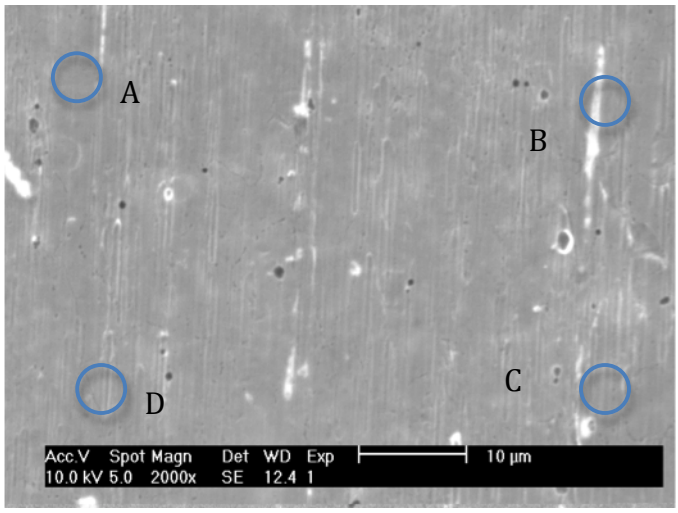

Element	At %			
	A	B	C	D
Cr	1	2	2	2
Fe	91	91	90	90
Ni	7	6	7	8
%Cr/%Ni	18/82	21/79	21/79	19/81

5)

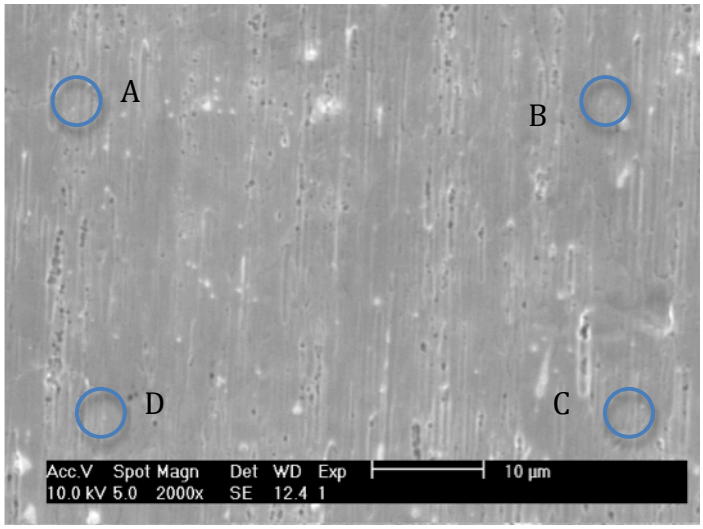

Element	At %			
	A	B	C	D
Cr	1	1	2	1
Fe	93	93	92	93
Ni	5	5	6	6
%Cr/%Ni	18/82	19/81	24/76	16/84

Fig.III.47. The elemental analysis for the Ni-20%Cr alloy electroplated in the flow cell from the solution containing 4.26 g dm^{-3} Cr(III) sulphate, 5.37 g dm^{-3} Ni(II) sulphate, 0.66 g dm^{-3} thiourea, 0.4 g dm^{-3} saccharin, 6 g dm^{-3} boric acid and 100 g dm^{-3} potassium sulphate. The electroplating conditions were: solution temperature 318 – 328 K, current density -60 mA cm^{-2}, deposition charge 108 C cm^{-2}. Five regions on the alloy were examined and percentage of Cr and Ni in the Ni-20%Cr alloy was estimated.

It can also be recognized that a large amount of Fe was detected suggesting again a thin layer of the deposited alloy. Deposition charge was therefore increased to a 108 C cm^{-2} instead of 15 C cm^{-2}. Fig.III.47 shows SEM and EDX analysis for the alloy deposited in the flow cell with deposition charge 108 C cm^{-2}. The EDX analysis was conducted for the same five points on the alloy according to procedure shown in the same figure.

SEM pictures from the fig.III.47 show a relatively smooth layer on a 10 μm scale and the white patches, seen in the Ni-Cr alloy deposited in the parallel plate beaker cell, seemed to appear to a lesser extent. After the electroplating, the sample had a metallic colour. The EDX analysis revealed no changes in the composition of the alloy upon passing 15 C cm^{-2} and 108 C cm^{-2}. Approximate numbers of the 80% of Ni and 20% of Cr in the Ni-Cr alloy were detected. Also the percentage of Fe was similar for both depositions and this implies that the alloy layer is not thickening with charge passed. Perhaps H_2 evolution is taking over completely and this observation is consistent with strong catalysis of H_2 evolution by the alloys in the array experiments.

The aim of this investigation was to find a practical method to electroplate the Ni – 20%Cr alloy, which is known to be very good corrosion resistant material. Deposition of the Ni-Cr alloys with different Cr content prepared by PVD confirmed that the Ni – 20%Cr alloy could be used as a next protective layer for the steel coated bipolar plates. Compact structure of the all Ni-Cr alloys deposited by PVD was obtained and the thickness of the film could satisfactory be of the order of 200 nm.

In the case of the Ni – 20% Cr alloy electroplated from sulphate solution, the alloy was successfully deposited, however the thickness was not clearly determined – tens of nanometers layer might be an estimate. More uniform and better distribution of the Cr and Ni in the Ni–Cr alloy was achieved in the rectangular flow cell (see fig.III.47), than in the parallel plate beaker cell.

2.1.6. Heat treatment for bipolar plates

Apart from the electroplating or PVD deposition of the Ni-20%Cr alloy, the other approach to obtaining the alloy was to deposit thin layer of Cr onto Ni coated carbon steel and then apply a heat treatment. It was important to find an appropriate heating temperature and heating time. Those parameters will clearly depend on the thickness of the Cr layer.

A 20 nm of Cr layer was evaporated onto the Ni coated carbon steel (prepared in the flow cell). The Cr was evaporated in the small vacuum chamber (see experimental chapter *II.2.6. Cr onto Ni coated carbon steel*). The sample after counting had a characteristic light blue metallic color. The SEM and EDX analysis were carried out for the Cr evaporated onto Ni coated carbon steel and the results are shown in fig.III.48. The surface of the deposited Cr was practically featureless. The EDX analysis revealed uniform Cr distribution, however a substantial amount of oxide film was present on the surface of the Cr. The surface of the Cr evaporated onto Ni coated carbon steel was studied using cyclic voltammetry technique. The current density was recorded from -1.2 V vs. Hg/Hg_2SO_4 to +0.2 V vs. Hg/Hg_2SO_4 and the first scan is presented in fig.III.49. No anodic peak for Ni oxidation was seen in the forward scan and the current density was very low in both directions - the surface of the Cr layer was already in the passivation state.

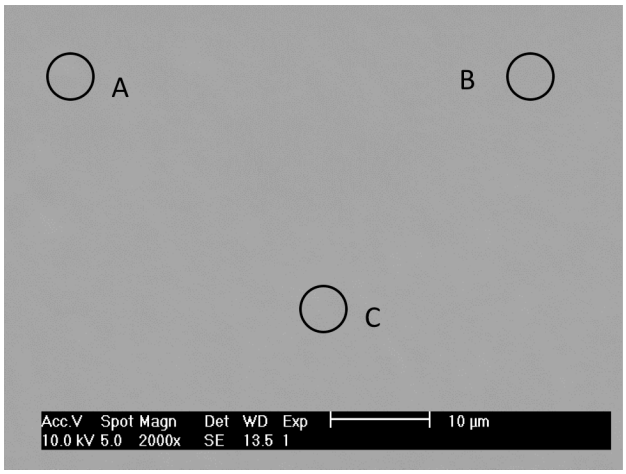

Elements	*At %*		
	A	***B***	***C***
O	15	14	15
Fe	2	4	3
Ni	63	61	61
Cr	20	20	20

Fig.III.48. SEM and EDX analysis for 20 nm Cr evaporated onto Ni coated carbon steel.

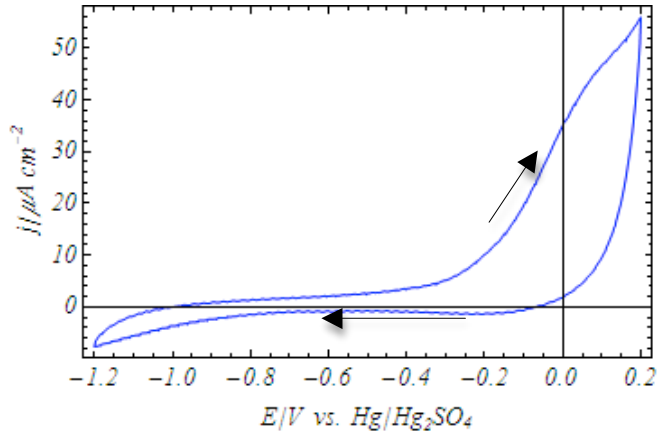

Fig.III.49. Voltammogram recorded for the 20 nm Cr layer evaporated onto Ni coated carbon steel. Scan rate 20 mV s^{-1}. The sulphate medium, pH 4 at 333 K was saturated with N_2 and N_2 was passed over the solution surface whilst experiment was running.

The heat treatment for the Cr evaporated onto Ni coated carbon steel with different temperatures for various times in N_2 and Ar/5%H_2 atmosphere was investigated (see the Experimental chapters: *II.3.6 Equipment for heat treatment* and *II.6 Heat treatment procedures)*. The air in the glass tube was directly replaced with N_2 or Ar/5%H_2 by purging the gas through the glass tube and therefore the air was "pushed out" of the tube. This reducing atmosphere was intended to avoid surface oxidation during the heating. The objectives were to form a Ni-Cr alloy on the surface of the Ni hence to reduce further the corrosion rate. The heat treatment and the heating temperatures as well as dwell times are listed in table III.13. The appearance of the Cr and Ni samples after the heat treatment is also reported in the same table.

Before the heat treatment, the samples were cut into small pieces, 2 cm x 4 cm in order to fit to the glass tube. Several heating procedures were investigated. In all cases, the emphasis was to obtain oxygen free atmosphere before the heating commences. The attempts were as follows:

1. Purging with N_2 gas for 40 minutes. After 40 minutes, the sample was inserted in to the furnace in the room temperature and then the temperature was increased with rate of 16 degrees per minute until the final temperature was achieved. After the heat treatment, the sample remained in the furnace until cooled down to room temperature.

The N_2 was purging to the glass tube whilst heating and cooling the sample, however, during the heating and cooling the rate of purging was much reduced.

Sample	Heat treatment		Appearance
	Temperature T/K	Time t/h and minutes	
Cr 20 nm onto Ni coated mild steel	573	½ h	Deep and very distinct colours over the whole surface, e.g., deep blue, yellow, brown
	773	1 h	
	873	½ h	
	973	1 h	
	1273	1 h	
	973	1 minute	Less intense colours e.g., light gold, pale yellow
	1173	1 minute, 5 minutes	
	1273	1 minute, 10 minutes	
	1283	1 minute, 3 minutes, 10 minutes	
Ni coated carbon steel	573	1 h	No colours on the surface were observed after the heat treatment
	673	1 h	
	773	1 h	
	873	½ h	
	1283	10 min	

Table.III.13. Heat treatment and dwell time for Cr with thickness 20 nm onto Ni coated carbon steel and Ni coated carbon steel, coating thickness 3 μm.

2. Purging with Ar/5%H_2 mixture for 40 minutes prior to the heat treatment. In the meantime, the furnace was heated up to the appropriate temperature. The glass tube under the Ar/5%H_2 atmosphere was inserted into the hot furnace and left there during the heating. After the heat treatment, the glass tube still remained in the furnace under the Ar/5%H_2 atmosphere until cooled down to the room temperature.

3. The same heating procedure was applied as it was described above (in 2), but instead of cooling the sample in the furnace to the room temperature; the sample was pulled out from the hot zone of the furnace (middle of the furnace) toward the entrance of the furnace where the temperature was lower. The glass tube with the sample was kept there for 10 minutes. After this time, the glass tube was completely removed from the furnace and cooled down to the room temperature. The overall cooling time was 30

minutes. All the time, the sample remained in Ar/5%H_2 atmosphere until cooled down to room temperature.

Each procedure described above, gave similar results after the heat treatment - different colours on the surface were observed. The colours result from oxidation of the Cr and this was confirmed by applying similar heat treatment to uncoated Ni. The longer the samples were kept in furnace the deeper the colour was observed (see table.III.13). Upon heating the sample with higher temperatures and shorter times, for instance at 1173 K for 1 minute and at 1273 K for 10 minutes, the colours were less intense. For the heat-treated Cr onto Ni coated carbon steel for 1 minute, the sample had a pale yellow colour but if the dwell time was increased to 10 minutes and the temperature was increased to about 100 degrees, a gold-like colour was observed. The oxidation of Cr surface during the heat treatment was a clear indication of the presence of oxygen in the glass tube. Therefore, the heat treatment performed by direct replacing the air with purging the inert gases, was a not satisfactory method to obtain surface free of oxidation.

In spite of different colours on the surface of the Cr sample, one-hour corrosion test in 0.1 M Na_2SO_4 solution with addition of 2 ppm NaF, pH 4 at 333 K was performed for the heat-treated and as deposited Cr onto Ni coated carbon steel. The heat-treated samples with less intense colours were chosen for the tests. Fig.III.50 reports results after the one-hour corrosion test. It can be immediately seen that all transients decreased with time. The corrosion current density in the first 1000 s decreased faster than for the as deposited Cr onto Ni coated carbon steel. At the end of the test, the corrosion current density for the as deposited sample was approximately 0.4 $\mu A\ cm^{-2}$ whereas for the heat-treated samples at two different temperatures, the current density was approximately 0.1 $\mu A\ cm^{-2}$. Almost negligible difference was observed in the corrosion current density after the samples were heated at two different temperatures.

As it was mentioned earlier, the Cr evaporated onto Ni coated carbon steel had different colours after the heat treatment, which was attributed to the formation of oxide layer on the surface. Therefore, it is believed that the chromium oxide layer contributed to a very low corrosion current density. It is important to emphasize that the passive layer formed on the metallic bipolar plates is likely to decrease the electrical contact between MEA and bipolar plates in the PEM fuel cell. This will result in a poor fuel cell performance.

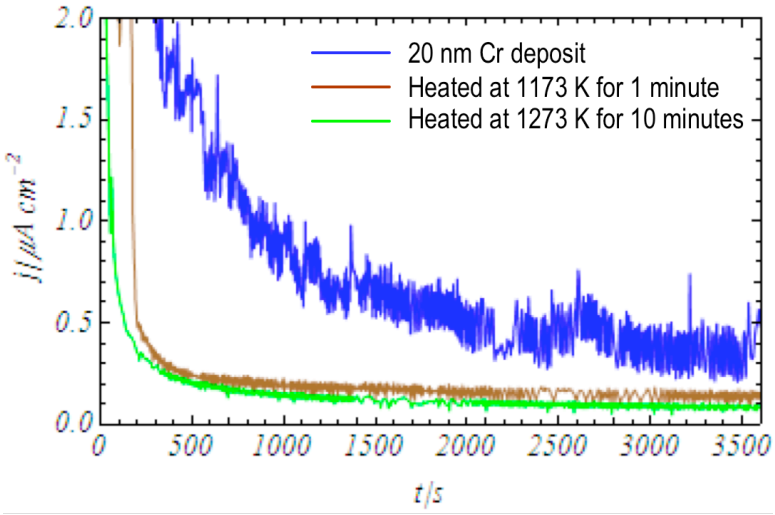

Fig.III.50. One-hour corrosion test for the 20 nm Cr evaporated onto Ni coated carbon steel and the heat-treated sample at two different temperatures. 0.1 M Na_2SO_4 with 2 ppm NaF, pH 4 at T = 333 K was used for corrosion test. The solution was saturated with N_2 and N_2 was passed over the solution surface whilst experiment was running.

IV. Concluding remarks

This thesis has sought to probe the possibility of a bipolar plate for H_2/O_2 PEM fuel cells based on a cheap carbon steel base. The approach to be used is set out in the Introuction, section I.1 and I.2, pages 3 – 7 and figures I.1 and I.2.

Employing a medium and conditions selected to mimic the environment of the bipolar plate in the operating fuel cell, preliminary studies established:

- Mild steel corrodes very rapidly and shows no evidance of passivation
- Stainless steel corrodes only very slowly but was considered too expensive
- Nickel shows active corrosion at a substantial rate but passivates at more positive potentials. Although, even passivated, the corrosion rate is too high for the application.

Repeating literature procedures, Ni was successfully deposited from Watts bath. Such Ni layers can show identical corrosion rates to bulk Ni but only in the absence of pinholes. Pinholes lead to very rapid corrosion. The deposition of uniform layers without pinholes requires careful control of plating conditions and deposition of relatively thick layer was more readily achieved in a flow cell with strong convection. A simple impedance procedure was developed to monitor the quality of the deposit.

The introduction of graphite particles into Ni to form a composite was intended to decrease the contact resistance between the bipolar plate and the MEA in the fuel cell. Because of the intention of modifying the surface by PVD, there was also the need to obtain a composite layer with minimum shadowing by particles during the PVD procedure; hence low graphite content and single particles without clumping was targeted. The surface required was very different from those produced by CORUS for a battery application. In particular, it was necessary to use a low content of graphite particles in the solution, 1 g dm^{-3}. Also 1 g dm^{-3} graphite particles in the solution gave better results when the flow cell was used and showed the possibility to create surface with isolated single particles that easily meet the target contact resistance.

A combinatorial approach using physical vapour deposition (PVD) and a 10 x 10 electrode array was developed to investigate corrosion and to define the Cr content of NiCr alloys that give low corrosion rates. The method was first tested by a study of Ni in 1 M NaOH solution at room temperature. Ni-Cr alloys were next successfully deposited by PVD and their electrochemistry defined in the acid sulphate medium at 333 K. It was found that there was little advantage in increasing the Cr content above 20%. It was also shown that for suitable corrosion studies it is essential to deposit thick layers (by PVD standard) in order to avoid initial, irreversible changes to the surface before or during the electrochemical experiment and also to allow multiple experiments. This approach shows promise for identifying alloys with the lowest corrosion rates.

Electroplating of Cr from Cr(III) sulphate bath is possible and according to the literature, the corrosion rate is low. There was also possible to deposit thin layer of Ni-Cr alloys from a sulfate bath containing thiourea but the layer did not thicken because of H_2 evolution, as these alloys are good catalysts for this reaction. On the other hand, a very thin layer onto Ni-graphite composite may be sufficient to protect Ni-graphite layers.

It was intended that the surface of Ni layers could be modified by the deposition of a Cr layer (by electroplating or PVD) and a heat treatment employed to diffuse the Cr into the Ni to form a surface alloy. Heat treatments always led to coloured surfaces resulting from Cr oxidation and it was concluded that heat treatments are only likely to be successful if carried out with the total exclusion of O_2, e.g. with a high vacuum system. Indeed, the samples heat-treated in the PVD chamber did not colour although, since they involved very thin layers, they were carried out at much lower temperatures.

In general, as yet bipolar plate based on carbon steel is not viable. Procedures for deposition of Ni-graphite composites seem to be acceptable methods for the further protection of the Ni need to be improved further.

References

[1] *Metal Bipolar Plates For PEM Fuel Cell—A Review*, H. Tawfika, Y. Hunga,, D. Mahajan, Journal of Power Sources 163,2007, pages 755-767

[2] *Modern Aspects in Electrochemistry 40, PEM Fuel Cell Bipolar Plates*, V. Bloomfield, D. Bloomfield, 2007, pages 1 – 35

[3] www.fuelcells.org

[4] *Applications of Proton Exchange Membrane Fuel Cell System*, Jung-Ho Wee, Renewable and Sustainable Energy Reviews 11, 2007, pages 1720-1738

[5] *Portable and Military Fuel Cells*, K. Cowey, K. J. Green, G. O. Mepsed, R.Reeve, Current Opinion in Solid state and Material Science 8, 2004, pages 367-371

[6] *The Car and Fuel of The Future*, J. Romm, Energy Policy 34, 2006, pages 2609-2614

[7] *A First Course in Electrode Process*, 2nd edition, D.Pletcher,, RSC Publishing , 2009

[8] *Ni-Cr Thin Film Resistor Fabrication for GaAs Monolithic Microwave Integrated Circuits*, S. Vinayak, H. P. Vyas, K. Maruleedharn, V .D. Vankar, Thin Solid Films 514, 2006, 52-57

[9] *Metallurgical, Surface, and Corrosion Analysis of Ni–Cr Dental Casting Alloys Before and After Porcelain Firing*, H. Lin, B. Bowers, J. T. Wolan, Z. Cai, J. D. Bumgardner, Dental Materials 24, 2008, pages 378-385

[10] *Thermodynamics and Kinetics in Material Science: A Short Course*, B. S. Bokstain, M. I. Mendelev D. J. Srolovitz, Oxford University Press, 2005, pages 278-279

[11] *Electrochemical Methods, Fundamental and Applications*, A. J. Bard, L. Faulkner, John Wiley and Sons, 2nd edition, 2004

[12] *Physicochemical Hydrodynamics*, V. G. Levitch, Prentice-Hall Inc., 1962

[13] *A First Course in Electrochemical Engineering*, F. C. Walsh, The Electrochemical Consultancy, 1993

[14] *Reconstruction of Hydrodynamic Flow Profiles in a Rectangular Flow Channels Using Electrochemical Methods of Analysis,* O. V. Klymenko, A. Oleinick, Ch. Amatore, I. Svir, Electrocheimica Acta 53, 2007, pages 1100-1106

[15] *Atlas of Electrochemical Equilibria in Aqueous Aolutions*, M. Pourbaix, Pergamon Press, Oxford, 1966

[16] *Electrochemical Polarization. I. A Theoretical Analysis of The Shape of Polarization Curve*, M. Stern and A. L. Geary, Journal of The Electrochemical Society 104, 1957, pages 56 - 63

[17] *Encyclopedia of Electrochemistry, vol.4, Corrosion and Oxide Films*, A.J. Bard, M. Stratman, G. Frankel, Wiley-VCH Verlag GmbH and Co. KGaA, 2003

[18] *Electrochemical Impedance Spectroscopy,* M. E. Orazem, B. Tribollet, The Electrochemical Society Series, Wiley and Son, 2008

[19] *ASM handbook, Volume 13A, Corrosion: Fundamentals, Testing and Protection*, S. D. Cramer, B. S. Covino, ASM International, 2003

[20] *Temperature Dependence of The Electrochemical Corrosion Characteristics of Carbon Steel In Salty Soil*, X. H. Nie, X. G. Li, C. W. Du, Y. F. Cheng, Journal of Applied Electrochemistry 39, 2009, pages 277 – 282

[21] *On The Corrosion Behaviour of Novel High Carbon Rail Steels in Simulated Cyclic Wet–Dry Salt Fog Conditions*, B. Panda, R. Balasubramaniam, G. Dwivedi, Corrosion Science 50, 2008, pages 1684-1692

[22] *Electrochemical Study On Carbon Steel Corrosion Process in Alkaline Sour Media*, R. Cabrera-Sierra, E. Sosa, M.T. Oropeza, I. Gonza´lez, Electrochimica Acta 47, 2002, pages 2149-2158

[23] *Steelwork Corrosion Control*, D. A. Bayliss, D. H. Deacon, Taylor and Francis, 2nd edition, 2002

[24] *Corrosion and Corrosion Protection Handbook*, Philip A. Schewitzer, CRC Press, 2nd edition, 1988

[25] *The Corrosion Handbook*, H. H. Uhlig, John Wiley and Son, 1948

[26] *Steels and Its Heat Treatment*, 2nd edition, Karl-Erik Thelning, Butterworths, 1984

[27] *Steels, Microstructure and Properties*, R. W. K. Honeycombe, Edward Arnold Ltd, 1981

[28] *Corrosion of Iron in Aqueous Solutions Containing a Chemical Cleaning Agent*, A.M. A1-Mayouf, Desalination 114, 1997, pages 29-36

[29] *ASM Handbook, Volume 13B, Corrosion: Materials*, ASM International, 2005

[30] *On The Corrosion Inhibition of Low Carbon Steel in Concentrated Sulphuric Acid Solutions. Part I: Chemical and Electrochemical (AC and DC) Studies,* S. S. Abdel Rehim, O. A. Hazzazi, M. A. Amin, K. F. Khaled, Corrosion Science 50, 2008, pages 2258-2271

[31] *Experimental and Theoretical Study For Corrosion Inhibition of Mild Steel in Hydrochloric Acid Solution by Some New Hydrazine Carbodithioic Acid Derivatives*, K. F. Khaled, Applied Surface Science 252, 2006, pages 4120-4128

[32] *Annual Book of ASTM Standards*, Vol. 02.05, 1996, American Society for Testing and Materials, West Conshohocken, PA

[33] *Industrial Electrochemistry, Chapter 9,* "Corrosion Control", D. Pletcher, Springer, 1982,

[34] *Integrated Circuit Manufacture*, P. C. Sukanek, A. Sekiguchi, J. G. Ryan, W. R. Wilcox, Encyclopedia of Physical Science Technology 2004, pages 861-882

[35] *Modern Electroplating*, M. Paunovic, M. Schlesinger, J. Wiley and Son, 4th edition, 2000

[36] *Semiconducting Properties of Passive Films Formed On Electroplated Ni and Ni-Co Alloys*, J. Kang, Y. Yang, X. Jiang, H. Shao, Corrosion Science 50, 2008, pages 3576-3580

[37] *Young's Modulus of Electroplated Ni Thin Film For MEMS Applications,* J. K. Luo, J. Flewitt, S. M. Spearing, A. N. Fleck, W. I. Milne, Material Letters 58, 2004, pages 2306-2309

[38] *Electrodeposition of Ni From a High Internal Phase Emulsion (HIPE) Template*, I. J. Brown, S. Sotiropoulos, Electrochimica Acta 46, 2001, pages 2711-2720

[39] *www.growel.com*

[40] *Effect of Boric Acid On Electrodeposition of Iron, Nickel and Iron-Nickel*, K. M. Yin, B. T. Lin, Surface and Coating Technology 78, 1996, pages 205-210

[41] *Electroplating and Electroless Plating of Nickel Through/onto a Porous Polymer In a Flow Cell*, I. J. Brown, S. Sotiropoulos, Journal of Applied Electrochemistry 31, 2001, pages 1203-1212

[42] *Fundamental of Electrochemical Deposition*, M. Paunovic, M. Schlesinger, John Wiley and Son, Inc, 2nd Edition, 2006

[43] *The effect of Current Density On The Grain Size of Electrodeposited Nanocrystalline Nickel Coatings*, A. M. Rashidi, A. Amadeh, Surface and Coating Technology, 202, 2008, pages 3772 – 3776

[44] *The Effect of Parameters On The Mechanical Properties of Ni-Based Coatings Prepared by Automatic Brush Plating Technology*, B. Wu, B. S. Xu, B. Zhang, S. Dong, Surface and Coating Technology 201, 2007, pages 5757-5765

[45] *Current Distribution In Gavlanic cells Involving Natural Convection*, C. Wagner, Journal of Electrochemical Society 104, 1957, pages 129 - 131

[46] *To The Electric Conductivity of The Solutions*, R. R Salem, Protection of Metals 42, 2006, pages 60-65

[47] *Secondary Current Distribution in a Hull Cell*, M. Matlosz, C. Creton, C. Clerc, D. Landolt, Electroplating Science and Technology 134, 1987, pages 3015-3021

[48] *Studies On Cathodic Protection Using the Hull Cell. Action of Corrosion Inhibitors*, K. S. Rajagopalan and Y. V. P. Ramachandra**,** Journal of Electrochemical Society 107, 1960, pages 379-382

[49] *Investigation of The Secondary Current Distribution in a Hull Cell*, Z. Zhang, J. Q. Zhang, W. H. Leng, and C. N. Caoa, Journal of Electrochemical Society 148(7), 2001, pages C448-C491

[50] *Influence of Electrolyte Flow on The Alloy Electrodeposition of Zinc-Iron*, T. UDA, K. Asano A. Shibuya, Transaction of The Iron and Steel Institute of Japan 26, 1986, pages 53-60

[51] *Comprehensive Treatise of Electrochemistry, Volume 6: Electrodics: Transport*, E. Yeager, J.O'M. Bockris, B. Conway, S. Srangapani, Plennum Press, New York, 1983

[52] *Beneficial Role of Surfactants In Electrochemistry and in The Modification of Electrodes*, R. Vittal, H. Gomathi, K. Kim, Advances in Colloid and Interfacial Science 119, 2006, pages 55 - 68

[53] *Influence Of a Cationic Surfactant in The Properties of Cobalt-Nickel Electrodeposit*, E. Gomez, S. Pane, X. Aclobe, E. Valles, Electrochimica Acta 51, 2006, pages 5703-5709

[54] *Nickel and Nickel-Phosphorous Matrix Composite Electrocoatings*, N. Spyrellis, E. A. Pavlatou, S. Spanaou, A. Zoikis-Karathanasis, Transactions of Nonferrus Metals Society of China 19, 2009, pages 800-804

[55] *Composition Control of Electroplated Nickel-Phosphorus Deposits*, C.-C. Hu, A. Bai, Surface and Coatings Technology 137, 2001, pages 181-187

[56] *Electrodeposition of Particle-Strengthened Nickel Films*, H. Ferkel, B. Mtiller , W. Riehemann, Material Science and Engineering A 234-236, 1997, pages 474-476

[57] *Friction and Wear Behaviour of Ni–Graphite Composites Prepared by Electroforming*, H. Zhao, L. Liu, W. Hu, B. Shen, Materials and Designs 28, 2007, pages 1374-1378

[58] *Preparation and Characterization of Graphite–Nickel Composite Coatings by Automatic Brush Plating,* B. Wu, X. Yu, B. Zhang, B. Xu, Surface Coating Technology 202, 2008, pages 1975-1979

[59] *Synthesis of Super Hard Ni-B/Diamond Composite Coatings by Wet Process*, H. Ogihara, A. Hara, K. Miyamoto, N. K.Shrestha, T. Keneda, S. Ito, T. Saji, Chemical Communication 46, 2010, pages 442-444

[60] *Preparation and Investigation of Nanostructured SiC–Nickel Layers by Electrodeposition*, L. Benea, P. Bonora, A. Borello, S. Martelli, F. Wenger, P. Ponthiaux, J. Galland, Solid State Ionics 151, 2002, pages 89-95

[61] *Electrodeposition of Ni-SiC Nano-Composite Coatings and Evaluation of Wear and Corrosion Resistance and Electroplating Characteristics*, M. R. Vaezi, S. K. Sadrnezhaad, L. Nikzad, Colloids and Surfaces A: Physicochemical Engineering Aspects 315, 2008, pages 176-182

[62] *Electrodeposition of Ni–RuAl Composite Coating On Steel Surface*, A. A. Aal, H.A. Gobran, F. Muecklich, Journal of Alloys and Compounds 473, 2009, pages 250-254

[63] *Electrochemical Impedance Spectroscopy and Corrosion Behaviour of Al_2O_3–Ni Nano Composite Coatings*, A. Ciubotariu, L. Benea, M. Lakatos–Varsanyi, V. Dragan, Electrochimica Acta 53, 2008, pages 4557-4563

[64] *Corrosion Behaviours of Carbon Nanotubes-Ni Composite Coating,* X. H. Chen, C. S. Chen, N. H. Xiao, F. Q. Cheng, G. Zhang, G. J. Yi, Surface and Coatings Technology 191, 2005, pages 351-356

[65] *Ni/Nano-TiO_2 Composite Electrodeposits: Textural and Structural Modifications*, S. Spanou, E. A. Pavlatou, N. Spyrellis, Electrochimica Acta 54, 2009, pages 2547-2555

[66] *Nickel and Chromium Plating*, J. K. Dennis, T. E. Such, Woodhead Publishing Ltd., and ASM International, 1993

[67] *Practical Problems in Bright and Hard Chromium Electroplating – Part I to Part VII*, N. V. Mandich, Metal Finishing, pages 97,1999,

[68] *Hard Chromium Plating of EDT Mill Work Rolls*, J. SimaÄo, D. K. Aspinwall, Journal of Material Processing Technology 92-93, 1999, pages 281-287

[69] *Studies of Corrosion Resistance of Amorphous Chromium Deposit in Acidic Solution,* X. Wang, H.J iang, B. Guo, Transactions of the Institute of Metal finishing 78(3), 2000, pages 101-104

[70] *Characterization of Black and White Chromium Electrodeposition Films: Surface and Optical Properties*, M. Aguilar, E. Barrera, M. Palomar-Pardave, L. Huerta, S. Muhl, Journal of Non-Crystalline Solids 329, 2003, pages 31-38

[71] *A Novel Trivalent Chromium Electroplating Bath*, D. Smart, T. E. Such, S. J. Wake, Transaction of Institute of Metal Finishing 61, 1983, pages 105-110

[72] *Bright Chromium Alloy Plating*, W. H. Safranek, U.S. Patent Number 2822326, 1958

[73] *Electrodeposition of Chromium And Its Alloys*, D. J. Barcley, W. M. Morgan, J. M. Vigar, U.S. Patent Number 4502927, 1985

[74] *Inorganic Chemistry*, A. G. Sharp, Longman Scientific and Technical, John Wiley and Sons, 3rd Edition, 1991, pages 580-581

[75] *The Metallic Elements*, R.V. Parish, Longman Group Limited, 1977

[76] *Complexes and First-Row Transition Elements*, D. Nicholls, Macmillan Press LTD, 1974

[77] *PhD Thesis: Electrode Studies of Electroplating Systems*, J. N. Howarth, University of Southampton, October 1987

[78] *Elimination of Anode Hydrogen Cyanide Formation in Trivalent Chromium Plating*, D. J. Barclay, J. M. L. Vigar, U.S. Patent No 4256548, 1981

[79] *The Electrodeposition of Chromium from Chromium(III) solutions – a Study Using Microelectrodes*, J. N. Howarth, D. Pletcher, Journal of Applied Chemistry 18, 1988, pages 644 – 652

[80] *Passivation of Chrome-Plated Sheet Iron in Electrolytes Based on Chromium(III) Salts*, V. A. Paramanov, N. G. Filatove, Protection of Metals 38, 2002, pages 475-478

[81] *Theory of The Potential and The Technical Practice of Electrodeposition. I. The General Problem and The Cases of Uniform Flow*, C. Kasper, 77 General Meeting in Wernersville, Pa., April 27, 1940

[82] *Alloy and Microstructure Design*, J. K. Tien, G. S. Ansell, Academic Press, 1976

[83] *The Strengthening of Metals*, D. Pecker, Chapman and Hall, 1964

[84] *The Role of Additives in The Electrodeposition of Nickel–Cobalt Alloy From acetate Electrolyte*, K. R. Marikkannu, G. P. Kalaignan, T. Vasudevan, Journal of Alloys and Compounds 438, 2007, pages 332 – 336

[85] *Temperature Effect in Corrosion Resistance of Ni-Fe-Cr Alloy In Chloride Medium*, M. V. Cardoso, S. T. Amaral, E. M. A. Martini, Corrosion Science 50, 2008, pages 2429-2436

[86] *Electrodeposition of Zn-Ni Alloys in Sulfate Electrolytes I. Experimental Approach*, F. J. Fabri O. Miranda. E. Barcia O. R. Mattos and R. Wiart, Journal of Electrochemical Society 144, 1997, pages 3442 - 3451

[87] *Electrodeposition, Characterization and Mathematical Model of Nickel-Iron Film in a Parallel Plate Flow System*, K. M. Yin, H. F. Huang, Y. T. Lin, Transaction of the Institute of Metal Finishing, 2005, pages 82-89

[88] *Electrochemical Studies of Zinc-Nickel Codeposition in Sulphate Bath*, M. M. Abou-Krisha, Applied Surface Science 252, 2005, pages 1035-1048

[89] *Electrodeposition of Zn-Ni Protective Coatings From Sulphate-Acetate Baths,* E. Beltowska-Lehman, P. Ozga, Z. Swiatek, C. Lupi, Surface and Coatings Technology 151-152, 2002, pages 444-448

[90] *The Anomalous Codeposition of Iron-Nickel Alloys*, H. Dahms, I. M. Croll, Journal of Electrochemical Society 112, 1965, pages 771 – 776

[91] *Mechanism of The Electrodeposition of Zinc Alloys Containing a Small Amount of Cobalt*, K. Higashi, H. Fukushima, T. Urakawa, Journal of Electrochemical Society 128, 1981, pages 2081 – 2086

[92] *Development of Electroplated Magnetic Materials For MEMS,* N. V. Myung, D. Y. Park, B. Y. Yoo, P. T. A. Sumodjo, Journal of Magnetism and Magnetic Materials 265, 2003, pages 189-198

[93] *Electrochemical Study of The Passive Behaviour of Ni-Cr Alloys in a Borate Solution – a Mixed-Conduction Model Approach*, M. Bojinov, G. Fabricius, T. Laitinen, K. Makela, T. Saario, G. Sundholm, Journal of Electroanalytical Chemistry 504, 2001, pages 29-44

[94] *The Mechanism of Transpassive Dissolution of Ni-Cr Alloys in Sulphate Solution*, M. Bojinov, G. Fabricius, P. Kinnunen, T. Laitinen, K. Makela, T. Saario, G. Sundholm, Electrochimica Acta 45, 2000, pages 2791-2802

[95] *Electrical Resistivity Measurement in Ni-Cr Alloys*, A.A.Al-Aql, Materials and Design 24, 2003, pages 547-550

[96] *The Electrical Resistance and Enthalpy of Industrial Alloys Based On Nickel and Copper*, V. N. Korobenko, A.I. Savvatimski, Journal of Non-Crystalline Solids 205-207, 1996, pages 678-682

[97] *Preparation and Characterization of Electroplated Amorphous Gold–Nickel Alloy Film For Electrical Contact Applications*, N. Togasaki, Y. Okinaka, T. Homma, T. Osaka, Electrochimica Acta 51, 2005, pages 882-887

[98] *Characerisation of Cr-Ni Multilayers Electroplated From Chromium(III) – Nickel(II) Bath Using Pulse Current*, C. A. Huang, C. Y. Chen, C. C. Hsu, C. S. Lin, Scripta Materialia 57, 2007, pages 61-64

[99] *Hardness Variation and Corrosion Behaviour of as Plated and Annealed Cr-Ni Alloy Deposits Electroplated In a Trivalent Chromium Based Bath,* C. A. Chuang, C. K. Lin, C. Y. Chen, Surface and Coatings Technology 203, 2009, pages 3686-3691

[100] *Technological Advances in Physical Vapour Deposition*, G. Herklotz, H. Eligehausen, Institute of Electrical and Electronics engineers, Transaction on Components Hybrids and Manufacturing Technology, CHMT-6, 2,1983, pages 173-180

[101] *A Combinatorial Approach to The Study of Particle Effect On Supported Electrocatalysts: Oxygen Reduction On Gold*, S. Guerin, B. E. Hayden, D. Pletcher, M. E. Rendall and J. P. Suchsland, Journal of Combinatorial Chemistry 8, 2006, pages 679-686

[102] *Physical Vapor Deposition Method For High-Throughput Synthesis of Solid State Material Libraries,* S. Guerin, B. E.Hayden, Journal of Combinatorial Chemistry 8(1), 2006, pages 66-73

[103] *High Throughput Synthesis and Screening of Ternary Metal Alloys For Electrocatalysis*, S. Guerin, B. E.Hayden, C. E. Lee, C. Mormiche and A. E. Russell, Journal of Physical Chemistry B, 110, 2006, pages 14355-14362

[104] *Combinatorial Electrochemical Screening of Fuel Cell Electrocatalysts*, S. Guerin, B. E. Hayden, C. E. Lee, C. Mormiche, J. R. Owen and A. Russell, Journal of Combinatorial Chemistry 6(1), 2004, pages 149-158

[105] *Cold-rolled products*, CORUS Strip Products UK, p.28-29,

[106] *Combinatorial Electrochemical Screening of Fuel Cell Electrocatalysts*, S. Guerin, B. E. Hayden, C. E. Lee, C. Mormiche, J. R. Owen and A. Russell, Journal of Combinatorial Chemistry 6, 2004, pages 49-158,

[107] *A First Course in Electrochemical Engineering,* F. C. Walsh, The Electrochemical Consultancy, 1993,

[108] *Electrochemical Reactor Design,* D. J. Picket, Elsevier Scientific Publishing Amsterdam-Oxford-New York, 1977,

[109] *Physical Vapor Deposition Method for High-Throughput Synthesis of Solid State Material Libraries*, .I Guerin, B. E.Hayden, Journal of Combinatorial Chemistry 5, 2006, pages 66-73,

[110] *A First Course in Electrode Process,* D. Pletcher, The Electrochemical Consultancy, 1991,

[111] *High Throughput Synthesis and Screening of Ternary Metal Alloys for Electrocatalysis,* S. Guerin, B. E. Hayden, C. E. Lee, C. Mormiche and A. E. Russell, Journal of Physical Chemistry B 110, 2006, pages 14355-14362,

[112] *Secondary Current Distribution in a Hull Cell*, M. Matlosz, C. Creton, C. Clerc, D. Landolt, Electroplating Science and Technology 134, 1987, pages 3015-3021

[113] *Structural and Electrochemical Characterization of Ni Nanostructure Films on Steel With Brush Plating and Sputter Deposition,* B. Subramanian, S. Mohan, S. Jayakrishnan, M.J ayachandran, Current Applied Physics 7, 2007, pages 305-313

[114] *Crystals and Crystal Structures*, R. Tilley, John Wiley and Son, 2006

[115] *Corrosion of Graphite in Industrial Phosphoric Acid,* A. Guenbour, H. Iken, N. Kebkab, A. Ballaouchou, R. Bouli, A. B. Bachir, Applied Surface Science 252, 2006, pages 8710-8715

[116] *Comprehensive Treatise of Electrochemistry, Volume 4: Electrochemical Material Science*, E. Yeager, J. O'M. Bockris, B. Conway, R. E. White, Plennum Press, New York, 1981

[117] *The Corrosion of Carbon Black Anodes in Alkaline Electrolyte II. Acetylene Black and the Effect of Oxygen Evolution Catalysts on Corrosion*, N. Staud, P. N. Ross, Journal of Electrochemical Society 133, 1986, pages 1079 – 1085

[118] *Stress, Resistance and Phase Transition in NiCr (60 wt%) Thin Films*, W. Bruckner, W. Pitshike, J. Thomas, Journal of Applied Physics 87, 2000, pages 2219-2226

[119] *Ni-Cr Thin Film Resistor Fabrication for GaAs Monolithic Microwave Integrated Circuits,* S. Vinayak, H. P. Vyas, K. Maruleedharn, V. D. Vankar, Thin Solid Films 514, 2006, pages 52-57

[120] *The Mechanism of Transpassive Dissolution of Ni-Cr Alloys in Sulphate Solution*, M. Bojinov, G. Fabricius, P. Kinnunen, T. Laitinen, K. Makela, T. Saario, G. Sundholm, Electrochimica Acta 45, 2000, pages 2791-2802

[121] *Electrochemical Processes in Fuel Cells*, M. W. Breiter, Springer-Verlag New York Inc., 1969

[122] *Analysis of the Charge-Discharge Characteristics of Nickel-Oxide Electrodes by Infrared Spectroscopy*, F. P. Kober, Journal of Electrochemical Society 112, 1965, pages 1064 – 1069

[123] *Effect of Crystal Structure on the Anodic Oxidation of Nickel*, J. L. Weininger, M. W. Breiter, Journal of Electrochemical Society 110, 1963, pages 484 - 491

[124] *Nickel-Cadmium Cells I. Thermodynamics and X-Ray Studies*, A. J. Salkind, P. F. Bruins, Journal of Electrochemical Society 109, 1962, pages 356 – 361

[125] *Structure and Stoichiometry of Nickel Hydroxides in Sintered Nickel Positive Electrodes*, M. A. Aia, Journal of Electrochemical Society 114, 1967, pages 418 – 424

[126] *A Novel Trivalent Chromium Electroplating Bath*, D. Smart, T. E. Such, S. J. Wake, Transaction of Institute of Metal Finishing 61, 1983, pages 105 -110